PROCEEDINGS OF THE
5th CANADIAN ROCK
MECHANICS SYMPOSIUM

TORONTO DECEMBER 1968

Sponsored by:
The Canadian Advisory Committee on Rock Mechanics,
and The University of Toronto.

PUBLISHED BY
MINES BRANCH
DEPARTMENT OF ENERGY, MINES AND RESOURCES, OTTAWA, 1969

Available by mail from the Queen's Printer, Ottawa
and at the following Canadian Government bookshops

HALIFAX
1735 Barrington Street

MONTREAL
Æterna-Vie Building, 1182 St. Catherine St. West

OTTAWA
Daly Building, Corner Mackenzie and Rideau

TORONTO
221 Yonge Street

WINNIPEG
Mall Center Bldg., 499 Portage Avenue

VANCOUVER
657 Granville Street

or through your bookseller

Price: $6.50 Catalogue No.: M37-1370

Price subject to change without notice

Queen's Printer for Canada
Ottawa, 1970

Production editor, Jack Hughes.
Technical editorial assistance, K. Barron,
Department of Energy, Mines and Resources,
Ottawa, Canada.

Contents

1 *The Influence and Control of Groundwater in Open Pit Mining*, by C.O. Brawner

15 *In Situ Dynamic Strain Measurements in Rock*, by R.F. Favreau and S. Chung

19 *Behavior of the Underground Powerhouse Arch at the W.A.C. Bennett Dam During Excavation*, by A.S. Imrie and L.T. Jory

41 *Insights into Undercutting in Block Caving*, by Giovanni Barla and Stefan Boshkov

59 *Rock Stress Measurement at the Sullivan Mine*, by M.J. Royea

75 *Rock Mechanics in Damsite Location*, by E.W. Brooker and I.H. Anderson

91 *Design and Application of Microseismic Devices*, by C.D. Broadbent and C.W. Armstrong

105 *Underground Measurements in a Steeply Dipping Orebody*, by D.G.F. Hedley, G. Zahary, H.W. Soderlund and D.F. Coates

127 *Ultrasonic Compressional and Shear-wave Velocities of Confined Rock Samples*, by M.S. King

157 *Projectile Penetration in Rock*, by Alan Bauer and P.N. Calder

171 *Fracture Characteristics of Rock Particles Tested Under Impact*, by K.D. Lyall and R.O. Tervo

185 *Closure Studies Improve Ground Control of Falconbridge Mine*, by K.R. Notley

197 List of Registrants

Foreword

Since the series of Canadian symposia on rock mechanics was inaugurated at McGill University in September 1962, one of its more encouraging features has been the broadening of the spectra of the fields of interest, and of the people who have been brought together to produce its most significant event to date, the fifth symposium. Though its parent body, the Canadian Advisory Committee on Rock Mechanics, is informal in its constitution, has no specialized home office, and collects no dues, its interest and enthusiasm are of high order. More importantly, the Committee has continually adjusted its viewpoints and terms of reference, and now offers a unique Canadian forum for the exchange and interchange of knowledge among practitioners and researchers in all activities which are concerned with crustal engineering materials and the residual structures influenced by them and the earth's body forces. The evidence of this effect lies in the 220 registrations for the event to which these Proceedings bear record, and whose quality and breadth speak for themselves.

A most successful and popular innovation of the third symposium held in Toronto in January 1965 was the mounting of a series of preliminary lectures in areas basic to studies in rock mechanics. This was repeated in the present case, and the response from the hundred or so people who registered for its benefits has been so gratifying that it is strongly recommended that future symposia contain the same optional feature.

The lectures, which were given on 5 December, were:

"Rock Fabric Analysis," by J.E.G. Schwellnus, Department of Mining Engineering and Applied Geophysics, McGill University.

"The State of the Art of *in situ* Stress Measurement," by Kenneth Barron, Mining Research Centre, Mines Branch, Department of Energy, Mines and Resources, Ottawa.

"Visco-Plastic Behaviour of Rocks," by M.S. King, Department of Geological Sciences, University of Saskatchewan.

"Rock Failure Theories," by B. Ladanyi, Department of Mining Engineering, École Polytechnique, Université de Montréal.

"Borehole Extensometers and Other Instrumentation in Field Applications," by A.V. Pegler, Department of Mining Engineering, Queen's University.

To these lecturers, and to the authors and presenters of papers in the main body of the Symposium, grateful thanks are due. The structure was also ably supported by Messrs. A.V. Corlett, W.M. Gray, N.R. Morgenstern, and T.H. Patching, who chaired the various sessions with tact and resolve.

The entire series of Canadian symposia owes much to the Mines Branch, Department of Energy, Mines and Resources, which assumes the burden of publishing these Proceedings, and whose officers take a leading part in Canadian mining research.

Again, a special acknowledgment is recorded to the Board of Education of the City of Toronto, for the use of the conference room and related facilities and personnel in its Education Centre, with its remarkable combination of efficiency, comfort, and aesthetic quality.

To close on a personal note, a recognition is made of the support in all decisional matters rendered by the Canadian Advisory Committee on Rock Mechanics, and especially by its chairman, D.F. Coates.

Department of Civil Engineering,
University of Toronto,
Toronto 5, Ontario.
7 December 1968

H.R. Rice,
General Chairman

Abstract

The presence of groundwater in areas of open pit mines can create serious problems. The most important problem is generally a reduction in stability of the pit slopes. This is caused by cleft water pressures and hydrodynamic shock reducing the shear strength, seepage pressures, water in tension cracks and increased unit weight increasing the shear stress.

Groundwater and seepage also increase the cost of pit drainage, shipping, drilling and blasting, and equipment maintenance. Surface erosion may also be increased and, in northern climates, ice flows on the slopes may occur.

Procedures have been developed in soil mechanics and engineering of dams to obtain quantitative data on cleft water pressures and rock permeability, to evaluate the influence of cleft water and seepage pressures on stability and to estimate the magnitude of groundwater flow.

Based on a field investigation program, a design can be prepared for the control of groundwater in the pit. Methods of control include the use of horizontal drains, the use of large blasted toe drains, construction of adits or drainage galleries or pumping from wells in or outside of the pit. Instruments should be installed to monitor the groundwater conditions during drainage.

Two typical case histories are described that indicate the approach used to evaluate groundwater conditions.

The Influence and Control of Groundwater in Open Pit Mining

by C.O. BRAWNER,
Principal, Golder, Brawner & Associates Ltd.,
Vancouver, B.C.

The Influence of Groundwater

In most open pit mines a certain amount of groundwater will generally be encountered. The amount of groundwater present, the rate at which it will flow through the rock, the effect it may have on stability and the influence it will have on the economical development of the pit will vary depending on many factors. The most important of these will be the topography of the general area, the amount of precipitation, the temperatures which occur throughout the year, the permeability of the rock mass and overburden soil and the orientation of the rock structure.

The most important effect of groundwater in open pit mining is the effect it has upon the stability of the rock slopes. The more important effects of groundwater on stability are described in the following text.

a. Reduction in Shear Strength

Shear strength is normally expressed by the Coulomb Equation:

$$s = c + (\sigma - u)\tan\phi$$

where
c = cohesion
σ = the weight normal to the slip surface
u = the neutral or buoyant pressure
ϕ = angle of internal friction.

Where the groundwater table is above the potential failure surface, the weight above that surface and below the groundwater table which develops friction along the failure surface is reduced by the buoyant uplift of the groundwater. Assuming the weight of rock to be approximately 170 pounds per cubic foot and the weight of water to be 62.4 pounds per cubic foot, frictional resistance developed by the rock in this zone would be reduced by 37%. If the groundwater table were to extend to the ground surface, the overall reduction in stability as compared to a zero cleft water pressure condition, would approximate this value. A typical example of the influence of drainage on stability is given in Figure 1.

In mountainous regions where the open pit may be well below the level of surrounding mountains, it is possible that cleft water pressures in excess of the total height of the slopes can be encountered. In this case the reduction in stability will exceed 37%.

In intact rock the cohesion is significantly influenced by changes in moisture content.

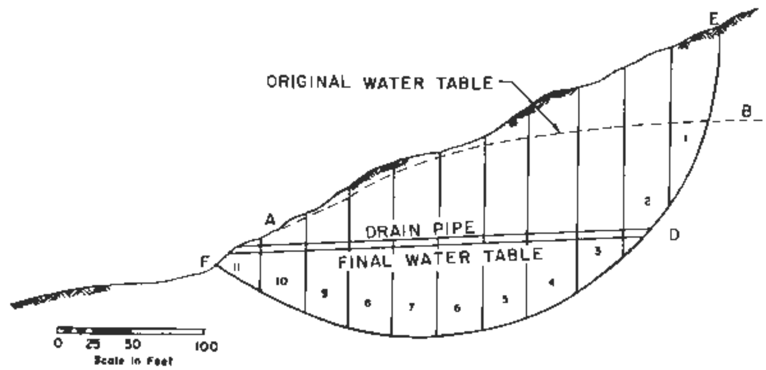

NOTES

$\mu 1_A$ = NEUTRAL PRESSURES BEFORE DRAINAGE (AREA);

$\mu 2_A$ = NEUTRAL PRESSURES AFTER DRAINAGE (AREA);

h_1 = HEIGHT OF PIEZOMETRIC SURFACE ABOVE SLIP-PLANE BEFORE DRAINAGE.

h_2 = HEIGHT OF PIEZOMETRIC SURFACE ABOVE SLIP-PLANE AFTER DRAINAGE (BOTTOM OF PIPE).

ASSUMPTIONS

1. THE NEW WATER TABLE WILL LIE AT THE ELEVATION OF THE DRAIN.
2. A STATIC CONDITION (NO SEEPAGE) EXISTS FOR THE CONVENTIONAL FLOW LINE.

VOLUMES AND LOADS WITHIN ARC EF

	1	2	3	4	5	6	7	8	9	10	11	TOTAL
AREA (A), SQ.FT.	2460	3730	4120	4450	4150	4100	3650	3280	2300	1340	390	33,970
NORMAL (N_A)	900	2500	3300	4000	3900	3950	3600	3200	2150	1150	300	28,950
TANGENTIAL (T_A)	2300	2800	2450	1850	1100	500	-200	-700	-800	-700	-250	8,350
AVERAGE h_1	30	80	96	119	125	123	115	96	70	45	18	
AVERAGE I	65	50	40	38	32	32	32	32	35	35	30	
$\mu 1_A$, SQ.FT.	1950	4000	3920	4520	4000	3930	3680	3070	2450	1575	540	33,635
AVERAGE h_2	0	2	23	44	55	61	60	56	45	30	13	
$\mu 2_A$, SQ.FT.	0	100	920	1670	1760	1950	1920	1790	1575	1050	390	13,125

$$\text{SAFETY FACTOR} = \frac{\Sigma(N-\mu)\tan\phi + CL}{\Sigma T}$$

CASE 1 - NO DRAINAGE

$$\text{SAFETY FACTOR} = \frac{1{,}520{,}000 \times 0{\cdot}1763 + 1660 \times 465}{1{,}040{,}000} = \underline{\underline{1{\cdot}0}}$$

CASE 2 - DRAINAGE

$$\text{SAFETY FACTOR} = \frac{2{,}800{,}000 \times 0{\cdot}1763 + 1660 \times 465}{1{,}040{,}000} = \underline{\underline{1{\cdot}2}}$$

INCREASE IN STABILITY IN LOWERING WATER TABLE FROM FB TO FD = 20 %

(AFTER LANDSLIDES AND ENGINEERING PRACTICE, 1958)

FIGURE 1 – Typical example of influence on stability of lowering groundwater pressures by drainage

Colbach and Wiid(1) found that the angle of shearing resistance remains essentially unchanged with the change in moisture but that the cohesion is reduced considerably as the moisture content of the rock increases.

The greatest reduction in stability can be expected to occur during and shortly after spring thaw, following heavy rainfall, and in northern climates, during the late stages of winter. In the past it has frequently been assumed that winter conditions should be conducive to stability since the surface of the rock slope is frozen. However, the water which normally is free to flow out through the cracks in the rock during the summer period becomes frozen during the winter and greatly reduces the permeability of the surface of the rock slope. This may result in a build-up of very high cleft water pressures behind the face, a condition which is particularly dangerous because the generally low permeability of the rock material. The force acts in the direction of flow of the water, i.e. into the open pit. Seepage forces can become very high. Coates and Brown(2) quote an example where seepage forces were computed to increase the shear stress by 24%. Figure 2 illustrates seepage forces acting in a slide area.

Seepage forces and cleft water pressures can occur in slopes which on the surface appear to be dry. If the permeability of the rock is moderately low it is possible that the rate of evaporation from the surface of the rock may exceed the rate of seepage. As a result, rock slopes which appear dry on the surface may experience high cleft water pressures at shallow depth. It is important to remember that high cleft water pressures can be developed by small amounts of water. Large water flow is not a necessity for instability to occur.

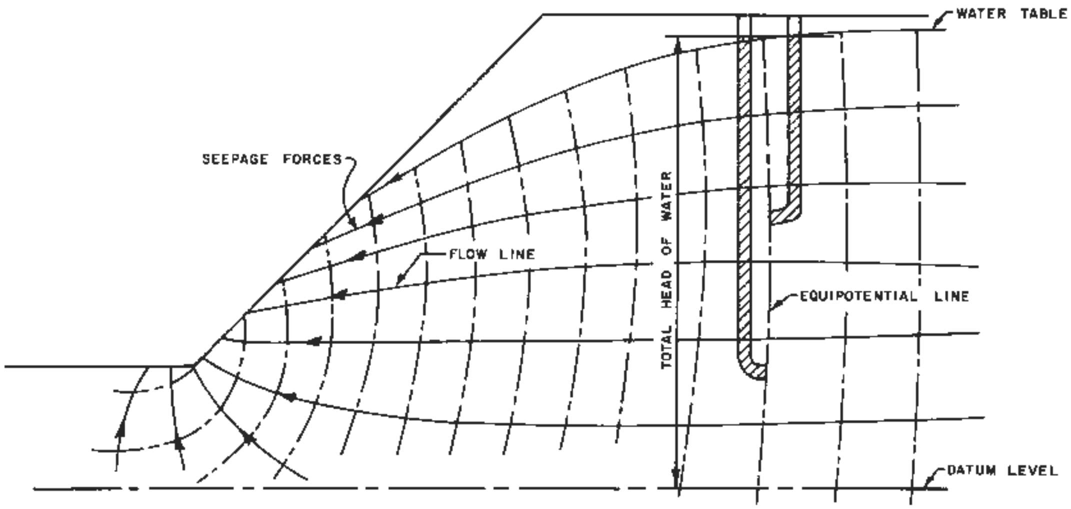

FIGURE 2 — Two-dimensional water flow net in a slope showing seepage forces (after Hoek and Pentz, 1968)

shear strength of the rock would diminish quite rapidly with the result that sudden failure of the rock may take place. Also, during the winter months, the rock slopes are frequently covered with snow so that tension cracks, which normally warn of impending movement, are not noticeable.

b. Development of Seepage Forces

As water flows through rock slopes, seepage forces develop as a result of the resistance offered to the flow of the water by the

The statement is frequently observed in the literature that the influence of cleft water and seepage pressures on stability can be ignored where massive rock exists. This statement is theoretically valid. However, from a practical standpoint, there is usually insufficient evidence obtained on most projects to guarantee that unfavourably oriented discontinuities do not exist. Therefore, the consequences of failure would usually be sufficiently serious that extreme caution in the use of this assumption is advised.

c. Water in Tension Cracks

Tension cracks frequently develop at and around the top of slides. These cracks are normally treated as indicators of instability. However, should rain occur while these cracks are open, these openings will fill with water. This water in the cracks creates a horizontal hydrostatic pressure on the sliding mass.

In practice, tension cracks may extend to depths of more than 20 to 40 feet so that hydrostatic pressures in these cracks can significantly influence stability. It is desirable, when tension cracks are first observed, that movement measuring devices or hubs be installed in the slide area and that tension cracks be filled immediately so that water cannot enter them and aggravate the already borderline stability. A typical example of hydrostatic pressure in a tension crack is shown in Figure 3.

d. Increase in Weight

The weight of a rock mass increases as the level of the water table increases due to the weight of the water in the joints, discontinuities and voids in the rock. This additional weight increases the shearing stress in the slope and therefore acts to reduce stability.

e. Liquefaction

Fault zones in rock are occasionally filled with a rock flour like gouge. If this gouge is in a loose density, is uniformly graded and is completely saturated, there is danger that vibration due to earthquakes or blasting may cause the gouge to liquefy. Failures due to this mechanism have been more commonly associated with failures of spoil dumps or tailings dams such as the El Cobre slides in Chile in 1966 [Dobry and Alvarez,(3)].

f. Dynamic Hydrostatic Shock Due to Blasting

It appears possible that large short-term cleft water pressures develop in rock slopes during blasting. This occurrence would reduce effective pressures and therefore would reduce stability. However, information is not available on this subject to date and the magnitude of the pressures which may be involved or the influence of high-pressure short-term loading on rock stability is unknown. Research on this subject is necessary at an early date.

In addition to possible adverse influence on stability, groundwater may have other detrimental effects. Some of these are briefly noted.

i. Pit Drainage – In areas of heavy precipitation or low evaporation and moderately pervious bedrock, extensive seepage from the slopes may occur which requires expensive drainage control and pumping from the bottom of the pit. Pit drainage control frequently costs thousands of dollars annually.

ii. Increase in Shipping Costs – On some projects the ore excavated from the pit is transported considerable distances. If the ore is moved in the saturated state, considerable water is transported. On major projects, transportation costs for hauling this water may be significant. Stubbins and Munro(4) state that an extra 2 % moisutre in the iron ore at Knob Lake, Que., increased transportation costs 12 cents per ton.

iii. Drilling and Blasting in Wet Holes – Where excavation is required below the groundwater table and the bedrock is moderately pervious, blast holes may fill up very rapidly with groundwater. This requires more expensive powder and blasting techniques and may result in caving prior to loading the hole. Blasting costs for wet holes are approximately double those which are normally incurred for dry holes.

iv. Increased Equipment Costs – During the spring thaw or heavy rainfall, excess seepage water may collect on the floor of the pit and on haul roads causing them to become muddy. Such conditions reduce the life of tires, tracks and brakes. In addition, hazards with electric cables are increased.

v. Surface Erosion – Occasionally relatively large amounts of water will occur as springs from the rock slopes. If the rocks are badly fractured, soft or weathered, the flow of water may cause detrimental erosion on the slopes.

vi. Ice Flows – In northern climates water issuing from the slopes may continue to freeze and build up ice mounds. In the spring, during the thaw period, these ice mounds can create a serious menace by sliding down the slopes.

Measurement of Groundwater Pressures and Permeability

Cleft water pressures can have a great influence on stability and the amount of seepage water can greatly influence the economics of pit and mine drainage. It is therefore desirable to determine the general groundwater conditions prior to final feasibility studies.

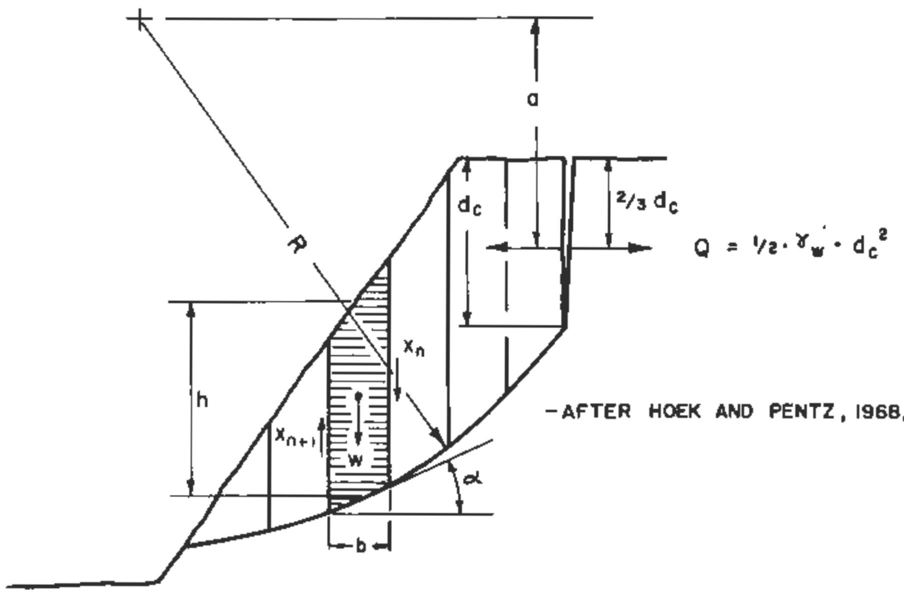

CIRCULAR ANALYSIS

$$F = \frac{R}{\sum (W \cdot R \cdot \sin\alpha) + Q \cdot a} \sum \left[\frac{c' \cdot b + \left[W(1 - u/\gamma_h) + X_n - X_{n+1} \right] \tan\phi'}{\cos\alpha \left[1 + \frac{\tan\phi' \cdot \tan\alpha}{F} \right]} \right]$$

F = FACTOR OF SAFETY

c' = EFFECTIVE COHESION

u = NEUTRAL PRESSURE AT BASE OF SLICE

γ = UNIT WEIGHT OF SOIL

ϕ' = EFFECTIVE ANGLE OF INTERNAL FRICTION

Q for 20' deep tension crack = $1/2 \times 62.4 \times (20)^2$ = 12400 lb/lineal ft.

Q for 40' deep tension crack = $1/2 \times 62.4 \times (40)^2$ = 49920 lb/lineal ft.

FIGURE 3 — Influence of tension crack filled with water on stability

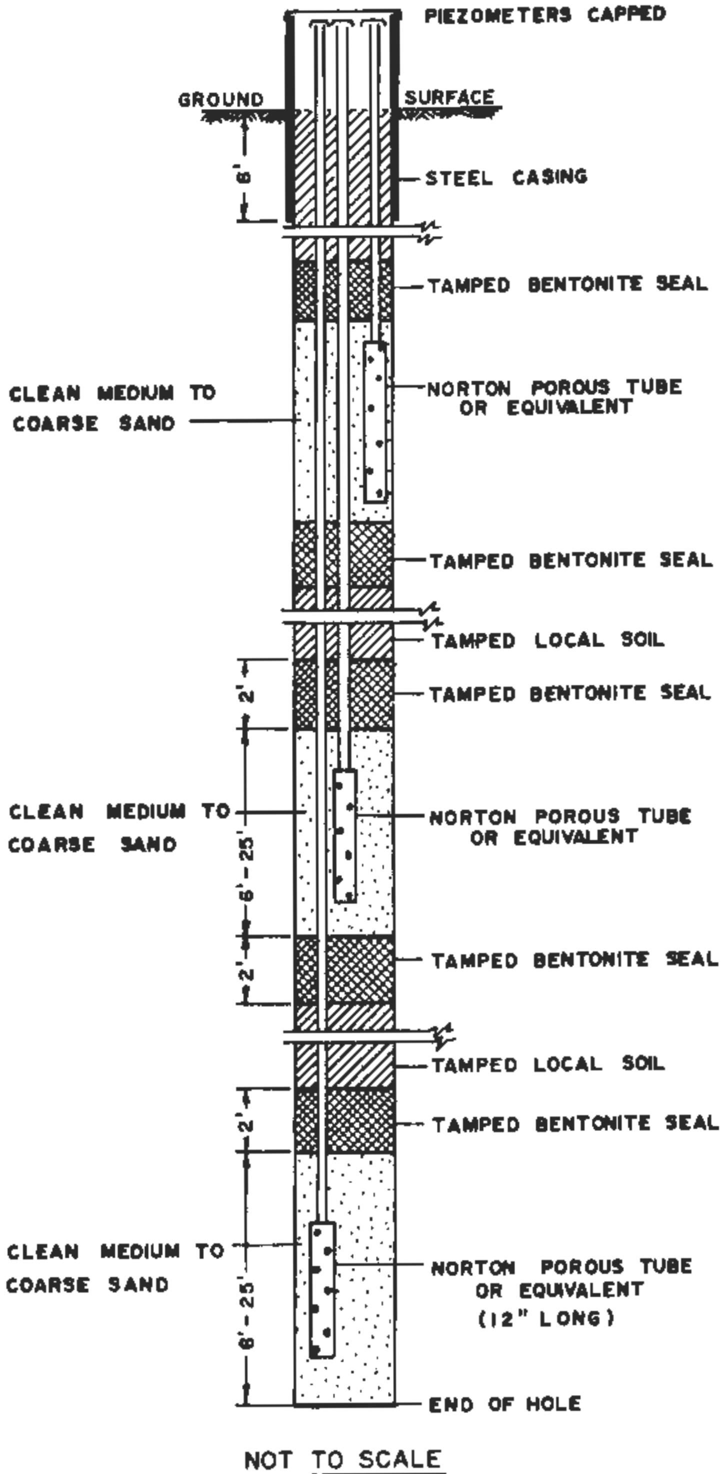

FIGURE 4 – Simple piezometer installation for measurement of cleft water pressures. Two or three piezometers are recommended per hole

The civil engineer can provide the mining engineer with considerable assistance in this regard. Extensive experience has been gained in soils engineering and groundwater studies performed in the investigation, design and construction of major dams throughout the world. With limited modification, the procedures for measurement of cleft water pressures, permeability of rock and groundwater flow developed for dam engineering can be used in groundwater studies for mine development. The cost of major dams generally compares with that of large mining developments. The importance of the influence of water on stability of dams has been sufficiently large to result in the development of refined methods of groundwater testing and evaluation.

Determination of cleft water pressures in the general pit area is desirable. The simplest procedure is to install porous pot or equivalent piezometers. (Figure 4.) These can be installed in boreholes that are drilled to determine the location and grade of ore. One piezometer can be installed in an AX size hole and up to three can be installed in an NX size borehole. Since it is not uncommon to find perched water tables in bedrock, two or three piezometers are recommended per hole. In order to install instruments in the best located boreholes it is recommended that all exploration holes that are drilled be cased to bedrock and protected so they can be used at a later date if necessary. The depth to the water level in the piezometers is usually determined by lowering an electrical resistance probe. (Figure 5.)

The coaxial cable is unwound from the reel and lowered down the piezometer tube. The ammeter is actuated when the two electrodes in the tip of the coaxial cable come in contact with the water, completing the electric circuit.

FIGURE 5 – Water level finder

Where water pressure data is required at a great depth, it may be necessary to install special transducerized piezometers. The most common electrical water pressure transducer is the Maihak vibrating wire piezometer. [Terzaghi and Peck,(5)]. This instrument is suitable for short-term installation. On a long-term basis, difficulties often develop with calibration and the instrument is easily damaged by nearby blasting. The disadvantages of the Maihak instrument appear to have been overcome in a prototype Solartron quartz-strut piezometer recently developed in England [Hoek and Pentz,(6)]. The vibrating wire has been replaced by a quartz-strut loaded in compression through a diaphragm upon which the water pressure acts.

Water levels should be read at least once per month, or following rain or thaw conditions, and the data compared with precipitation and spring thaw information. All piezometers installed outside the final pit should be established as permanent installations.

To evaluate stability and potential drainage problems, it is also necessary to know the general permeability of the bedrock. In most rocks, more water flows through discontinuities than through the intact rock. In this case, laboratory tests on rock core will not provide useful permeability data.

Pumping tests can be performed to determine average permeability. In these tests groundwater is pumped from a central hole or well and water level readings are measured continuously in observation holes located in several directions from the centre hole. (Figure 6.) This procedure is practical and reasonably economical for depths up to about 100 feet. Beyond this depth pumping tests become very expensive. With the great depths encountered in most open pit mines, this type of test has limited application.

At present, the borehole water packer permeability test is the most suitable and economical technique to measure the range of rock permeability. Usually a packer with a 10- to 20-foot spacing is installed in the borehole at any desired depth. Water is pumped into the hole between the packers under a moderate pressure and the volume of water forced into the rock is determined. Using standard permeability formulae [Cedergren(7)] the average permeability of the rock in the zone tested can be estimated. Rock permeability has been tested to a depth of 900 feet in BX boreholes

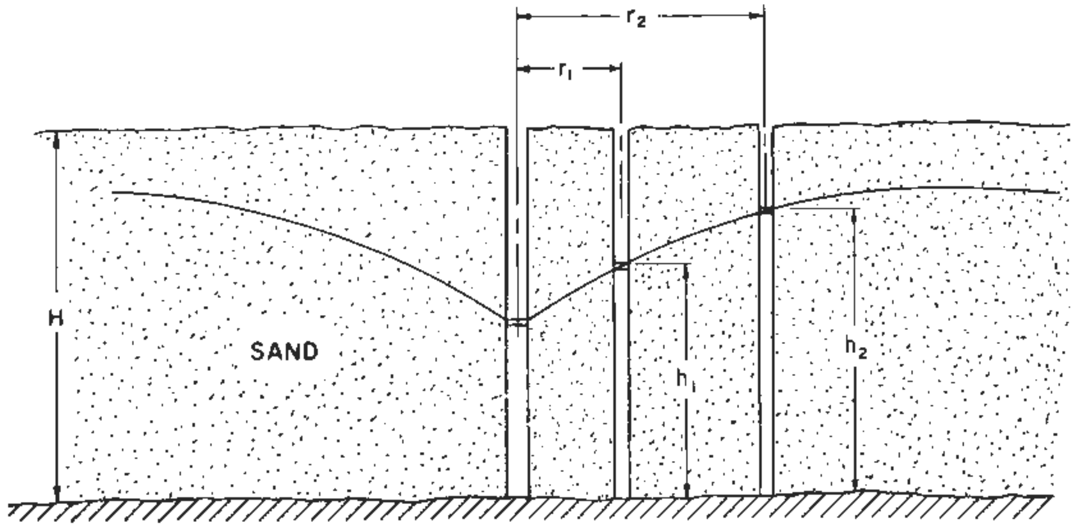

$$\text{Coefficient of permeability} = k = \frac{2.3q}{2\pi H(h_2 - h_1)} \log_{10} \frac{r_2}{r_1}$$

q = quantity of water pumped from the well per unit of time

FIGURE 6 — Illustration of influence of pumping test on ground water and determination of coefficient of permeability

under the author's direction. Providing the exploration boreholes have been maintained open and can be used, 6 to 10 boreholes around the pit area can usually be tested to depths of 800 to 900 feet in a one to two month period.

To obtain a rapid estimate of general permeability, falling head tests in boreholes can be performed [Golder and Gass(8)]. This involves filling the borehole with water to the surface and measuring the rate of drop of the water level with time. Standard formulae for this type of analysis are shown in Figure 7.

On many mining projects, adits are driven to check ore grades and metallurgy. By measuring water levels in boreholes situated above and adjacent to the adit during and following adit excavation and by measuring the flow of water in the adit using weirs, the average permeability of the rock can be estimated. The calculations are based on the assumption of symmetrical flow into the adit. The most convenient means of presentation and evaluation of cleft water pressures, seepage pressures and groundwater flow is by the use of a two dimensional flow net (Figure 2). It is assumed that the flow of water follows Darcy's law which states that:

$v = ki$

where v = discharge velocity (centimetres per second), k = coefficient of permeability (centimetres per second), and i = hydraulic gradient (a pure number), and that the LaPlace differential equation governs the flow of an incompressible fluid through an incompressible porous medium when the flow can be considered to be two dimensional. Since the LaPlace equation also governs the flow of electricity, water flow problems can conveniently be studied using an electrical analogue with the permeability of the rock represented by the circuit resistance [Karplus(9)]. With a variable resistance network, anisotropic conditions and variable boundary conditions can be evaluated.

Based on the permeability test results and the flow net, seepage volumes can be computed [Harr(10), Cedergren(7)]. By analyzing the field cleft water-pressure data and geometry of the flow net, cleft water pressures can be predicted for any slope geometry. The influence on stability can be estimated using the standard stability analysis employed in the field of soil mechanics [Brawner(11), Hoek and Pentz(6)].

Control of Groundwater

If the evaluation of groundwater conditions indicates excessive inflow into the pit or adverse effects on stability, several procedures to improve conditions are available to the mining engineer.

One technique which may be used to improve the stability of the rock slopes is to install horizontal drains, a technique which is commonly used to stabilize earth landslides [Brawner and Huculak(12)]. Percussion holes 2 to 3 inches in diameter are drilled near the toe of the slope on about a 5% grade for a distance of 50 to 100 feet into the slope. A typical installation in a soil slope is shown in Figure 8. To reduce drilling time it is common to fan 3 to 5 holes from one drill location. Groundwater flows into the drain holes, lowers the groundwater level and improves stability. In stabilizing landslides in soil it is necessary to install perforated pipe in each of the horizontal holes. In bedrock, however, the pipes are not normally necessary. During the cold winter weather in Canada it may be necessary to protect the outlets of the drains from freezing and to

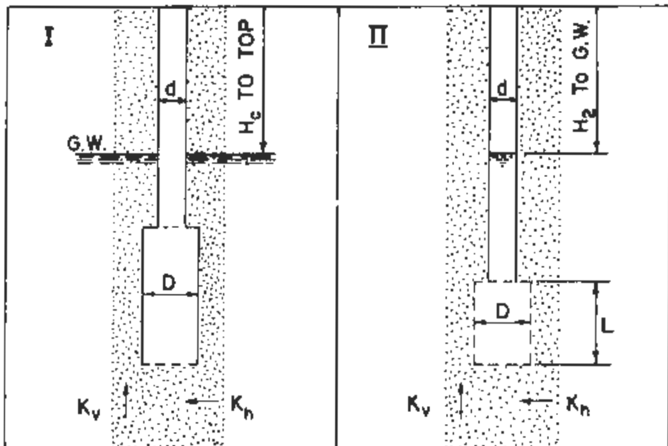

Flush Bottom in Uniform Soil

Well Point - Filter in Uniform Soil

LEGEND

- D = Diam., Intake, Sample, Cm.
- d = Diameter, Standpipe, Cm.
- L = Length, Intake, Sample, Cm.
- H_c = Constant Piez. Head, Cm.
- H_1 = Piez. Head For $t = t_1$, Cm.
- H_2 = Piez. Head For $t = t_2$, Cm.
- q = Flow of Water, Cm^3/Sec.
- t = Time, Seconds
- K_v = Vert. Perm. Ground, Cm./Sec.
- K_h = Horz. Perm. Ground, Cm./Sec.
- K_m = Mean Coeff. Perm., Cm./Sec.
- m = Transformation Ratio

$K_m = \sqrt{K_h \cdot K_v} \quad m = \sqrt{K_h / K_v}$

Case	Constant Head	Variable Head
I	$K_m = \frac{q}{2.75 \cdot D \cdot H_c}$	$K_m = \frac{\pi \cdot d^2}{11 \cdot D \cdot (t_2 - t_1)} \ln \frac{H_1}{H_2}$ $K_m = \frac{\pi \cdot D}{11 \cdot (t_2 - t_1)} \ln \frac{H_1}{H_2}$ For $d = D$
II	$K_h = \frac{q \cdot \ln\left[\frac{mL}{D} + \sqrt{1 + \left(\frac{mL}{D}\right)^2}\right]}{2 \cdot \pi \cdot L \cdot H_c}$	$K_h = \frac{d^2 \ln\left[\frac{mL}{D} + \sqrt{1 + \left(\frac{mL}{D}\right)^2}\right]}{8 \cdot L \cdot (t_2 - t_1)} \ln \frac{H_1}{H_2}$ $K_h = \frac{d^2 \ln\left(\frac{2mL}{D}\right)}{8 \cdot L \cdot (t_2 - t_1)} \ln \frac{H_1}{H_2}$ For $\frac{mL}{D} > 4$

FIGURE 7 — Formulas to determine permeability in bore holes (after Hvorslev, 1951 and Golder & Gass, 1962)

collect the water with a frost-free collector system.

In the winter months in northern climates it is common for the pit slopes to freeze so that seepage does not exit from the slopes. As a result high cleft water pressures frequently develop. This factor appears to account for the fact that many failures occur in the February to April period in Canada. An alternative to horizontal drainage to minimize the buildup of porewater pressures in the slopes is to blast the entire lower bench 30 to 40 feet wide around the toe of the slope in the open pit and not to excavate this blasted toe during the winter months. This area will have high permeability and will act as a large drain in allowing water to seep from the slope. Water from this area must be collected in one or more sump areas and pumped from the pit.

In some instances it may be practicable to construct an adit under the ore body and use it as a drainage gallery from which water is pumped. For large volumes of water or for deep pits, drainage galleries at more than one elevation may be required. To increase the effectiveness of the drainage gallery, drill holes can be drilled on a fan pattern outward from the adit to intercept additional water. As a further refinement to improve drainage efficiency, it may be possible to place the entire adit under a partial or complete vacuum. Drainage galleries may be particularly adaptable where open pits are located on steep mountain side slopes so that the adit may be drained by gravity.

Where very heavy seepage is expected, pumping from deep wells located around the periphery of the pit may prove practical and economical. Facilities of this type have been installed at more than 400 feet with success [Stubbins and Munro(4)]. Where the groundwater flow is large and if the influence on stability of cleft water pressures and seepage pressures is significant, the pumping system must be designed with reasonable over-capacity so that if one pumping unit becomes inoperative there is sufficient overlap of pumping capacity to prevent the development of local areas of excess water pressure which might cause instability.

The design of drainage control in open pit mines should always be preceded by a moderately detailed field permeability testing program unless extensive previous experience at the site is available.

FIGURE 8 – Typical horizontal drain installation in soil slope to reduce pore water pressure and improve stability

In addition to drainage control within the pit itself the control of surface drainage outside the pit boundaries is necessary to ensure that surface water does not flow into the pit. Besides the extra pumping capacity required, water flowing into the pit percolates into surface fractures and openings—many of which have been created by blasting—develops cleft water pressures and enhances rock breakup by freezing and thawing action. This aggravates rock falls and the occurrence of local slides between benches.

Not only is it desirable to determine the influence of groundwater on stability but it will be desirable to determine whether drainage of the pit slopes will allow an increase in the overall slope angle. For the same safety factor, reducing the cleft water pressures by 20 feet will usually allow an increase in slope angle approximating 3 to 6 degrees. An evaluation can be made of the cost of drainage versus the economical benefit to be gained by the increase of the slope angle that the drainage will allow.

In order to evaluate the effectiveness of drainage it is necessary to install piezometers at key points in and around the pit to measure cleft water pressures. Normally it will be adequate to read this instrumentation on a monthly basis, with more frequent readings during the spring runoff period, following heavy rains and during the late winter.

As the open pit deepens, the probability of high cleft water pressures developing in the base area of the pit increases and they could conceivably become sufficiently large to cause a blow up of the base of the pit. This probability increases where the bedrock structure is horizontal or if significant horizontal tectonic stress exists in the rock.

Typical Case Histories of Groundwater Evaluation

Two typical examples of groundwater evaluation are given. The first deals with an open pit mine. The techniques described are also applicable to underground problems for which the second example is typical.

Example No. 1

The present depth of the open pit is approximately 400 feet. Increasing amounts of seepage were observed with pit depth. The frequency of water filled blast holes was also increasing with depth. As a result it was desired to evaluate the amount of seepage and influence on stability of increasing cleft water pressures which would be expected as the pit depth gradually increased to 1,000 feet. Several holes which had been drilled two years previously were found to be open to depths up to 900 feet around the periphery of the pit. Water packer permeability tests with packers spaced 15 feet apart were performed at 50-foot intervals in each of the four boreholes. A typical summary of the data from one of the boreholes is shown on Figure 9. Rock permeability results ranged from 1×10^{-4} cm/sec. to 1×10^{-9} cm/sec. The average value computed for all the tests was 1×10^{-6} cm/sec. For design purposes, an average permeability of 1×10^{-5} cm/sec. was used. Flow nets for several different sections of the proposed pit at ultimate depth were drawn and the flow into the pit was estimated. It was computed that total seepage for a depth of pit of 1,000 feet would approximate 5 cu.ft/sec. Based on the evaluation of rainfall records for the area it was estimated that rainfall and snow melt could account for an additional 5 cu.ft/sec. As a result a continuous pumping capacity of 10 cu.ft/sec. at a 1,000-foot head was recommended for drainage capacity for the ultimate pit.

Piezometers were installed in the four boreholes following the permeability testing. These indicated that groundwater pressures would exist in the slope as the pit was deepened. The major concern for stability is during the winter months. For long-term control it is proposed that the lowest bench be blasted and left unexcavated during the winter months to provide a major frost free toe drain to minimize the buildup of cleft water pressures. It is also proposed that a series of piezometers at 400- to 600-foot intervals bc installed along the toe of the pit slope. These piezometers are installed in holes drilled with the staudard rotary equipment.

Example No. 2

At a potential underground mine in eastern Canada there was concern that excess underground water may be encountered. A study was performed to estimate the rate of groundwater flow into the mine stopes. This required an estimate to be made of the permeability of the bedrock formations and the cleft water pressures in the area. The most practical type of

PRESSURE TESTS IN ROCK

Sheet 3 of ____

Date: Oct. 12/67 | Weather: Wet snow | Engineer: Tilk | Borehole No. J-148

Borehole diameter: BX core | Gauge height: 2.0 | Stable W.L. in borehole: 119.5 | Depth of test: 515' to 530'

Project: 67065 | Location: East side | Datum: Geodetic | Elevation: 1849.3

REMARKS:- Water intake to hole during test 3.5' above ground level.

DESCRIPTION OF CORE:- Quartz Rock and Marble

Applied Pressure	Pressure increasing: t (min.)	Meter (gal.)	Δ Take (gal.)	Σ Take (gal.)	Pressure decreasing: t (min.)	Meter (gal.)	Δ Take (gal.)	Σ Take (gal.)
11:00	Filled System Before Test							
30 P.S.I. Very steady press.	0	983.5	-	-				
	1	984.0	0.5	0.5				
	2	984.4	0.4	0.9				
	3	984.6	0.2	1.1				
	4	984.8	0.2	1.3				
	5	985.0	0.2	1.5				
60 P.S.I. Very steady press.	0	985.0	-	-	0	996.6	-	-
	1	985.5	0.5	0.5	1	996.7	0.1	0.1
	2	985.9	0.4	0.8	2	996.9	0.2	0.3
	3	986.2	0.3	1.2	3	997.1	0.2	0.5
	4	986.5	0.3	1.5				
	5	986.8	0.3	1.8	Had to discontinue test as mine had to be cleaned for blasting			
90 P.S.I. steady press.	0	986.8	-	-				
	1	987.4	0.6	0.6				
	2	987.8	0.4	1.0				
	3	988.3	0.5	1.5				
	4	988.8	0.5	2.0				
	5	989.2	0.4	2.4				
120 P.S.I. steady press.	0	989.2	-	-				
	1	990.0	0.8	0.8				
	2	991.0	1.0	1.8				
	3	991.5	0.5	2.3				
	4	992.2	0.7	3.0				
	5	992.9	0.7	3.7				
150 P.S.I. Varies ±5 psi	0	992.8	-	-				
	1	993.7	0.8	0.8				
	2	994.5	0.8	1.6				
	3	995.2	0.7	2.3				
	4	995.9	0.7	3.0				
	5	996.6	0.7	3.7				

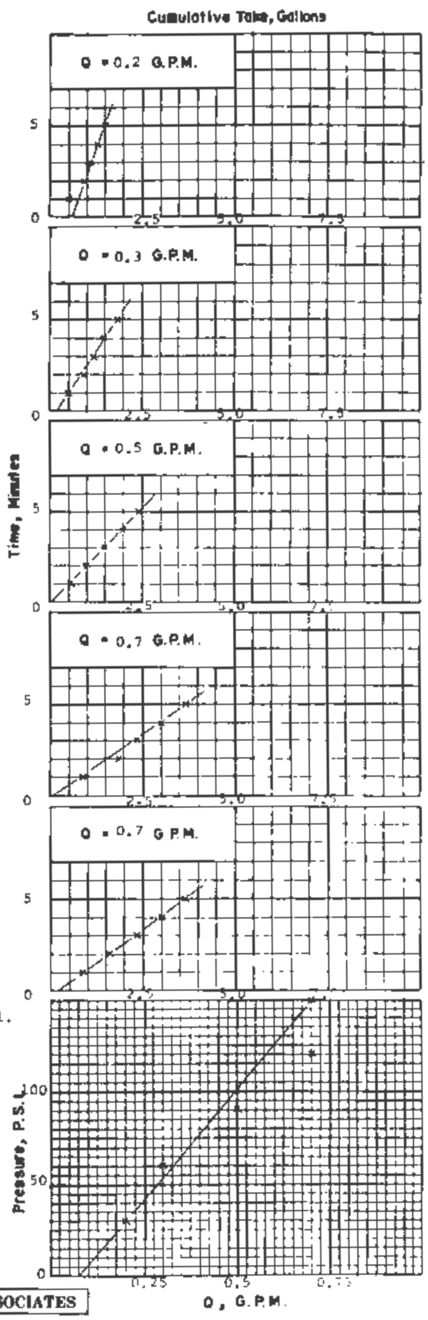

COMPUTATIONS:- No leakage anywhere above ground level.

$k = \frac{Q}{2\pi L H} \ln \frac{L}{r}$ or $k = C_p \frac{Q}{H}$

where
- k = permeability
- Q = constant rate of flow into the wall of hole
- L = length of hole pressurized
- H = differential head of water
- r = hole radius

for a 15 ft. packer in a Bx hole $C_p = 3{,}700 \ \frac{\text{min.}}{\text{ft.yr.}}$

therefore $k = \frac{3{,}700 \times 0.4}{100 \times 2.3} = 6.4$ ft/yr. or

6.6×10^{-6} cm/sec.

GOLDER, BRAWNER & ASSOCIATES

FIGURE 9 — Record sheet for water packer permeability test. Test performed at a depth of 515 to 530 feet. Average permeability at this depth was computed to be 6.6 X 10^{-6} cm/sec

test was found to be water packer permeability tests in diamond drill holes.

An expanding packer was used and sealed off, and water was pumped into the section under pressure. The rate of inflow of water into the hole was measured and the average value of permeability of the rock was computed. Water packer tests were performed at numerous depths in six boreholes and average permeability values were determined for these zones. The computed coefficient of permeability varied from 3×10^{-4} cm/sec. to 4×10^{-6} cm/sec.

As a comparison, permeability tests were performed on samples of rock core in the laboratory. The rock core was, in general, 100 times less pervious than the field formations. This indicated that most of the groundwater flow would occur through fractures, fissures and joints in the rock. Using a flow net analysis and the permeability values obtained from the field testing program it was estimated that seepage into the stopes would range from about 0.2 to 3.4 gallons per minute per foot width of stope.

The volume of water encountered during mining was within 25% of that predicted.

References

1. Colback, P.F.B. and Wiid, B.L., 1965. The influence of moisture content on the compressive strengths of rocks, *Proc. Rock Mech. Symp.*, Dept. of Mines and Tech. Surv., Ottawa.
2. Coates, D.F. and Brown, A., 1961. Stability of slopes at mines, *Can. Mining & Met. Bull.* Can. Inst. of Mining & Met., Montreal.
3. Dobry, R. and Alvarez, L., 1967. Seismic failures of Chilean tailings dams, Proc. Am. Soc. Civil Engrs., *Soil Mech. J.*, Paper No. 5582.
4. Stubbins, J.B. and Munro P., 1965. Open pit mine dewatering – Knob Lake, *Can. Mining & Met. Bull.* Can. Inst. Mining & Met., Montreal.
5. Terzaghi, K. and Peck, R.B., 1967. *Soil Mechanics in Engineering Practice*, 2nd ed., John Wiley and Sons.
6. Hoek, E. and Pentz, D.L., 1968. *The Stability of Open Pit Mines,* Imperial College Rock Mech. Res. Rept. No. 5.
7. Cedergren, H.R., 1967. *Seepage, Drainage and Flow Nets,* John Wiley and Sons.
8. Golder, H.Q. and Gass, A., 1962. *Field Tests for Determining Permeability of Soil Strata,* ASTM Conference, New York, June.
9. Karplus, W.J., 1968. *Analog Simulation. Solution of Field Problems,* McGraw Hill Co.
10. Harr, M.E., 1962. *Groundwater and Seepage*, McGraw Hill Co.
11. Brawner, C.O., 1966. Slope stability in open pit mines, *Western Miner*, Oct.
12. Brawner, C.O. and Huculak, N., 1961. "The Use of Horizontal Drains in Landslide Stabilization", 42nd Conf., Can. Good Roads Assoc.
13. Eckel, Edwin B., 1968. *Landslides and Engineering Practice*, Highway Res. Board, Special Rept. 29.

C.O. Brawner

Education – B Sc, civil engineering, University of Manitoba, 1963; M Sc, soil, foundations and geology, Nova Scotia Technical College, 1958.

Employment Summary – 1953-56, soils engineer for British Columbia Dept. of Highways; 1956-63, senior materials and testing engineer for British Columbia Dept. of Highways; 1963 to the present, vice-president of Golder, Brawner & Associates Ltd.

In Situ Dynamic Strain Measurements in Rock

R.F. Favreau,
Collège militaire royal de Saint Jean,
Saint Jean, Québec.

S. Chung,
Explosives Research Lab. of
Canadian Industries Ltd.,
Beloeil, Québec.

Abstract

In situ dynamic strain measurements in rock by means of strain gauges remain one of the more absolute techniques for evaluating the blasting action of different explosives on a given rock, especially since they do not require the use of any theoretical formulae for converting from stress to strain. Although such measurements have been carried out previously, especially by the United States Bureau of Mines, it is possible to suspect the reliability of strains measured with gauges embedded in the usual manner, described in the literature, when such gauges are at distances of less than about 5 ft from the borehole. A modified technique of embedding gauges is described in the present paper; some field data of results obtained with the new technique at distances of only a few inches from the borehole will be presented. The relative merits and drawbacks of the new method will be discussed.

Introduction

Means of predicting the blasting performance of different explosives in a given rock can be of assistance in designing economical blasting patterns in the mining and quarrying industries. Even though theoretical methods of making such predictions are becoming available (1), it is of great interest to have experimental techniques available to verify the validity of the assumptions made in theoretical calculations. Moreover, it is desirable that such techniques be not only inexpensive but also suitable for on-site measurements near actual blasts.

Experimental methods reported in the literature usually fall into one of two categories: (i) fast camera techniques where photographs record the particle velocity induced at a free face of a rock body or specimen, when the rock body is subjected to explosive loading, or (ii) transducer techniques where some calibrated transducer (e.g. velocity meter, acceleration meter, strain gauge) is attached to the rock face, or embedded in a cavity in the rock, to record the movement of the latter under explosive loading.

In such tests, because transducers are often irrecoverable, strain gauges, which are significantly less expensive than other types of calibrated transducers, appear especially attractive for large-scale in situ measurements.

Previous Work

Many references (2) (3) can be found in the literature of dynamic in situ strain measurements in rock subjected to explosive loading, particular mention going to the U.S. Bureau of Mines who carried out extensive tests with strain gauges. In this work, the strain gauges were grouted in separate circular boreholes drilled parallel to the shot-hole and some distance from it. The location of the strain gauge (Figure 1) was usually along a diameter of the gauge-hole, oriented so as to be on a radius from the centre of the shot-hole.

This technique, however, suffers from several disadvantages. For one, the fact that the gauge is in a circular hole implies that the stress wave must first strain the cylindrical grouting material, and then the grouting material must itself strain the gauge. This leads to loss of response, as can be realized by imagining the difficulty in deforming a long, thin cylinder, not along its length but along one of its diameters – especially considering the fact that this deformation depends on the degree of bonding between the cylinder wall and the

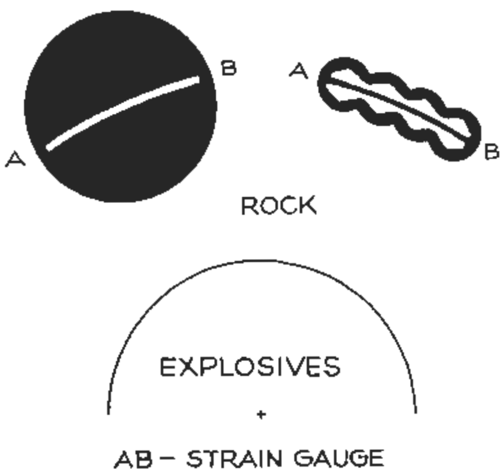

FIGURE 1

surrounding medium. Moreover, for short shot-hole to gauge-hole distances, the stress wavefront is narrower than the length of the gauge, so that the latter is not acted upon simultaneously along its entire length; thus the measurement obtained is some complicated spatial/time average of the true strain.

For these reasons, previous workers have usually placed their gauges well away from the shot-hole, at distances normally 5 ft and greater. Being so far away, it was necessary to place a series of gauges at various distances from the shot-hole, so as to be able to extrapolate back to it. This not only imposed a large number of measurements, but also introduced uncertainty in the extrapolated results, since it was necessary to assume that linear extrapolation* was valid; more recent work (1) suggests that linear extrapolation is improper in the region near the shot-hole.

Present Technique

The present technique attempts to overcome these drawbacks by using a differently shaped enclosure to embed the gauge. By means of a coromant cut, that is, a series of adjacent parallel holes of half-inch diameter, the circular gauge-hole is replaced by a slit (Figure 1). Moreover, the slit, and the strain gauge grouted in it, are oriented along the circumference of a circle centred at the shot-hole. This affords several advantages. For one, the gauge now measures "circumferential" or "tangent" strain, a quantity which can theoretically be shown (1) to display a gradual rise in magnitude with time, while the "radial" strain previously measured displays a very abrupt rise in value on arrival of the stress wavefront; thus the strain gauge is less likely to be broken by the first impact.

Moreover, in view of the close proximity between gauge and solid rock, and due to the additional grip afforded by the teeth along the wall of the slit, loss of response is less likely to occur due to slipping along a plane parallel to the gauge. A further possible advantage, in the opinion of the authors, is that a knowledge of "tangent" strain is more applicable than "radial" strain in predicting the actual blasting performance of an explosive, since most of the useful disruption of rock in a blast results from tension failure, not compression failure. Thus, it has been possible with the new technique to reduce the shot-hole to gauge-hole distance to some few inches, thereby almost completely removing the need for extrapolation.

It might be mentioned that the present in situ method evolved from earlier miniature tests, carried out with a small charge in a borehole in a small cylinder of synthetic rock into the wall of which strain gauges had been cast directly. The superior bonding achieved there allowed tests to be done within about one inch of the explosive; however, this procedure is rather limited to miniature experiments where normal commercial explosives cannot usually be used due to their restricted critical diameter.

Typical Experimental Results

The technique has now been applied to actual large-scale blasts. Some typical results are as follows.

TABLE I
Strain Gauge Comparison of Different Explosives in Limestone

Explosive	ANFO	Commercial Slurry No. 1	Commercial Slurry No. 2
Shot hole radius (cm)	5.1	5.1	5.1
Rock thickness (cm)	10.1	9.9	10.8
Induced particle velocity (m/sec)	67	314	91

In this table, the induced particle velocity u is used as the chief criterion for comparison,

*Linear extrapolation on plots of log strain vs. log distance is meant here.

since it represents a direct measure of the action of the explosive; it is, moreover, a result unadulterated by theoretical conversions. It is obtained from the rather straight initial slope of the strain-vs.-time curve recorded on an oscilloscope. Usually, the strain gauge breaks after some few tens of microseconds; however, this does not prevent the slope from being evaluated independently of the time elapsed before the gauge breaks. It is evident from the table that the technique can indeed discriminate between different explosives, and this on the basis of a measurement that is directly related to actual blasting in rock (as against methods that measure the action of explosives on some medium like water).

Conclusions

A modified method has been described for embedding strain gauges to measure in situ dynamic strains induced in rock by explosive loading; it appears to present advantages over previous methods: (i) it affords better gauge response; (ii) with it, measurements closer to the shot-hole are possible, thus removing the need for ambiguous extrapolation and lessening the number of results required; (iii) it is relatively inexpensive; and (iv) it appears to discriminate adequately between different explosives. It presents certain disadvantages: (i) gauge holes cannot be made more than about one foot deep, so a collar problem arises; and (ii) the method does not usually obtain the peak strain since the gauge normally breaks before maximum strain is attained.

Acknowledgment

The cooperation of DOMTAR, who permitted the tests reported on in the table to be conducted at their limestone quarry, is gratefully acknowledged.

References

1. Favreau, R.F. The generation of strain waves in rock by an explosion in a spherical cavity. *J. Geophys. Res.* (in press).
2. Atchison, T.C. and Tournay, W.E. *Comparative Studies of Explosives in Granite,* U.S. Bureau of Mines Report 5509.
3. Larocque, G.E.; Sassa, K.; Darling, J.A. and Coates, D.F., 1967. Field blasting studies, *Proc. 4th Can. Rock. Mech. Symp.*, Mines Branch, Dept. Energy, Mines and Resources, Ottawa.

R.F. Favreau

Education — Ph D, McGill University.

Employment Summary — 1960-63, research physicist at Explosives Research Laboratory; 1963 to the present, professor of physics, Collège militaire royal de Saint Jean.

S. Chung

Education — B Sc, physics, National Taiwan University, 1965; M Sc, applied physics, University of Waterloo, 1967.

Employment Summary — 1967 to the present, physicist at Explosives Research Laboratory, Canadian Industries Limited.

Behavior of the Underground Powerhouse Arch at the W.A.C. Bennett Dam During Excavation

A.S. Imrie
Engineering Geologist, International Power and Engineering Consultants Limited, Vancouver, B.C.

L.T. Jory
Consulting Geologist, Dolmage, Campbell and Associates, Vancouver, B.C.

Abstract

W.A.C. Bennett Dam is the first stage of hydro-electric development of the Peace River in northeastern British Columbia (Figure 1). The damsite is located near the head of a deep bedrock canyon at the eastern edge of the Rocky Mountain Foothills. The reservoir extends 75 miles west to the Rocky Mountain Trench and then 150 miles along the Trench in a northwest-southeast direction.

The present development includes a 600-ft-high dam; 3 diversion tunnels through the right abutment, of which 2 are now serving as low level outlets; a gated chute spillway on top of the right abutment; and an underground powerhouse within the left abutment (Figure 2). Construction of the project began in 1962; first power was generated in September of 1968.

The powerhouse roof was designed to be a parabolic arch in cross-section and to be supported by a pattern of grouted rock bolts spaced 5 ft apart. Rock mechanics studies conducted prior to the excavation of the arch suggested the presence of high residual stresses in the bedrock. During the excavation, downward movements of the overlying bedrock were recorded by a number of different methods. The measurement and suggested nature of this deformation are discussed in this paper.

The owner of the project is the British Columbia Hydro and Power Authority. Design and supervision of construction was carried out by International Power and Engineering Consultants Limited of Vancouver.

Technical Description of Site

The dam is zoned, gravel-fill embankment 600 ft high and 6,700 ft long, built of glacial outwash material conveyed from a borrow area 3 miles away. Figure 3 shows a cross-section of the dam illustrating the different zones of gravel fill. The total volume of the dam is 57,200,000 cu yds of compacted material. The spillway at the top of the right abutment has a discharge capacity of 375,000 cfs.

The powerplant is located within the left abutment beneath the downstream toe of the dam. Water enters the intakes upstream of the left wing of the dam before flowing down 18-ft-diameter penstocks to the turbines in the lower part of the powerhouse chamber. The chamber is 890 ft long, 153 ft high and 67 ft wide. At full development, ten 310,000-horsepower Francis turbines will each drive a 227-megawatt generator.

Power generated at 13,800 volts is transferred up lead shafts to the surface switchyard downstream of the dam where it is transformed to 500,000 volts. From here the power is transmitted to southern British Columbia by two 550-mile-long transmission lines.

Water, after passing through the turbines, discharges into two separate manifolds via 150-ft-long draft tubes. Each manifold is 330 ft long, 105 ft high and 45 ft wide and is connected to a 66-ft-high horseshoe-shaped tailrace tunnel which conveys the water to an excavated channel downstream from the dam.

Geology

Regional Geology

The damsite is situated on the eastern border of the Rocky Mountain Foothills which are composed of deformed Mesozoic sedimentary rocks. The interior plains to the east are underlain by flat-lying Upper Cretaceous sedimentary rocks. To the west are the main ranges of the Rocky Mountains which are separated from the Western Cordillera by the Rocky Mountain Trench. The Rockies consist of strongly deformed Paleozoic sedimentary

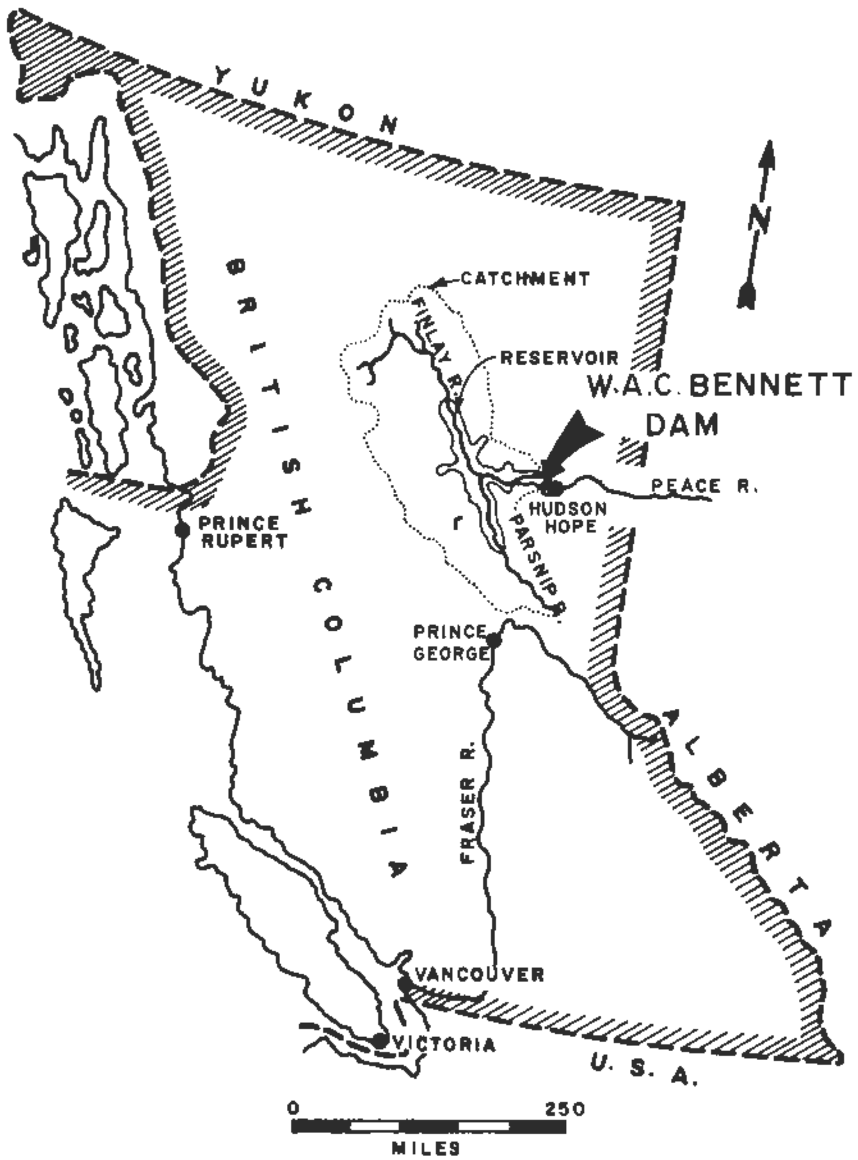

FIGURE 1 — Locality plan

rocks, mainly limestone and quartzite. Westerly-dipping thrust faults are common in both the Rockies and Foothills.

The pre-glacial Peace River flowed between Bullhead and Portage mountains through what is now known as Portage Pass (Figure 4). During the Pleistocene epoch this portion of northeastern British Columbia was located between two ice fronts: the Laurentide and Cordilleran ice sheets advancing from the north-east and west, respectively. Toward the end of the Pleistocene, a Cordilleran glacier occupying the Peace River valley reached at least as far east as Portage Pass as evidenced by a well-defined terminal moraine which remained there.

This and other glacial debris remaining in Portage Pass after the ice receded, forced melt and glacial lake water to flow south around Portage Mountain and form the Peace River Canyon, a deep, narrow structure some 17 miles long.

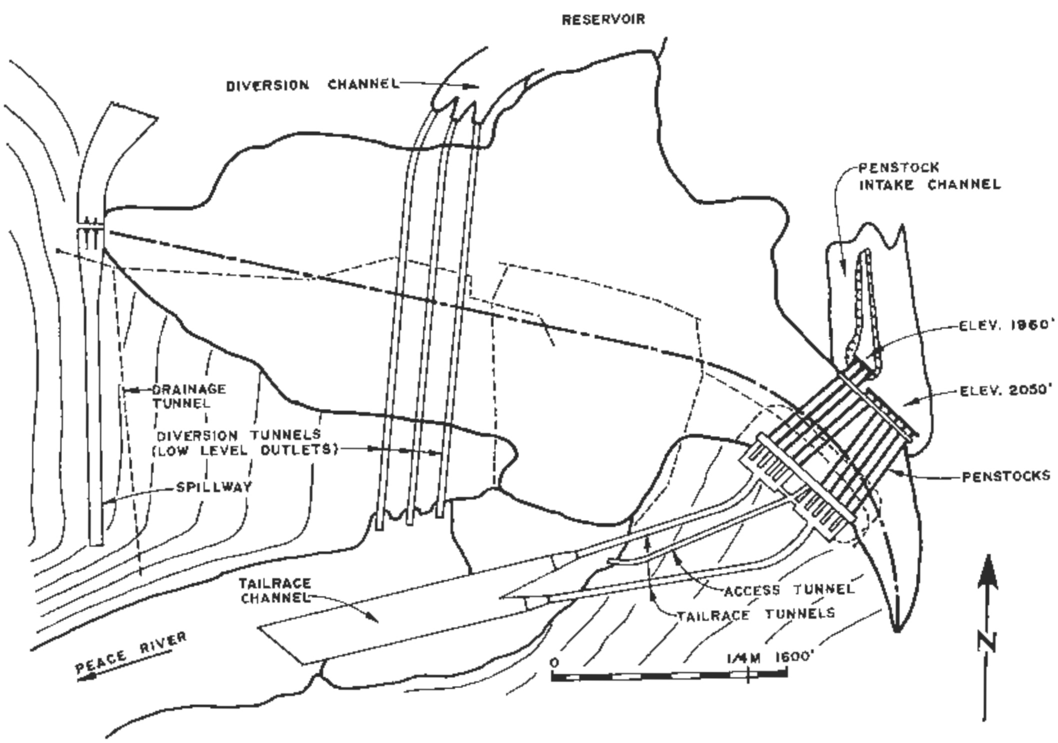

FIGURE 2 – Plan, W.A.C. Bennett Dam

Damsite Geology

The geology of W.A.C. Bennett Dam has been described in detail by Dolmage and Campbell (2). Lower Cretaceous strata belonging to the Dunlevy and Gething formations underlie the damsite. Lithologically these formations are similar and consist of interbedded sandstones, siltstones, shales and coals of continental deposition.

The Dunlevy Formation contains massive sandstone beds 20 to 100 ft thick separated by much thinner shale and coal sequences. The sandstone is well indurated and contains a chert cement. The shale members are generally 5 to 40 ft thick and are composed of compact, brownish-black, relatively soft silty shale. The shales do not compress significantly when subjected to high loading, nor do they swell significantly when saturated with water. However, freshly exposed shales on the surface tend to crumble under changing conditions of temperature and humidity. In the controlled atmosphere of underground exposures, deterioration of the shales seems to be due almost entirely to mechanical relaxation of joint planes.

The Gething Formation crops out only on the upper portions of the right and left abutments. Thick shale and coal sequences predominate in the Gething rocks.

Structurally, Dunlevy and Gething strata comprise part of the western limb of a large anticlinorium which strikes N 10° W and plunges southerly. At the site the formations strike northwest and dip 5 to 10 degrees to the southwest. No major faulting is present. Bedding plane slip associated with folding led to the development of gouge seams in various coal and shale horizons. Well-developed cleating exists in the coal whereas poor to well-developed jointing is present in the siltstone and shale. Pronounced jointing is generally absent from the massive sandstones.

Rock Mechanics Studies

During construction of a large underground structure, the possibility of having high residual stresses in the bedrock must be considered

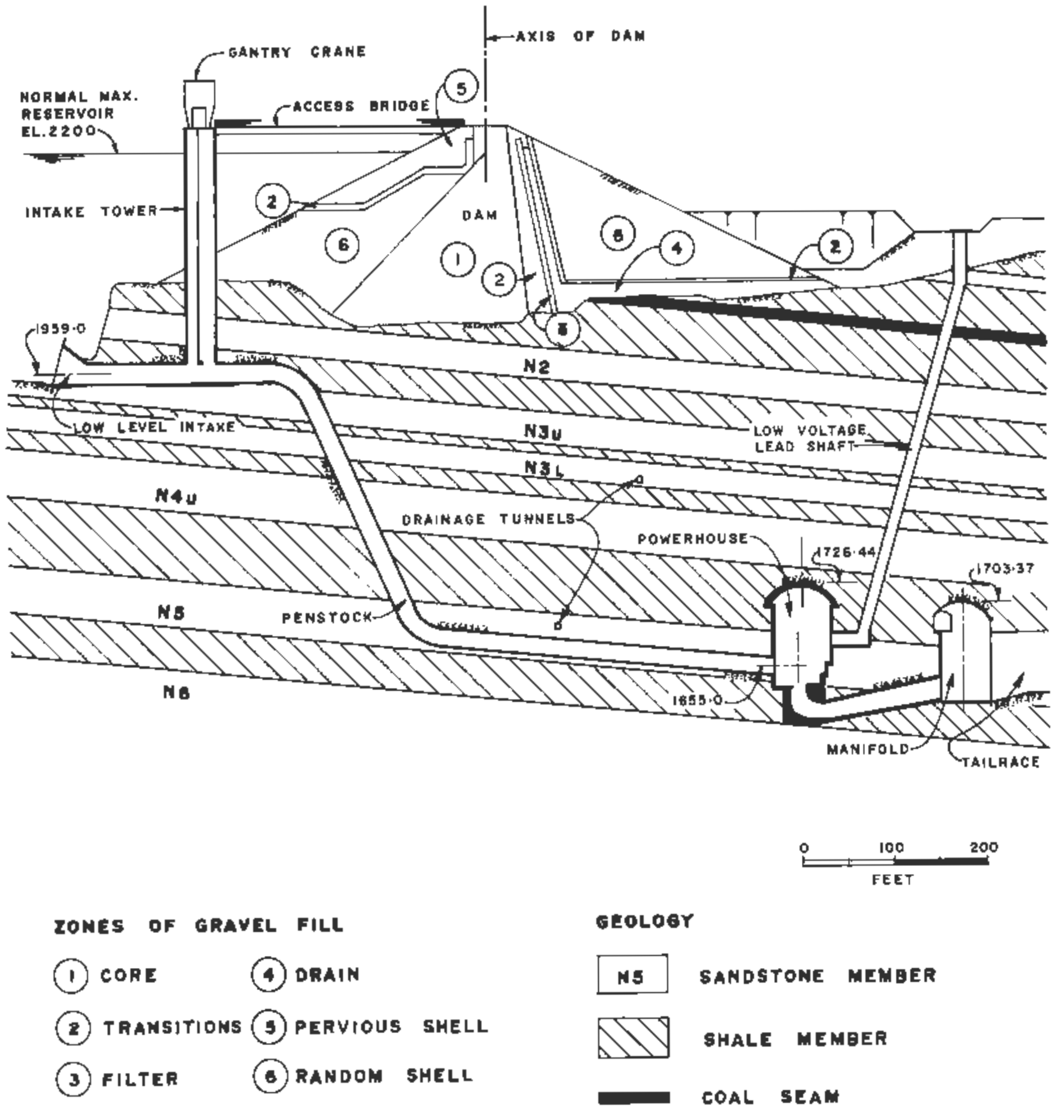

FIGURE 3 — Typical section, left abutment

when calculating the increased stress created by the opening.

At W.A.C. Bennett Dam two methods of measuring in situ stresses were used. The first was an over-coring drill hole method conducted in the powerhouse exploratory tunnel (Figure 5). The second method measured time-dependent strains of oriented samples by photoelastic means. Both methods indicated that the bedrock at the damsite is subjected to horizontal compressive stresses higher than would be expected due to the weight of overlying rock. Assuming a Poisson's ration of 0.25 the overburden depth of 450 ft in the powerhouse area would produce a vertical stress of about 500 psi and horizontal stress of 175 psi.

As measured, the maximum horizontal stress in the central and southeastern portions of the powerhouse area has a magnitude of 1,920 psi acting in a direction N 76° E (Figure 6). The minimum horizontal stress is 1,070 psi acting S 14° E. The vertical stress in this region is 1,050 psi. In the northwest area of the

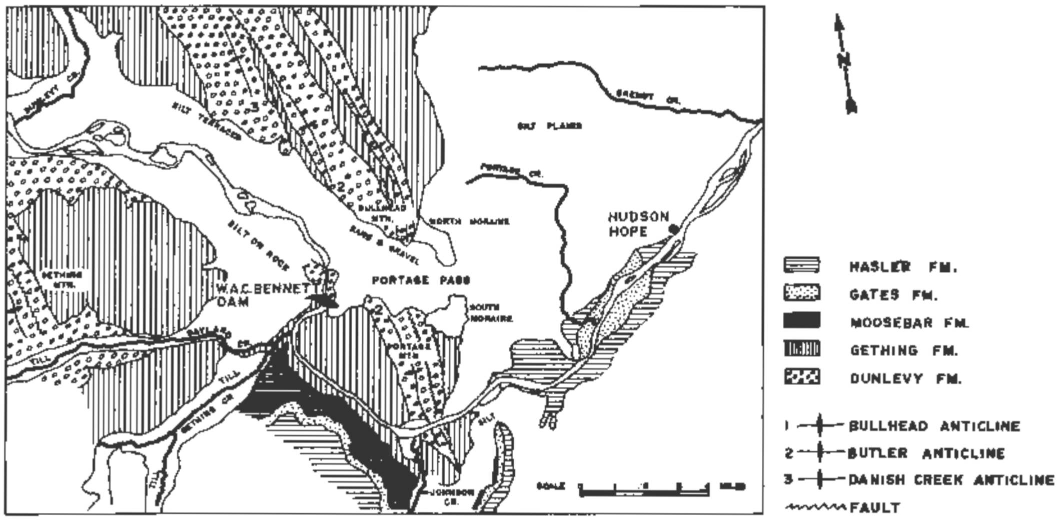

FIGURE 4 – Geology of the Peace River Canyon

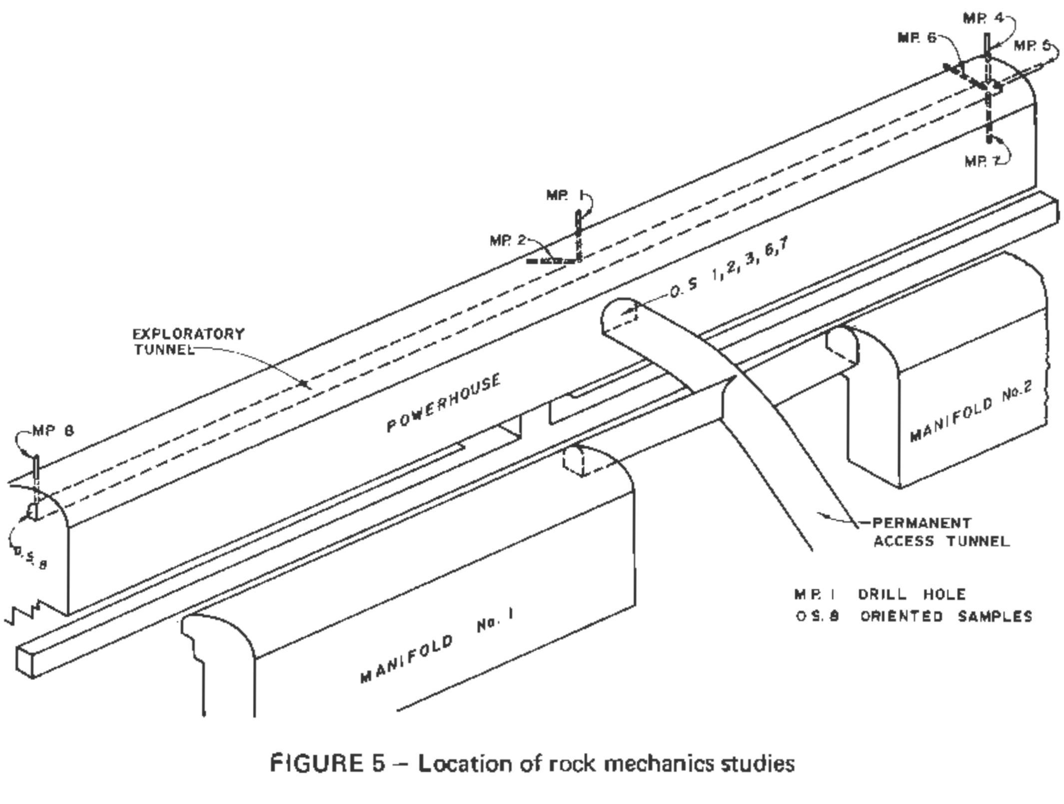

FIGURE 5 – Location of rock mechanics studies

powerhouse the maximum horizontal stress is 1,300 psi (N 20° E) and the minimum horizontal stress is 900 psi (S 70° E). The vertical stress was not measured at this point.

In the central and eastern area of the powerhouse the direction of the maximum horizontal stress (N 76° E) compares favourably with that expected from the regional structure. The trend of the Portage Mountain – Butler Ridge anticlinorium at the damsite is N 10° W. A regional stress normal to this would have a bearing of N 80° E. The stress magnitudes in the west end of the powerhouse are lower and the orientations have changed as would be expected due to the proximity of the canyon wall. The maximum horizontal stress trends N 20° E while the canyon wall trends N 16° E.

Moduli and compressive strength measurements were obtained from a number of rock cores in the powerhouse area (Table 1). These results clearly show the anisotropic nature of the bedrock at the damsite. The higher modulus obtained for shale compared to sandstone indicates the difficulties in extrapolating laboratory values to the field. The results are the opposite of what would be expected from in situ tests which would have taken into account the structural discontinuities that are more prevalent in the shale than in the sandstone.

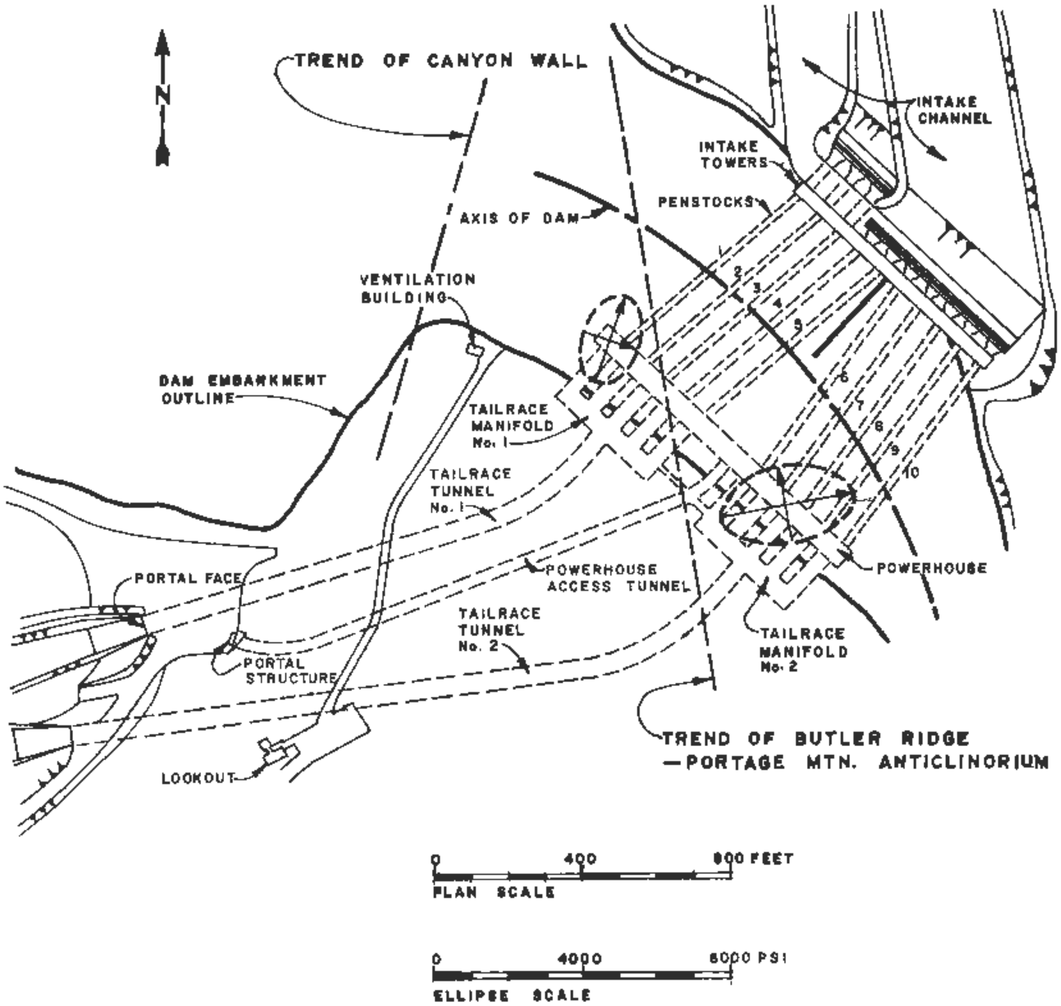

FIGURE 6 — Orientation of stress ellipses horizontal plane

Design of Powerhouse Arch Support

The long axis of the powerhouse chamber was oriented along the strike of bedding which subparalleled the dam axis on the left abutment (Figure 6). A parabolic arch was chosen for the roof of the powerhouse as this cross-section theoretically provides satisfactory stress distribution around the opening. The top of the

TABLE 1

Summary of Powerhouse Compression Tests

Type of Rock	Elastic Modulus (10^6 psi)			Ultimate Compressive Strength (psi)		
	Along Strike	Along Dip	Normal to Bedding	Along Strike	Along Dip	Normal to Bedding
N4 Sandstone	2.6	2.4	2.3	19,800	19,300	17,700
N5 Shale	5.6	4.4	5.3	13,700	11,800	16,300
N5 Sandstone	2.5	2.2	2.6	16,400	18,800	20,300

arch was positioned in a shale horizon 17 ft below the massive N4U sandstone member (Figure 3). Pattern rock bolts in conjunction with a relatively thin concrete arch were selected for permanent support.

Experience gained from the excavation of three 50-ft-diameter diversion tunnels assisted the consulting geological engineers in laying out the rock bolt pattern for the arch. In the diversion tunnels 3/4-in.-diameter, 10-ft-long high-tensile steel rock bolts spaced 5 ft apart had been stipulated for only those areas where shale formed the arch of the tunnels. During actual excavation it became apparent that rock bolts 6 to 8 ft long would be sufficient except where anchorage in sandstone was desirable. No rock failures occurred in the diversion tunnels.

High-tensile steel bolts with minimum lengths of 8 to 10 ft and installed 5 ft apart were considered necessary for the powerhouse. Geological cross-sections of the arch rock suggested that the best anchorage would be provided approximately 14 ft above the "A" line and the minimum length of bolt was therefore

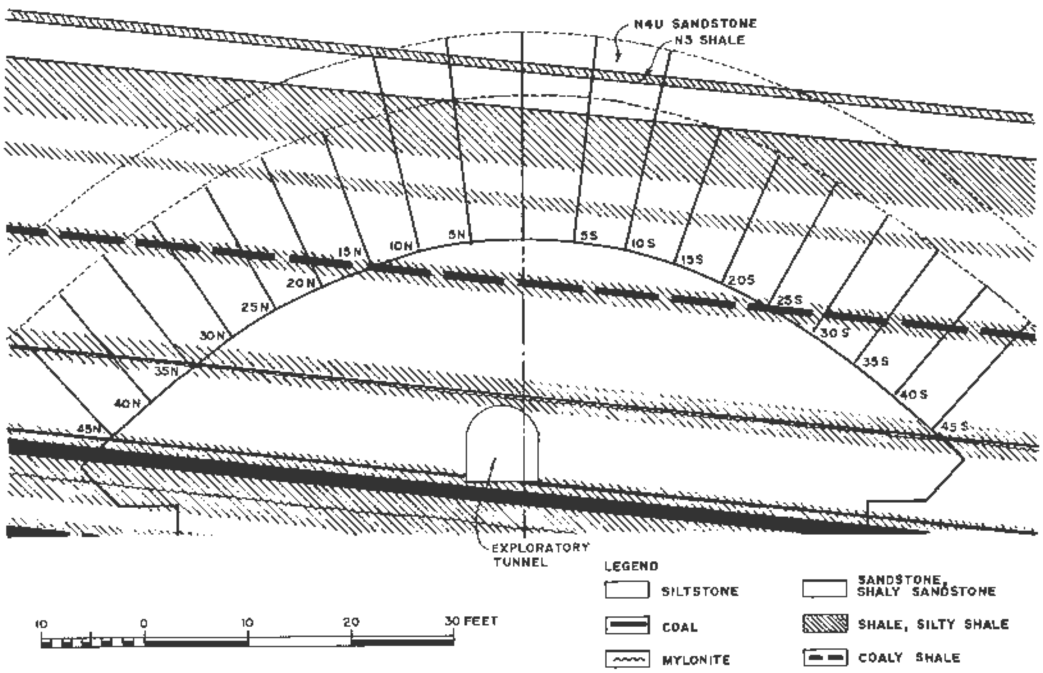

FIGURE 7 — Geology of powerhouse arch

increased to 14 ft (Figure 7). This pattern of fanned 14-ft-long bolts, at 5-ft spacing, in addition to arching from the abutments, was judged to be adequate for the basic support of the powerhouse roof. The N5 shale – N4U sandstone contact, approximately 17 ft above the top of the arch, was known to be a potential parting plane and the length of the central five bolts was increased to 20 ft so as to anchor in sandstone and increase the friction across this plane. A preliminary testing program was conducted prior to excavation in order to determine a torque-tension relation and the best anchorage for the rock bolts. Bail-type expansion shells were selected for the anchorage.

The contract specification called for the pattern rock bolts to be installed within 5 ft of the working face within 8 hours after blasting. These bolts were to be tensioned to two thirds of the yield strength of the rock bolt (23,000 lb) at the time of installation. If the rock was found to be incapable of developing the specified anchorage, allowance was made for a reduction in spacing of the rock bolts and a corresponding reduction in the anchorage requirements to suit the capability of the rock. The torques of bolts within 30 ft of a working face were to be checked after each blast and the bolts re-tightened if necessary. Wire mesh and steel strapping were specified for use as conditions required. Finally, all pattern bolts were grouted for permanent support, although no grouting was to be permitted within 100 ft horizontally of an excavation face. After stress relieving, described below, a reinforced concrete arch was emplaced.

Deformation of Powerhouse Arch

In the initial stages of excavation in the area where the arch was breached by a construction access ramp, routine torque checking of previously installed bolts showed that the torque on a number of bolts was increasing, suggesting a downward movement of the arch rock. Quantitative measurements of the downward movement were obtained from rock relaxation gauges. These measurement data, which were used as a guide for supplementary rock bolting, are presented following a brief description of the excavation sequence.

Excavation Sequence

The contractor began the excavation of the powerhouse arch by ramping up from the previously excavated permanent access tunnel (Figure 5). This ramp entered near the top of the arch in approximately the centre of the powerhouse and provided two working faces so that excavation could proceed simultaneously to both ends of the chamber.

Initially, central headings, 26 ft wide and 25 ft high, were driven towards the extremities of the powerhouse. This first stage of excavation was followed by excavation of two side faces, 20 ft wide, and two haunch faces, 10 ft wide (Figure 8). The mining sequence in the northwest end of the powerhouse proceeded uniformly with the side and haunch faces generally in close proximity to the central heading. In the southeast end of the chamber, excavation did not advance in the same manner, for the central heading was driven well ahead of the side and haunch faces, especially those on the southern side of the powerhouse. Figure 9 shows the progress of the arch excavation.

As previously stated, installation of pattern rock bolts was specified to follow blasting of each face. Supplementary bolts required in certain areas were either installed at the time of excavation or later, depending on information available from instrument readings.

After excavation of the arch and grouting of the rock bolts the contractor pre-sheared the powerhouse walls to an elevation of 1,667 ft. This pre-shearing was accomplished by drilling 3-in.-diameter vertical holes, 34 ft long at 1-ft intervals for the entire length of the chamber. Alternate holes were then blasted. Removal of a 22-ft-wide slot in the centre of the powerhouse from elevation 1,701 ft to elevation 1,667 ft for the full length of the chamber was the fifth stage of the excavation. In stage 6 the side benches on either side of this slot were blasted so that the muck expanded to elevation 1,701 ft. The pre-shearing and partial bench excavation were to allow wall rock relaxation and inward wall movement to occur before concrete emplacement. Following concreting of the arch and subsequent removal of the broken rock, the downward excavation of the main body of the powerhouse proceeded.

Deformation Measurements

Rock Relaxation Gauges – The main portion of each rock relaxation gauge consisted of a steel rod 4 1/2 ft long and 3/16 in. in diameter, coupled to a standard 16-ft-long, 3/4-in.-diameter rock bolt (Figure 10). This main portion of the gauge was anchored near

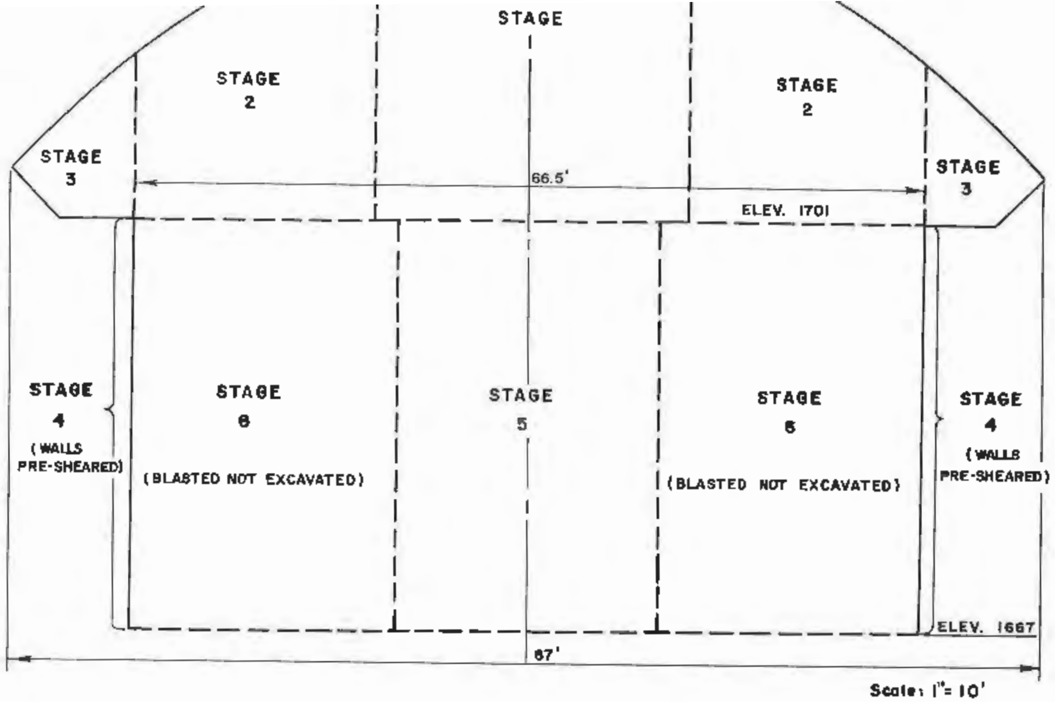

FIGURE 8 – Powerhouse excavation sequence, elev. 1,726 – 1,667

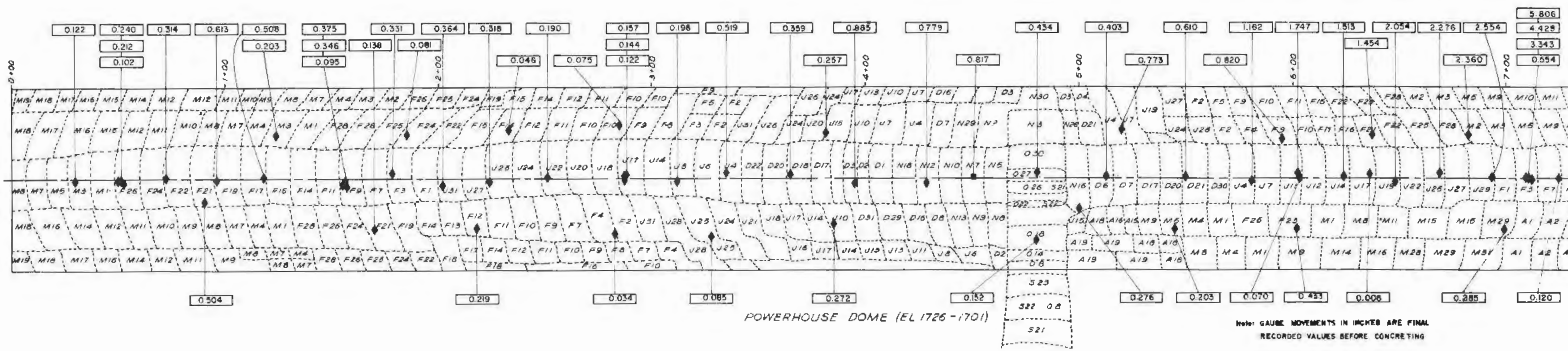

FIGURE 9 – Plan of powerhouse arch showing excavation sequence and relaxation gauges

the top of a vertical 22-ft-long drill hole using a special hollow wrench. At the collar of the hole a 2-ft-long, 1-in.-diameter hollow rock bolt was anchored in the surface rock. The lower end of the 3/16-in. steel rod rested freely within the hollow rock bolt. The distance between the lower end of the rock bolt and the end of the steel rod was measured at the time of installation and at subsequent intervals. An increase in this distance indicated a relative downward movement of the strata lying between the 2-ft rock bolt and the upper end of the gauge.

Gauges were installed along the centreline of the powerhouse arch every 20 to 30 ft (Figure 9). The standard gauge was 20.5 ft long so that it was anchored in N4U sandstone just above the contact with the underlying N5 shale. The movement measured below this upper anchor approximates the total downward movement in the shale which formed the immediate arch if the relaxation of the massive N4U sandstone is assumed to be very small. At five locations in the arch a set of three gauges of different lengths (6.5, 12.5 or 14.5, and 20.5 ft) was installed to try to determine if most of the movement was restricted to a particular horizon.

Gauges were also installed at the sides of the arch north and south of the centreline but on a wider spacing.

A total of 70 gauges were installed between December 28, 1965 and June 1, 1966. The gauges were all installed at the time of arch excavation at each location except in the vicinity of the powerhouse ramp (station 3+65 to station 5+50). The arch movement in the region northwest of the powerhouse ramp was far less than that recorded in the region to the southeast. In the latter region, gauge movements along the centreline averaged 2.5 in. reaching a maximum of 5.8 in. near station 7+10; to the northwest, the movements averaged 0.40 in. reaching a maximum of about 1 in. in the vicinity of station 3+50 to station 4+50. the movement recorded by each side gauge was less than for the adjacent centreline gauge but the pattern of movement was similar.

Displacement - time graphs plotted for the gauge sets at stations 7+10 and 8+05 reveal some significant factors about the nature of the arch movements (Figures 11 to 16). The arch

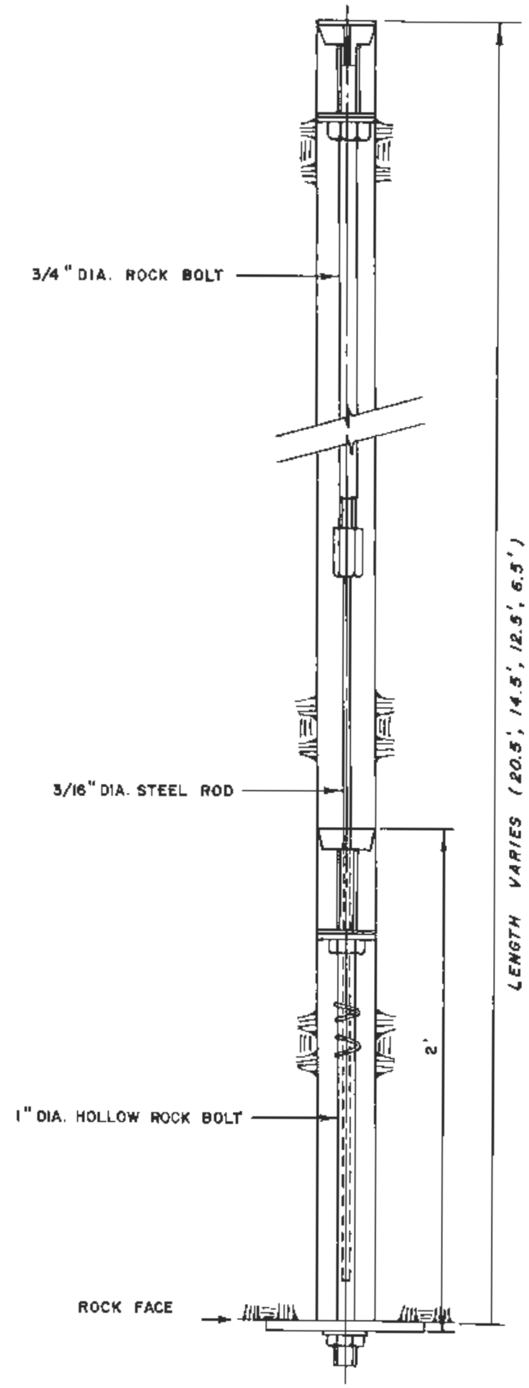

FIGURE 10 — Installed rock relaxation gauge

during a blasting delay, March 18 to March 25, and ceased altogether with the completion of arch excavation in the second week of May. This was true of all gauges in the southeast half of the chamber. To the northwest the arch movements diminished considerably after the full arch opposite a gauge had been opened for about two weeks (Figure 17). During this time the excavation face had advanced 60 to 70 ft. Minor movement occurred, however, until early May.

Although arch blasting definitely affected the movements recorded by the gauges, the pre-shearing and the excavation of the underlying bench, carried out at the times indicated on the graphs, had no marked tendency to accelerate or retard these movements. The supplementary rock support installed in certain areas slightly retarded the rate of movement.

With regard to the shape of the displacement - time graphs, gauge readings were generally made on a daily basis rather than immediately before and after blasting of a certain portion of the arch. The slopes of the graphs (Figure 18a) are therefore not a true indication of the movement pattern which probably resembled a step-like pattern (Figure 18b). In the few instances where readings were obtained just prior to and then after a blast this movement pattern was confirmed.

Results from four of the five sets of three gauges show that virtually all the movement measured occurred within 14.5 ft of the arch and that this strain was distributed fairly uniformly throughout the distance. The fifth gauge set at station 7+10 showed that 1.4 in. of movement occurred between 12.5 and 20.5 ft above the arch. Slightly more than 1 in. of movement was measured in the interval between 6.5 and 12.5 ft, and 3.3 in. of movement was measured in the lower 6.5 ft of rock.

The structural rock bolts were grouted during April and May 1966. To ensure that inadvertent grouting of a gauge was not responsible for the lack of recorded movement afterwards, three additional relaxation gauges were installed after completion of the grouting. These last three gauges were read until August 1966 and recorded only minor creep of the arch.

Seismophone — A portable seismophone unit, consisting of a geophone, amplifier, earphones and tape recorder, was used during the last half of the arch excavation. This instrument, developed by an American insurance

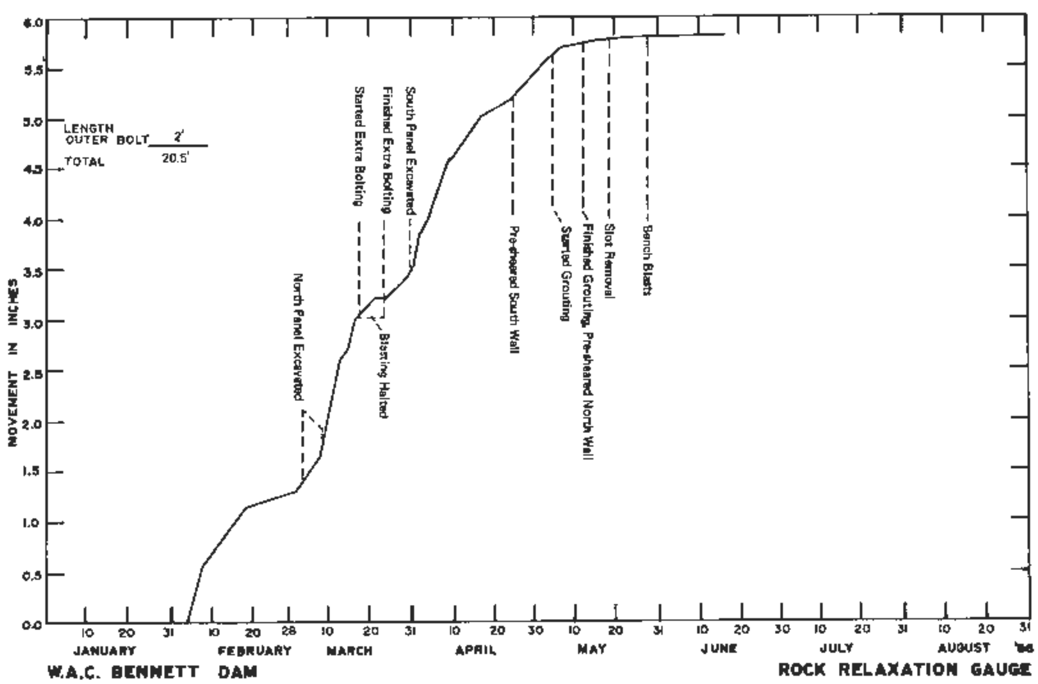

FIGURE 11 — Powerhouse roof arch at 709

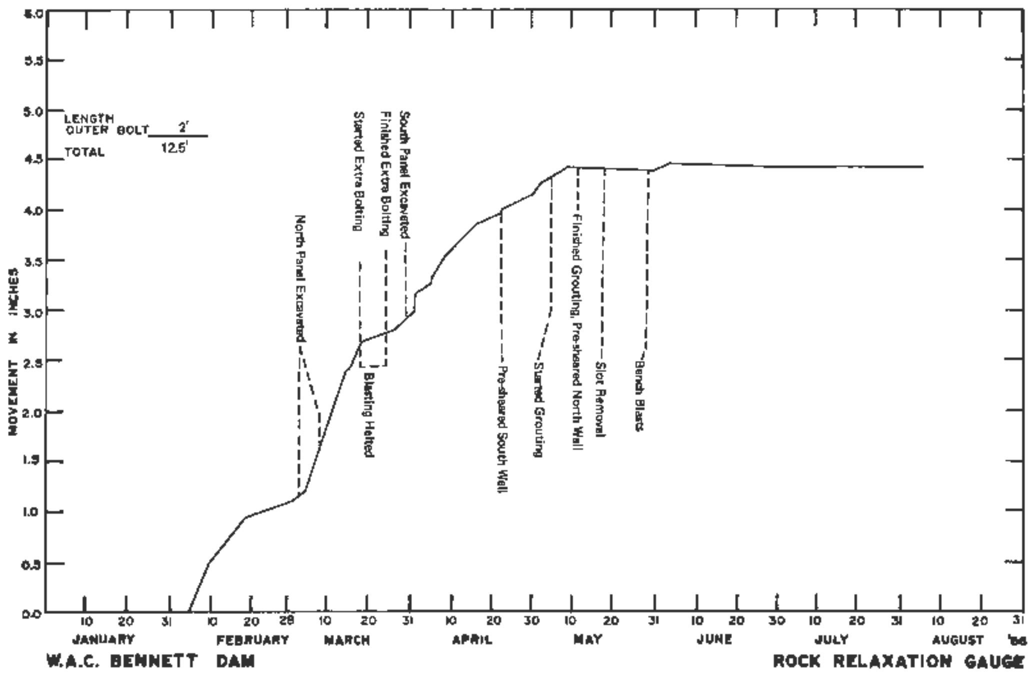

FIGURE 12 — Powerhouse roof arch at 710

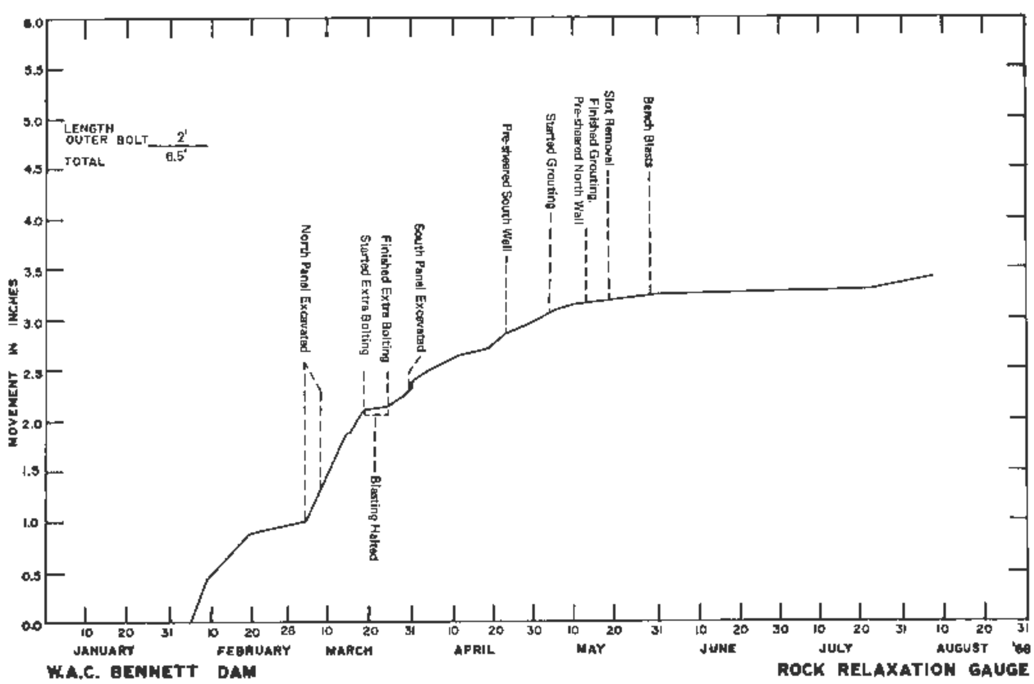

FIGURE 13 — Powerhouse roof arch at 712

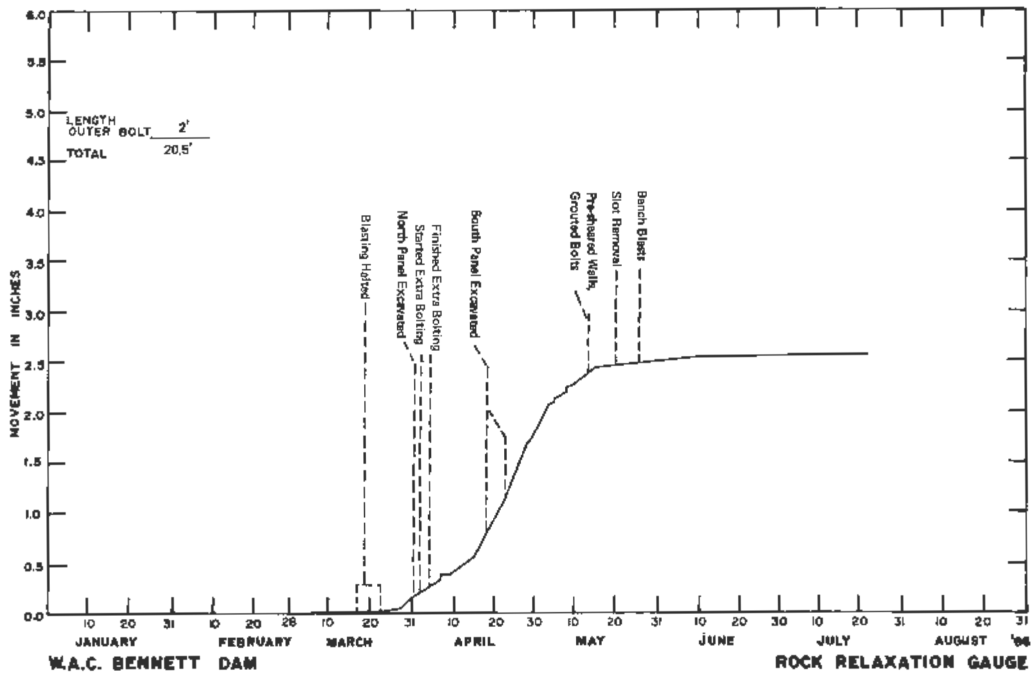

FIGURE 14 – Powerhouse roof arch at 804

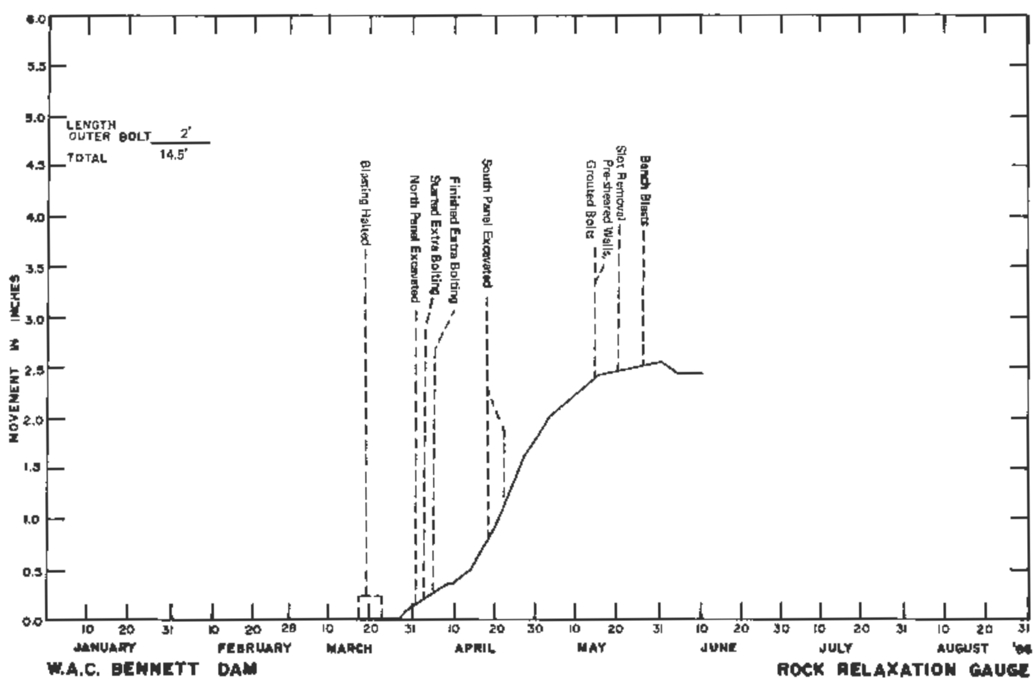

FIGURE 15 – Powerhouse roof arch at 805

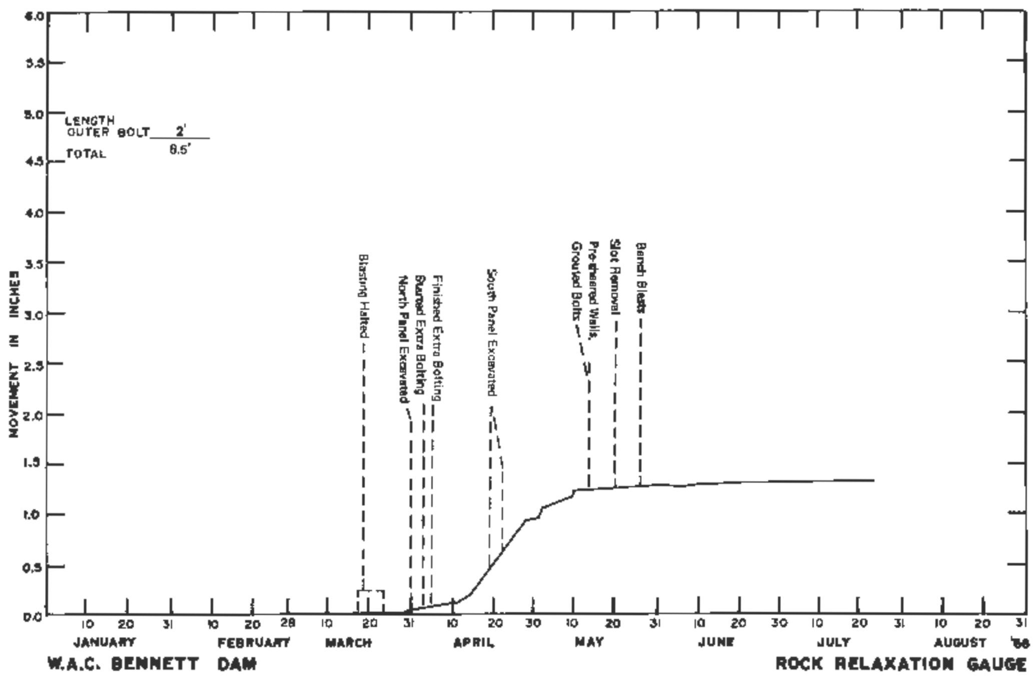

FIGURE 16 — Powerhouse roof arch at 806

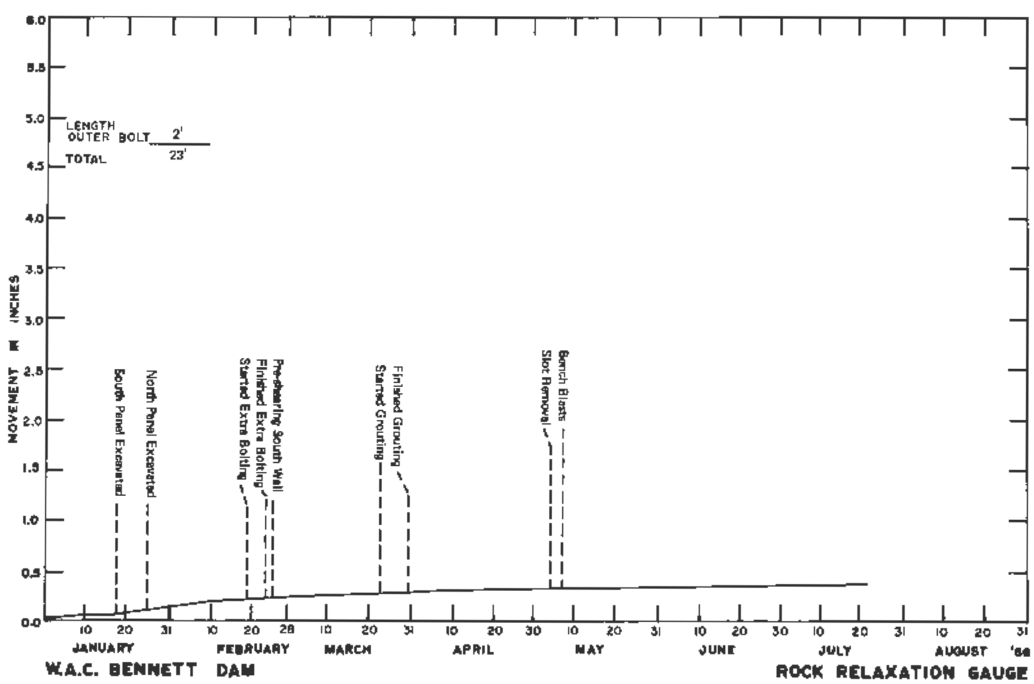

FIGURE 17 — Powerhouse roof arch at 365

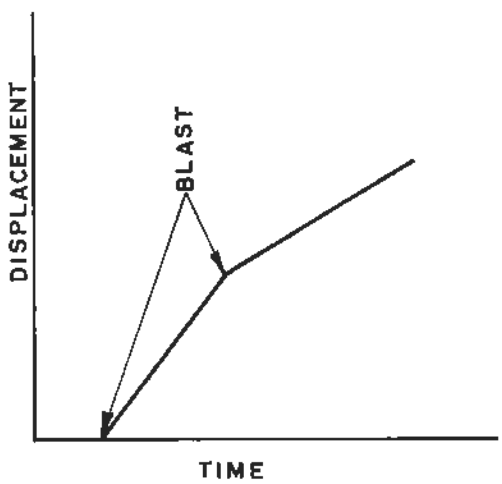

a. INDICATED SHAPE

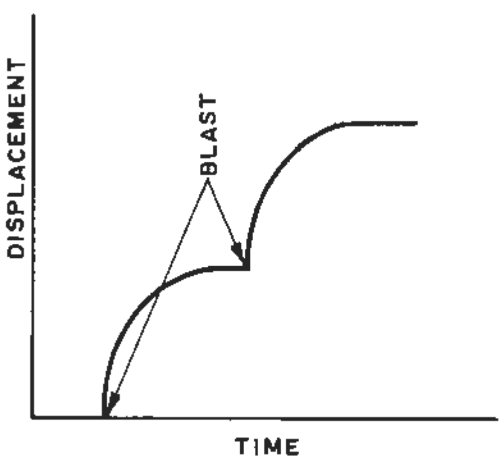

b. PROBABLE SHAPE

FIGURE 18 – Shape of time displacement graphs

firm in conjunction with the United States Bureau of Mines (Crandell (1)), detects microseismic activity in rock undergoing relaxation or readjustment.

Horizontal holes 5 ft long were drilled at intervals of 100 ft in the upstream haunch or side headings of the powerhouse for use as measuring stations. These stations were all at the arch invert level except for one located near the top of the arch at station 7+00. Seismophone readings could only be taken during the rather rare periods of construction stoppage, thus severely limiting the instrument's use. The rock noise measured consisted of individual "pops", which were counted by an observer during listening period of 5 to 10 minutes. Tape recordings of the noise were made for permanent record.

Little activity was observed, even at measuring stations near relaxation gauges which showed relatively high rock movements. The average rate of noise was under five "pops" a minute, exceeding this value only at stations near recent excavation. The low activity again suggests that the major amount of movement occurred at the instant of blasting.

Drill Hole Probing – Eight vertical diamond drill holes were cored in the powerhouse arch during March 1966 in order to observe the physical state of the rock immediately overlying the partially completed arch. Three holes were drilled from staging at the top of the arch at stations 5+62, 6+60 and 7+30. Five holes were collared near the north haunch and drilled from the invert at stations 2+50, 4+00, 6+85, 7+00 and 7+15. In November 1966 three additional vertical holes were cored through the concrete arch along the centreline of the powerhouse at stations 3+00, 5+00 and 7+20.

The three vertical core holes (NX) drilled along the centreline of the chamber in March 1966 provided a limited visual observation of the rock immediately above the arch. Horizontal fractures could be seen in the rock immediately above the collar of each hole and an attempt was made to measure these observed cracks and those suspected above them.. Measurements were taken using a graduated, wooden loading stick with a nail probe attached to one end. Readings were taken at two different times in April 1966 and the results are given in Tables 2, 3 and 4.

The results of this probing cannot be used to estimate directly the amount of rock relaxation which occurred between April 6 and April 19, 1966, because slightly different methods of measurement were used. In the first set of readings care was taken to try to distinguish between fractures in the rock and chipping of the side of the hole at a fracture during drilling. This precaution was not taken for the April 19 readings.

TABLE 2

Drill Hole Probing, Station 5 + 62

	Estimated Size of Crack	
Distance from Collar	April 6/66 16' Probe	April 19/66 20' Probe
1' 6"	1/16"	NR
1' 8½"	NR	1/8"
1' 9"	1/16"	1/8"
7' 0"	1/16"	1/8"
8' 10¼"	NR	1/16"
9' 0"	1/16"	NR
9' 2"	1/8"	1/8"
9' 9½"	NR	1/8"
10'0"	1/16"	1/8"
10'9"	1/16"	NR
11'0"	1/16"	3/8"
11'10¾"	NR	1/4"
12'0"	1/16"	1/16"
16' to 20'	No measurements	NR
Estimated total	5/8"	1½"

NR – No fracture(s) recorded

TABLE 3

Drill Hole Probing, Station 6 + 60

	Estimated Size of Crack	
Distance from Collar	April 6/66 16' Probe	April 19/66 20' Probe
1' 4"	1/8"	NR
1' 8"	1/8"	1/4"
2' 0"	1/4"	NR
2' 1½"	1/4"	3/8"
2' 2½"	1/8"	NR
2' 6"	1/8"	3/8"
6' 6"	NR	1/16"
6' 9"	1/16"	1/4"
6' 11"	1/8	NR
9' 4¼"	NR	1/8"
10'0"	1/16"	1/4"
10'2"	1/16"	NR
10'5"	1/16"	NR
11'4¾"	NR	1/16"
12'6½"	NR	1/8"
13'5"	1/16"	1/8"
15'0"	NR	1/4"
16' to 20'	No measurements	NR
Estimated total	1 7/16"	2¼"

NR – No fracture(s) recorded

Table 5 gives a comparison of the total amount of fracturing measured by the probe and the movements measured by adjacent gauges. The data suggests that 60 to 80 % of the gauge movements recorded to April 6 can be accounted for by the opening of the fractures. The results of April 19 readings show that the amount of fracturing exceeds the gauge movements probably due to mistaking chipping for open fractures.

TABLE 4

Drill Hole Probing, Station 7 + 30

	Estimated Size of Crack	
Distance from Collar	April 6/66 16' Probe	April 19/66 20' Probe
0' 8"	1/8"	3/8"
1' 1"	1/16"	1/4"
1' 10½"	1/16"	1/16"
2' 10"	1/16"	1/8"
3' 4"	1/8"	3/8"
3' 5½"	1/8"	NR
4' 3"	3/16"	7/8"
4' 7¼"	NR	3/8"
4' 8½"	1/16"	NR
4' 11"	1/16"	NR
7' 2"	1/16"	NR
7' 3½"	NR	1/4"
7' 5"	1/16"	NR
7' 7"	1/16"	NR
8' 7¾"	NR	1/8"
8' 9½"	1/16"	NR
9' 7¼"	NR	1/16"
10'6"	NR	1/16"
11'6"	NR	1/8"
11'8"	1/16"	1/8"
12'0"	NR	7/8"
12'3"	1/16"	3/8"
12'9"	NR	1/16"
12'10¾"	NR	1/16"
13'0"	NR	1/16"
14'4"	1/16"	NR
Estimated total	1 5/16"	4 5/8"

NR – No fracture(s) recorded

From Tables 2, 3 and 4 the limit of fracturing appears to be 12 to 14 ft from the collar of the hole. This agrees with the relaxation gauge information of the sets of gauges. It was also noted in the probing that two slight offsets (0.5 and 0.75 in.) had occurred in the strata near the collars of two of the holes after drilling. The underlying rock moved toward the southern side of the chamber relative to the overlying rock.

The results of the coring conducted at station 7+20 through the concrete arch are of

TABLE 5

Comparison of Gauge and Probe Measurements

	Inches of Movement Gauge 5 + 81	Inches of Opening Probe 5 + 62
April 6	0.91	0.6
April 19	1.05	1.5
	Gauge 6 + 69	Probe 6 + 60
April 6	1.72	1.4
April 19	2.10	2.3
	Gauge 7 + 32	Probe 7 + 30
April 6	2.00	1.3
April 19	3.08	4.6

interest because apparently no grout was intersected in the area where the arch had undergone the maximum deformation (5.8 in.) during excavation. The NX borehole camera available at the site could not be used to substantiate this finding because the drill hole was BX in size.

Absolute Movement Measurements — As indicated above, the rock movements measured by the relaxation gauges are relative movements only, although if the relaxation in the massive N4U sandstone in which the gauges are anchored is considered negligible, the recorded values should approximate the total downward movement. An attempt was made to check this assumption during the latter stages of excavation by precise survey methods. As with the seismophone, periods of measurement were very limited. There was no evidence to indicate downward rock movements in excess of those measured by the relaxation gauges.

Nature of Arch Movement

Because of the anisotropic state of the rock, it is difficult to form definite conclusions regarding the nature of the arch relaxation recorded by the gauges. A comparison of the measurement readings in the east and west ends of the powerhouse, however, gives some insight into this relaxation. Rocks above the arch are thought to have moved by the following mechanisms: 1. homogenous elastic and elastico-viscous expansion, 2. downward bending, and 3. opening of horizontal tension cracks.

Elastic and elastico-viscous dilation probably contributed the least amount to the total movement measured by the relaxation gauges. These gauges were installed near the face of the centre heading up to 8 hours after blasting and most of the truly elastic deformation would have occurred by then. Elastico-viscous movements (time-dependent strain) occurred for some time after this but these movements are believed to have been small. At the Poatina underground powerhouse a downward roof movement of only 0.07 in. was accounted for by dilation in rock of similar lithology and in situ stress conditions [Endersbee and Hofto, (4)].

Downward bending of the strata under the influence of the horizontal compressive stresses also contributed to the arch movements but this mechanism is not believed to have contributed the major part. While the horizontal stresses are higher in the east end of the chamber than the west end (Figure 6), the large differences in maximum movement between the two areas (5.8 in. as opposed to 1 in.) cannot be entirely due to the difference in stress levels.

The main mechanism of arch movement would appear to have been the opening of horizontal tension cracks caused by blasting. One theory of blasting [Duvall and Atchison (3)] is that most of the fracturing in rock exposed to a blast is the result of compression waves being reflected into tension waves at a free surface; the rocks fail in tension, the tensile strength of rocks being much less than their compressive strength. At W.A.C. Bennett Dam the stress distribution in the rocks above the arch during blasting was very complex. Compression waves, reflected from the overlying N4U sandstone contact as tension waves, were probably a factor in the formation of the fracturing observed above the arch.

The east end of the powerhouse was subjected to dynamic loading over a longer period of time than the west end. At any one point in the excavation sequence (Figure 9), the central heading advanced far ahead of the other faces. Following the excavation of the side faces on the north side of the powerhouse, the excavation of the south faces was carried out up to two months behind the central heading. Each episode of side blasting subjected the arch to severe vertical loading and kept the rock active so that it relaxed considerably. In the west end of the powerhouse the excavation was more rapid and uniform, and the dynamic loading had less effect.

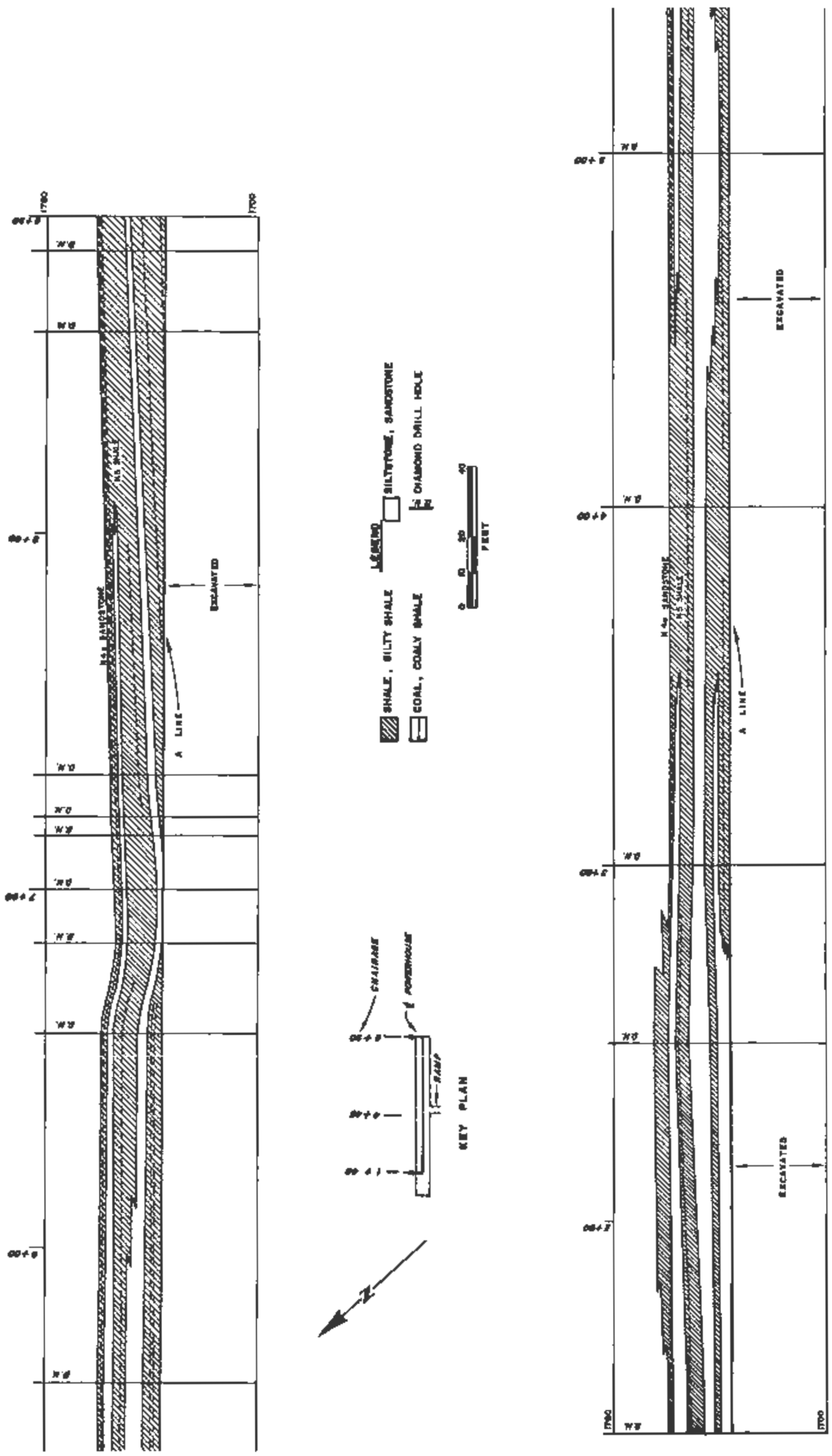

FIGURE 19 — Powerhouse arch centreline stratigraphic section

Evidence, however, suggests that the movements recorded in the southeast end of the powerhouse would have been higher than in the northwest end regardless of the excavation rate. The shale sequence above the arch in the southeast end (Figure 19) contains more coal seams than the shale sequence in the northwest end, giving the former a lower tensile strength. The formation of horizontal tension fractures would thus occur more readily in the southeast end of the powerhouse.

This situation can partially explain why more than 1 in. of movement occurred at station 7+10 before the excavation of any side or haunch faces. Of perhaps greater significance, however, is a structural flexure which occurs in this vicinity (station 6+60 to station 7+15, Figure 19). The stress conditions in this region would probably be higher than in the surrounding rock and the resulting movement either by dilation or bending of the strata would also be higher.

Conclusions

1. Elastic theory presently serves as the basis for trying to predict the behaviour of homogeneous rock masses under changing stress conditions. Deviations from elastic theory may be considerable as was observed with the anisotropic rock formations in the powerhouse roof at W.A.C. Bennett Dam. Assuming an elastic, isotropic rock mass, inward wall and roof movements of somewhat less than 1 in. would be expected. During excavation, localized roof movements of over 5 in. were recorded. The need for a flexible support design to meet conditions such as these is very important in anisotropic rocks.

2. During excavation of a large underground opening, it is necessary that the effects of forces on the rock immediately surrounding the opening be carefully monitored in order to determine whether the design support is functioning as intended. If these forces, which may be the result of dynamic loading or in situ stresses, give rise to larger rock readjustments than expected, supplementary support can then be installed without delay. At W.A.C. Bennett Dam, rock relaxation gauges were successfully used for this monitoring.

3. For a large underground opening the most critical period for the support system occurs during excavation. Complex dynamic loading results from the blasting used in conventional mining methods. Control over excavation procedures must be carefully exercised so that this loading has the least possible effect on rock readjustments. The problems created by dynamic loading would be overcome by the adaptation of tunnel boring machines for use in powerhouse and similar excavations. Rock disturbance and the amount of support required would be significantly less.

Acknowledgments

The authors are indebted to H.K. Pratt, Manager, Generation and Supply Division, British Columbia Hydro and Power Authority, for permission to present this paper.

We would like to acknowledge the assistance of the staff of International Power and Engineering Consultants Limited, especially E.L. Miller and E.A. Shabatura, who were Resident Engineer and Powerhouse Engineer, respectively, during excavation of the powerhouse.

We would also like to express our appreciation to the consulting geological engineers, Dr. V. Dolmage and Dr. D.D. Campbell whose comments and criticisms proved very helpful during preparation of this paper.

References

1. Crandell, F.J., 1955, Determination of incipient roof failures in rock tunnels by micro-seismic detection. *Boston Soc. Civil Engrs.* Jan.
2. Dolmage, V. and Campbell, D.D., 1963, The geology of the Portage Mountain damsite, Peace River, B.C.; *Trans. Can. Inst. Mining Met.*, Vol. 66
3. Duvall, W.I. and Atchison, R.C., 1957, Rock *Breakage by Explosives;* U.S. Bur. Mines Rept. Invest. S356
4. Endersbee, L.A. and Hofto, E.O., 1963, Civil engineering design and studies in rock mechanics for Poatina underground power station, Tasmania; *J. Inst. Engrs.*, Australia, Vol. 35, No. 9

DISCUSSION

Barry Voight,
College of Earth and Mineral Sciences,
The Pennsylvania State University,
University Park, Pa., USA.

Included in the rock mechanics investigations reported for the powerhouse exploratory tunnel are two independent studies of in situ stresses. The practical aspects of this work is of interest because stress measurement procedures in general have been regarded as controversial. In the last few years ill will on the part of mine managers and practicing engineers has been understandably generated, in many instances, due both to misunderstandings and to statements by certain stress measurement specialists in which the case for immediate practical application of "measured" stresses had been overstated, while at the same time the technical difficulties and simplifying assumptions required for stress determination were being ignored or minimized.

In order to increase understanding of the practical application of the stress measurement work reported for the Bennett site, I would, therefore, ask for further clarification of the following points:

1. How were the ground stresses reported for the Bennett powerhouse site actually employed in design of the powerhouse arch?

2. Were the stress measurements used in formulating an excavation sequence ? In this regard, was the pre-shearing of the powerhouse walls predicated by the high lateral stresses reported, or would this procedure have been followed irrespective of stress measurement results?

3. The paper suggests that agreement between time-dependent photoelastic methods and drill hole overcoring was obtained. What level of agreement was in fact obtained? Were the principal stress magnitudes and orientations approximately duplicated, or does "agreement" simply suggest that both methods indicated high lateral stresses. Further elaboration on the results of the time-dependent photoelastic method and environmental controls (e.g., temperature, humidity) would be useful, for several workers (myself included) have expressed serious reservations as to the adequacy of the method.

4. With respect to the results due to the overcoring method, further elaboration would be useful. I would like to see the individual results from boreholes M. P. 1 to M. P. 8. If multiple measurements were made in each borehole, would the authors please list these results; if averages of multiple results were ultimately chosen to represent the state of stress in each hole, would the authors illustrate the methods of data selection and averaging used?

Furthermore, the vertical stresses as given are approximately double the value which can be accounted for by the weight of overburden rock. While precise equality of the overburden pressure component with the vertical stress is a special case (see p. 334, *Proceedings of the First Congress, Inter. Soc. Rock Mechanics,* 1966, v. III), a disparity of the present proportions may lead to difficulties, both with respect to the vertical stress itself and with the confidence attached to the determined lateral stresses. Would the authors care to comment on this question?

5. Finally, it is claimed that the measured stresses are oriented in a manner that might be expected from considerations of regional structure (i.e., the anticlinorium) and local topography. This seems to be an oversimplification of the problem of principal stress orientation predictions. In fact, the relation between geologic structural features and in situ stresses is simply not known at the present state of the art. Detailed geologic structural work coupled with unambiguously determined field stresses will be required at a number of localities before we can make any such predictions with confidence. Studies of this kind are only beginning, and the interpretive problems attached to field stresses and their related geologic mechanisms are very much open questions at this time.

K. Barron,
Mining Research Centre,
Department of Energy, Mines
and Resources, Ottawa.

1. Additional details on the rock stress measurements would be appreciated. In view of the anisotropic nature of the bed rock and of the nature of the techniques used there would

have been problems with interpreting the measurements. Further it would have been of interest to know whether sufficient measurements were taken to enable an estimate of the errors to be made.

2. From the magnitude of the reported deflection measurements it would be appreciated that loose rock and, possibly, some falls would have occurred; an evaluation of this would have been of interest.

A.S. Imrie

Education — B Sc, mining geology, University of Alberta, 1963; M Sc, structural geology, University of Alberta, 1967.

Employment Summary — 1964-67, assistant engineering geologist for IPEC Ltd.; 1967 party chief for J. Foster Irwin Engineering and Management Services; 1967 to the present, engineering geologist for IPEC.

L.T. Jory

Education — BA Sc, geological engineering, University of British Columbia, 1950; Ph D, economic geology and geochemistry, California Institute of Technology, 1964.

Employment Summary — 1950-63, engaged in mining and mining exploration for various companies including 6 years with Eldorado Mining and Refining Co. Ltd. as chief geologist, 1963-66, senior engineering geologist for IPEC; 1966 to the present, consulting geologist for Dolmage, Campbell and Associates.

Insights into Undercutting in Block Caving

Giovanni Barla
Preceptor, Henry Krumb School of Mines, Columbia University, New York, N.Y.

Stefan Boshkov
Professor of Mining and Chairman, Henry Krumb School of Mines, Columbia University, New York, N.Y.

Abstract

Numerous instrumental observations have proved that large changes in stress and deformation occur on the rock and concrete linings around development workings below undercuts while the latter are being created in block caving. It is shown that some insight into these phenomena can be gained by reference to existing mathematical solutions of the plane, statical theory of elasticity. Further, the application of gelatin mixture models in conjunction with photoelastic methods can be used as a potentially fruitful approach to the problem. Three undercutting methods in a linearly elastic, homogeneous and isotropic rock under gravitational loading have been analyzed. The aim of the study is the determination of the influence of the geometric parameters involved and the optimum layout. An annulus of mechanical properties different from those of the rock medium is also introduced in some cases to simulate the effect due to the existence of a lining in the opening below the undercut.

Introduction

Numerous instrumental observations, reported by the United States Bureau of Mines (1) (2), show that large changes in stress and deformation occur in the rock and concrete linings around the openings below the undercut, while the latter is created.

These phenomena may be explained on the general assumption that the undercut removes the effect of the vertical stress to which the openings were formerly subjected. Existing mathematical solutions in the classical theory of elasticity may be used based on this assumption (3).

Although this approach may be a good first approximation, it is insufficient to completely describe the conditions encountered in an actual block caving operation. Not only must one allow that the rock may not be expected to behave as a linearly elastic, homogeneous and isotropic medium, but also that it may be fractured and that the geometry defining the shapes and relative locations of the openings may be quite complicated. Further, it may be reasoned that the interaction between these openings must be studied in an appropriate initial stress field.

Although numerical techniques have already been developed to cope with some of the factors which make the problem difficult of formal solution, one faces, in addition, the existing lack of knowledge of the rock mass physical and geological properties.

The application of concepts of the classical theory of elasticity and experimental methods involving two-dimensional photoelastic analysis is justified, particularly when the assumption of zero vertical stress component by undercutting is removed and gravity effects are considered.

In this paper an approximate theoretical solution for such a case is obtained by the method of superposition. Then, gelatin mixture models and photoelastic techniques are used to analyze three typical undercutting sequences.

The Problem

The choice of a proper procedure for undercutting in block caving is of primary importance in mining practice. It determines the stability of the extraction openings and, consequently, the maintenance costs. Progress in this respect has come mainly from field tests. Theoretical and experimental investigations are limited. This results from the difficulty of conceiving a complete, either mathematical or experimental, representative model.

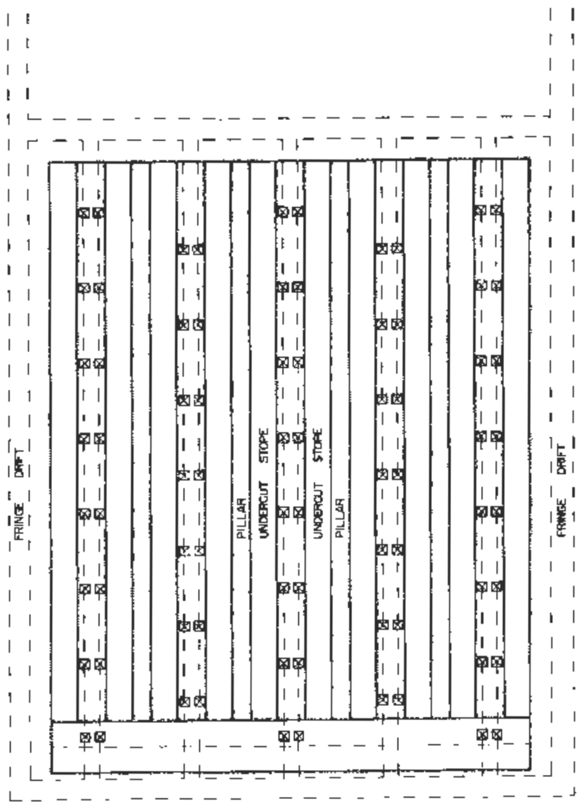

FIGURE 1 – Stope plan at undercut level in a blockcaving operation.

Considerable simplification is gained when specific situations which occur in block caving are examined.

Figure 1 shows a stope plan at the undercut level in a typical undercut caving operation, where undercut stopes are driven and pillars left on top of the drifts. Another typical caving method is illustrated in Figure 2. Pillars of ore are left to create a series of adjacent panels which are then worked together.

An analysis of Figures 1 and 2 suggests that one consider the following undercutting sequences:

(I) Undercut passing over a drift.

(II) Undercut advancing toward the sides of a block.

(III) Undercut advancing toward a pillar.

These three undercutting sequences are depicted in Figure 3 together with a schematic idealization which may be deemed representative. This is intended to be a two-dimensional idealization and introduces considerable simplifications into the problem. It must be recognized that a three-dimensional idealization would be more appropriate particularly when studying the undercutting sequence (II) (See Figure 2).

Formulation of a Theoretical Solution

The problem defined in the previous paragraph is a particular case of the most general two-dimensional situation where adjacent, equally or differently shaped, openings are located in a gravity loaded continuum. Numerical methods are being used to obtain a complete solution for this problem (4). A procedure to evaluate the approximate tangential stress at the contour only of the circular drift, based upon the application of the superposition principle and known solutions in the classical theory of elasticity, may make use of the following information:

a. Tangential stress around a circular hole in a half space of zero weight under a uniform normal load applied to a segment of the straight line edge.

b. Tangential stress around a circular hole in a half space of zero weight under a uniform normal load "extended to the right" and/or "extended to the left" and applied to the straight line edge.

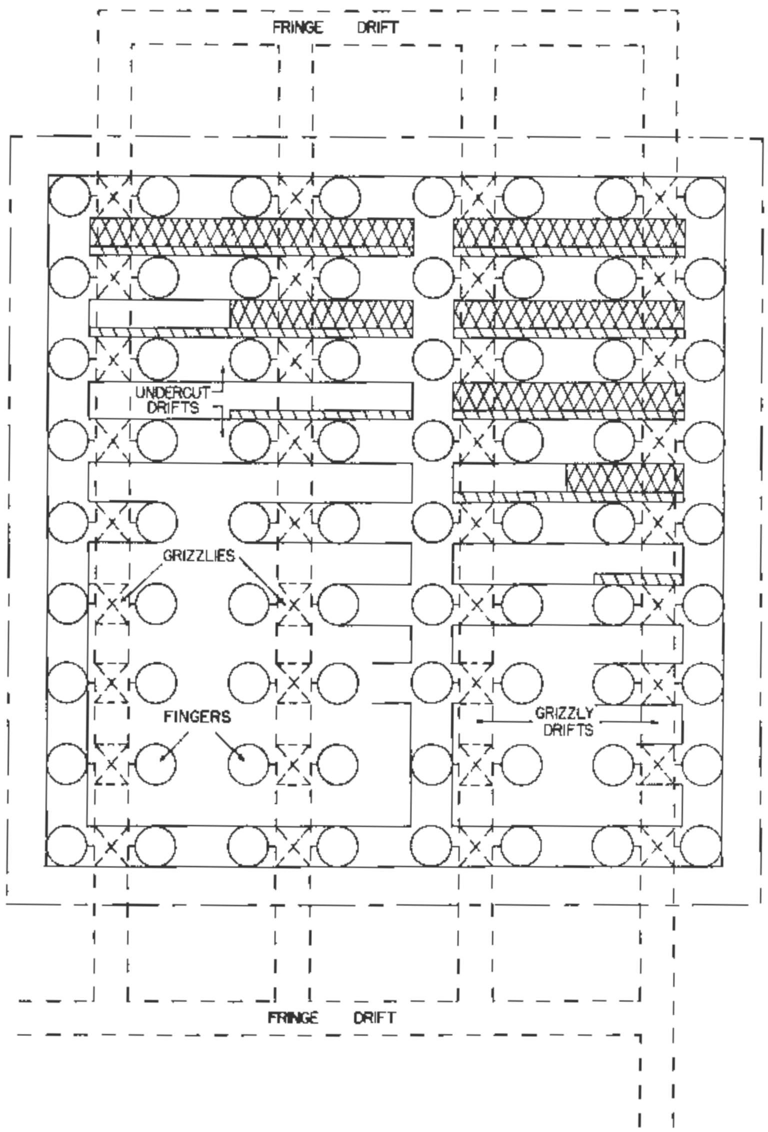

FIGURE 2 – Stope plan at undercut level in a panel caving operation.

c. Tangential stress around a circular hole in a half space of zero weight under a uniform load parallel to the straight line edge (5).
d. Tangential stress around a circular hole in a half space of non-zero weight (6).

For the sake of completeness, solutions for these problems are given in Table 1. For problems c. and d. above, exact solutions are available; for problems a. and b., the solutions are only approximate. To estimate the order of this approximation, we consider first the existing solution obtained by Barjansky (7) for the tangential stress around a circular hole which is located in a so-called plane Boussinesq field. Due to the complexity of such a solution, the analysis is limited to the case when the normal point load acts along the line passing through the center of the circular hole, as represented in Figure 4. We have, in this case, the following series solution for the tangential stress around the hole (7):

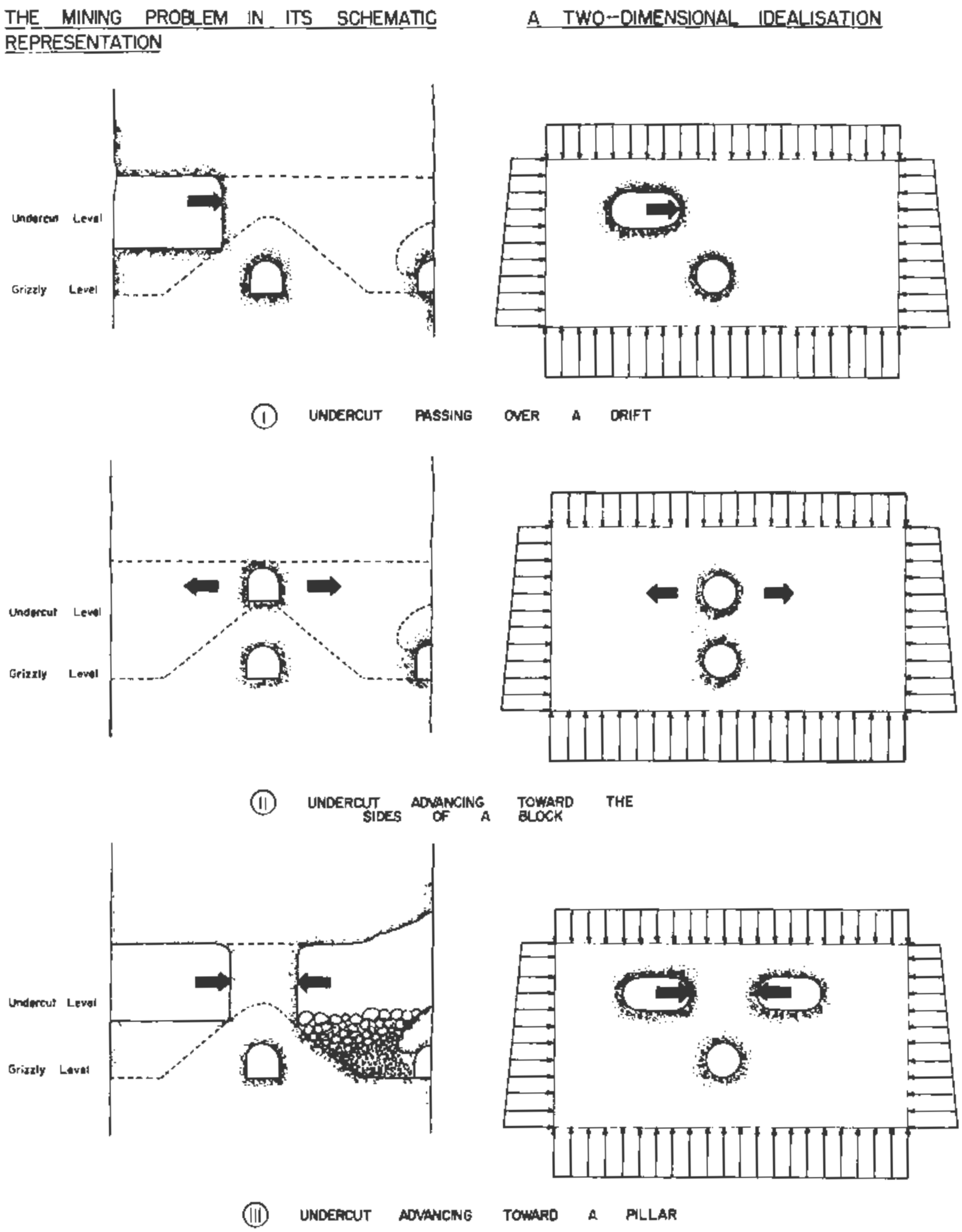

FIGURE 3 – Undercutting sequences

$$a\tau_{tt} = -\frac{p}{\pi}(1 + \coth^2 \xi_o)$$

$$-\frac{2p}{\pi}\frac{\cosh \xi_o}{\sinh^2 \xi_o}\cos\eta$$

$$+\frac{p}{\pi}(5\coth^2\xi_o - 1)\cos 2\eta$$

$$-\frac{2p}{\pi}\left[\frac{2\sinh\xi_o \sinh 2\xi_o}{\sinh^2 2\xi_o - 4\sinh^2\xi_o}\right.$$

$$\left.+\frac{4\sinh\xi_o\sinh 4\xi_o}{\sinh^2 4\xi_o - 16\sinh^2\xi_o}\right]\cos 3\eta$$

$$+\frac{4p}{\pi}\left[\frac{4\sinh\xi_o\sinh 4\xi_o}{\sinh^2 4\xi_o - 16\sinh^2\xi_o}\right]\cos 4\eta$$

$$-\frac{2p}{\pi}\left[\frac{4\sinh\xi_o\sinh 4\xi_o}{\sinh^2 4\xi_o - 16\sinh^2\xi_o}\right.$$

$$\left.+\frac{6\sinh\xi_o\sinh 6\xi_o}{\sinh^2 6\xi_o - 36\sinh^2\xi_o}\right]\cos 5\eta \qquad \text{Eq. 1}$$

where a system of bipolar coordinates (ξ,η) is used so that

$$\eta = x_1 = 0$$

and

$$\xi = \xi_o \cos^{-1}\frac{h}{a}$$

represents the periphery of the circular hole, h, p, and a are defined in Figure 4.

A compromise solution for the same problem can be obtained in the same way as those for a. and b., by using the principle of superposition:

$$\tau_{tt} = \frac{2p}{\pi r}(4\cos^2\beta - 1) \qquad \text{Eq. 2}$$

if the circular hole is assumed to be in a uniform stress field $(\frac{2p}{\pi r})$, equal to that which would have existed along its contour under the same loading conditions if the hole had not been created. β and r are shown in Figure 4. The stress concentration ratio $\tau_{tt}/\frac{2p}{\pi x_1}$ vs. position along the circular boundary is plotted in Figure 4, for cases in which h/a = 2 and 5. The solid lines relate τ_{tt} derived from equation 1 and the dashed line, the value derived from equation 2, $2p/\pi x_1$, is the value of stress which would have existed under the same load conditions at a point located at the same depth along the center line, if the hole were not present.

One may notice that when compromise solution, equation 2, is used instead of equation 1, errors are introduced, especially for values of h/a less than 2. Both curves tend toward a limit curve (when $h/a \to \infty$) which is simply the plot of the term $(1 - 2\cos 2\alpha)$. If this is kept in mind, solutions (a) and (b) of Table 1 can be placed in proper perspective.

Gelatin Mixture Models

It has been shown in (8) that a prototype rock may be replaced in a model with a "soft material" sensitive to body force effects and chosen in such a manner that its mechanical properties may be related to those of the rock structure by a change in the scales of stresses, time and displacements. Possible applications for gelatin mixtures are suggested by the following.

If the rock structure under investigation is composed of linearly elastic materials, and uniform conditions are assumed to exist for the model and prototype,

a. the equation for conservation of mass,

b. the equation for balance of linear momentum,

c. the conditions for equilibrium on the surface boundary, and

d. the constitutive equations of the rock mass give (8)

$$\frac{x'}{x} = \frac{u'}{u} \qquad \text{Eq. 3}$$

$$\frac{E'}{E} = \frac{\epsilon}{\epsilon'}\frac{\rho'}{\rho}\frac{x'}{x} \qquad \text{Eq. 4}$$

$$\frac{\sigma'}{\sigma} = 1 \qquad \text{Eq. 5}$$

$$\frac{T'}{T} = \frac{\tau}{\tau'} \qquad \text{Eq. 6}$$

where

- x = rectangular coordinate
- u = component of displacement
- E = Young's modulus
- ϵ = strain component
- ρ = mass density
- σ = Poisson's ratio
- T = boundary force
- τ = stress component

and the primes denote the same quantities in the model.

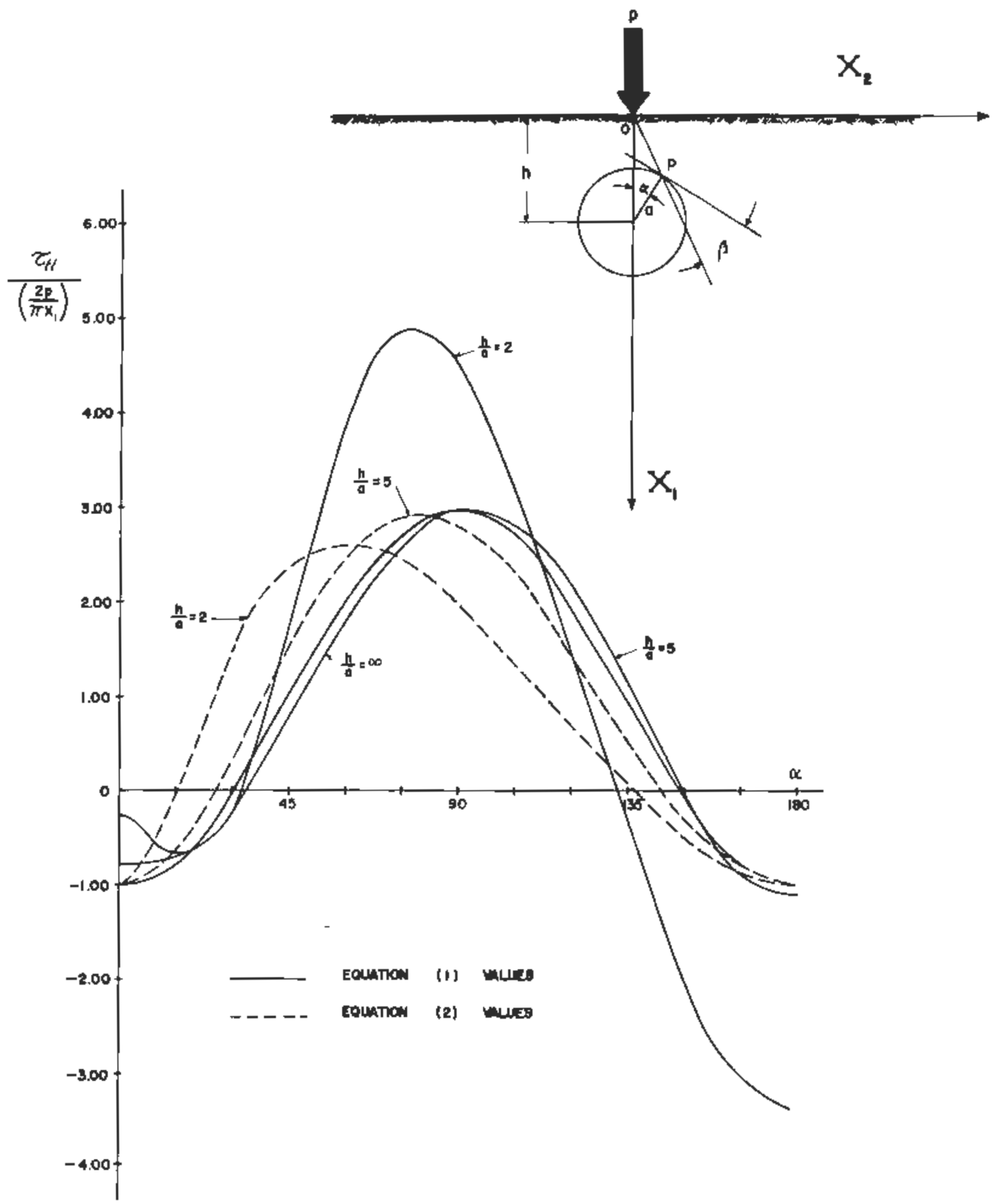

FIGURE 4

The above design criteria must be valid simultaneously if complete similarity between the model and prototype is to be ensured. However, some limitations arise. Equation 4 can be satisfied only if a large ratio between the strains of the model and those of the prototype is allowed. Then, if this fact is related to equations 3 and 6, which require the strain to be equal at analogous points in the model and prototype, a limitation becomes immediately evident. Furthermore, the requirement that the Poisson's ratios of the model and the prototype be identical cannot be satisfied, because the gelatin mixtures have a $\sigma' = .5$.

Gelatin mixture models used in conjunction with photoelastic methods require one to choose a proper calibration technique. In the present case, the extremely high dependence of the mechanical and optical properties of gelatin mixtures upon variations in temperature, relative humidity, mold time and gelatin composition, requires the simultaneous conduct of both calibration and model tests. A calibration procedure for gelatin mixtures known as the "block test" was described in (8). This permits one to evaluate, at any time: 1. the modulus function in shear, 2. the photoelastic stress coefficient, and 3. the photoelastic strain coefficient. In addition, creep curves can be obtained which allow one to determine, at any time, the maximum shearing stress–maximum shearing strain relationship, defining the physical behavior of the mixture. Thus, the gelatin mixture can be checked for physical linearity.

Results and Discussion

Following the schematic idealization of Figure 3, gelatin mixture models* were constructed to analyze undercutting sequences (I) to (III). The experiments dealt with three series of such models which were classified in accordance with the undercutting sequences they represented:

Series A – Undercut passing over a drift.

Series B – Undercut advancing toward the sides of a block.

Series C – Undercut advancing toward a pillar.

The models were tested within a frame over which two thick plexiglass plates were clamped and careful lubrication was provided. In this manner, conditions of plane strain were represented quite satisfactorily throughout the test. The experimental methodology used is described in (8).

The photoelastic analysis consisted of taking photographs of dark-field and light-field isochromatics at various times during the experiment. The simultaneous conduct of the calibration test furnished values of the photoelastic stress coefficient, thus allowing the determination of the maximum shearing stress at each point in the model and of the tangential stresses on a free boundary. In order to furnish additional information for the analysis, isoclinic lines were also traced. Techniques for the determination of the sign of the stresses and of the fractional fringe orders could also have been applied. However, the latter are used very rarely in such work because of the high optical sensitivity of the gelatin mixtures and the ability to utilize their time-dependent behavior to advantage with shifting isochromatic lines covering different areas of the model at different times.

The experimental results are presented for each series in Tables 2 and 3, and Figures 5 and 6. Figure 5(f) and Figure 6(c) and (f) describe the history of stress concentration changes at the circular drift boundary points defined by $\theta = 0°, 90°$. The tangential stresses are calculated using the method given in the Tables. The final results, for each model, are given in terms of stress concentration factors, i.e. the average value of the tangential stress $(\tau_{tt})_\theta = 0°$ or $90°$, normalized to the weight of the gelatin mixture above the circular drift ($\rho g h_1$).

Since previous tests had proved the desirability for increasing the value of h_1 proportionally to the maximum linear dimension of the opening, Table 2 is arranged to reflect this change for models 1A to 4A. In Figure 5(a), (b), (c) and (d), and Figure 6 (a), (b), (d) and (e), the lines of equal maximum shearing stress normalized to ($\rho g h_1$) are depicted for each model series.

The following behavior patterns may be noted for the series of experiments.

Series A

1. A sharp rise of both the back (at $\theta = 0°$) and rib (at $\theta = 90°$) tangential stresses around the drift occurs when the undercut passes over it ($x_2 = 4a$ in Figure 5). The relative increase is 90% and 55%, for the back and rib tangential stresses respectively, of the value before undercutting.

2. When the undercut increases further in lateral dimension, both stresses decrease. However, the back tangential stress decreases smoothly (15% of the maximum value relative variation), whereas approximately 90% variation occurs for the rib tangential stress.

3. A large increase in stress concentration at the abutments of the undercut follows the relief of stresses around the circular drift.

*Gelatin mixtures with 15% of gelatin and a water-glycerin ratio 3:1 were used for all tests. Experiments were carried on in air-conditioned room under continuous recording of temperature and relative humidity.

TABLE 1

PROBLEM	SCHEMATIC REPRESENTATION	TANGENTIAL STRESS
(a) Approximate tangential stress around a circular hole in a half space of zero weight under a uniform normal load applied to a segment of the straight line edge.	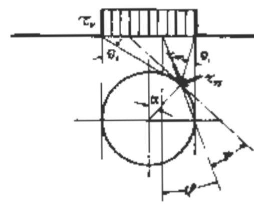	$\tau_{tt} = \tau_{nn}(4\cos^2\psi - 1) + \tau_{ss}(4\sin^2\psi - 1)$ (approximate) where: $\tau_{nn} = \frac{\tau_v}{\pi}[(\theta_1 - \theta_2) + \sin(\theta_1 - \theta_2)]$ $\tau_{ss} = \frac{\tau_v}{\pi}[(\theta_1 - \theta_2) - \sin(\theta_1 - \theta_2)]$ $\varphi = \frac{\theta_1 + \theta_2}{2}$
(b) Approximate tangential stress around a circular hole in a half space of zero weight under a uniform normal load "extended to the right" and applied to the straight line edge. (solution for uniform normal load "extended to the left" is analogous by symmetry)	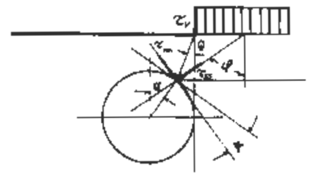	$\tau_{tt} = \tau_{nn}(4\cos^2_2\psi - 1) + \tau_{ss}(4\sin^2\psi - 1)$ (approximate) where: $\tau_{nn} = \frac{\tau_v}{2\pi}\left[\frac{\pi}{2} + \theta - \cos\theta\right]$ $\tau_{ss} = \frac{\tau_v}{2\pi}\left[\frac{\pi}{2} + \theta + \cos\theta\right]$ $\varphi = \theta + \frac{\pi}{2}$
(c) Tangential stress around a circular hole in a half space of zero weight under a uniform load parallel to the straight line edge [5]	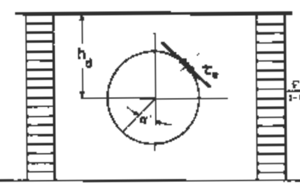	$\tau_{tt} = 2\tau_v \left\{1 + \frac{2\mathrm{sh}^2\xi_0 \sin^2\eta - (\mathrm{ch}\xi_0 + \cos\eta)}{(\mathrm{ch}\xi_0 - \cos\eta)^2}\right.$ $\left.\left[\mathrm{sh}\xi_0 \mathrm{sch}\, 2\xi_0 - 2e^{-2\xi_0}\cos\eta - \sum_{n=2}^{\infty} N_n \cos n\eta\right]\right\}$ where: $h_d = a \tan h\, \xi_0$ $\sin\alpha' = \frac{\mathrm{sh}\xi_0 \sin\eta}{\mathrm{ch}\xi_0 - \cos\eta}$, values of N_n are given in [5]
(d) Tangential stress around a circular hole in a half space of non-zero weight. [6]	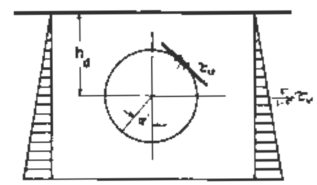	$\tau_{tt} = \rho g a M(\mathrm{ch}\xi_0 - \cos\eta)\left\{6 \cot h\, \xi_0 \csc h\xi_0 + 6\mathrm{csch}\, \xi_0 \cos\eta\right.$ $\left. + 4\sin h\, \xi_0 \sum_{n=2}^{\infty} T_n \cos n\eta\right\} + 6\rho g a M \mathrm{csch}\xi_0 \times (\cos\psi +$ $+ 2\cos h\, \xi_0 \cos 2\psi + \cos 3\psi) + \frac{2\rho g a(\mathrm{ch}\xi_0 - \cos\eta)}{\mathrm{sh}}$ $\left\{\frac{1 - \mathrm{ch}\xi_0\cos\eta}{(\mathrm{ch} - \cos)} - \cot h\, \xi_0 - \frac{(7 - 8\eta)\cos\eta + 2e^{\xi_0}\cos\eta}{4(1-\eta)\,\mathrm{sh}\,\xi_0}\right.$ $\left. - \sum_{n=2}^{\infty} R_n \cos n\eta\right\}$ where: $\cos\psi = \frac{\mathrm{ch}\xi_0\cos\eta - 1}{\mathrm{ch}\xi_0 - \cos\eta}$; $\sin\psi = \frac{\mathrm{sh}\xi_0 \sin\eta}{\mathrm{ch}\xi_0 - \cos\eta}$; ξ_0 and α' are defined above; values of M, T_n, and R_n are given in [6]

TABLE 2

MODEL	1A			2A			3A			4A		
Fringe value at $\theta = 0^\circ$	4.5	4.5	5.0	7.5	8.0	8.5	7.5	8.0	8.5	–	9.5	10.0
Fringe value at $\theta = 0^\circ$	5.0	5.0	5.5	6.5	7.0	7.5	5.0	5.5	6.0	–	1.0	1.0
Photoelastic stress coefficient [lbs/fringe in.]	.208	.184	.177	.216	.211	.191	.224	.213	.205	–	.225	.225
Tangential stress at $\theta = 90^\circ$ [p.s.i.]	1.247	1.105	1.179	2.156	2.251	2.161	2.240	2.272	2.327	–	2.850	3.000
Tangential stress at $\theta = 0^\circ$ [p.s.i.] average	1.197			2.190			2.280			2.925		
Tangential stress at $\theta = 90^\circ$ [p.s.i.]	1.386	1.227	1.297	1.869	1.970	1.907	1.493	1.562	1.463	–	.300	.300
Tangential stress at $\theta = 90^\circ$ [p.s.i.] average	1.303			1.915			1.566			.300		
Time of analysis [hour]	.5	1.0	2.0	.5	1.0	2.0	.5	1.0	2.0	.5	1.0	2.0
Depth (h_1) [inch]	12.0			12.0			17.0			21.0		
Stress concentration factor $\frac{(\zeta_{tt})}{\rho g h_1}$ $\theta = 0^\circ$	2.03			3.78			3.35			3.48		
Stress concentration factor $\frac{(\zeta_{tt})}{\rho g h_1}$ $\theta = 90^\circ$	2.25			3.88			2.30			.36		

4. Large changes in deformation occur as a result of the undercutting. Noticeable is the increase in dimension of the circular drift in the direction of the line joining its geometric center with that of the undercut. A rotation of the major axis of the drift below the undercut also occurs.

Series B

1. The back tangential stress reaches a maximum value comparable to that of the previous sequence. This occurs when the undercut is extended, symmetrically with respect to the circular drift, for a length equal to its diameter ($x_2 = 3a$ in Figure 5(c)). The rib tangential stress follows a similar pattern, but the relative variation is only 35% of the value before undercutting.

2. When the undercut is extended to its full length, the back tangential stress decreases with a relative variation of 15% of the maximum value. The rib tangential stress undergoes a change (decrease) of 64%.

TABLE 3

MODEL	1B			2B			1C			2C		
Fringe value at $\theta = 0°$	6.5	6.5	6.5	6.0	8.0	8.0	5.5	5.5	6.5	5.0	5.0	6.5
Fringe value at $\theta = 90°$	5.5	5.5	5.5	3.5	4.0	4.0	6.5	6.5	7.5	6.5	7.0	8.0
Photoelastic stress coefficient [lbs/fringe in.]	.225	.192	.204	.234	.222	.201	.205	.194	.182	.210	.203	.205
Tangential stress at $\theta = 0°$ [p.s.i.]	1.954	1.663	1.772	1.870	2.367	2.141	1.500	1.420	1.580	1.400	1.353	1.640
Tangential stress at $\theta = 0°$ [p.s.i.] average	1.796			2.126			1.500			1.464		
Tangential stress at $\theta = 90°$ [p.s.i.]	1.653	1.407	1.499	1.184	1.070	1.115	1.780	1.680	1.820	1.823	1.892	2.191
Tangential stress at $\theta = 90°$ [p.s.i.] average	1.520			1.115			1.760			1.968		
Time of analysis [hour]	.5	1.0	2.0	.5	1.0	2.0	.5	1.0	2.0	.5	1.0	2.0
Depth (h_1) [inch]	14.5			14.5			14.5			14.5		
Stress concentration factor $\frac{(\zeta_{tt})}{\rho g h_1}$ $\theta = 0°$	3.10			3.67			2.58			2.52		
Stress concentration factor $\frac{(\zeta_{tt})}{\rho g h_1}$ $\theta = 90°$	2.62			1.92			3.63			3.39		

3. The deformation does not reveal any rotation of the major axis of the drift below the undercut.

4. The increase of the vertical dimension of the drift is gradual and the adverse conditions which take place when the pillar is suddenly removed do not occur as in the sequence depicted in Series C.

Series C

1. The back tangential stress increases smoothly toward the value corresponding to the stress relief due to undercutting. The rib tangential stress reveals a behavior similar to that of Series A. The maximum value for this stress is reached as the undercut is extended to leave a pillar over the circular drift ($x_2 = 3a$ in Figure 5(f)).

2. When the pillar is removed the rib tangential stress decreases with a relative change of 85% of the maximum value.

3. Changes in deformation follow the undercutting. However, the symmetry of this

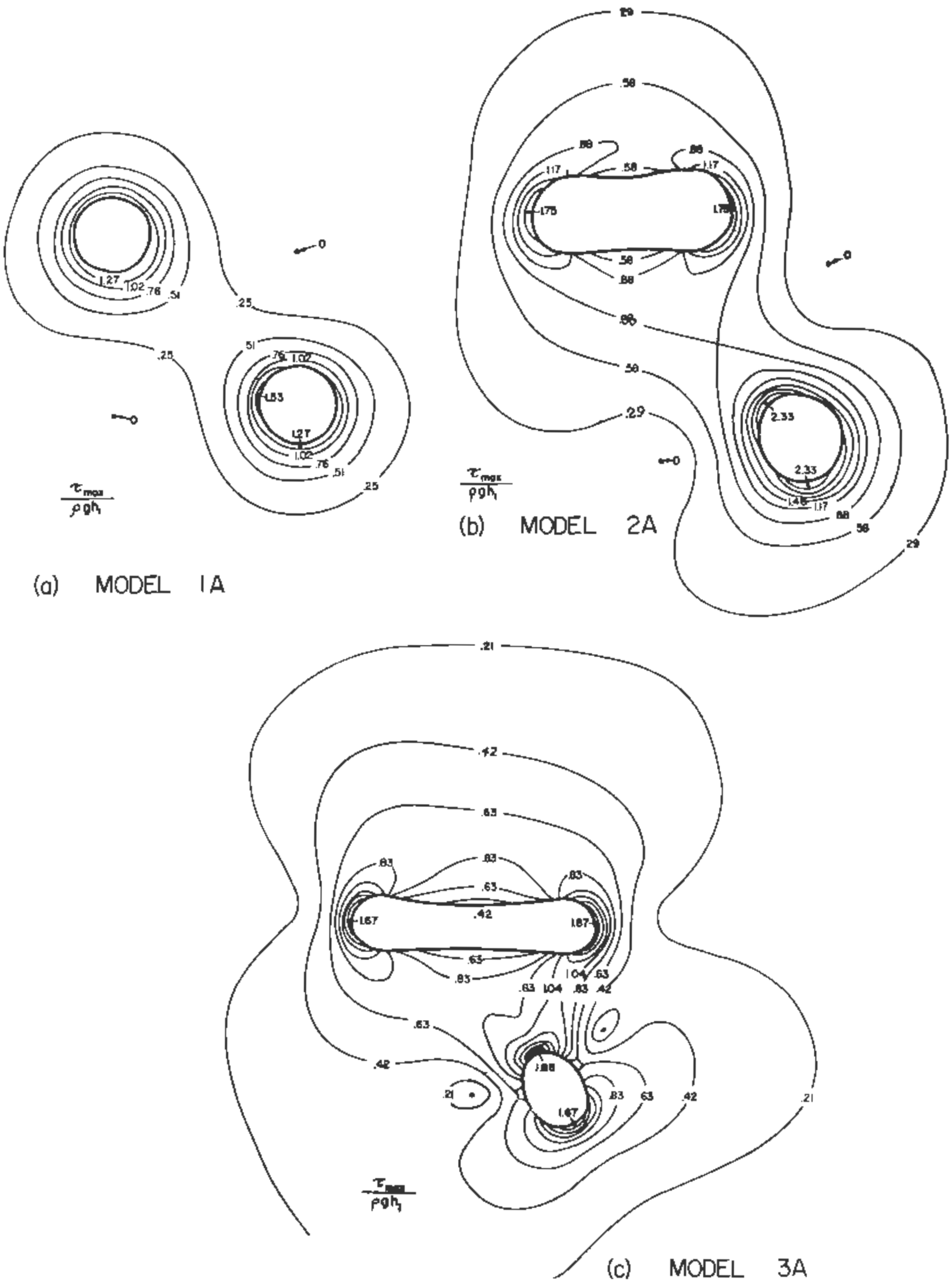

FIGURE 5 -- (a), (b) and (c) lines of equal maximum shear stress.

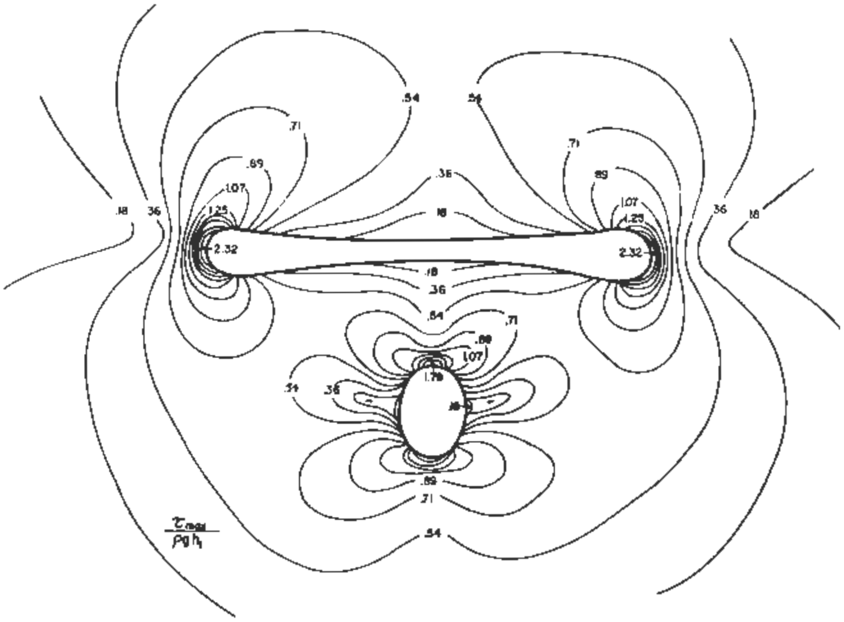

(d) MODEL 4A

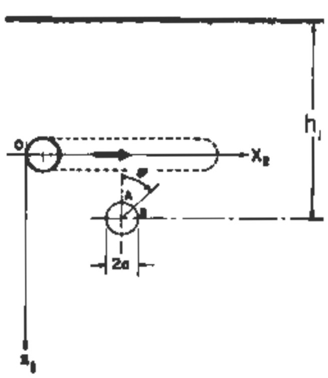

(e) DIAGRAM OF THE MODEL

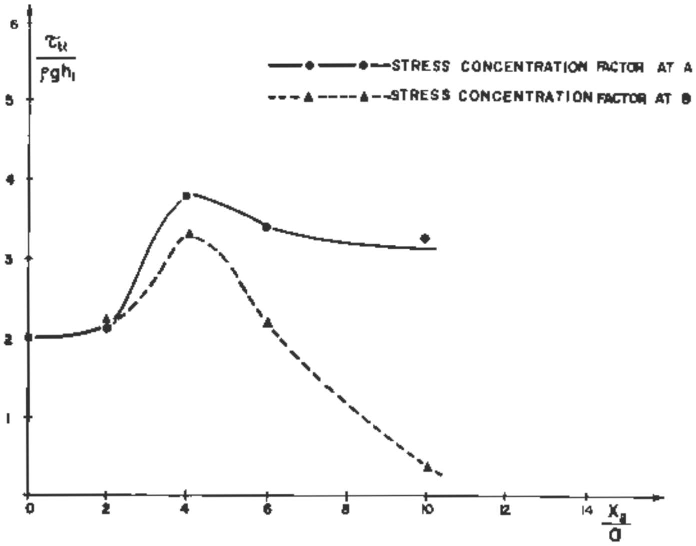

(f) STRESS CONCENTRATION FACTORS OF MODEL SERIES "A"

FIGURE 5 (cont'd) -- (d) lines of equal maximum shear stress, (e) diagram of the model, (f) stress concentration factors of the circular drift.

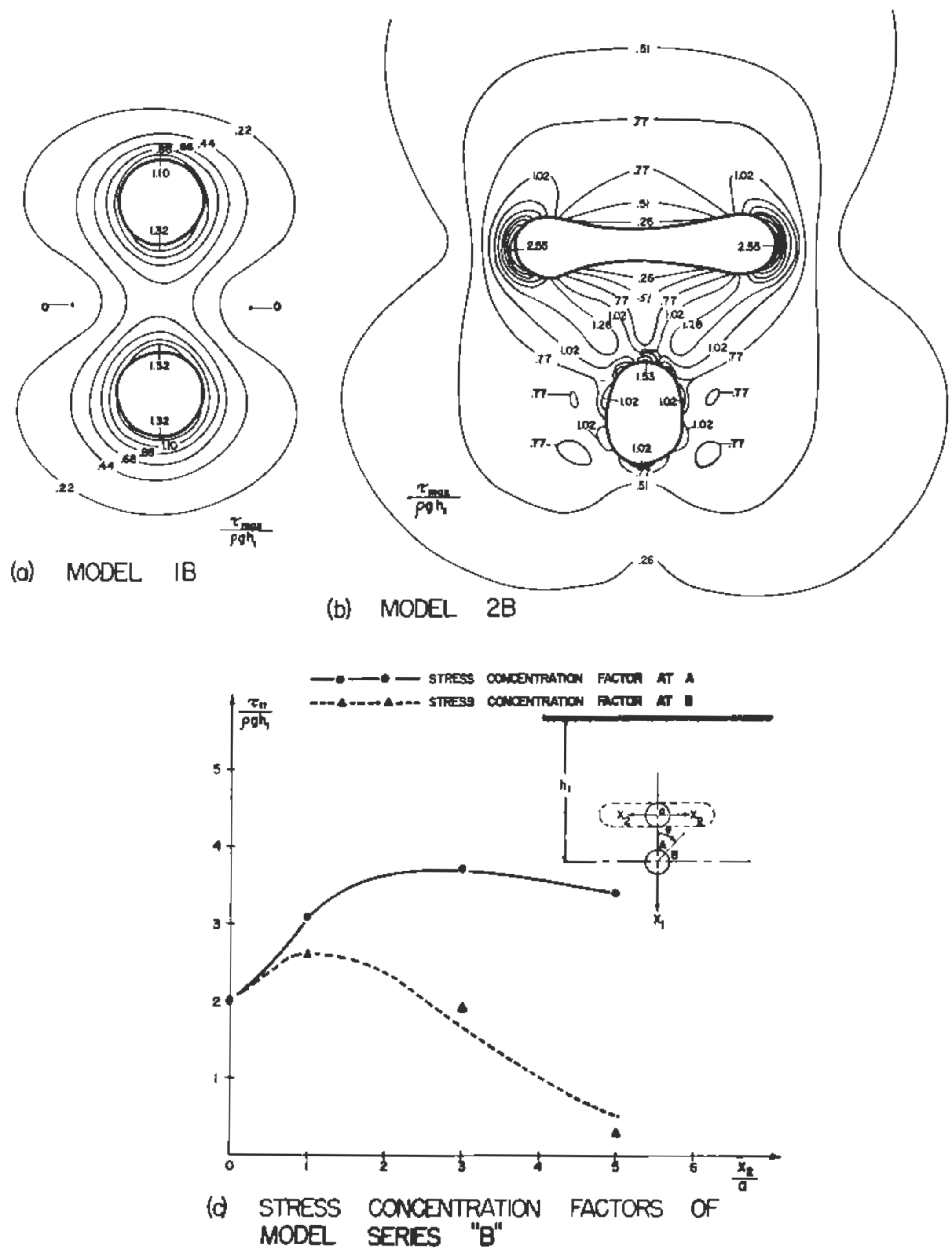

FIGURE 6 – (a) and (b) lines of equal maximum shear stress (c) stress concentration factors of the circular drift.

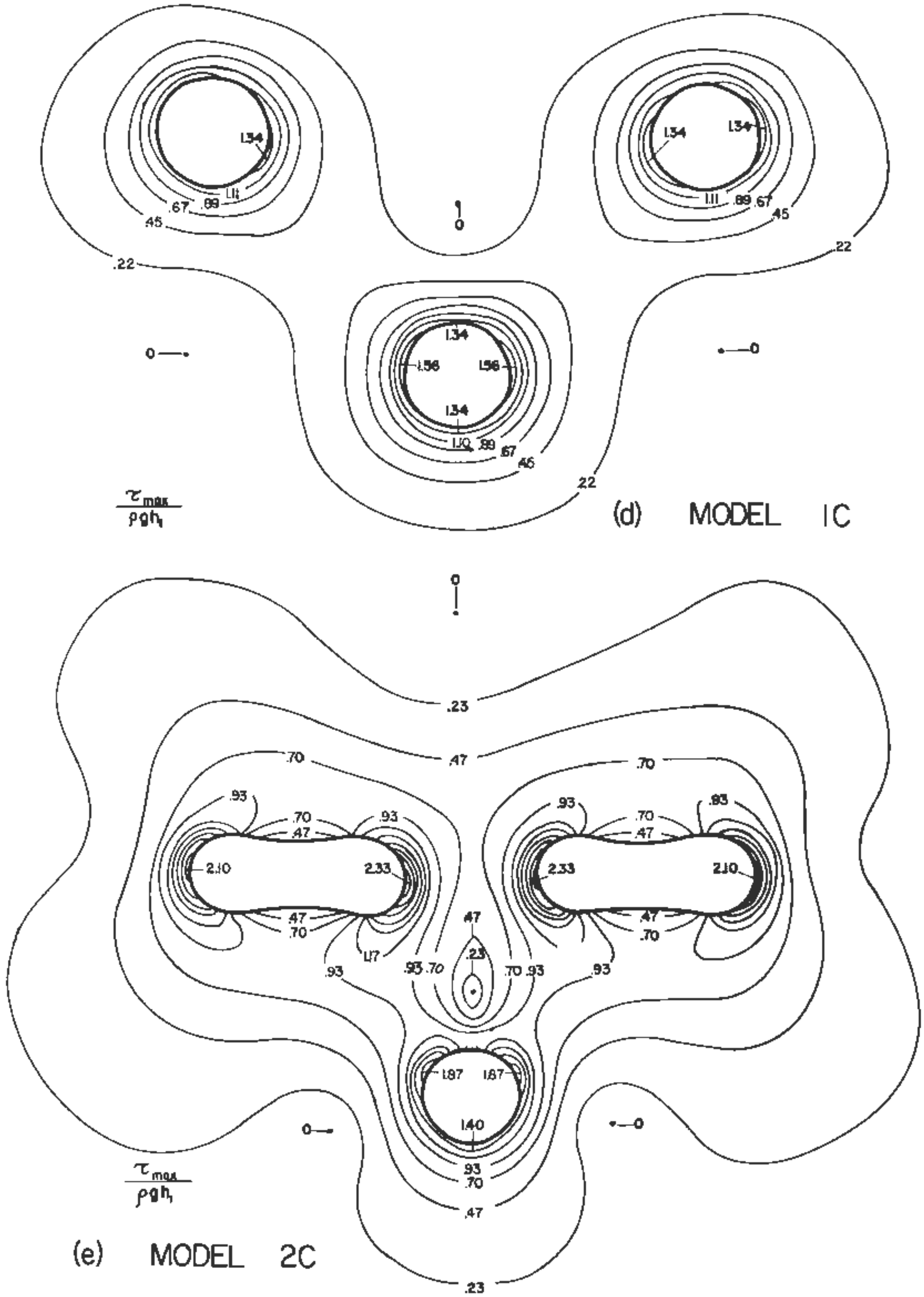

FIGURE 6 (cont'd) – (d) and (e) lines of equal maximum shear stress

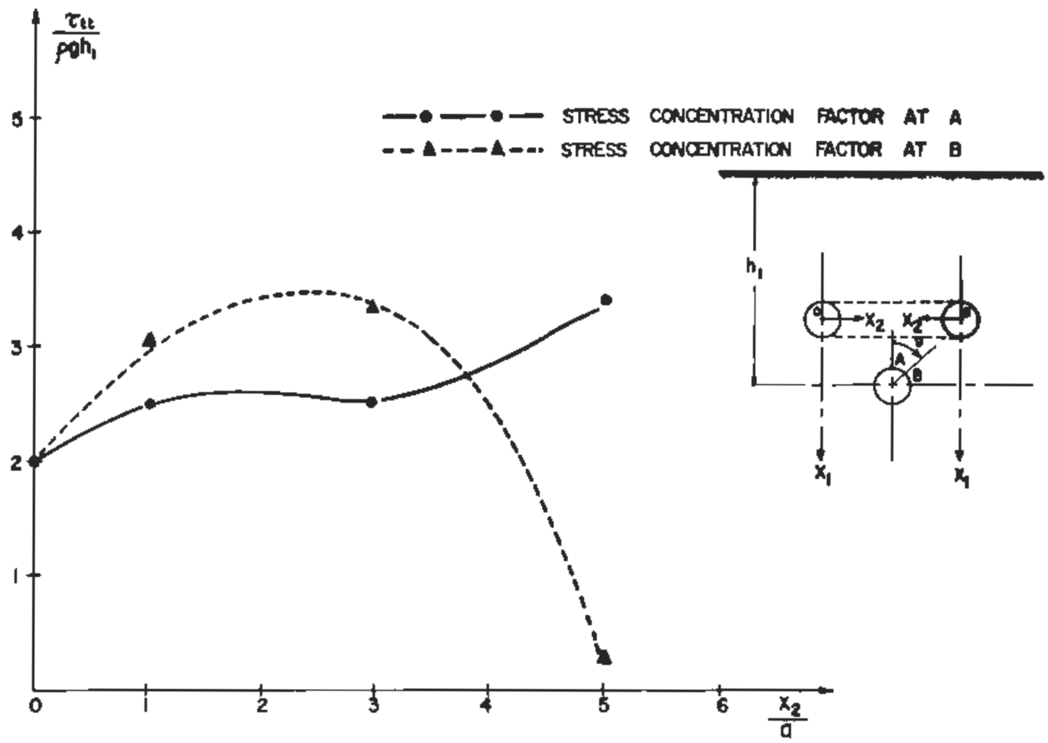

(f) STRESS CONCENTRATION FACTORS OF MODEL SERIES "C"

FIGURE 6 (cont'd) — (f) stress concentration factors of the circular drift

undercutting sequence confirms the expected fact that no rotation of the major axis of the drift occurs.

Conclusions

The history of stress and deformation changes which occur as a consequence of undercutting in block caving have been studied by experimental means. An approximate theoretical solution has also been formulated by using simple concepts of the classical theory of elasticity.

It is concluded that, when applying undercutting sequences (II) and (III), more stable conditions for the openings below the undercut will prevail. Further, undercutting sequence (II) seems to be more desirable than (III), since it is conducive to a gradual change in deformation.

The application of gelatin mixture models in conjunction with photoelastic methods appears to be a suitable technique for the analysis of structures in rock under gravitational loading.

Cognizance must be taken, however, of the inherent limitation of the experimental method resulting from large deformations in the model and the inherent assumption of an hydrostatic initial stress field.

Despite such drawbacks, it is felt that studies of this type allow the investigator to gain some insight into some of the phenomena peculiar to the behavior of mine structures.

References

1. Merrill, R.H. and Johnson, G., 1964. Changes in strain and displacement created by undercutting in block caving. *Proc. 4th Internat. Conf. Strata Control and Rock Mech.* Columbia U. Press.
2. Bolmer, R.L., 1965. *Stresses Induced around Development Workings by Undercutting and Caving. Climax Molybdenum*

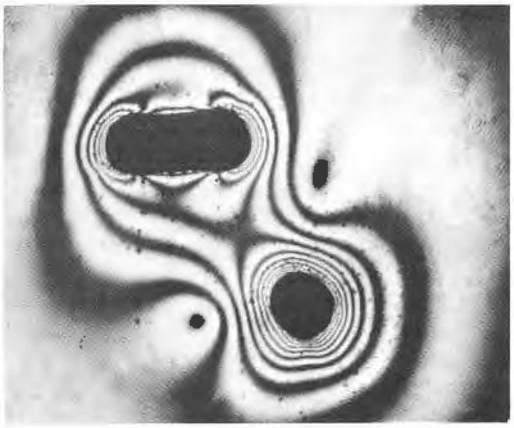

Model 2A (time = 1 hour)

Model 2B (time = 1 hour)

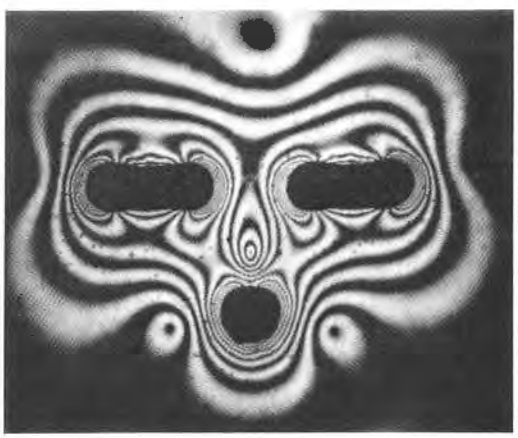

Model 2C (time = 1 hour)

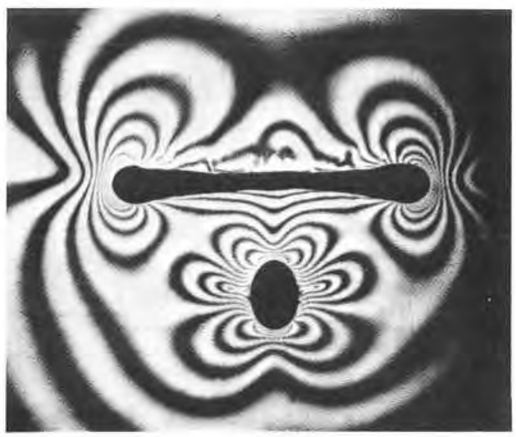

Models 4A,3B,3C (time = 1 hour)

FIGURE 7 – Typical dark-field isochromatic patterns

Mine, Colorado. (In two parts). 2) *Strain and Deformation Measurement.* U.S. Bureau of Mines Rept. of Invest. 6666.

3. Merrill, R.H., 1961. *Changes in Stress Concentrations Created by Undercutting in Block Caving.* U.S. Bureau of Mines Rept. of Invest. 5881.
4. Barla, G. On the stress distribution around adjacent equally or differently shaped openings non-symmetrically located in a rock mass. (In preparation.)
5. Savin, G.N., 1961. *Stress Concentration around Holes.* Pergamon Press.
6. Mindlin, R.D., 1939. Stress distribution around a tunnel. *Proc. A.S.C.E.* April.
7. Barjansky, A., 1944. The distortion of the Boussinesq field due to a circular hole. *Quart. Applied Math.* Vol. 2.
8. Barla, G. and Boshkov, S.H., 1969. Two dimensional photoelastic analysis of gravity loaded rock structures using gelatin mixture models. *Trans. Soc. Mining Engrs.* of A.I.M.E., Vol. 244, No. 1, Mar.

DISCUSSION

D.F. Coates
Mining Research Centre,
Department of Energy, Mines
and Resources, Ottawa.

This is a useful paper as it does, as suggested by the title, provide some additional insights into a practical problem. Furthermore, we know from our experience that the work must have been done very carefully. In attempting to use gelatin for models in our projects, concerned with developing theories for predicting stresses in pillars and in slopes, we found gelatin not to be an easy material to use being somewhat unstable under temperature changes and with the passage of time.

This led us to develop an alternate deformable material that M. Gyenge has named Mirelite (1). However, this new material was not as deformable as gelatin leading us to apply the previously developed concept of "excavation stresses" (2) whereby for a material with a Poisson's ratio close to 0.5 we could obtain the same stress distribution by applying a boundary pressure on the surfaces where the excavation stresses would act. As mercury was used in this reverse loading technique, a high order of isochromatic fringes could be obtained. The results were useful although there were still difficulties in determining maximum fringe orders at boundaries and stress trajectories in areas of low gradients.

Our photoelastic work was quickly superseded by the advent of the finite element method. With the assistance of Y. Yu this technique was used initially to compare the results with the photoelastic work, which showed very good agreement. The technique, as is well known, is fast and has great scope particularly in dealing with heterogeneous materials.

Field work subsequently has substantially confirmed the model results on pillar loadings but has also shown that models can be misleading with respect to the actual conditions. It seems that heterogeneous residual field stress conditions might occur more often than the homogeneous conditions that have to be assumed in simple models and theory. The relating of such residual stresses to the geological structure with the hope of being able to predict more accurately the environment for mining is being pursued at present by Dr. G. Eisbacher, Geological Survey of Canada, and H. Bielenstein the Mines Branch at Elliot Lake.

References

1. Gyenge, M., "Canadian Mining Research Centre Develops New Photoelastic Model Material", *Materially Speaking,* Thiokol Chemical Corp., Trenton, N.Y., Dec. 1968.
2. Coates, D.F., *Pillar Loading. Part I: Literature Survey and New Hypothesis,* Mines Branch Research Report R 168, Oct. 1965, Dept. Energy, Mines & Resources, Ottawa.

Giovanni Barla

The calibration technique used for gelatin mixture models allows one to take into account the dependence of physical and optical properties on time, humidity and temperature variations, and gelatin composition. The fact that gelatin models undergo large deformations in the course of the experiment is a serious detriment of the method if the model must abide by the requirement of the classical theory of elasticity.

The advantage of using the finite element method of stress analysis with respect to two-dimensional photoelastic techniques must be recognized. The finite element method makes

The first phase of the stress measurement project involved the development of suitable gauges and apparatus. Succeeding sections of this paper describe the present state in the evolutionary process of developing instruments and techniques to suit the particular ground conditions encountered at the Sullivan Mine. The data from a number of stress measurement projects are included.

Instruments and Equipment

Instruments

A great deal has been written on the subject of rheology. In addition to exhibiting elastic behaviour, under certain conditions rocks are known to possess both viscous and plastic characteristics. It seems fairly certain however, that hard rock in the normal underground mining environment behaves in an essentially elastic manner. Our approach to the problem of measuring stresses has been therefore based on elastic rock properties. During the course of the program, several verifications of this assumption have been made.

Three basic features are required of the stress measuring system. First, it must produce reliable readings in a great variety of ground conditions. This implies that there must be incorporated checks and means by which the quality of readings can be assessed. It is particularly important when working in fractured ground.

Second, the instruments' stress measuring sensitivity must be high. A precision of a few hundred pounds per square inch is acceptable but one of 1,000 or 2,000 psi is not.

Finally, the entire procedure must be simple enough that a measurement project can be completed in a reasonable length of time. This requirement is brought about by the large volume of work to be done at the Sullivan Mine, and also by the condition that a statistically significant number of individual readings be made at each site. The imposition of this feature creates a distinction between an economic mining tool and one which is of high scientific calibre but at the same time unwieldy under field conditions.

A review of existing literature at the beginning of the program indicated that a gauge which is simply pushed into a borehole and then overcored would best satisfy the requirements. The instrument measures the change in hole diameter as a large bit advances concentrically over the gauge, thereby relieving the stress in the rock surrounding the hole. A knowledge of rock properties and instrument characteristics is used to convert change in hole diameters to stresses originally present in the rock. Initial gauge development was based on concepts published by Griswold (2).

Four factors were incorporated in the design of resistance strain gauge transducers. Unless costly procedures are adopted, all diamond drill holes tend to wander slightly, producing very tightly spiralling grooves and ridges on the hole surface. If a transducer is rigidly fixed to the gauge body, as it is pushed down the hole its passage over these indulations could tend to overstrain the strain gauge. Of course this problem can be avoided by employing compressed air or other pressure systems to pre-strain the transducers once the gauge is in position. However, simplicity in tools used underground is a very great virtue. As an alternative, a floating transducer, not rigidly fixed to the gauge body, avoids this overstrain effect because the hole diameter is very nearly constant at any point along its length. The "C-ring" transducer shown in Figure 1 is of this type.

A second criterion is that the sensitivity of the transducer must be adequate. Following the equations for converting hole diameter change to stress values, outlined by Merrill and Peterson (3), one finds that for a sensitivity of 200 psi in each of the major and minor plane stress values the changes in hole diameters must be measured to within 0.000050 in.

$$S + T = \frac{E}{3d}(U_1 + U_2 + U_3) = 200 + 200 \text{ psi}$$

$$S - T = 0$$

$$400 \text{ psi} = \frac{9 \times 10^6 \text{ psi}}{3\,(1.16 \text{ in.})}\,(3U \text{ in.})$$

$$3U = 155 \times 10^{-6} \text{ in.}$$

$$U = 50 \text{ microinches}$$

Since most strain gauge read-out systems have an accuracy of about 10 microstrain, this means that the single strain gauge must accurately detect one fifth of the diameter change, or the transducer calibration factor (CF) should be:

$$CF = \frac{\text{change in hole diameter}}{\text{corresponding strain reading}} = \frac{50 \text{ microinches}}{10 \text{ microinches/in.}} = 5 \text{ in.}$$

strains are recoverable. Since the transducers are inserted in a pre-strained condition to permit measurement of the normal increases in hole diameter, careful strain gauge mounting techniques are used to eliminate the possibility of creep in the cement.

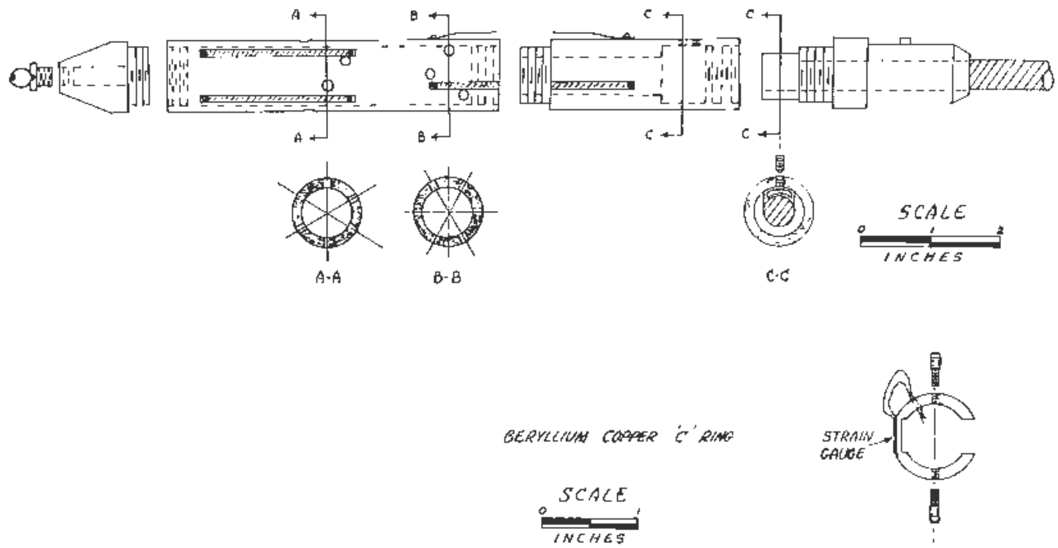

FIGURE 1 — Details of overcoring gauge and 'C'-ring transducer.

Transducer "softness" is another design parameter. The spring effect of the transducer must be relatively small so that it has no effect on hole deformation. The entire assembly also has to be pushed into the hole with ease. Furthermore, the use of soft rings reduces wear on the transducer contact points which slide along the hole and makes it easier to maintain constant pre-strain on the rings without resorting to frequent adjustment.

Ring softness is closely associated with sensitivity, in that the reduced section of the C-ring shown in Figure 1 obviously affects both features. Optimum design was achieved partially on a trial and error basis. Rings with calibration factors in the range of 2 to 10 have been fabricated. If required, it is of course an easy matter to mount an additional strain gauge on the inside of the ring and thereby approximately double its sensitivity by connecting the gauges in a half bridge configuration.

The fourth factor in transducer design is that the unit must be stable, exhibiting no creep effects during the overcoring process. Beryllium copper, or watch spring metal, is used for the rings to ensure that all imposed

Details of the gauge housing are shown in Figure 1. Shielded cable is used primarily to increase the durability under severe conditions, but also to guard against the signal interference if such should exist. The grease nipple at the front of the gauge permits filling the entire assembly with a waterproof grease. It was found that this measure greatly prolongs strain gauge life. One unit was used on a regular daily basis for nearly 18 months before the strain gauges needed renewing.

It will be noted that the six transducers are oriented 30° apart, which permits a good evaluation of the quality of readings. This procedure will be detailed in a later section of the paper.

Drilling Equipment

A standard screw-feed core-drilling machine is used. The rate of bit advance selected is about one inch per minute at a speed of 250 rpm. As indicated in Figure 1, the gauge is inserted in a pilot hole 1.16 in. in diameter. This is drilled with an XRT core bit. The present overcoring bit is an NX casing shoe, 3-in. ID, 3 5/8-in. OD; although a thinwall 6-in.

ID bit with an 18-in. barrel was originally used with an AXWL pilot hole. The drill string consists of standard AX Wire Line rods and a 2 1/2-foot or 5-foot NX casing rod. A special water swivel was designed to permit the passage of cable and insertion rods.

Auxiliary Apparatus

The gauge insertion/extraction tool consists of 7/8 in. square aluminum channel in 5-foot lengths with a device at the end for attaching it to the gauge.

Gauge orientation in the hole is determined by a Brunton reading on the open side of the channel. Since the sections of channel are solidly bolted together, the accuracy of reading is within 2°. This is probably as good as that achieved by a small mercury switch and has the additional advantage that the gauge does not have to be turned to a particular orientation.

Biaxial testing equipment is used to determine the elastic modulus value of the overcore. The cell is similar to that described by Fitzpatrick (4). The overcore is painted with an epoxy coating to prevent hydraulic oil penetration. It was found that a length of biaxial cell equal to one and a half overcore diameters provided a region at the centre where end effects did not influence the modulus values. This is shown diagrammatically in Figure 2.

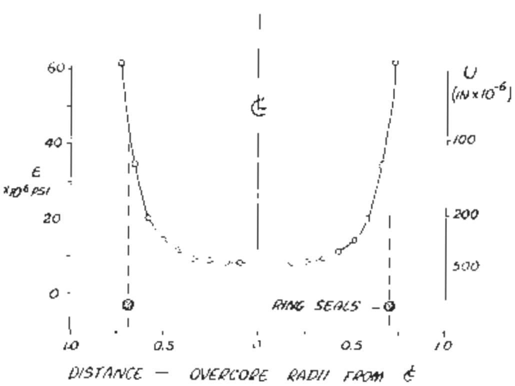

FIGURE 2 — Deformation of overcore under biaxial loading.

Overcoring Techniques

It has been found that stress concentrations similar to those predicted by theory do exist around underground openings. Figure 3 shows four such cases. Examples A and B are from the same location. The former shows the usual pattern, while the latter illustrates the effects of a pronounced fracture upon the stress concentration. Features such as these suggest that it is not always possible to adjust measured stress values near an opening to average field stress conditions by applying a theoretical reduction factor. Furthermore, the extent of the fracture zone around an opening and hence its effective size, are not always easy to determine. From the stress pattern in example C for instance, one suspects that the effective size of the opening is that shown by the dotted outline rather than as seen underground. To avoid the problem of dealing with these stress concentrations, our present practice is to drill a distance equal to one half the opening diameter before attempting any stress measurements.

The pilot hole is then drilled 3 to 5 feet ahead. The core from this small hole is carefully logged for fractures. It becomes very important to distinguish between actual rock fractures and breaks in the core caused by drilling, because much better overcoring success is achieved if the gauge is located in areas free of fractures.

At this point the gauge is inserted in the pilot hole, its orientation is determined, and transducer pre-strain is checked. Two to four thousand microstrain has proven to be an appropriate level of pre-strain. The gauge cable is threaded through the overcoring bit and drill string before the assembly is pushed into the hole. No waiting time is required for the gauges to stabilize. An appropriate length is then overcored. The procedure of overcoring to obtain complete relief on all six transducers is termed a "run". For moderate stress, it has been found that a distance of one overcore hole diameter before the first transducer and the same distance beyond the last transducer is adequate to obtain complete relief and also to avoid measuring the stress concentration ahead of the large hole face.

For stress fields in the order of 10,000 psi it has been found that a couple of extra inches before and after the transducers is required to satisfy these conditions. Upon the completion of a run, the drill string is broken and the insertion rods are pushed inside the string until the instrument is engaged. It is then moved ahead to a pre-selected position in solid ground, and the process is repeated. At the end of several such cycles, ideally about seven runs in a 5-foot length; the drill string, core and gauge are removed from the hole. The maximum depth overcored to date is 30 feet. Although the process would be slower, stress measurements at depths of 50 feet or more would be feasible.

In a full 8-hour shift, in ideal ground conditions, a two-man crew would produce an average of about ten runs. Difficulties caused by fractured ground reduce our current average to somewhat less than half this figure.

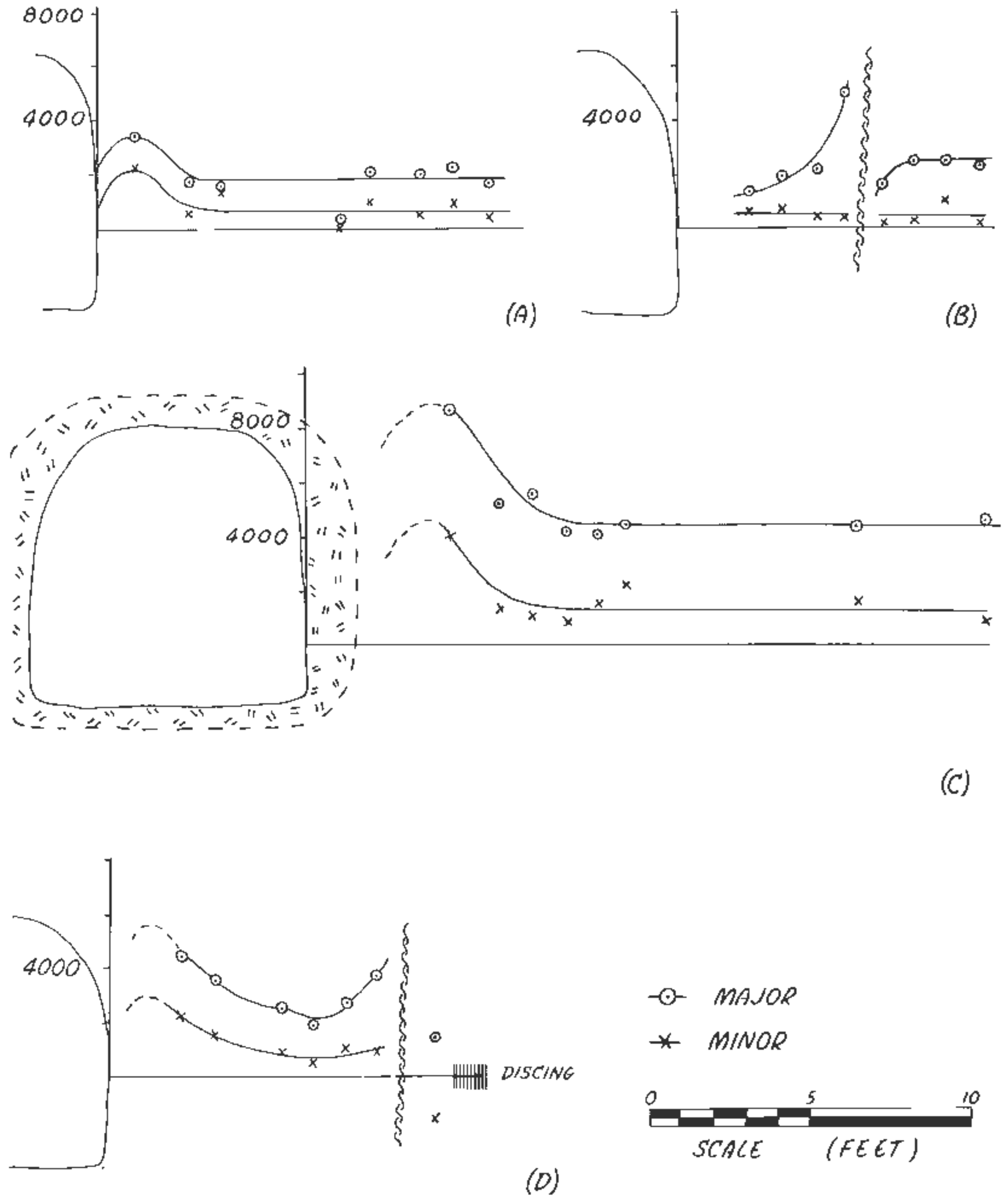

FIGURE 3 — Plane stress data.

During each overcoring run, the transducers are monitored, in rotation, through a switch and balance unit to a portable strain indicator. The normal pattern shows continuous change with bit advance until relief is complete. When a transducer is located on or very near a fracture, it behaves erratically. If the core breaks during a run, wild fluctuations are generally noted on the strain indicator as either the rotating core hits the gauge, or gauge and core rotate through a few revolutions before the drill can be stopped. When this happens, the gauge is usually pushed ahead to solid ground and another run is started. Should a transducer point be located on a crack that tends to separate slightly as overcoring proceeds, extreme strain relief is noted and that particular value becomes suspect. It is given special attention during the data evaluation process. Figure 4 shows a typical overcoring set-up.

Data Treatment

Strain relief patterns from the overcoring run are plotted against distance of bit advance. Two examples are shown in Figure 5. It is apparent that, in example A, strain concentrations caused by the approaching bit are roughly proportional to the eventual total relief at each hole diameter orientation. Transducers 2,4 and 6 show maximum relief shortly after the bit passes over them, the relief then approaches final value. The final change on one or two transducers can be, and often is a negative value. The validity of these seemingly anomalous patterns can be demonstrated by calculating the stresses at increments of bit advance. Example A is typical of readings which are aligned with the major principal stress.

When the orientation of the hole is such that the major principal stress is not perpendicular to it, the patterns are more of the type shown in example B. The hole in this case is

FIGURE 4 – Overcoring run in progress.

oriented at azimuth 311°, inclination +3 1/2°. The major principal stress was found to be oriented at azimuth 313°, inclination + 71 1/2°. A detailed description of this phenomenon was recently given by Bonnechère and Fairhurst (5). These plots of strain relief patterns are invaluable in obtaining the first qualitative check on any overcoring run.

Calibration factors are applied to the final strain relief readings of the six transducers. These data are then used to plot, to an exaggerated scale, the cross-sectional outline of the stress-relieved pilot hole. Depending on the scale used, the best fit outline is an ellipse or a lemniscate figure. It is immediately apparent if one or two transducer readings are incompatible with the rest. This procedure detects erratic readings which would not be apparent, except in extreme cases, when using a three-component gauge. Figure 6 shows two such strain relief outlines. In example A no readings are erratic; in example B some of the points are not on the extrapolated ellipse.

statistical basis. However, reasonably good approximations are obtained with the aid of the following additional check. The sum of readings on pairs of perpendicular transducers should be constant.

$$U_n = \frac{d}{E}\left[(S+T) + 2(S-T)\cos 2\theta_n\right]$$

$$U_{(n+90^\circ)} = \frac{d}{E}\left[(S+T) + 2(S-T)\cos 2(\theta_n + 90^\circ)\right]$$

$$= \frac{d}{E}\left[(S+T) + 2(S-T)(-\cos 2\theta_n)\right]$$

$$U_n + U_{(n+90^\circ)} = \frac{2d}{E}(S+T)$$

$$= U_{(n+30^\circ)} + U_{(n+120^\circ)}$$

$$= U_{(n+60^\circ)} + U_{(n+150^\circ)}$$

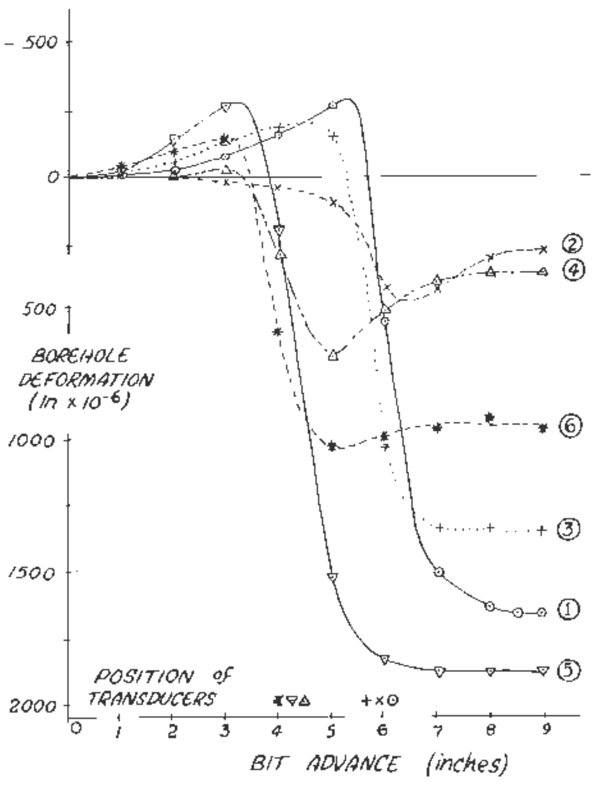

FIGURE 5A — Overcoring strain relief pattern (reading No. 6564-78).

It is recognized that six sets of data are not sufficient to apply corrections on a highly

Figure 7A lists data obtained in a single hole. By applying obvious corrections to the strain ellipse, with assistance from the above relationship, the data in Figure 7B are obtained. Since the stress level is not constant along the hole, there are variations in overcoring readings. To illustrate the small error caused by the fact that the three (U_n + $U_{(n+90°)}$) pairs are not always equal, the data in Figure 7C eliminate the effects of stress variation by equating the mean of each group to the overall mean. The standard deviation is thereby reduced to a very acceptable level. This exercise can be summarized by saying that, in this series of overcoring readings, the total standard deviation of 20% is composed of roughly 5% due to measuring error and 15% due to stress variations.

Elastic modulus values of the rock are required to convert hole deformation measurements to rock stress. Using the biaxial testing apparatus described earlier, one potential problem was anticipated. Since nearly all our overcoring work is done in banded sulphides, it was suspected that rock anisotropy might be so severe that the standard formulae for isotropic material would not apply.

During the course of routine biaxial testing, sufficient data were accumulated to permit an examination of this feature. It has been found that elastic modulus values either parallel to, or perpendicular to the bedding do not deviate from the mean by more than 25%, the average deviation being in the order of 10%. Following the reasoning of Becker and Hooker (6), these variations do not cause appreciable error in stresses calculated under the assumption that the rock is isotropic.

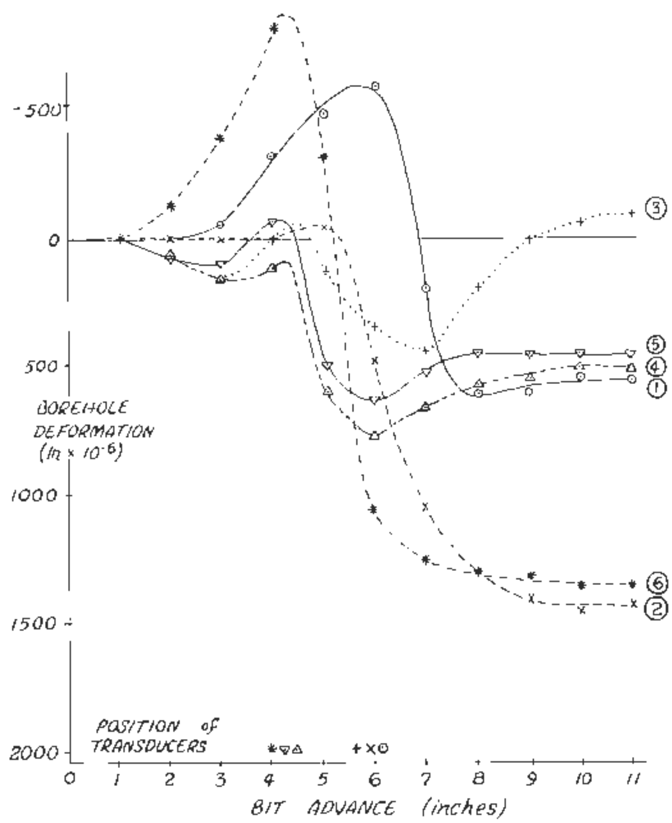

FIGURE 5B — Overcoring strain relief pattern (reading No. 6566-101).

A number of tests were performed on uniaxial specimens to determine the Poisson's ratio of banded sulphides. Again, deviation from the mean value is small. Individual tests are not run on every specimen, the average of a series of tests is used.

After having obtained elastic modulus values on every usable piece of overcore, plane principal stresses are calculated for each overcoring run, using the method first outlined by

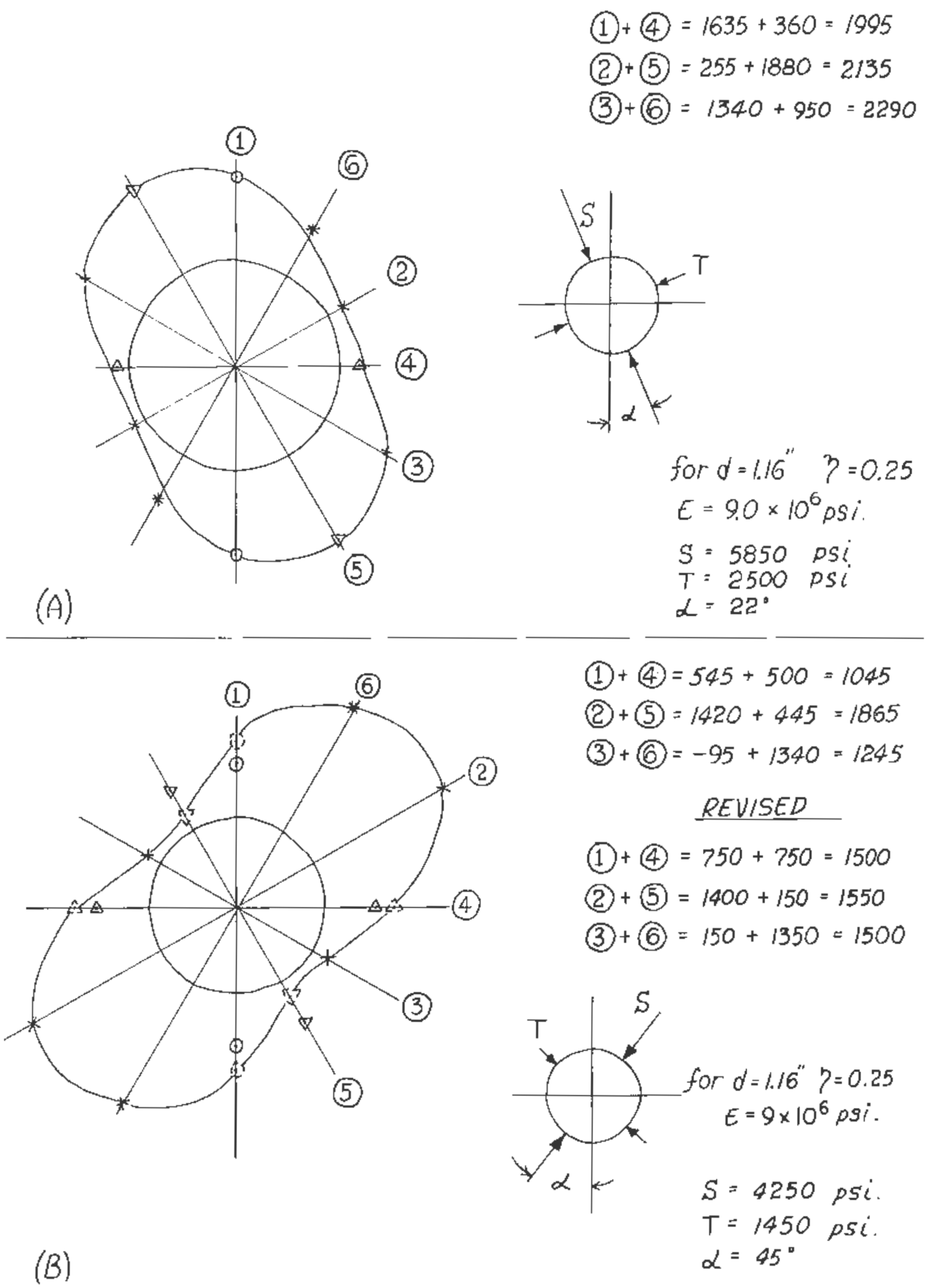

FIGURE 6 — Overcoring strain ellipses.

READING NO.	(A) ORIGINAL			(B) CORRECTED			(C) ADJUSTED TO MEAN STRESS LEVEL		
	U_1+U_4	U_2+U_5	U_3+U_6	U_1+U_4	U_2+U_5	U_3+U_6	U_1+U_4	U_2+U_5	U_3+U_6
6564 -52	1740	1840	2020	1850	1840	1900	2050	2040	2105
-60	2815	2170	2460	2350	2500	2200	2064	2195	1930
-78	1995	2135	2290	1995	2135	2290	1920	2055	2205
-94	1910	2680	3040	2360	2550	2550	1960	2115	2115
-104	2410	2405	2490	2400	2450	2450	2035	2080	2080
-113	2320	2535	1850	2275	2300	2200	2080	2100	2010
-126	1290	1655	1280	1290	1360	1280	2030	2145	2015
-146	1945	1635	1640	1680	1820	1500	2080	2255	1855
	MEAN = 2106 Std. Dev. = 21.7%			MEAN = 2064 Std. Dev. = 19.7%			MEAN EACH GROUP = 2064 Std. Dev. = 4.4%		

FIGURE 7 — Evaluation of overcoring readings.

Merrill and Peterson (3). Conditions of plane stress are assumed. By calculating plane stresses as soon as the readings are taken, an estimate can be made of the number of runs required to give good statistical reliability to the end result.

Plane stress patterns along a hole also serve to define zones of stress concentration within the rock mass. It is particularly important to define high stress differentials across fractures, since these features usually give warning of impending difficulties in mining.

Following completion of a minimum of three overcoring holes, with a minimum of five runs per hole, the data are assembled for computer processing. The computer program was developed on the basis that a uniform state of stress exists in a body of elastic, homogeneous, isotropic rock encompassed by the array of overcoring holes. It defines a three-dimensional state of stress which best fits the data supplied. The methods used are similar to those outlined by Panek (7), Leeman (8), and Gray and Toews (9). Essentially, for five overcoring runs in each of three holes, the computer solves 90 simultaneous equations in six unknowns. These latter are the three normal and three shear stress components referred to a standard coordinate system. Principal stresses and their orientations are then computed from the six stress components.

Except where work has been confined to one side of a pronounced pillar discontinuity, the computed principal stress values are said to represent the average state of pillar stress.

Stress Measurement Data

The following table, Figure 8, includes the three-dimensional pillar stress data obtained to date. Several early pillar overcoring projects comprised only two holes or two pairs of parallel holes, which configuration of course is not sufficient for three-dimensional analysis. The data in Figure 8 represent stress conditions in pillars totalling about three million tons of ore.

The quantity "Standard Deviation of Regression" gives a combined evaluation of four parameters: the uniformity of the stress field, variation of hole orientations from the ideal, quality of overcoring readings, and the sensitivity of the stress measuring system. The effect of the latter can be ascertained from the "Ideal Case" listed at the end of the table. In this example, effects of the first three parameters above were eliminated by selecting arbitrary values for each of the six stress components, referred to the usual coordinate system north-east-vertical. From these data, diametral deformations at arbitrarily selected orientations in three orthogonal holes were calculated. These values were then rounded off to the normal degree of precision obtained in overcoring readings. The standard deviation of regression derived is thus an evaluation of transducer precision.

By comparing this value of 114 psi with those reported in Figure 8, it will be noted that most of the pillar stress determinations have a quite acceptable standard deviation of regression. A few selected examples of this type, as well as the exceptions, will be considered in detail in the remainder of this section.

R-9-1 Project

The data in Figure 9 are generally typical of the majority of such projects. The ground is quite solid and therefore the stress field is reasonably uniform. Sufficient time was available to obtain a good number of readings. After

PILLAR	S.D.R. *	S_1 P.S.I.	S.E.S S_1	AZIMUTH S_1	INCL. S_1	S_2 P.S.I.	S.E.S S_2	AZIMUTH S_2	INCL. S_2	S_3 P.S.I.	S.E.S. S_2	AZIMUTH S_3	INCL. S_3
R-9-1	353	4650	103	313°	71°	2290	122	92°	14°	580	207	185°	12°
S-8-1	647	2860	171	199°	63°	2210	528	357°	25°	630	223	92°	9°
S-9-1	239	1440	81	316°	68°	540	140	218°	3°	50	91	126°	22°
T-9-1	506	2270	109	40°	88°	1610	137	257°	1°	-630	385	167°	1°
T-10-30	485	2190	118	322°	81°	1070	213	96°	7°	280	171	187°	7°
U-9-1	324	2390	69	281°	76°	1440	176	166°	6°	930	84	75°	13°
U-10-30	387	1850	144	35°	15°	490	99	251°	72°	-10	200	127°	10°
V-11-1(B)	2554	7170	1160	93°	80°	6110	1555	238°	8°	-3850	4076	328°	5°
(A)	2145	5700	580	30°	22°	4600	610	212°	68°	-18700	3360	120°	0°
4-52	574	4510	146	121°	59°	2060	143	337°	26°	1270	367	239°	16°
4-58,60	704	5490	493	217°	65°	1710	375	330°	11°	-5100	2270	65°	22°
5-52	730	7290	550	200°	10°	4990	272	339°	77°	1400	464	109°	9°
IDEAL CASE	114	3220	69	60°	70°	1200	138	234°	20°	40	91	324°	2°

* S.D.R. STANDARD DEVIATION of REGRESSION (PSI).
S.E.S. STANDARD ERROR of STRESS (PSI).
INCL. INCLINATION.

FIGURE 8 — Overcoring data.

the three-dimensional stress state is calculated, a computer sub-routine is used to work back and calculate the "best fit" plane stresses S and T for each of the holes.

S-9-1 Project

Figure 10 lists the results of a rather hurried project. Although the number of readings is limited, the stress sampling is considered adequate because the stress field is again reasonably uniform.

V-11-1 Project

The actual overcoring data are listed in Figure 11A. This pillar was quite solid and competent. However, numerous incipient fractures caused core breaks as drilling progressed. In areas where there were few incipient fractures, core discing occurred.

It was therefore difficult to obtain reliable stress readings, and the stress field being sampled varied considerably between fractures. The tabulated standard errors of stress of the six stress components indicate that the results obtained are not suitable for analysis on the basis of a homogeneous stress field.

In an attempt to reduce the greater scatter of readings, each overcoring run was re-assessed. One set of readings was selected as being representative of each hole. In the first hole, the last two pairs of readings were considered more valid than the first two pairs and so an average of the former was taken. The first two runs in the second hole appeared more suspect than the third, so the latter was used to represent the hole. A straight arithmetic average was again made in the third hole. The results of this very arbitrary procedure appear in Figure 11 B as well as in Figure 8. The degree of improvement is questionable, except that the 12,500 psi tensile stress is eliminated from the first computation. This exercise confirmed that the stress field was much too inhomogenous for any meaningful average pillar stress calculations to be made.

This project was summarized by saying that the pillar stress was high. Individual major plane stress values ranged from 1,500 psi to 16,000 psi, with several in the 8,000 to 12,000 range. Furthermore, a number of runs showing early indications of high readings could not be completed because discing occurred. Considering these facts in assigning a quantitative value to the average major principal pillar stress, the figure 10,000 psi was chosen as probably being more representative than 5,000 or 15,000 psi.

While this project is admittedly of doubtful scientific value, it afforded a distinction between two types of mining phenomena, a distinction which had a significant effect upon the mining method used. Poor ground conditions in a particular location within a pillar can either be caused by a general high pillar load and consequent deterioration or it can be caused by the localized effects of a major

E PSI x 10^6	ORIENTATION U_1 WRT. HORIZ.	U_1	U_2	U_3	U_4	U_5	U_6
HOLE 1 AZIMUTH 352.0° INCLINATION 1.5°							
BEST FIT S= 4180 PSI T= 2190 PSI							
8.42	61.0°	925	280	1495	815	1560	525
8.4	85.0°	2065	520	1545	750	1650	915
8.37	75.5°	1630	260	1340	365	1875	950
8.38	88.0°	1550	560	1180	360	2120	1860
8.4	175.0°	430	1405	1275	1980	1000	1215
8.40	97.0°	2040	535	980	280	2000	870
8.4	54.5°	405	360	1215	885	1295	65
8.4	75.0°	1765	120	1180	180	1515	460
HOLE 2 AZIMUTH 37.5° INCLINATION 10.5°							
BEST FIT S= 4260 PSI T= 1560 PSI							
9.2	64.0°	970	200	1000	750	1270	425
9.20	76.0°				590	1430	195
9.77	80.0°				430	1140	260
9.23	71.0°	545	240	1115	635	935	130
9.2	83.0°				45	535	165
HOLE 3 AZIMUTH 311.2° INCLINATION 3.5°							
BEST FIT S= 3910 PSI T= 1030 PSI							
7.6	94.0°	1630	480	310	-225	1110	1700
7.62	85.0°	1660	360	-155			
7.6	102.0°	545	1420	-95	500	455	1340
7.6	65.0°	1085	0	280	-350	1045	525
7.6	67.0°	815	200	590	-225	1070	455
7.6	75.0°				90	1740	260
		σ_x	σ_y	σ_z	τ_{xy}	τ_{yz}	τ_{xz}
		2407	774	4344	-259	818	-496
STANDARD ERROR OF STRESS :		(223)	(539)	(182)	(222)	(203)	(127)

HOLE DIAMETER = 1.16"
POISSON'S RATIO = 0.25

FIGURE 9 — R-9-1 Overcoring results.

fracture. This latter feature, while affecting the rock in its immediate vicinity, may have relatively little influence on the bulk of the pillar. As outlined in an earlier paper (1), the principle of overcutting the pillar eliminates the difficulties in this type of situation.

In the case of the pillar under discussion, it is certain that extensive overcut development could not have been driven and maintained with any degree of economy. Alternate methods were used to successfully mine this pillar. Fortunately, the conditions encountered

E PSI X 10^6	ORIENTATION U_1 WRT. HORIZ.	U_1	U_2	U_3	U_4	U_5	U_6
HOLE 1 AZIMUTH 2.4° INCLINATION 4.8° BEST FIT S = 1220 PSI T = 140 PSI							
9.7	97.0°	800	270	145			
HOLE 2 AZIMUTH 45.5° INCLINATION 3.5° BEST FIT S = 1325 PSI T = 40 PSI							
9.7	81.0°	1120	-360	580			
9.7	90.0°	500	-90	385			
9.7	90.0°	650	-180	580			
9.7	75.0°	750	0	630			
9.7	82.0°	575	-625	775			
HOLE 3 AZIMUTH 316.4° INCLINATION 4.0° BEST FIT S = 1110 PSI T = 500 PSI							
9.7	101.5°	550	-45	290			
9.7	102.0°	120	270	100			
9.7	120.0°	220	180	100			
HOLE 4 AZIMUTH 23.3° INCLINATION 4.0° BEST FIT S = 1290 PSI T = 40 PSI							
9.7	88.0°	320	-180	290			
9.7	92.5°	570	-360	290			

	σ_x	σ_y	σ_z	τ_{xy}	τ_{yz}	τ_{xz}
	328	457	1240	134	325	-356
STANDARD ERROR OF STRESS :	(285)	(449)	(143)	(137)	(140)	(109)

HOLE DIAMETER = 1.91"
POISSON'S RATIO = 0.25

FIGURE 10 – S-9-1 Overcoring results.

represent an isolated case which has not been repeated.

5-52 Project

The data in Figure 12 were obtained over a total elapsed time of about six months. While no significant stress changes due to mining activity were expected, it is possible that the moderate degree of scatter in the readings is partially due to a changing stress field.

Virgin Stress Field

A project to measure rock stress in an area undisturbed by mining has been in progress for

E PSI x 10^6	ORIENTATION U_1 WRT. HORIZ.	(A) ORIGINAL READINGS U_1	U_2	U_3	(B) REVISED READINGS U_1	U_2	U_3
HOLE 1 AZIMUTH 103.1° INCLINATION 0.4°							
(A) BEST FIT S = 6110 PSI, T = 1030 PSI					(B) BEST FIT S = 6760 PSI, T = 1050 PSI		
7.5	96.5°	3660	505	570			
7.5	83.0°	1430	-605	715			
7.5	64.0°	2860	-405	1140	1580	-405	1140
7.5	64.0°	305	-405	1085			
HOLE 2 AZIMUTH 131.0° INCLINATION 0.8°							
(A) BEST FIT S = 7820 PSI, T = 6850 PSI					(B) BEST FIT S = 7340 PSI, T = 5600 PSI		
7.5	61.0°	5290	7830	8180			
7.5	101.0°	5065	3770	820			
7.5	83.0°	7335	3490	2910	7330	3490	2910
HOLE 3 AZIMUTH 175.8° INCLINATION 0.4°							
(A) BEST FIT S = 6700 PSI, T = 4180 PSI					(B) BEST FIT S = 7280 PSI, T = 4250 PSI		
7.5	91.0°	4640	1510	3090	4280	1440	2770
7.5	100.0°	3915	1370	2450			

	σ_x	σ_y	σ_z	τ_{xy}	τ_{yz}	τ_{xz}
(A)	-12500	-700	4740	10600	500	-90
STANDARD ERROR OF STRESS :	(10660)	(2150)	(1730)	(4770)	(900)	(1580)
(B)	3450	-1070	7050	4395	-820	670
STANDARD ERROR OF STRESS :	(4400)	(6150)	(2380)	(5903)	(2090)	(2130)

HOLE DIAMETER = 1.91"
POISSON'S RATIO = 0.25

FIGURE 11 — V-11-1 Overcoring results.

several months. The site selected is a drift several hundred feet down dip from the farthest stoping front. The depth of overburden at this location is about 2,000 feet. The work has been delayed somewhat by higher priority overcoring in areas that will be mined in the near future.

Preliminary results in the first two holes indicate approximate average major and minor plane stress values of 6,000 and 5,000 psi.

ϵ PSI X 10^6	ORIENTATION U_1 WRT. HORIZ.	U_1	U_2	U_3	U_4	U_5	U_6
HOLE 1 AZIMUTH 74.7° INCLINATION 3.0° BEST FIT S = 4980 PSI T = 4580 PSI							
11.7	84.5°	1260	1280	600	720	650	1520
11.7	81.0°	2070	610	1410	710	2250	1030
HOLE 2 AZIMUTH 48.8° INCLINATION 7.0° BEST FIT S = 4360 PSI T = 2210 PSI							
9.9	85.0°	2800	645	930			
9.9	73.0°	2745	-270	1160			
9.9	99.0°	3900	895	500			
9.9	84.0°	800	1320	545			
9.9	94.0°	1700	1600	1820			
HOLE 3 AZIMUTH 140.5° INCLINATION 5.0° BEST FIT S = 5490 PSI T = 4490 PSI							
12.0	91.0°	50	1700	910			
12.0	93.0°	450	1510	1180			
12.0	97.0°	1200	1980	2090			
HOLE 4 AZIMUTH 102.2° INCLINATION 3.7° BEST FIT S = 6930 PSI T = 4860 PSI							
13.5	110.0°	560	415	1320	880	1010	190
13.5	103.0°	495	630	1950	1450	1245	315

	σ_x	σ_y	σ_z	τ_{xy}	τ_{yz}	τ_{xz}
	2134	6572	4980	1812	-196	-647
STANDARD ERROR OF STRESS:	(1772)	(1440)	(530)	(525)	(421)	(531)

DIAMETER HOLES 1,4 = 1.16"
DIAMETER HOLES 2,3 = 1.91"
POISSON'S RATIO = 0.25

FIGURE 12 — 5-52 Overcoring results.

Conclusions

This paper has described one particular method of stress measurement. It has concentrated on the tools and techniques developed at the Sullivan mine to suit our particular conditions and requirements, as they exist at present. The main features of the system include simplicity of operation and ruggedness, and incorporated checks on data quality.

References to theoretical considerations, upon which stress measurement is based, have been avoided as much as possible. This aspect is more than adequately covered in existing rock mechanics literature.

The measurement of mining stresses has proven to be an extremely valuable aid to a better understanding of rock behaviour. Consequently, it has provided much of the information needed to optimize mining methods.

This paper has outlined how a scientific approach to ground behaviour can be used directly in everyday mining practice. There is every reason to expect that similar techniques can be successfully applied at other mines, provided that the need for such information exists.

Acknowledgments

The author expresses his appreciation to the management of Cominco Ltd. for permission to publish this paper. Valuable contributions to the project have been made by present and past members of the Rock Mechanics Section, Sullivan Mine. The assistance of D.C. Jackson, who did most of the overcoring work, is acknowledged.

M.J. Royea

Education — B Sc math. and physics, Mount Allison University, 1960; B Eng., mining, McGill University, 1964; M Eng., mining, rock mechanics, McGill University, 1967.

Employment Summary — 1960-65, miner, mineral dressing researcher, geological exploration and mine planner in northern areas of Ontario, Quebec and Manitoba; 1965 to the present, program director of applied rock mechanics program, at Sullivan Mine, Cominco.

References

1. **Royea, M.J., and Davies, K.G., 1968.** Rock mechanics applied to the extraction of pillars at the Sullivan Mine, *Bull. Can. Inst. Min. and Met.*, v. 61, Oct.
2. **Griswold, G.B., 1963.** How to measure rock pressures: new tools and proved techniques aid mine design, *Eng. and Min. J.*, v. 164, Oct.
3. **Merrill, R.H., and Peterson, J.R., 1961.** *Deformation of a borehole in rock*, U.S. Dept. of the Int. BuMines RI5881.
4. **Fitzpatrick, J., 1962.** *Biaxial device for determining the Modulus of Elasticity of Stress Relief Cores*, U.S. Dept. of the Int., BuMines RI6128.
5. **Bonnechère, F., and Fairhurst, C., 1968.** Determination of the regional stress field from "doorstopper" measurements, *J. S. Af. Inst. Min. and Met.*, v. 68, July.
6. **Becker, R.M., and Hooker, V.E., 1967.** *Some Anisotropic Considerations in Rock Stress Determinations*, U.S. Dept. of the Int., BuMines RI6965.
7. **Panek, L.A., 1966.** *Calculation of the Average Ground Stress Components from Measurements of the Diametral Deformation of a Drill Hole*, U.S. Dept. of the Int., BuMines RI6732.
8. **Leeman, E.R., 1967.** The borehole deformation type of rock stress measuring instrument, *Int. J. of Rock Mech. and Min. Sci.*, v. 4.
9. **Gray, W.M., and Toews, N.A., 1967.** *Analysis of Accuracy in the Determination of the Ground Stress Tensor by Means of Borehole Devices*, Dept. Energy, Mines & Res., Mines Br. Rept. FMP 67/28-MRL.

Rock Mechanics in Damsite Location

E.W. Brooker,
Consulting engineer,
Edmonton, Alta.

I.H. Anderson,
Head, Development Planning,
Water Resources Division,
Alberta Department of Agriculture,
Edmonton, Alta.

Abstract

The development of water resources in Alberta will require a number of major engineering projects. Many of these projects will be constructed in Cretaceous rocks. In order to deal with the investigation and analysis of rock mechanics problems inherent in dam, tunnel, and spillway construction, an approach has been developed.

Problem areas have been defined and the geological and engineering factors pertinent to them are considered. Major aspects include the dam embankment as influenced by subsurface detail, abutment stability, and permeability of the rocks. In each case a means of attacking the problem is proposed. It is concluded that theoretical methods are very limited and that a rational analysis must be based on observed behaviour. It was found that an urgent need exists for a simple rock classification system.

Introduction

William Pearce, a noted early advocate for the development of water resources in Alberta, in 1919 first proposed the diversion of the North Saskatchewan and the Red Deer River into east central Alberta. Since this time various agencies have investigated his proposal, and recently detailed investigations have been undertaken by the Water Resources Division of the Alberta Department of Agriculture. In order to accomplish this development, not only must the North Saskatchewan and the Red Deer rivers be considered but also the Athabasca and Peace rivers. To make this development a reality, nine major dam and tunnel projects, which must be founded in Cretaceous bedrock materials, will be required.

Over the past two years, investigations have been focused on the central Alberta portion of the development plan. Figure 1 shows the location of two projects – the Rocky Mountain House damsite on the North Saskatchewan River and the Ardley damsite on the Red Deer River. A preliminary foundation investigation has been completed on the Rocky Mountain House site and a study of the feasibility of diverting a portion of the North Saskatchewan into the Red Deer River is now underway. Detailed foundation investigations and engineering studies have been concentrated on the Ardley site and these studies form the basis for this contribution.

Approach to Analysis

Many of the problems found at dam and tunnel sites are in the field of rock engineering. During the period of this study, the following working philosophy regarding rock engineering has been developed. Rock engineering involves the application of engineering mechanics, knowledge of geologic processes and materials, and the application of documented rock performance. In order to apply the theories from engineering mechanics, knowledge of the physical properties of rock must be available. In addition, the gross nature of the rock mass must be known in order to produce a realistic prediction of behaviour.

Based on these considerations, a damsite investigation is approached from two points of view:

(1) A consideration of the physical properties of intact rock, largely for classification purposes and for providing values for use in predictive theoretical equations.
(2) A definition of the character of the rock mass in relationship to the proposed new environment.

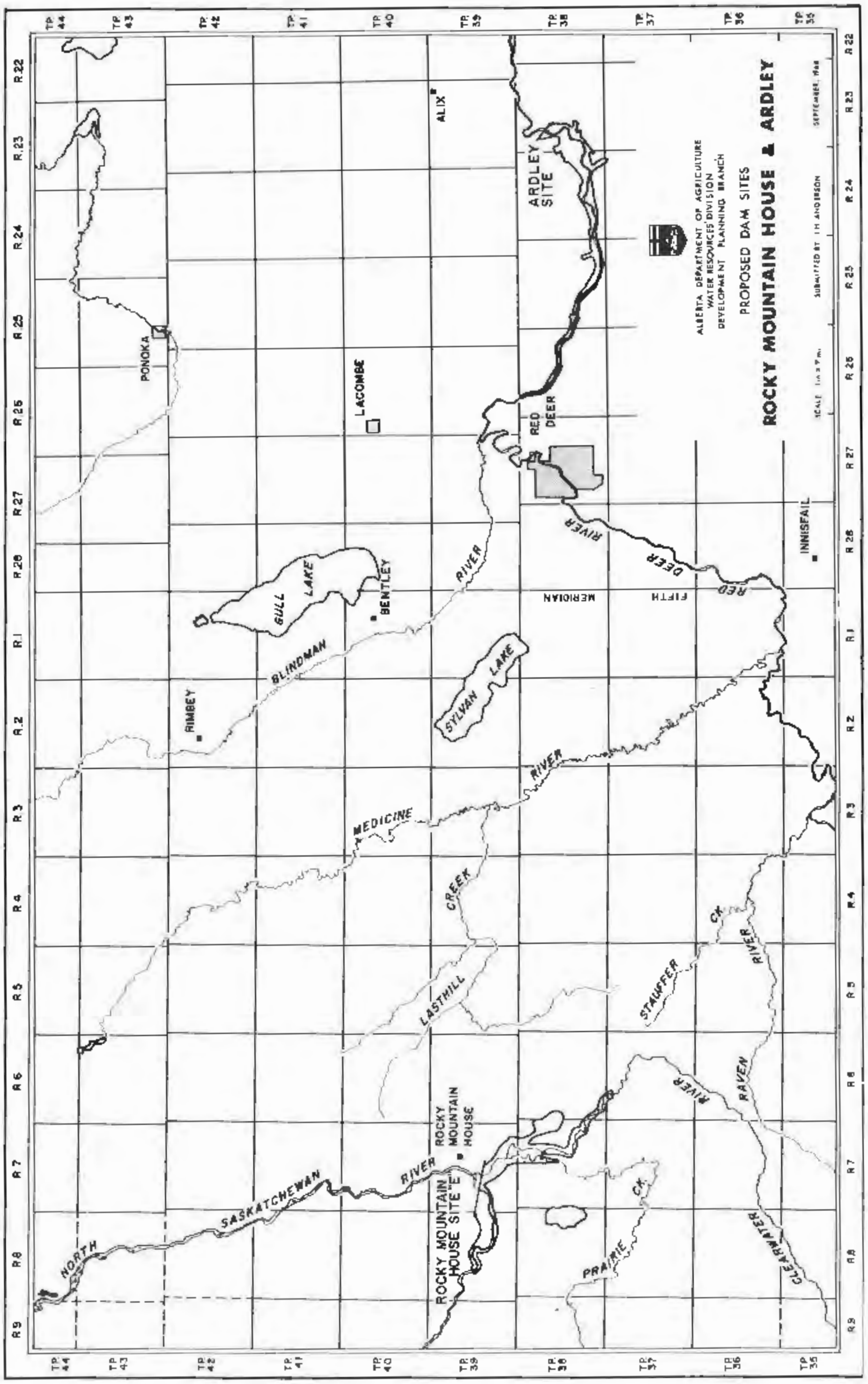

FIGURE 1 – Proposed dam sites – Rocky Mountain House and Ardley.

Attempts to apply theories alone directly to these situations have been of marginal value. The most valuable analytical procedure has been based on knowledge of performance as noted from field observations which were analyzed and organized on a scientific basis. The organization of this concept is demonstrated in Figure 2.

Problem Areas

Complications arise in the application of the concepts outlined. Most of the difficulties result from the need for an orderly means of organizing and analyzing data.

An area which has received much recent consideration is rock classification. Attempts were made, at an early stage in the investigations, to create a workable classification system based on simple index tests. The Panama hardness scale, illustrated in Table 1 was found useful. In addition to this, a standard pocket penetrometer and one modified so that the penetration needle had one tenth the usual area was used. This permitted an arbitrary measure of consistency, and provided a reasonable basis for the preliminary classification of soft rock.

A typical borehole log using the indices from these simple tests, as illustrated in Figure 3, provides a reasonable basis for the preliminary classification of soft rock. Attempts to utilize other aids such as the Rock Quality Designation (RQD) have been unsuccessful due to questionable sampling methods. Other methods described by Deere *et al.* (1967) and Coates (1964) are only marginally applicable to the materials under consideration. A simple and functional classification system remains a prime need. It is believed that recent attempts at the development of a rational system are helpful, but still require refinement for use in civil engineering, and, that too much attention has been given to minerologic and textural characteristics and too little to simple index tests together with broad genetic terminology.

The Ardley Damsite – Nature of Deposits

The Ardley damsite is located on the Red Deer River near Alix. The main elements of the project are the dam embankment, diversion tunnel and outlet works, and the spillway. Detailed maps of the site showing test hole locations and the orientation of the major components of the project are given in Figures 4A and 4B. A geologic section through the area is illustrated in Figure 5 and a detailed section of the damsite is given in Figure 6. The materials present are Upper Cretaceous sandstones and shales interbedded with coal and bentonite seams. A detail of the variation in material which occurs in the Edmonton formation is given in Figure 7. This figure shows an

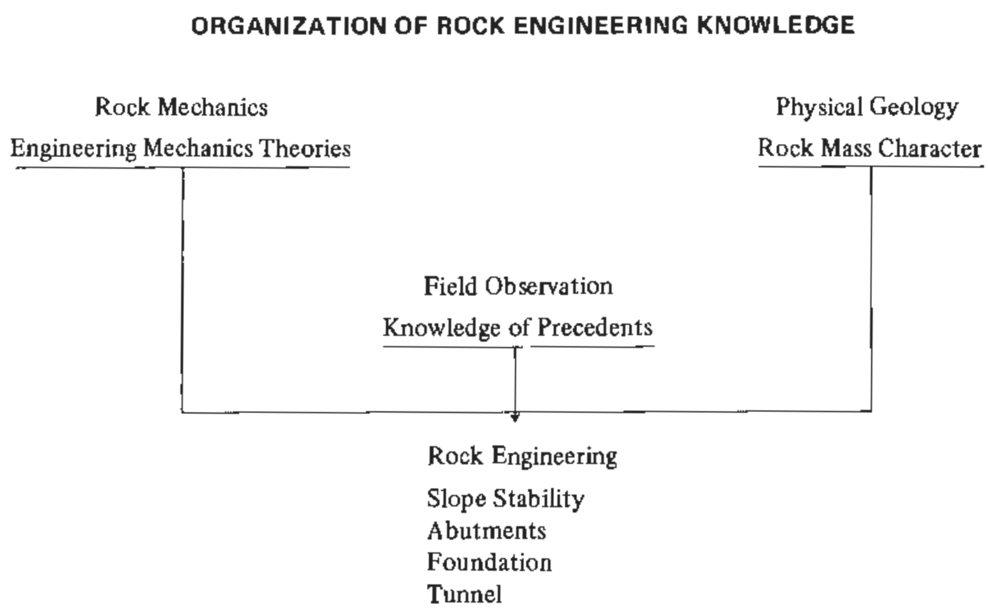

FIGURE 2 – Organization of rock engineering knowledge

TABLE 1

Hardness Scale Used in Material Classification

(Panama Hardness Scale)

OVERBURDEN

		Pocket Penetrometer tons/ft^2
OH–1	Easily squeezed through fingers. Consistency of fresh putty. (Muck, some clays.)	0 – 2
		Modified Pocket Penetrometer tons/ft^2
OH–2	Cannot be squeezed readily through the fingers, it is easily indented with the finger point at moderate pressure.	2 – 10
OH–3	Nonpenetrable at moderate finger pressure. A pencil point can be readily pushed into sample.	10 – 20
OH–4	Difficult to take drive sample. Difficult to punch pencil point into sample.	20 – 30
OH–5	Material of near rock character.	30 – 40

ROCK

RH–1	Slightly harder than very hard overburden, rock-like character but crumbles or breaks easily by hand. (Some clay-shales and uncemented sandstones and agglomerates.)	40 – 45
RH–2	Cannot be crumbled between fingers, but can be easily picked with light blows of the geology hammer. (Some shales and slightly cemented sandstones and agglomerates.)	45 +
RH–3	Can be picked with moderate blows of geology hammer. Can be cut with knife.	
RH–4	Cannot be picked with geology hammer, but can be chipped with moderate blows of the hammer.	
RH–5	Chips can be broken off only with heavy blows of the geology hammer.	

exposure of sandstone (RH2) overlying crushed shales (OH4). In cores, even more dramatic variations in lithology have been noted, as demonstrated by Figure 8 which shows a bentonite layer extruded laterally during a compression test and demonstrates the possibility of vast differences in stress-strain behaviour in the two materials.

Stress-strain curves for a sandstone and a shale in unconfined compression are given in Figure 9. It is obvious that there is a great difference in both modulus of elasticity and compressive strength. These materials constitute the practical extremes which are encountered at the site and it is important to realize that they are found adjacent to each other. It is a disturbing fact that the detail of variations may not be discovered from the results of ordinary boring and sampling procedures due to loss of recovery. This fact has a major influence on the confidence placed in slope stability and other theoretical design considerations.

Geologic Factors Requiring Consideration

In all engineering work which is concerned with real rock masses the geologic features outlined in Table 2 must be considered relative to both the existing and intended change in environment.

At the Ardley site the occurrence of major faults is questionable as there is little evidence of tectonic activity. The rocks, however, are jointed and strongly bedded as demonstrated in Figure 7B. Jointing is generally dominant in the sandstones and consists of two sets, spaced about 3 ft at right angles to each other. The joints are believed to be relatively tight as only a small amount of water intake was noted during pressure tests conducted in the field.

Piezometric heads of varying magnitude are encountered in the different strata. The sandstones appear to bear little groundwater. However, coal seams, which are common to the formation, are water bearing. It is believed that there is no readily definable groundwater pattern but this will require further attention during forthcoming field studies.

Problem Areas of the Damsite

There are four major problem areas which must be considered in detail: tunnels, embankment considerations, stability of abutments, and permeability of foundation and abutments.

1. Tunnels

The diversion facilities will involve three tunnels of 22-ft bore and total length of 6,000 ft. At the faces of the proposed tunnels, it is probable that sandstones of relatively high

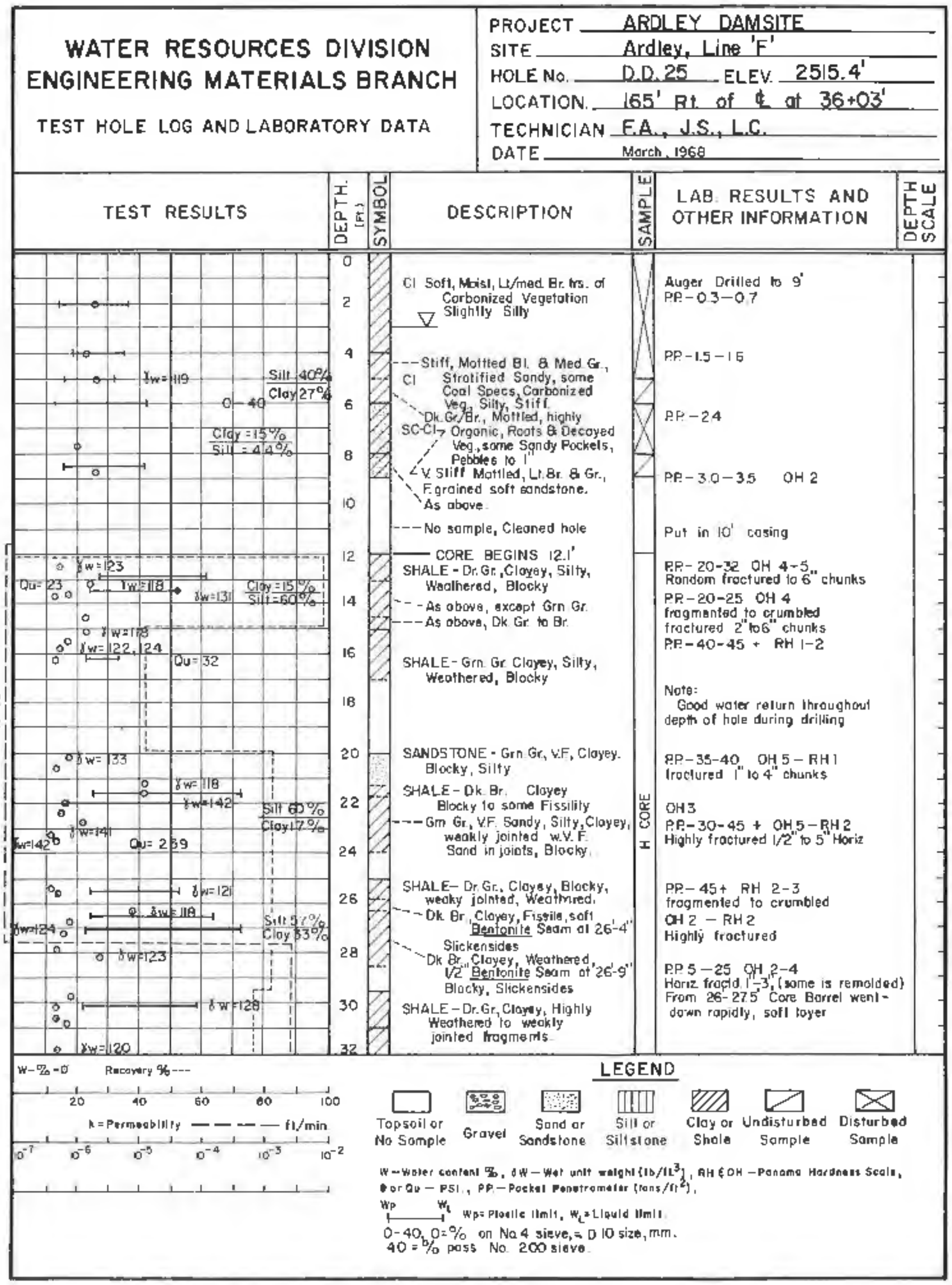

FIGURE 3 — Test hole log and laboratory data.

strength, crushed shale, bentonite layers or coal will be encountered. Because of the extreme variations in lithology and hardness, the use of a mechanical mole to accomplish the bores is questionable. Under these circumstances the ability of mechanical equipment to perform well is in question. These variations also control the amount and type of tunnel support which may be needed, and as a consequence, the construction time and cost. This part of the project is a major cost area and is the subject of further detailed consideration. It is hoped that the construction needs will be defined as a result of such studies.

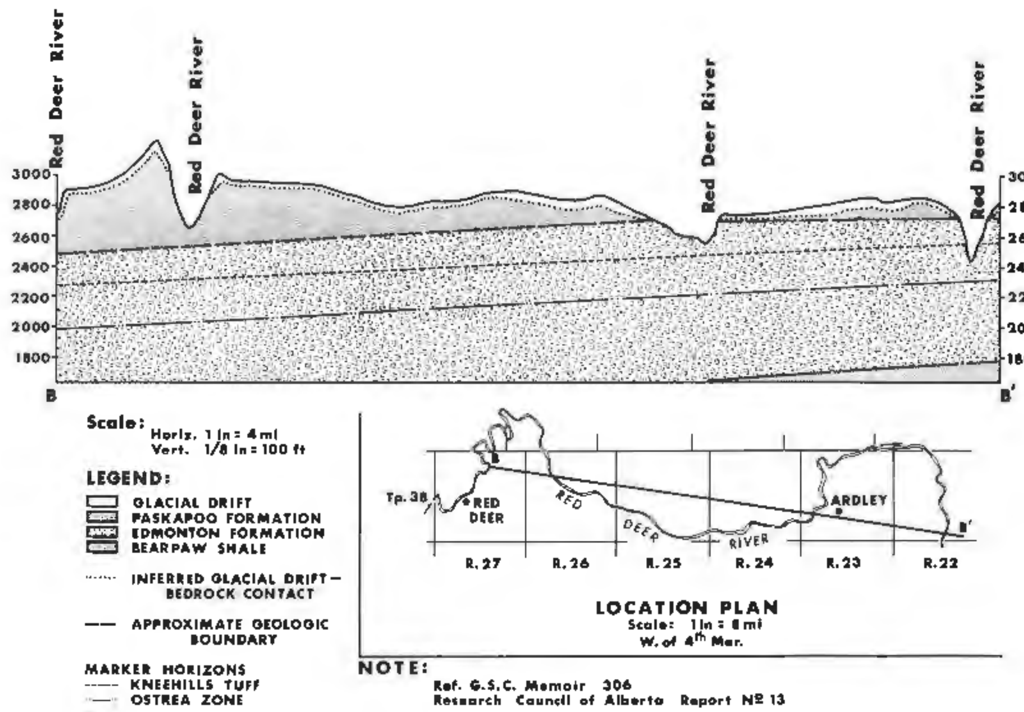

FIGURE 5 – Geologic section through the Red Deer – Ardley area.

2. Embankment Considerations

The design of the dam embankment is dependent upon the reaction of both foundation and fill materials to applied loads. In saturated soft rocks which possess a bulk modulus of compressibility substantially less than water, the application of an applied stress system results in the development of pore water pressure and thus little, if any, increase in effective stress. At Ardley, samples of the crushed shale zone, when tested in triaxial compression, Figure 10, displayed very high pore water pressures. At other damsite locations excess hydrostatic heads in similar rocks, during construction, equal to the vertical stress of the applied embankment loads, have been noted (Peterson, 1968, Binnie *et al.* 1967). As a consequence, it is concluded that the laboratory results obtained for this site relate to the observed field evidence from other projects. Consequently, it may be expected that high pore water pressures will be developed during construction of the Ardley dam. This feature may govern the design and construction sequence.

The overall stability of the cross section depends upon the ratio of the strength available to resist movement to the driving forces. Figure 11 illustrates the essential features of embankment stability at Ardley. The hydraulic head developed due to embankment loads, is represented by a b c. The heads, due to a full reservoir in the crushed zone are indicated by a' c' or a' d', depending upon the nature of drainage available in the crushed shale zone. The design head h, at any time depends on the reservoir head h_r and the hydrostatic excess head h_e, induced by the embankment construction. According to Coulomb's equation for the

$$s = c' + (\sigma - u) \tan \phi' \qquad \text{Eq. 1}$$

wherein s = shearing resistance
- c' = drained cohesive shear resistance
- σ = total normal stress
- u = hydrostatic head
- ϕ' = drained angle of shearing resistance.

If the value of u in this equation is equal to σ, then there is no frictional shearing resistance available. If this is the case, then all the driving forces will have to be resisted by cohesive

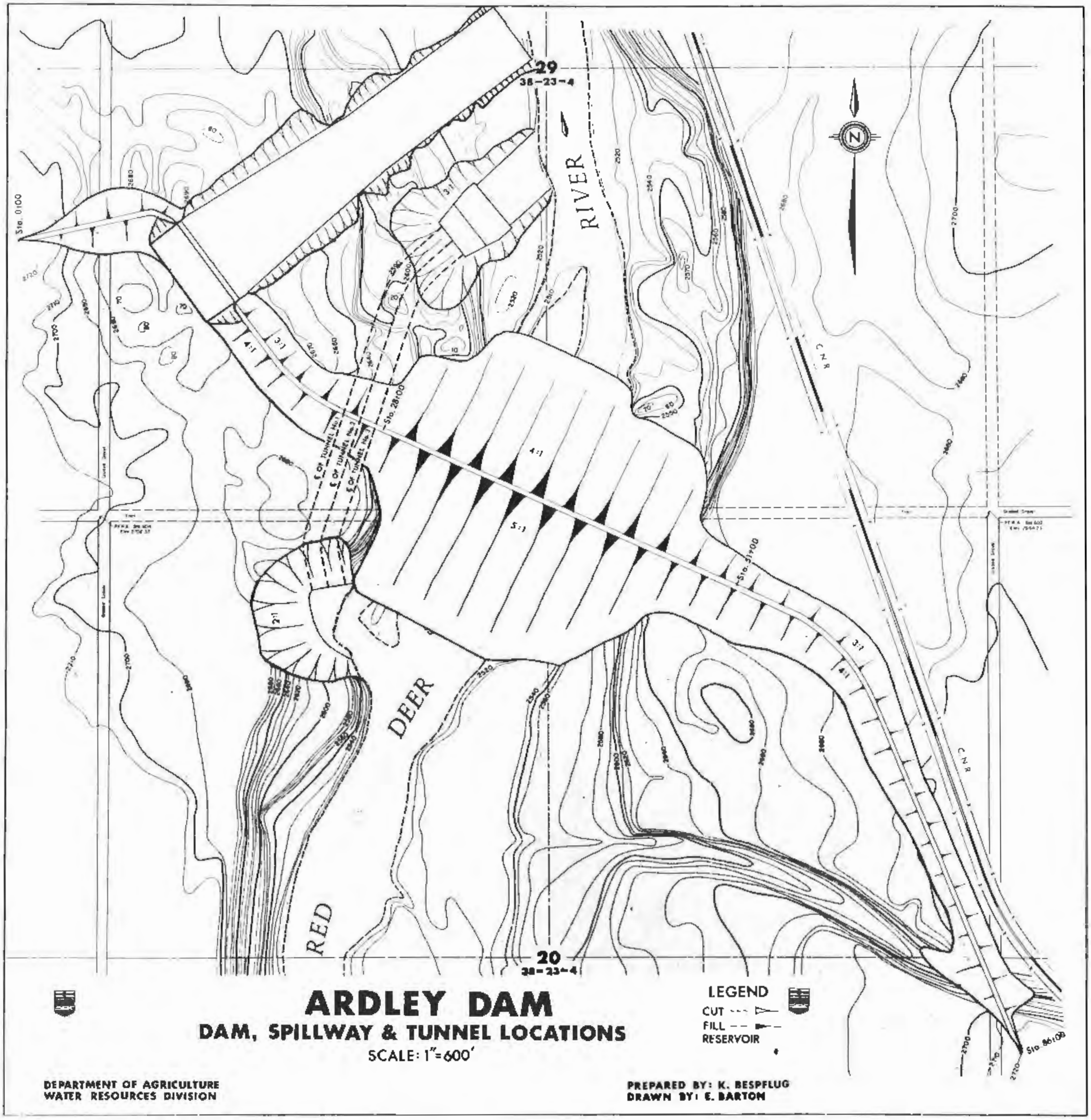

FIGURE 4A — Ardley Dam, spillway and tunnel locations.

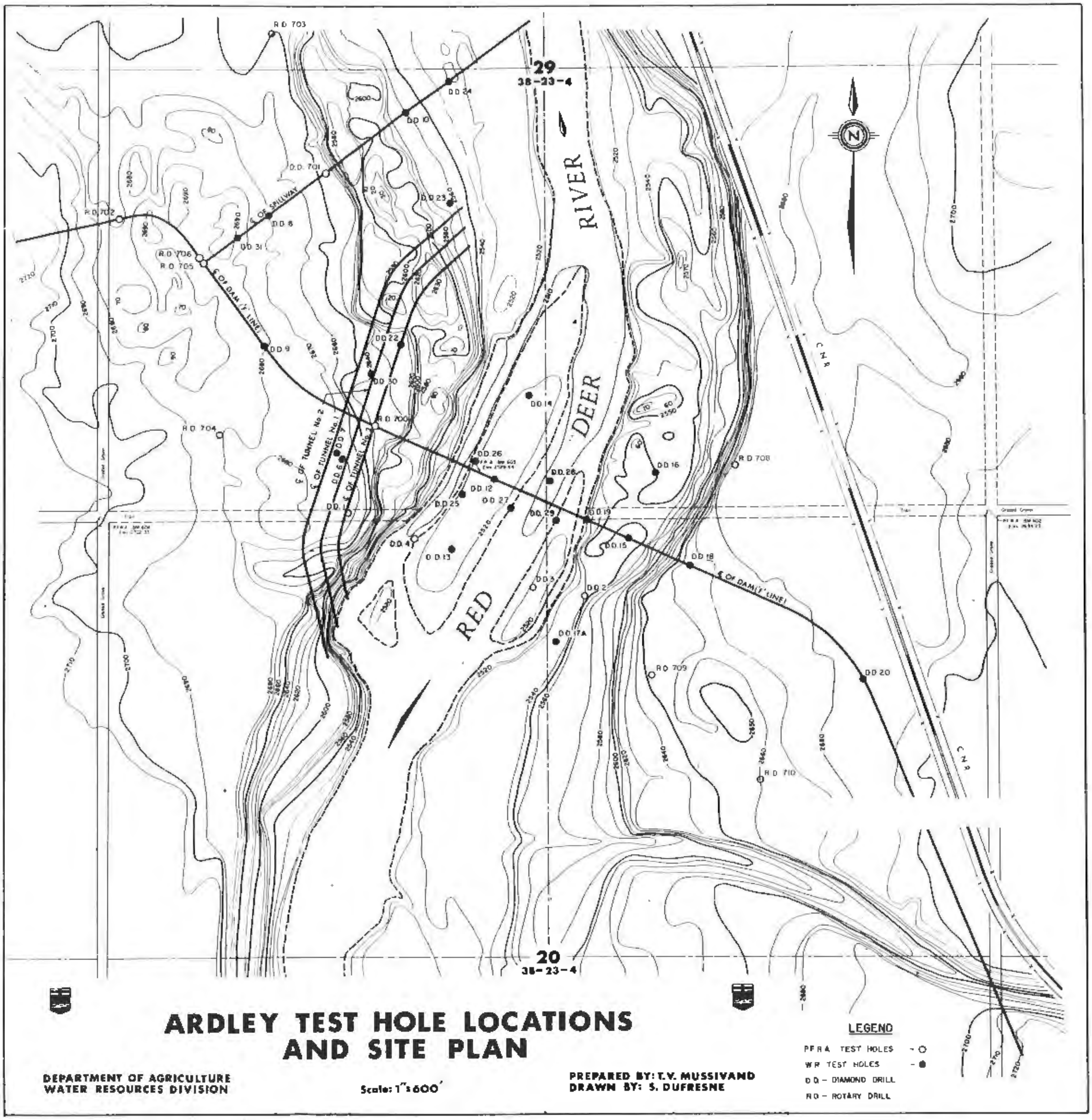

FIGURE 4B — Ardley test hole locations and site plan.

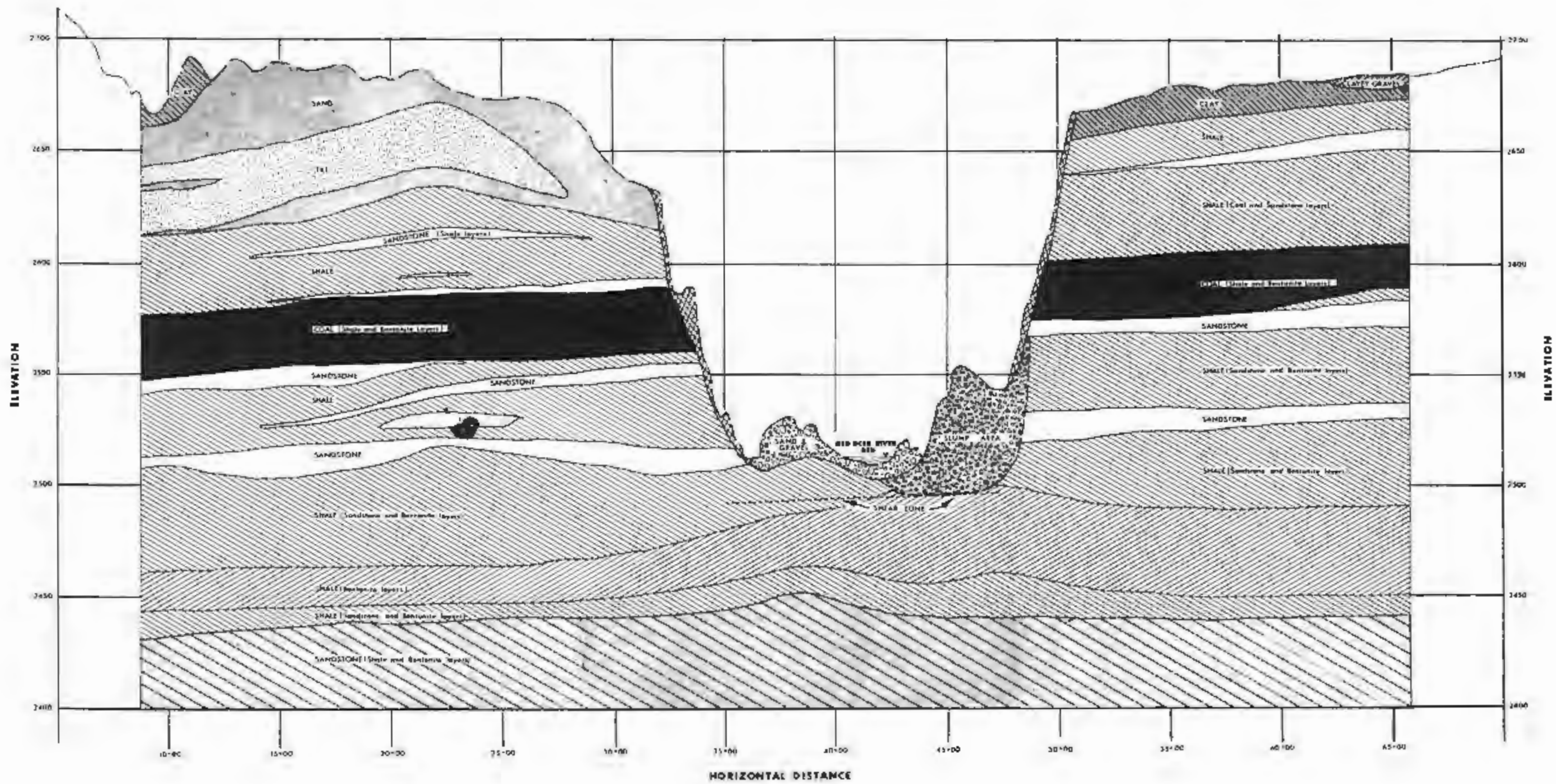

FIGURE 6 – Geological features of the Ardley damsite. Sta 8+75 to 65+75 on dam centreline.

TABLE 2
Geologic Factors Pertinent to Engineering Behaviour

Geologic Factors	Influence	Engineering Consequence
Depositional Environment:		
(a) Marine Deposition	Salt concentration in pore fluid.	High swelling potential.
(b) Shales, sandstones, coal, volcanic ash	Sediments generally of variable texture and structure.	Incompatible stress-strain properties of adjacent rock type.
(c) Variable depth of burial	Interparticle bonds – weak to permanent.	
Lithology and Stratigraphy:		
(a) Bentonite layers inter-stratified with shales, sandstone and coal	Controls movement of groundwater. Variable stress-strain behaviour.	Determines pore water pressure. Shear zones develop as a result of differential rebound during unloading
Stress History:		
(a) Loading by younger sediments	Consolidation.	Increase in shear strength.
(b) Diastrophism and preglacial erosion	Rebound.	Alteration of internal stress system.
(c) Glacial erosion, loading and unloading	Consolidation and rebound.	Indeterminant stresses at rest. Development of shear zones.
(d) Valley erosion	Relief of horizontal restraint.	Horizontal rebound and vertical jointing.
Structure:		
(a) Faults		
(b) Joints	Planes of weakness.	Controls strength and deformation of rock mass and as a result controls design.
(c) Bedding	Seepage paths.	
Weathering:		
(a) Precipitation	Disintegration of rock mass.	Develops structurally unsound rock mass.
(b) Temperature	Planes of weakness (Fig. 7A).	
Groundwater:		
(a) Quantity	Variations in flow affect leaching and pore pressure.	Changes in shearing resistance.
(b) Quality	Changes in free water and absorbed water chemistry.	Can result in swelling and loss in strength.

shearing resistance, provided that separation of the rock bedding does not occur. It is known from experience that the value of cohesive shearing resistance is questionable. Hence, there is substantial reason to be concerned, not only about the pressures which may be induced in the crushed zone by the embankment, but also about the selection of the parameters c' and ϕ' for use in equation 1.

Sinclair and Brooker (1967) have demonstrated that these rock materials possess both a peak and an ultimate (or residual) strength – the values of c' and ϕ for these two extreme conditions are widely different as illustrated by Figure 12. Not only is it necessary to make this distinction, but it is important to consider whether the value of c', determined from the results of laboratory tests, is applicable to the rock mass. Many of the answers to these questions can only be found during construction by comparing field measurements with hypothesized design assumptions.

3. Stability of Abutments

This constitutes an important aspect of overall dam stability. Recent research has indicated that the formation of valley slopes is closely related to stress relief and occurs retrogressively, Bjerrum (1967), Scott and Brooker (1966). Referring to the geologic section in Figure 6, a "shear zone" is noted at an elevation of about 30 ft below river bed. We have defined a shear zone, or crushed zone to be an apparently plane zone of crushed shale particles in plastic matrix. The particles are generally of one-eighth to one-half-inch size and the plastic matrix has the consistency of a highly plastic and stiff clay. This zone is found

FIGURE 7A – Weathered shale surface below the sandstone.

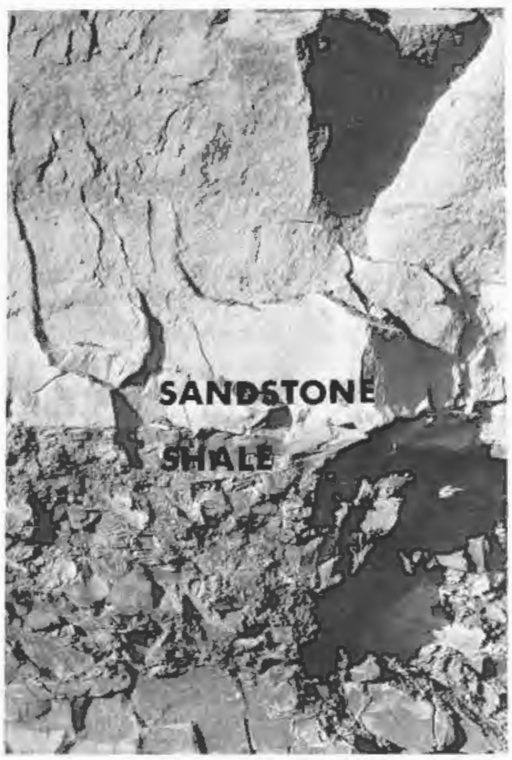

FIGURE 7B – Detail of the variation of material in the Edmonton formation

to be nearly horizontal and is believed to be the result of differential movements during rebound. It is apparently the seat of movements in abutment landslides. A schematic section of the right abutment in Figure 13 illustrates our concept of the development of the slope.

Initially, block A fails as a wedge shaped mass with it's base at the elevation of the crushed zone. This failure is followed by other wedges – B, C, etc. Each of the wedges when analyzed separately as a free body has a factor of safety of approximately unity (Hayley, 1968). The consequence of this is that we are faced with a difficult problem of assessing slope stability of the rock mass. Analyzed on the basis of residual strength, a factor of safety near unity is obtained. Yet, if a peak strength is used the factor of safety may be 2 or 3. The actual factor of safety is bounded by these values. It is believed that "setting" or consolidation of the disturbed zone since its original remoulding results in a strength greater than residual. As a consequence of the developed strength, a marginally stable situation may now prevail. However, minor movements may cause the material to revert again to the residual strength and result in further sliding.

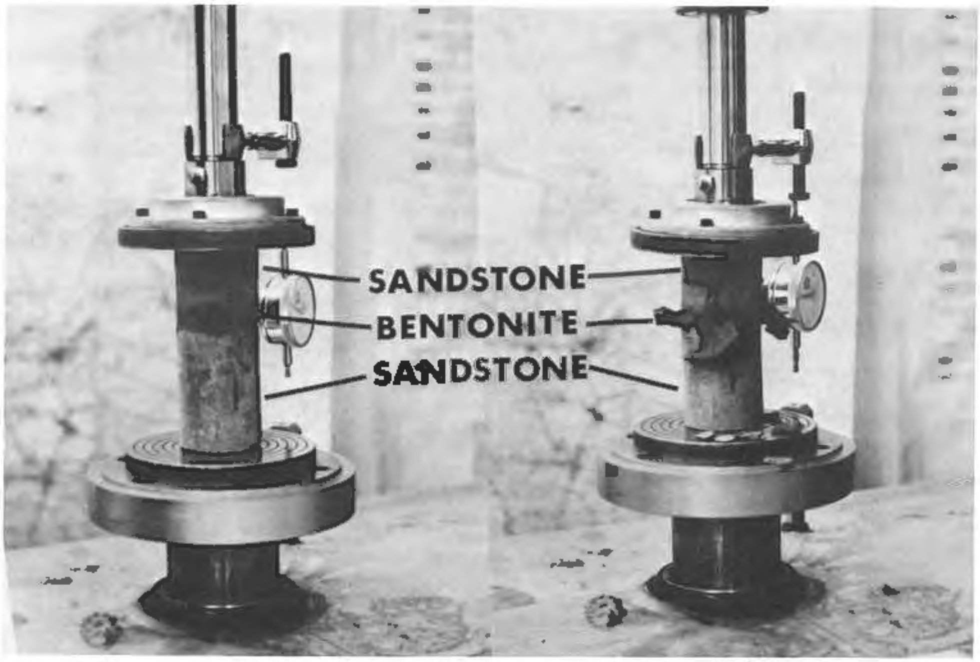

FIGURE 8 – Bentonite layer in sandstone A. before test, B. after test.

Figure 9 indicates the wide range of values in modulus of elasticity of materials tested. Associated with the stress relief which occurs during the formation of the valleys is differential rebound. As a result, shear zones form on or near the contact faces between strata possessing different modulus of elasticity. It is believed that these zones of weakness will have their peak strength reduced to a residual strength. However, additional research is required to substantiate this hypothesis.

4. Permeability of Foundation and Abutments

It has been noted on occasion that water will flow from a drill hole for several minutes after the core barrel has been withdrawn. In drilling the Edmonton or similar formations, water pressure is generally held as low as possible but when necessary the water pressure is brought up to 100 psi. It is believed that the flow of water from the drilled zones is a result of either of the following.

(a) Existing fissures in various strata are widened by water being forced into them, and on release of the water pressure, the earth pressure forces the water out of the fissures to the ground surface.

(b) Trapped air in fissures is compressed by the drilling water pressure and on release of the water pressure the trapped air forces the drilling water out of the drill hole.

Pressure testing techniques presently being developed to determine if fissures are widened by water pressure indicate that this is the case. However, further investigation will be required to determine if a "burst pressure" exists and what effect this will have on dam design. It is conceivable that drilling or pressure testing with high water-pressure may in fact damage the formation during a grouting program.

At this time, each of the aspects outlined above is under detailed consideration and the following steps are being taken toward answering the questions:

A Study of Alternate Damsite Centre Lines

This study will be concerned with the orientation of the embankment, diversion tunnel and spillway elements relative to the altitude of geologic features. From these layouts the advantages and economics of alternate proposals may be studied and the optimum scheme selected.

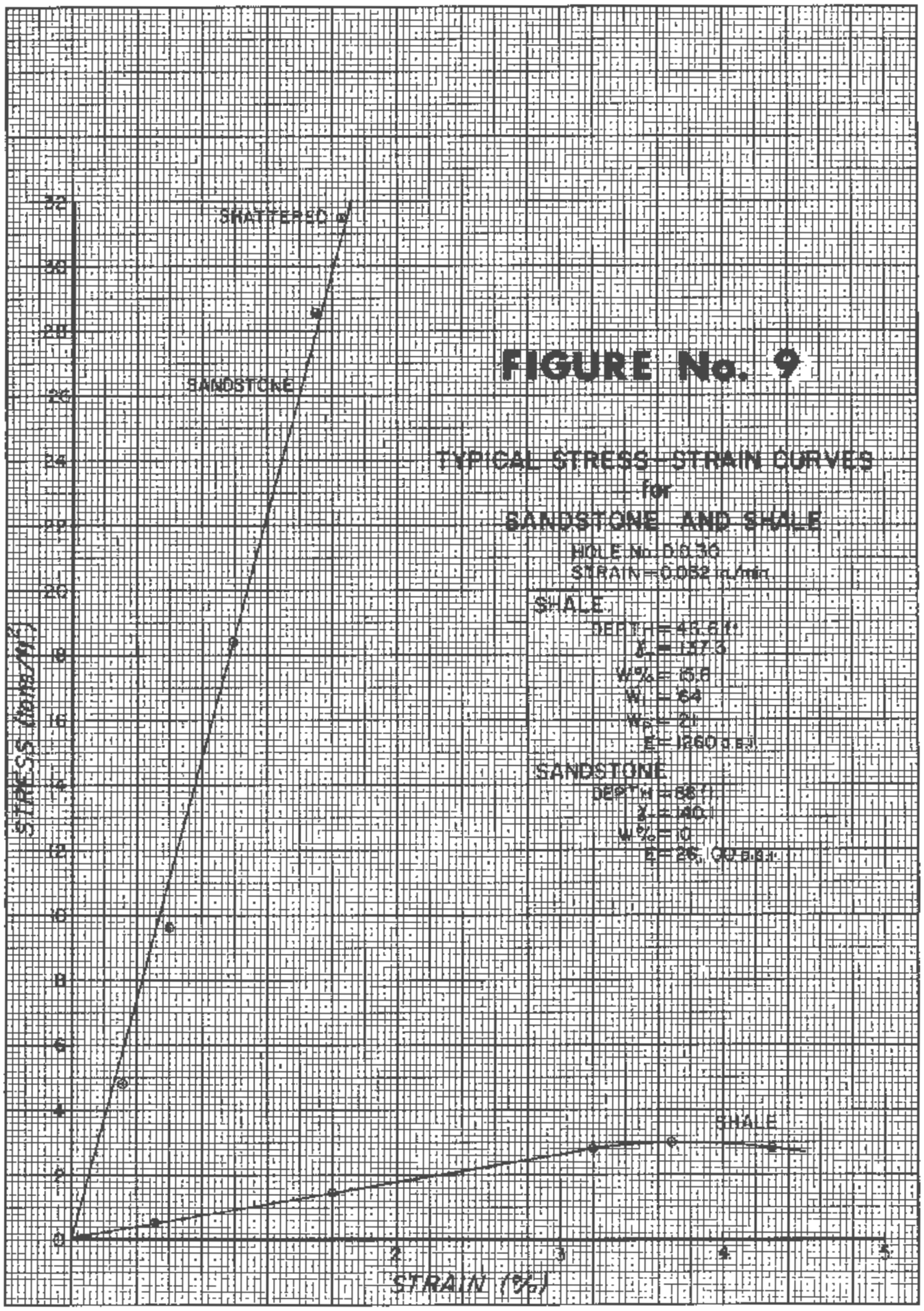

FIGURE 9 – Typical stress-strain curves for sandstone and shale.

A Detailed Study of Valley Slope Stability

This study will be made to define the mechanisms involved in the large block slides which have been noted at several locations.

From analysis of actual slides, it is believed that the study will give some insight into the shearing strength and deformation characteristics of the rock mass. Since the possibility of

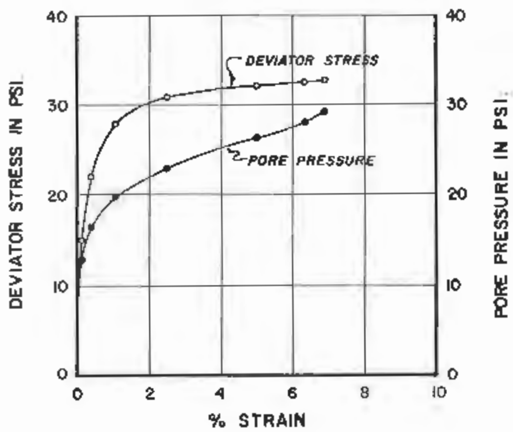

HOLE No. — D.D.29
MATERIAL — SHALE
DEPTH — 20 to 21 ft.
CELL PRESSURE — 50 psi.

SYMBOL	INITIAL	FINAL
W_o	31.6	22.0
γD_o	34.2	98.6
e	0.80	0.72

FIGURE 10 — Pore pressure reaction to deviator stress, Hole — D.D. 29, Ardley, Alta. Test No. 1.

relating the results of such analysis to laboratory tests exists, other local slopes could be analyzed without further intensive study.

Exploration

Although the test holes shown in Figure 4B have provided useful data, core recovery and disturbance in softer rocks have been unsatisfactory. As a result, identification of geological detail is questionable. In addition to this, the detailed stratigraphy over large areas has been difficult to correlate. One solution to this problem would be the use of large diameter bore holes which would allow not only visual inspection, but detailed and undisturbed sampling as well. Since the possibility of performing *in situ* shear tests is a very appealing feature, a number of 40-in. diameter exploratory shafts are being planned to be drilled into soft or weak zones.

Embankment Fill

It has been proposed that a test fill be constructed to determine if the embankment fill could utilize excavated and recompacted sandstones and shales. The test fill will indicate the difficulty to be encountered in ripping the bedrocks and compacting them to an acceptable standard, and possibly, problems which may be encountered in pore pressure build-up.

The swelling potential or rebound of the sandstones and shales has been considered by the Prairie Farm Rehabilition administration on a laboratory scale and, as a consequence, a potential swelling problem was defined. The

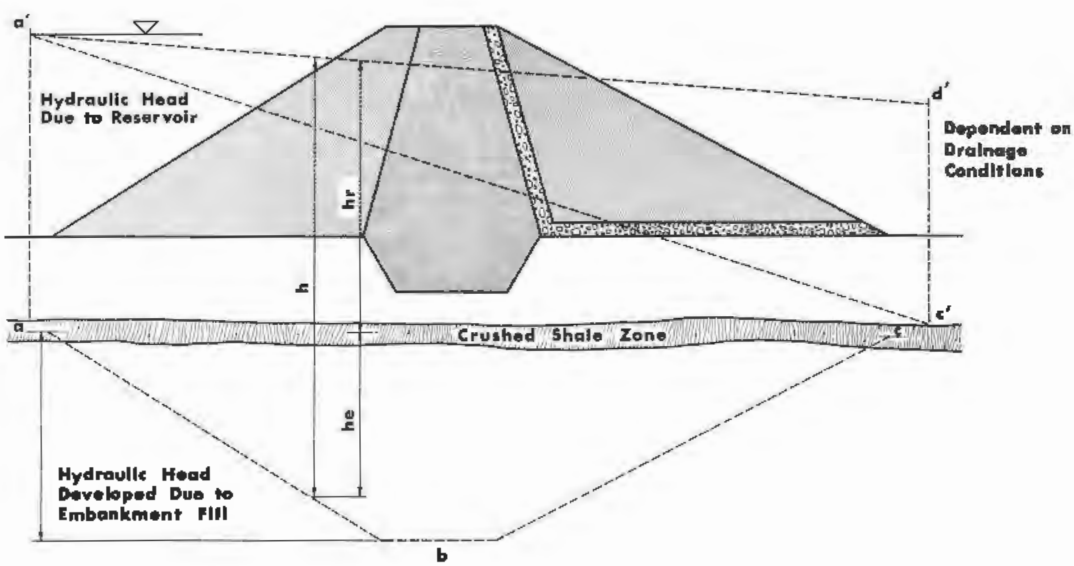

FIGURE 11 — Schematic diagram illustrating essential features of Ardley Dam stability.

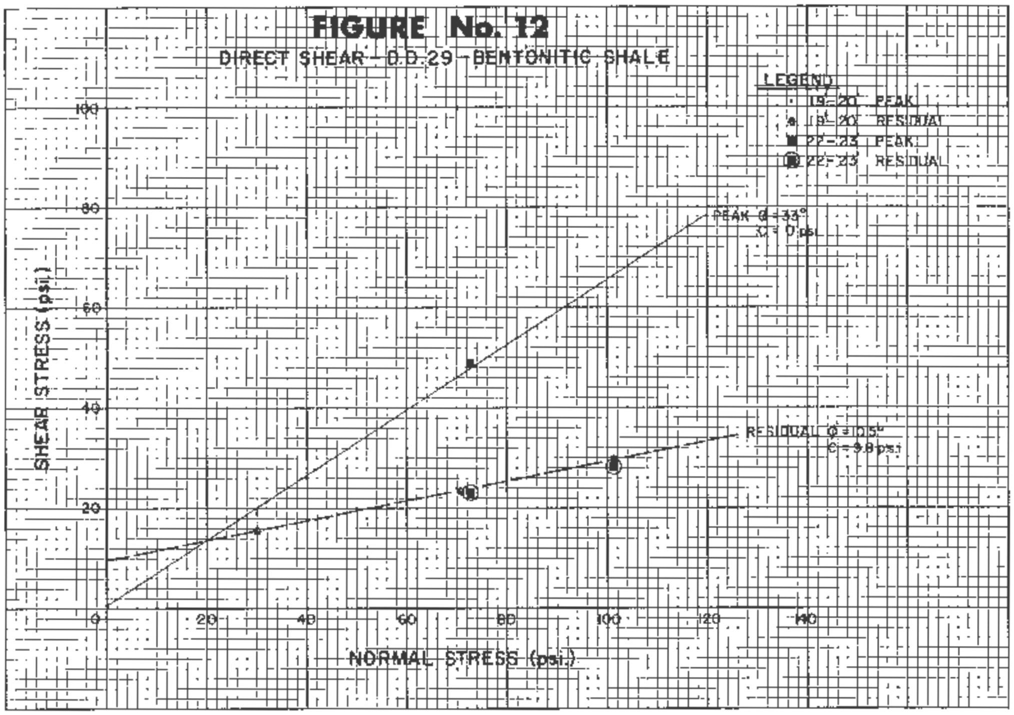

FIGURE 12 — Direct shear — D.D. 29 — Bentonitic shale.

magnitude of this rebound and the effect of pressures and movement of structures in the field is presently speculative. In order to gain more knowledge, the possibility of an instrumented test cut is being considered. The location of the cut would be in the spillway area, and the material excavated would be utilized in the proposed fill.

Instrumentation

The use of field measurements provides the most useful data for predicting present and future performance of structures. Instrumentation in this project during construction has been estimated at $250,000 and will include settlement gauges, slope indicators, piezometers, extensometers and *in situ* shear tests of various types.

Other Areas

Other areas where study needs to be concentrated include tunneling methods, strength of the rocks, drainage and the location of abandoned mines.

Summary

The Upper Cretaceous shales at the Ardley damsite pose challenging rock mechanics problems. The role of rock classification and strength testing has been important to date and much effort has been spent on a conventional soil mechanics approach which is not unlike the direction in which rock mechanics must evolve.

A major distinction between laboratory and analytical, as opposed to field behaviour, has been recognized. Further efforts will emphasize field studies and testing. In this regard the use of instrumentation is planned to measure deformation, pressures, and strengths throughout the stages of design, construction and operation. In applying rock engineering to damsite location, the factors outlined in Table 2 require consideration.

The problems outlined are challenging and they fall in the general field of rock engineering. The application of existing rock mechanics principles with methods being developed to meet the specific needs of civil engineers is providing the basis for solving the problems.

One of the greatest present needs in this project and perhaps rock engineering in general, is a simple but functional classification system. The other areas which appear to justify intensive consideration are the nature of the rock

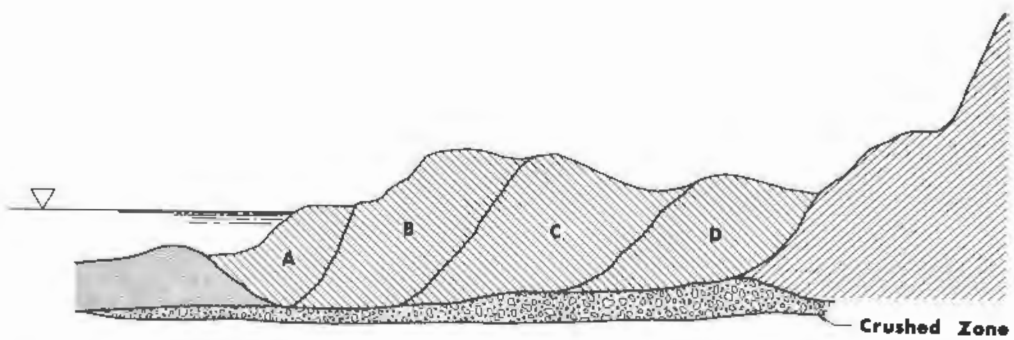

FIGURE 13 — Schematic diagram of stability of right abutment.

mass and its relationship to proposed changes in environment.

Acknowledgments

This paper was based on information collected during a damsite study for the Water Resources Division, Alberta Department of Agriculture. It is presented with the kind permission of R.E. Bailey, Director of Water Resources Division, Alberta Department of Agriculture.

The assistance of all Water Resources staff in preparing this paper is gratefully acknowledged. The efforts of Prof. T.H. Patching in reviewing the manuscript is also acknowledged.

References

1. **Binnie, G.M.; Clark, J.E.F.; Skempton, A.W. 1967.** The effect of discontinuities in clay bedrock on the design of dams in the Mangla project. Ninth Cong. on Large Dams, Istanbul, 1967.
2. **Bjerrum, L. 1967.** Progressive failure in slopes of overconsolidated plastic clay and clay shales. ASCE *J. Soil Mech. Found.*, vol. 93, SM5, Sept.
3. **Coates, D.F. 1964.** Classification of rocks for rock mechanics. *Inter. J. Rock Mech. Mining Sci.*, vol. 1, pp 421-429.
4. **Deere, D.U.; Hendron, A.J.; Patton, F.D., Cording, E.J. 1967.** Design of surface and near-surface construction in Rock. *Proc. 8th Rock Mech. Symp.*, AIME, U. of Minnesota, Minneapolis.
5. **Hayley, D.W. 1968.** *Progressive Failure of a Clay Shale Slope in Northern Alberta.* M. Sc. Thesis, Department of Civil Engineering, U. of Alberta.
6. **Peterson, A.F. 1968.** Personal communication.
7. **Scott, J.S.; Brooker, E.W. 1966.** *Geological and Engineering Aspects of Upper Cretaceous Shales in Western Canada.* Paper 66-37. Geological Survey of Canada.
8. **Sinclair, S.R.; Brooker, E.W. 1967.** Shear strength of Edmonton shale. *Proc. Geotech. Conf.*, Oslo.

E.W. Brooker

Education — B Sc, University of Alberta, 1955; M Sc, University of Alberta, 1958; Ph D, University of Illinois, 1964.

Employment Summary — 1964-68, associate professor of civil engineering at University of Alberta; 1968 to the present, consulting engineer in foundation engineering.

I.H. Anderson

Education — B Sc, University of Alberta, 1957.

Employment Summary — 1957, Water Resources Branch, Alberta Dept. of Agriculture; 1964 head of Development Planning Division of Water Resources Branch.

Abstract

Recent activity in slope stability research has brought the promise of rational slope design. However, old slopes of unknown stability will exist for many years, and the stability of engineered slopes will still be subject to unique and unforeseen rock conditions. It is imperative, therefore, that reliable slope failure warning systems be developed. Kennecott has been testing a microseismic detection system as one such pre-failure warning system.

It has been generally recognized that the rate at which microseisms are generated in rock increases as the rock approaches failure. The paper describes the general mechanical and electronic requirements for microseismic monitoring systems. Alternate techniques for sensing, amplifying, and recording data are compared. Also described is the microseismic unit used by Kennecott which was designed as a small, rugged and portable piece of electronics hardware to simply count and register microseismic events. In contrast to the conventional devices utilizing geophones, an accelerometer is used as the sensing unit. The counter then registers any microseisms above a pre-set threshold value without regard to the magnitude or duration of the disturbance. In this way, it is possible to utilize a precision electronics package which can be calibrated with a micro-g scale.

Raw field data, some related slide-displacement data and typical analyses are presented. Finally, the experimental technique is reviewed in the light of the results to date.

Design and Application of Microseismic Devices

C.D. Broadbent,
Mining Engineer, Metal Mining Division,
Kennecott Copper Corporation,
Salt Lake City, Utah

C.W. Armstrong,
Process Instrumentation Engineer,
Metal Mining Division,
Kennecott Copper Corporation,
Salt Lake City, Utah

1. Introduction

Increased activity in slope stability research will lead to substantial improvements and greater reliability in mine design techniques. However, rock is a natural and imperfect material and will always present unique and unforeseen structural problems. It is clear, therefore, that the industry must have methods for detecting slope failures early enough to take appropriate corrective action. Strain and displacement instruments have proven useful for this purpose but a back-up system would be desirable.

The acoustic emission generated by the sudden release of energy from internal deformation of rocks has been investigated by many authors. They have furnished evidence to show that such emissions, variously termed subaudible-rock noises or microseismims, often intensify as rock approaches failure. At the time that this study was initiated, work done in laboratories and in underground mines had resulted in operationally useful methods for predicting rock bursts. It appeared reasonable, therefore, to attempt the development of a practical slope-failure warning system based on the measurement of microseismic activity. Others had completed field tests or were then using microseismic systems for this purpose. Goodman and Blake (1) had reported a study of acoustic emissions at numerous highway cuts in California. U.S. Borax (2) was using a system in their open-pit mine for stability analysis. The United States Bureau of Mines (3) was evaluating a very extensive system installed at Kennecott's Kimbley pit in Nevada, site of our slope-stability research program. The systems being used were apparently well designed but were unproven for slope applications and did not meet the criteria that we had established for a practical open-pit mine system.

2. Slope Application

The mechanics of a rock slope failure must be recognized in order to arrive at the proper application of an open-pit microseismic system. The following are pertinent considerations.

2.1 Mechanics of Failures

Generally speaking, the absolute magnitude of compressive stresses in a mine slope decrease prove useful: (a) to detect "noise" due to sliding, (b) to detect a change in resonant characteristics of a zone, and (c) to detect progressive acoustic decoupling of a zone. Any of these phenomena might indicate the deterioration of bank stability.

3. System Design

Requirements for a microseismic monitor system vary from location to location. A well designed system of transducers and data-handling equipment for one mining installation may be too complex for another. Figure 3 illustrates the essential components of a micro-seismic system and some typical systems used for laboratory and field investigations. The success in getting such a group of units to work together harmoniously and to be able to gather experimental data is due in large part to the degree of understanding of the system. Many times a component may perform acceptably by itself, but by reason of incompatibility be unable to do so when connected into the system. The function of the main components and several factors worthy of careful considera-tion are outlined here.

3.1 Transducer

The transducer is used to convert the energy contained in a seismic wave into a suitable electric signal, much like a microphone converts acoustical energy from the air into electrical variations which are proportional to pressure changes in the atmosphere. In fact, early attempts at measuring microseismims utilized ordinary speech microphones which had been modified to survive in the environ-ment. Later, piezo-electric crystal geophones were developed which greatly improved trans-ducer response to seismic events. Many of these geophones, including those developed by the

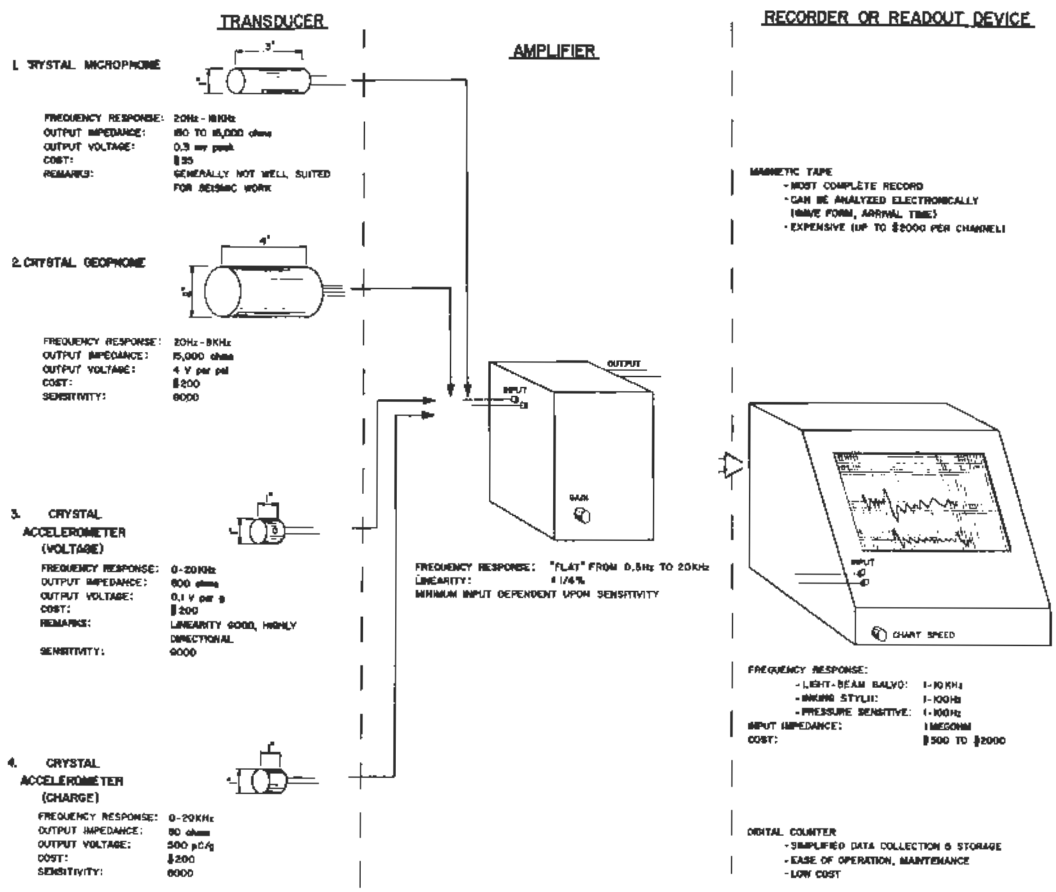

FIGURE 3—Typical microseismic system elements.

U.S. Bureau of Mines, incorporated the piezo-electric crystal as a cantilever which, when flexed by a seismic pulse, generated a relatively large electrical potential. More recently, developments and applications in the aerospace industry have brought about widespread use of very sensitive miniaturized accelerometers that are suitable for microseismic survey work. These transducers also use piezo-electric crystals, but not as cantilevers. Instead, a moving mass loads the crystal which in turn generates an electrical potential proportional to the acceleration of the seismic pulse. The accelerometers are rugged, very small, and are available in a large range of accurately calibrated sensitivities. Some of the more important transducer characteristics are:

3.1.1 Frequency Response — Accelerometers should be used below their resonant frequency to provide good response. As an example, a unit having a resonant frequency of 10,000 cps would be used where measurements in the 0 to 3,000 cps range are to be investigated. At frequencies above the resonant frequency of the accelerometer, output drops off rapidly because the mass of the transducer causes it to be unresponsive to the higher frequency vibrations.

3.1.2 Sensitivity — There is a "trade-off" between sensitivity and frequency response. A transducer which will operate over a wide frequency range generally has a low output; conversely, one which is designed for a narrow frequency range can be expected to yield a relatively high output.

3.1.3 Linearity — Operation of a transducer above its specified frequency range results in an output which is distorted. We say that it is "out of the region of linearity," so that the data from it will not be reliable. Obviously, one should operate transducers within the appropriate frequency range.

3.1.4 Impedance — Output impedance of the transducer dictates the type of cabling required. One of the reasons for using coaxial cable is that it has a characteristic impedance irrespective of the length of the cable. Therefore, the experimentor may connect up various lengths of cable to suit the application without disturbing the impedance "match" of the transducer to the cable. Because the maximum transfer of energy occurs when the transducer is matched to the cable, an effort should be made to maintain this impedance level. As an example, if the output impedance of the transducer is 600 ohms, a coaxial cable of 600 ohms should be used. In general, accelerometers having a voltage output need a high-impedance cable; those having charge output need a connecting cable of low impedance.

3.2 Cable and Connectors

The interconnection of units is often the most neglected area of low-level microseismic systems, and noise is the greatest enemy of low-level signals. Coaxial cable is almost exclusively used because of its ability to shield from noise. Therefore, any breaks in the cable or any splices which are made tend to introduce spurious electrical noise. It is in this regard that cables should not be spliced if at all possible, and where connectors are used they should be kept clean and protected from corrosion. Corrosion introduces extraneous resistance into the cable and causes the performance of the line to gradually deteriorate. Physical movement of cable can introduce electrical noise, because as the outer strands of the shield are flexed, the impedance changes slightly.

Where minute signals are to be transmitted over coax, best results are obtained by using a cable that has a low signal-to-noise ratio. The signal-to-noise ratio can be illustrated in this example: Suppose that the transducer will yield an output of 10 microvolts (0.000010 volt) and that the random electrical noise inherent in the coaxial cable is 1/10 microvolt. The signal-to-noise ratio is 100. Another way of stating the case would be that due to random noise in the system, it would not be possible to identify a microseismic event which was in the order of 1/10 microvolt. Now consider the use of a cable which is constructed in a superior way and which will introduce only 1/100 microvolt into our amplifier. We have now improved the system by an order of magnitude, the signal-to-noise ratio is 1,000, and a transducer output need only be greater than 1/100 microvolt to be distinguished at the amplifier input.

3.3 Amplifiers

The electrical output from the transducer is small and must be amplified to obtain a signal suitable for display or recording. The amplifier must have what is known as fidelity; that is, it must faithfully reproduce each variation of the weak signal and at the same time magnify its size. Modern amplifiers, with gains of up to 10 million, can easily satisfy these requirements. For research work where the investigation of microseismic wave shapes is of importance, an amplifier capable of reproducing all the frequency variations of the seismic pulse will be necessary. Such an amplifier may have a response of 0 – 100 KH. Conversely, if the event alone is of importance, then an amplifier with much less frequency response, say 0 – 20 KH. will suffice.

Because literally thousands of amplifiers are available today, it wonld be impossible to survey their characteristics in this paper. However, some of the parameters which are important to the proper selection of an amplifier for microseismic work are listed here:

3.3.1 Gain – The electrical signal from the transducer, i.e., the accelerometer or geophone, may be of the order of 1.0 microvolts, or 10^{-6} volt. Therefore, if a recorder requires a 1-volt drive, the amplifier must boost the transducer signal by a factor of 10^{6}. This factor, which expresses the amonnt of amplification the input signal will receive from the amplifier, is the amplifier gain. Often the decibel term (db) is used, which is merely a logarithmic expression of the same figure. As an example, a gain of 100 can be expressed as 20 db; a gain of 10,000 would be 40 db.

3.3.2 Frequency Response – The output of most off-the-shelf amplifiers can faithfully reproduce the input in a range of 0.1 to 10,000 Hz, while others may be rated for use in the range of 80 to 18,000 Hz. If the unit is to be used in a system where every excursion of the waveform must be reproduced, a wide-band amplifier should be used. An amplifier is said to have a flat response within its rated frequency range. Above and below these frequencies, the signal is degraded and is not a linear function of the input.

3.3.3 Filters – Devices known as filters are often used to restrict the operating range of an amplifier to a certain specified band of frequencies. Filters can also be inserted to screen unwanted frequencies or electrical noise so that they cannot be amplified along with the desired signal. In general, the greater the need for gain from an amplifier, the narrower will be the band over which that amplifier will respond without degrading the input signal. Again, this is a "trade-off" between the two design parameters, and one which should concern every purchaser-user. The converse is also true; if a low gain is acceptable, the frequency range can be quite broad, as much as 10 to 1,000,000 cps.

3.3.4 Distortion – This figure is the measure of degradation inside the amplifier, and although the *system* distortion can be considerably higher (due to the cumulative effects of distortion in all components) the distortion figure for a good wide-band amplifier should not be greater than 0.01%.

3.3.5 Output – Output is generally expressed as a maximum voltage available for a minimum input voltage level.

3.4 Recorders

Recorders take many forms, from magnetic tape units to electro-mechanical devices which are driven at the frequencies of the transducer system. A survey, taken in 1968 by the Instrument Society of America shows 72 different types and models of recorders from the simple stylus which marks on a pressure-sensitive paper to a complex high-speed light beam galvanometer. All these produce a permanent record on various types and sizes of chart paper. Often, however, a visual record is not desired. Here a magnetic tape recorder may be employed which operates on the same principle as the small personal recording machines – that of preserving the record on a thin magnetic tape.

The factors governing the selection of a recording device, whether for display or for permanent record, depend primarily upon the individual application. If portability is a criterion, the light beam galvanometer, because of its inherent makenp of delicate parts, will probably not be suitable. If accuracy or speed of response is an overriding factor, the galvanometer type of instrument will serve well.

A typical strip-chart analog recorder has been used here as an example to point up some of the principal considerations in the selection of such a unit.

3.4.1 Sensitivity – Sensitivity is generally listed as millivolts per chart line, or millivolts per mm of chart width. If the unit is equipped with an internal amplifier the sensitivity may be expressed in a range, i.e., 0.01, 0.02. . . . 10 volts per chart division.

3.4.2 **Stability** – This is a measure of the amount that the electronics may "drift" (however slight) while holding a specified signal input over a period of time. This is an important consideration, and should be no more than 0.25%.

3.4.3 **Frequency Response** – Generally, the upper frequency response of a chart recorder with an inking system is about 100 cps due to the inertia of the pen mechanism. The light-beam units, however, can reach 10,000 cps easily because of the relatively small mass of the galvanometer assembly.

3.4.4 **Drift** – The term given to the measure of stability that an amplifier exhibits is known as "drift," and denotes the small loss in stability or frequency response over a long period of time. If high-accuracy work is being carried out, a low-drift amplifier should be chosen.

3.4.5 **Input Impedance** – To effect a maximum transfer of energy from the transducer to the amplifier, the output impedance of the transducer should be matched to the input impedance of the amplifier. For example, if the transducer has a 600-ohm output, both the amplifier and coaxial cable impedance should be 600 ohms.

3.4.6 **Chart Speed** – This varies with the instrument. Again, a high-speed instrument can spew out paper at a rate of 12,500 mm per second; the average unit will reach top speed at 125 mm/sec. There is little reason to advance beyond 125 mm/sec unless an investigation of pulse width or arrival time is of overriding importance.

3.4.7 **Writing Methods** – Many methods are available; ink, electric imprint on voltage-sensitive paper, or light trace on light-sensitive paper. In some instances, the choice can be made favouring the relative ease of maintenance with electric imprint writings.

3.4.8 **Linearity** – The chart and pen must have a linear relation in order to minimize distortion. Once again, if a linear, true signal from the transducer and amplifier is distorted at the recorder, information is lost.

3.5 The Kennecott Design

Kennecott's requirements were for an inexpensive unit that would be portable, rugged, and simple to operate. On the other hand, the unit had to be flexible so its functions could be expanded according to the needs of the testing program.

Because transducers are difficult to design and construct, a standard off-the-shelf unit was used. Literature surveys indicated that a response to accelerations of 0.002 g's would be necessary for detection of microseismic activity. However, at such low levels the voltage response of a piezo-electric accelerometer is of the order of 10^{-5} volt and an acceptable signal-to-noise ratio is difficult to attain. Under these conditions, it was determined that it would be better to use the transducer as a charge, rather than voltage generator and then design the rest of the system accordingly.

The requirements of acceleration response, charge sensitivity, compactness, availability and low cost seemed to be met best by a unit such as the Columbia Research Laboratories accelerometer, model 902. An engineering firm was engaged to design a solid-state charge amplifier to work with this accelerometer. In the interests of operating simplicity, the recording function of the amplifier was limited to counting the number of microseismic events that exceeded a preset threshold level (calibrated in g's) which was continuously variable from .001 to .1 g. Take-off jacks for an analog recorder and for earphones were specified to aid field testing. In addition, because high frequencies are rapidly attenuated, it was felt that a response of .0 to 1,000 Hz would be adequate.

The specifications of the completed system (Figure 4) are shown in the Table.

4. Field Testing Program

Five identical systems having the noted specifications were purchased for field testing. Shortly before the instruments were delivered, a very large plane-shear type slope failure (Figure 1) occurred in Kennecott's Liberty pit in Nevada. Close inspection of the failure site revealed that new tension cracks were developing on the surface behind the failure. It appeared that a second failure, similar to the first but containing only about one million tons, might take place. Subsequent measurements indicated that an intact block was

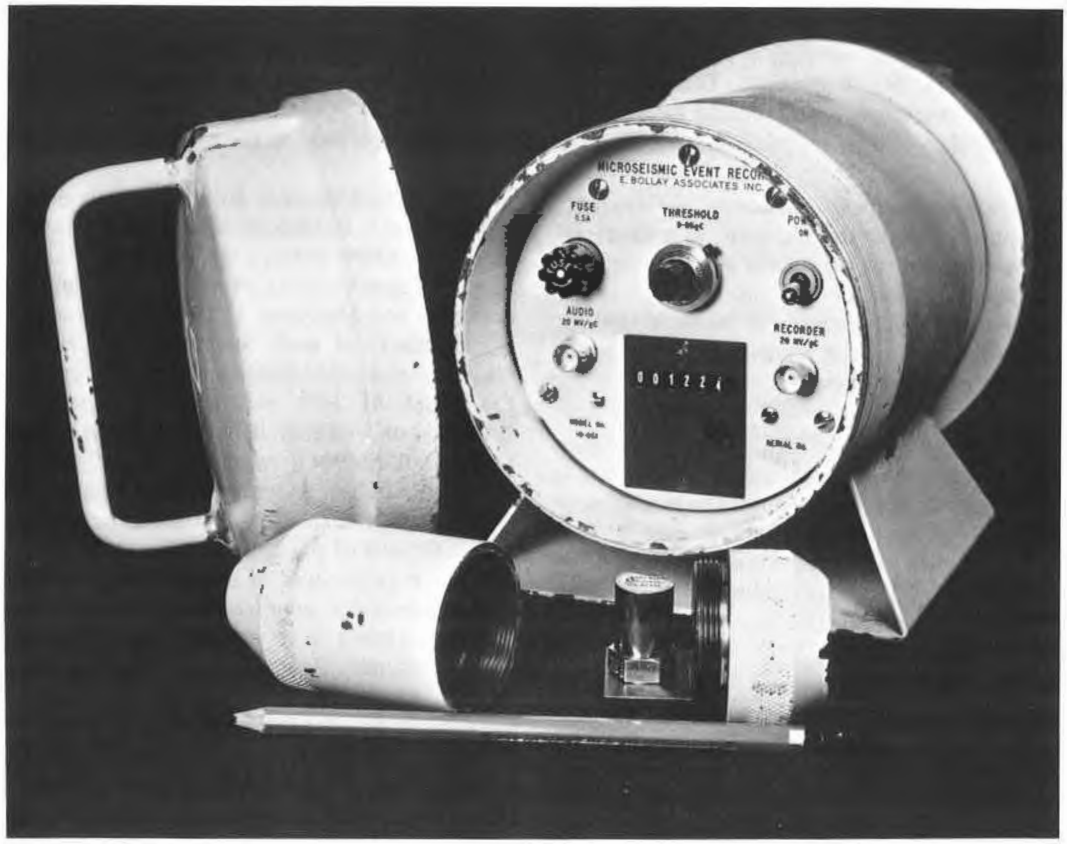

FIGURE 4—A microseismic event recorder. Provides a digital record of the number of events exceeding a chosen threshold level.

TABLE

Specifications of the Recording System

Transducer	
Acceleration range:	0.005 g to 20 kg
Charge sensitivity:	u 550 picocoulombs /g
Frequency range:	0.1 Hz to 3 KHz ± 2
Reasonant frequency:	20 KHz
Amplifier	
Power requirements:	20 to 24 vdc, 55 ma counting
Input:	Piezo-electric accelerometer
Charge gain:	20 mv/u coulomb
Noise:	Approx. 1 mv rms over 1 KHz bandwidth
Frequency response:	Approx. 3 to 1,000 Hz
Maximum sensitivity:	Approx. 0.001 g at 20 db S/N ratio
Counting threshold:	Variable 0.001 g to 0.10 g
Outputs	
Recorder:	Direct output from amplifier
Audio:	Capacitively coupled to amplifier
Data display:	Event counter

moving down a shallow plunge line at a rate of approximately 0.03 in./day. Although that particular section of the mine was not active and a failure would not create an operating hazard, it was decided that the five units in the immediate area should be deployed so they could be evaluated under actual field conditions. It was hoped that the microseismic data might help predict a violent failure if one were to occur. The zone has continued to slip, but unfortunately for our test program, has not yet failed. Nevertheless, the data accumulated to date has helped us evaluate the system and plan future applications.

4.1 Purpose of Tests

All the installations were made for the purpose of evaluating the instrumentation and its potential for stability analysis. Because microseismic data is highly variable, a long time-period was allowed for data collection after each parameter was changed. Even so, many of the tests are inconclusive at this time. Typical questions which we hoped to answer were: (a) What sensitivity is necessary to record naturally occurring seismic events and is the equipment capable of achieving this sensitivity? (b) How and where should the accelerometers be installed? (c) How can seismic activity in a stable area be distinguished from similar activity in a potentially unstable area, or from non-seismic noise? The tests answered some of these questions, raised others, and yielded data which have led to a better understanding of potential system applications. Details of some of the tests are presented below. New tests are being planned in accord with the results to date.

4.2 Field Tests

Test No. 1

Purpose: To compare the sensitivity of alternate mounting methods.
Location: Units 1 and 2 in failure block.
Data: Daily total of recorded events.
Mounting: Unit 1 – buried 12 in., sensitive axis vertical.
Unit 2 – bolted to 3 ft steel post driven 3 ft into the ground, sensitive axis vertical.
Threshold level:
0.002 g
Results (Figure 5):
$N = 7$ days
$X_1 = 51$ events
$X_2 = 556$ events
$r = .8391$

Comments:
Correlation at the 99+% confidence level indicates that both units were recording natural events as opposed to random system noise. Ground coupling is substantially improved by post mounting.

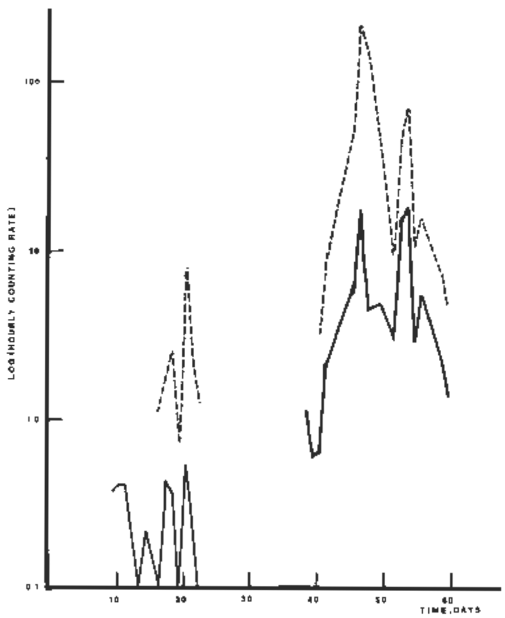

FIGURE 5--Sensitivity (left) and correlation (right) tests.

Test No. 2

Purpose: To compare two independent units at the same location and on identical mountings.
Location: 200 ft outside of failure zone.
Data: Daily total of number of events reduced to hourly rate.
Mounting: 3-ft steel posts, sensitive axis vertical.
Threshold: 0.002 g
Results (Figure 5):
$\underline{N} = 29$ days
$\bar{X}_1 = 16.2$ events/hr
$\bar{X}_2 = 27.5$ events/hr
$1 = 19.2$
$2 = 46.4$
$r = 0.69$

Comments:

Correlation at the 99+% confidence level indicates that both units were recording the same natural events without significant internal equipment noise. The average number of events recorded differed by a factor of nearly 2 even though care was taken to assure that the units were mounted as nearly alike as possible.

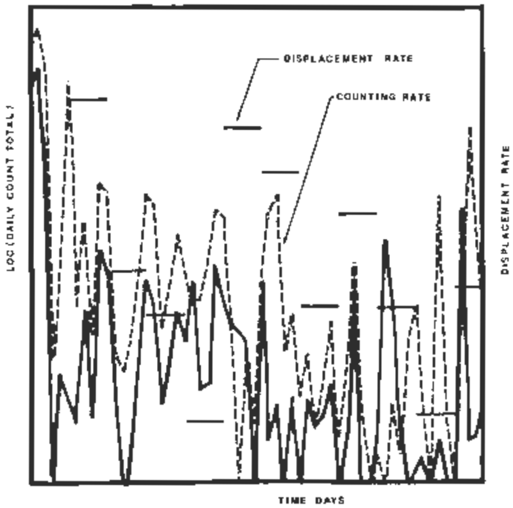

FIGURE 6—Typical data—test number 3

Test No. 3

Purpose: To determine the relative intensity of microseismic activity inside and outside of a failure zone, and its relationship to failure activity.

Location: Units 1 and 2 inside failure zone.
Unit 3 – 500 ft outside failure zone.

Data: 24-hour total of recorded events reduced to hourly rate, and measured daily failure displacement.

Mounting: 3-ft steel posts, sensitive axes vertical.

Threshold: 0.002 g

Results (Figure 6):

$N = 60$ days
$\bar{X}_1 = 2{,}422$ events/day
$\bar{X}_2 = 794$ events/day
$\bar{X}_3 = 256$ events/day
$\bar{X}_4 = 0.0035$ in./day
$r_{1-2} = .973$ – significant at 99.99% confidence level
$r_{1-3} = .202$ – not significant
$r_{1-4} = .093$ – not significant
$r_{2-3} = .163$ – not significant
$r_{2-4} = .093$ – not significant
$R_{4-12} = .344$ significant

Comments:

The test clearly showed the effects of failure, background seismic, and climatic noises on the micro seismic system. Failure noise increased the mean rate of events counted in the failure area, climatic noise correlated closely on all three units (although this is not shown in the above data), and background seismic noise was apparently local and showed little correlation from one location to another.

Test No. 4

Purpose: To ascertain the characteristics of noise associated with a failure displacement.

Location: Microseismic unit within the failure zone, displacement gauge spanning the peripheral cracks of that failure.

Data: Analog strip chart record of both seismic events and displacement, approximately 40 hrs.

Mounting: 3-ft steel post, sensitive axis vertical.

Threshold level: 0.002 g

Results: (See Figure 7).

Comments:

Three conditions were noted:

1. Displacements not associated with recorded noise.
2. Single cycle recorded noise not associated with displacements.
3. Multiple cycle noise, lasting up to 5 sec, always associated with recorded displacements.

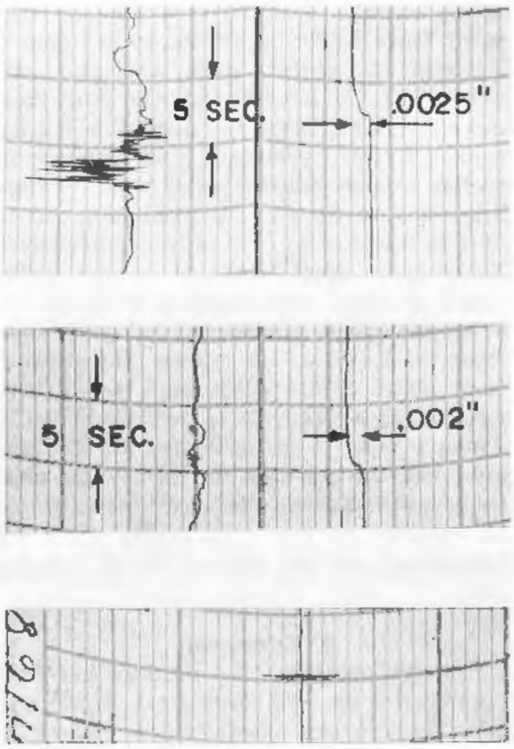

FIGURE 7–Examples of seismic "noise" associated with ground movement (top and centre), and a single microseismim (bottom). Chart enlarged 3x.

It was also noted that measured failure displacement was not at a continuous rate but occurred in discrect increments, and that these increments were irregularly spaced throughout daily periods.

4.3 Summary and Evaluation of Field Tests

The tests described cover only a small part of the total data recorded over a 2-year period. The following summary and evaluation is based on all available information.

4.3.1 Sensitivity – The system sensitivity is limited to approximately 1.5 x 10^{-3} g. Below this level, cable, amplifier, and recorder noise obscured the transducer signal. Satisfactory sensitivity of the system to ground motion was apparently achieved by post mounting. Other tests showed that the sensitivity was further improved by mounting the accelerometer on a rock bolt firmly anchored in rock. Surface post mounting made the unit highly sensitive to climatic noise, such as wind and thunderstorms, which was subtracted before the seismic noise could be evaluated.

4.3.2 Background Rate – The number of events counted per day at locations inside the failure zone was greater than the number counted outside the failure zone. Typical mean rates were 101/hr and 11/hr, respectively. It is interesting to note that many other investigators have reported similar rates. D. W. Wisecarver, for example, in a personal communication, made the following statement regarding data collected at another pit slope location which showed evidence of distress, "A small suspected weak zone is still being monitored with a single geophone ..... The area remained relatively stable until the August 16th earthquake. Seismic events soared from 10 events/hr to 716 events/hr on August 17th, dropped to 175 on August 18th, receded to 35 events/hr on August 19th, went back to 97 events/hr on August 20th and then gradually returned to the normal average 10 events/hr."

A 2-year record of underground rates compiled by Obert and Duvall (4) at one location showed normal monthly average rates of 10 to 30 events/hr and peak average rates of 90 to 180 events/hr. They noted the peak rates were associated with the development of a major new fracture.

4.3.3 Mining Noise – The effect of mining noise was apparently not significant at this particular location which was approximately 1,000 ft away from active operations. All blasts were recorded, but because the counting rate is limited to 1 count per 40 m sec, less than 5 counts were usually recorded per blast, and this number averaged over a 24-hour period was not significant. Mining was discontinued midway during the test program and no change in the average rate of recorded events was detected.

4.3.4 Variability of Data – The variability of the daily total of recorded events was large at all locations, partly due to an occasional count exceeding 5,000 events/day. Most of these high counts at locations outside the failure zone could be traced to severe storms; inside the zone, a lesser percentage could be so related.

For the most part, the standard deviation of events rate was slightly greater in the failure zone. The mean number of events was also greater but because of the large standard deviation, the differences in means and occasional high events could not be considered statistically significant. It was found that the frequency distribution of event rate was log normal and therefore some statistical tests were made in the log transformed data.

4.3.5 Correlation Between Recorders — The tests showed that the number of events recorded by different units in the same structural zone differed by factors of 2 - 3 but usually correlated at the 99.99 per cent confidence level. Data from units located in different structural zones correlated at a lower confidence level when all data was considered but showed little or no correlation after data known to be related to severe storms was removed.

Because each unit was operated completely independent of every other unit, the correlations indicate that the ratio of recorded natural events to recorded system noise must have been very high. It is not implied, however, that all natural events are of seismic origin. They might have been due in part to wind-blown static, tree-root movement, sonic booms, etc.

4.3.6 Correlation Between Events and Failure Displacement — The failure displacement was measured daily for a period of 2 years with a surveyor's chain. Total weekly displacement averaged 0.01 ft with minor seasonal variations. The percentage error in the daily measurement was, therefore, relatively high. Nevertheless, a correlation was shown to exist between the daily event rate and displacement. It is presumed that the occasional high event rates that could not be related to storm activity were related to the failure. A correlation test performed on the log-transformed data yielded a significantly lower correlation coefficient and this further indicated that the higher rates were not only related to the slide but are more important in the analysis than lower anomalous rates.

For test No. 4, a high-resolution displacement transducer was attached to a 60-ft wire spanning the peripheral cracks of the failure zone. Displacements and seismic activity were recorded simultaneously on a strip chart analog recorder operated at 1 mm/sec chart speed. Parts of that record, shown in Figure 7, illustrate the seismic noise associated with displacements of less than 0.003 in. From these records, it was apparent that displacement noise contained many cycles lasting over a period of several seconds whereas other noise, perhaps being strain-generated microseismims, consisted of 1 to 3 recorded cycles of higher frequency. These latter signals appeared on the analog record as single cycle traces as shown in the lower photograph of Figure 7, and would have registered 1 digit on the counter. The displacement noise, on the other hand, would have registered at a rate of 25 counts/second or 125 during a 5-second signal. Because the displacement rate changes from day to day, the noise count associated with that displacement would be expected to vary considerably above the background rate and this was found to be the case.

5. Conclusion

All test work on the program has been conducted in the field where access, power, and other desirably experimental conveniences were limited. Ideal test procedures could not be followed and results were, therefore, not always adequate for precise, unbiased interpretation. We have, nevertheless, drawn the following conclusions which we will temper with judgment for further application.

a. Displacement noise, as opposed to stress-generated rock noise, can be detected and should be the target for a microseismic system.
b. The digital register can be used in the system in place of analog recorders to indicate relative local seismic activity.
c. Surface mounting, or mounting in shallow drill holes can be adequate.
d. A reasonable level of mining noise can be tolerated.
e. The sensitivity to climatic noise must be reduced.
f. Trends, not absolute number of events, are the only reliable criteria at this time for slope analysis with microseismic recorders.
g. Depending on accelerometer mounting methods, a sensitivity level of 0.002 g is adequate.

The work to date has not proven the system for broad-coverage failure-warning application but has indicated that such an application is feasible. The results have given us an insight into the characteristics of the system, the seismic events, and the non-seismic noise. With this information, limitations and practical applications can be projected, and specific local analyses can be undertaken with a useful degree of confidence. We want the reader to understand that alternate equipment and other sites were not investigated. We therefore specifically refrain from making recommendations as to either equipment components or reliance on applications.

References

1. Goodman, R.E., and Blake, Wilson 1965. *Rock Mech. and Engineering Geol.* Supp. II, Safety in rock engineering, Proc. 15th Symp. Austrian Regional Group of Inter. Soc. Rock Mech., Sept. 1964, Salzburg Springer-Verlag, New York.
2. Paulsen, J.C., Kistler, R.B., and Thomas, L.L. 1967. *Slope stability monitoring at boron.* Mining Cong. J., Sept., 1967. Washington.
3. Wisecarver, D. W. 1968. *Changes in Stress, Strain and Displacement with Change in Slope Angle at the Kimbley Pit.* AIME preprint 68-AM-84.
4. Obert, Leonard, and Duvall, W. I. 1961. *Seismic Methods of Detecting and Delineating Subsurface Subsidence.* U.S. Bureau of Mines, Report of Investigations 5882.

C.D. Broadbent

Education — Engineer of Mines and M Sc, at Colorado School of Mines.

Employment Summary — Planning engineer for the Susquehanna Corporation; presently, mining engineer with Metal Mining Division, Kennecott Copper Corporation.

C.W. Armstrong

Employment Summary — Field engineer with General Electric Co.; professor of electrical engineering at Montana State University; consultant on process control at Kennecott Copper Corporation's Ozark Lead Company plant; and presently, head of process control section at Kennecott's Metal Mining Division.

Underground Measurements in a Steeply Dipping Orebody

D.G.F. Hedley and G. Zahary
Research Scientists, Elliot Lake Laboratory, Mining Research Centre, Mines Branch, Department of Energy, Mines and Resources, Elliot Lake, Ontario.
H.W. Soderlund
Chief Engineer, Algoma Ore Division, Algoma Steel Corporation, Wawa, Ontario.
D.F. Coates
Head, Mining Research Centre, Mines Branch, Department of Energy, Mines and Resources, Ottawa, Ontario.

Abstract

The problem of pillar stability at an iron mine was investigated by measuring field and pillar stresses, pillar deformation, sonic velocity and microseismic activity. Extensometer measurements of pillar deformation provided the most useful information on the extent of load transfer and stability of the pillar. These measurements in conjunction with the observed cases of pillar cracking indicate that the structural-weakness (fault and joint) planes are the main factors affecting stability. The in situ measurements of stress and deformation are compared to those calculated from a finite-element model, in an attempt to establish an analytical method of prediction.

Introduction

In 1963 a cooperative research program was established to carry out rock mechanics studies at the MacLeod Mine of the Algoma Steel Corporation. The objective of the work was to obtain basic information on the load, and deformation characteristics of the existing mine pillars, which would assist in the solution of the problems of mining at a greater depth. It was recognized that the results of any such rock mechanics investigations would only provide supplementary information that could be added to existing mining experience.

During the last six years a number of measuring techniques have been tried. Stress, deformation, microseismic and sonic measurements have been taken at several locations in the mine. This served the dual purpose of gathering data relevant to pillar stability and of evaluating the effectiveness of the measuring techniques in this mine. In many cases the measurements were designed to be complementary; for example, pillar cracking should be picked up by the extensometer, and by microseismic and sonic measurements.

In this paper the stress, deformation, microseismic and sonic measurements are summarized and compared. The case histories of pillars which have shown visible signs of cracking have been compiled, since these pillars show the first signs of instability. An analytical model, based on the theory of elasticity and using the finite-element technique, has been constructed to investigate the stress and deformation characteristics of a pillar as mining takes place. These stresses and deformations are compared to those measured in situ. Using all this information the critical parameters controlling the load applied to, and support offered by, the pillars can be more fully understood.

Description of the Mine

Algoma Ore Division of Algoma Steel Corporation operates both an underground mine and an open pit at Wawa, Ont., on the southwestern end of the Michipicoten iron range. The combined production from both operations is about 3,250,000 gross tons of siderite ore per year.

Geology

The Michipicoten iron range, which contains all the presently known orebodies, lies within a complex assemblage of Precambrian volcanic and sedimentary rocks. The siderite-pyrite orebody is bounded on the hangingwall by a volcanic series and on the footwall by a banded iron formation.

Structurally the orebody lies on the south limb of an east-to-west-trending syncline which has slightly overturned toward the north and plunges 40 to 60 degrees eastward. Thrust faults dipping 15 to 30 degrees south have displaced the ore zones northward and up. Two major thrust zones, separated vertically by 500 to 700 feet, are known to exist. These thrust zones considerably influence stope and pillar dimensions. The orebody dips generally at 70 to 80 degrees south but the flat thrust zones produce an overall dip of about 65 degrees.

In the central part of the orebody two steeply dipping diabase dikes intrude along major fault planes striking northwesterly, as shown on the plan of the M1 level, Figure 1. This major structural feature offsets the west and east section of the mine by about 300 to 400 feet. The mining zone terminates to the east at another diabase dike where major faulting displaces the iron formation.

Method of Mining

The George W. MacLeod mine has been developed along a strike length of one mile to a depth of 2,000 feet. The orebody is mined by a sub-level, longhole, open stope-and-pillar method. The main levels are driven on 300-ft vertical intervals and sub-levels on 75-ft centres. Stopes are 60 to 75 ft along strike and usually 230 ft high. Pillars are 75 to 80 ft along strike and take the form of an inverted letter 'L'. The crown pillar overlies the adjacent stope and extends to the level above. The stope and pillar dimensions in some sections of the orebody differ from the above because of geological structures, intrusives and grade considerations.

A stope is normally blasted, over a period of several months, in rings 5 ft apart. The pillars are taken out in two large blasts, first a 15-ft slash then the remainder of the pillar.

The dimensions of the MacLeod orebody and the overlying mined-out Helen orebody are such that large openings are created. The comparatively low grade of the ore precludes the use of back-filling and consequently the mining sequence is planned to take advantage of natural caving of the hangingwall. At present, in the west section of the MacLeod mine, the ore has been removed over a strike length of about 800 ft to a depth of 1,000 ft, as shown in the longitudinal section, Figure 1. Caving of the hangingwall and ore lost through dilution has

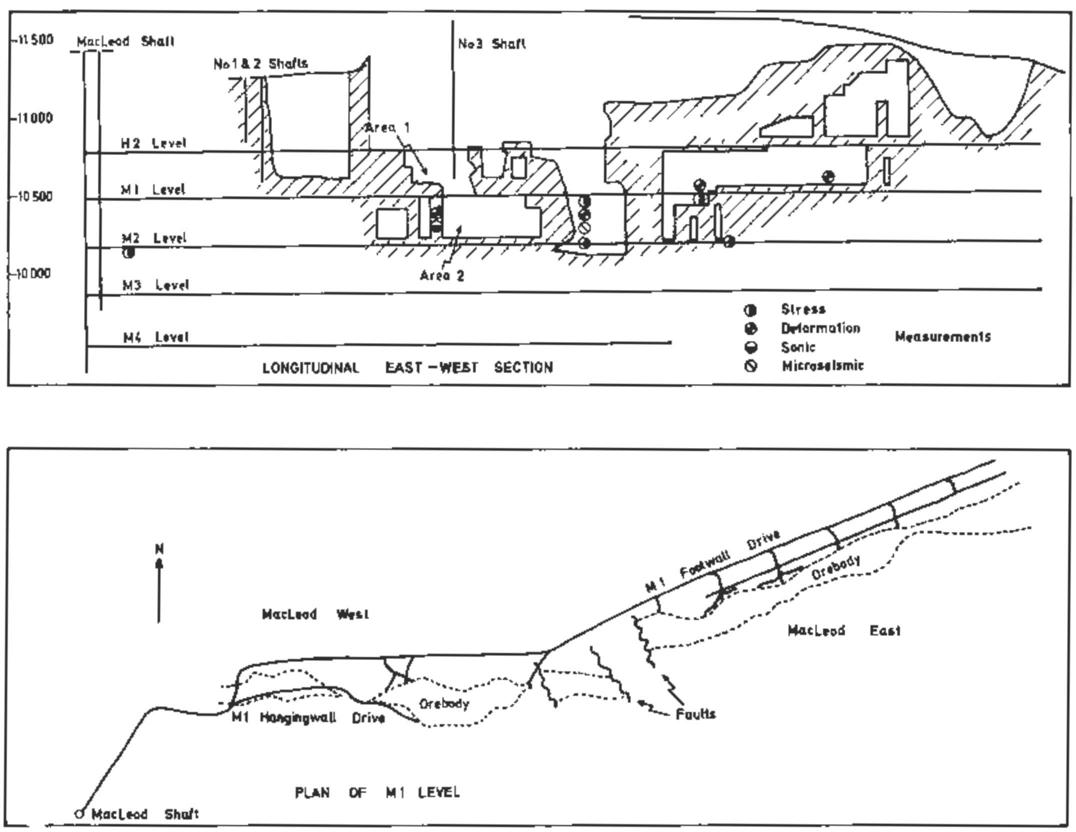

FIGURE 1 — Section and plan of the MacLeod mine showing location of instrumentation sites

provided a cover of about 200 feet of broken rock over the active workings.

It was expected in the early planning stages that the hangingwall would slough readily, but experience now indicates that the hangingwall will stand up vertically over the spans mined to date. Consequently, it is now the intention to leave four semi-permanent pillars, two in each of the east and west sections of the mine. These pillars will be approximately 225 feet wide at about 800-foot centres and extend from the top to the bottom mining level.

The overall mining sequence is planned to retreat east and west from the centre of the orebody, with the east and west mining faces on any level being 500 ft ahead of the mining faces on the level immediately below. Consequently, from the point of view of ground control there are no open stopes below active mining operations.

Measuring Techniques

The longitudinal section of the mine, Figure 1, shows the locations at which measurements of stress, pillar deformation, sonic velocity and microseismic activity were taken. The general methods of measurements are outlined in the following sections.

Stress

An overlying technique was used to determine the stresses acting on the orebody; the principle being that the rock, when the stresses are removed by overcoring, relaxes and the magnitude of the relaxation is proportional to the stresses originally acting on the rock. By measuring relaxation in three orientations in a borehole and knowing the elastic properties of the rock, the magnitudes and directions of the principal stresses can be calculated for the plane perpendicular to the axis of the borehole. This method of measurement gives the stress values at the time of overcoring but does not give directly the increase in stress resnlting from mining. The USBM deformation meter was used as the sensing device and the change in diameter of an EX borehole was measured when overcoring with a 6-in. dia. bit.

Extensometer

Borehole extensometers measure the relative movement between the collar and a point in the borehole. Usually the rock movement is the result of mining and it is measured over a period of time.

Both bolt and multi-wire extensometers have been used at the mine. The bolt extensometer consists of a rock-bolt shell and rod anchored in a borehole. The end of the rod protrudes through a sleeve at the borehole collar, and a dial gauge measures the movement between rod and sleeve. A separate borehole is required for each bolt. With the wire extensometer, as many as four wires can be installed in one borehole. The longer wires pass through holes drilled in the anchors. The extensometer is intermittently connected at the borehole collar and measures the relative movement between wire and borehole.

Sonic

This technique involves a measure of the transit time of a compressional sonic wave between a transmitter and a receiver probe anchored in two boreholes. A signal is generated by tapping a pipe connected to the transmitter, and the transit time is measured by means of an oscilloscope. The velocity of sour. through rock is basically dependent on the elastic properties of the rock; however, the velocity can be considerably altered by the structural-weakness planes in the rock mass.

Microseismic

The Seismitron is an instrument for detecting sub-audible noises in rock. Used in its simplest form a geophone is lowered into a short borehole and the number of amplified sounds, as heard on earphones, is recorded over a certain time interval. In an area where the background level of noise is constant, any increase in the number of sounds is an indication of increasing stress and possible instability.

Results of the Measurements

Stress

A program of measurements was undertaken to determine the field stresses acting in the orebody and the pillar stresses. It was expected that stress values, representing an order of magnitude, could be obtained from a few observations. This involved certain assumptions including a homogeneous stress field around the orebody and elastic behaviour of the rock mass.

The locations of the stress measurements are shown on the longitudinal section, Figure 1. Measurements were made at different locations in the borehole to a depth of 20 ft to define the stress concentration, and results from the bottom part of the hole were used. The stresses of greatest interest are those acting parallel and perpendicular to the axis of the pillars and consequently parallel and perpendicular to strike of the orebody. For practical purposes, all holes were horizontal and measurements were made in a vertical plane.

Pre-mining field stress parallel to strike was measured in a borehole drilled in hangingwall tuff. The site was on the M2 level near the shaft, 1,500 ft from the nearest mining and some 1,300 ft below surface. A maximum stress of 6,500 psi dipping 20 degrees to the east was obtained. A similar measurement was made, on the same level, 4,000 ft to the east in footwall iron formation. Mining had been completed 300 ft above and 700 ft to the west of the site. An average of 5,000 psi between 10 and 20 ft in the hole was obtained for the maximum stress which dipped 10 to 20 degrees to the east.

Another borehole was drilled in the footwall iron formation to measure stress perpendicular to strike of the orebody. The maximum stress was of the order of 4,000 psi acting perpendicular to the walls.

Pillar stresses of the order of 2,500 to 3,000 psi perpendicular to the hanging wall and footwall were measured in pillars 242 and 251. The mining geometry for both sites was similar in that an opening of about 200 ft existed on one side of the pillar and a 60 ft open stope on the other. In addition, a borehole was drilled on the M2 level directly below pillar 242. In this case a maximum stress of 5,000 psi was measured perpendicular to the hanging wall and footwall.

The vertical field stresses were found to vary between 1,700 psi and 2,900 psi. The gravitational load is of the order of 1,400 psi at all locations.

The data indicates that vertical stresses can be double the gravitational load; horizontal stresses are greater than the vertical; and the stress parallel to strike is greater than the perpendicular stress. Hence, if the data is accepted at face value, previous tectonic history rather than depth provides a more logical explanation for the observations.

On the other hand, the measurements obtained here are not conclusive. Departures from the original assumptions do occur. A high stress concentration around the mine opening and an area of uniform stress beyond was not always obtained. Planes of weakness in common mine rocks are considered to be a major contributing factor. Weakness planes on the scale at which the instrumentation operates produce large fluctuations in results.

On the basis of this work the concept of an average stress field around the orebody is retained. The principal stress acting parallel to strike is of the order of 5,000 psi, the intermediate stress acting perpendicular to strike, 2,500 to 5,000 psi, and the minor principal stress acting vertically, 1,500 to 3,000 psi. Other sources of information must be used to establish whether the measurements are adequate. Discontinuities in rock appear to be a significant factor in producing fluctuating results. This implies that measurements should be made with much closer geological correlation.

Extensometer

In general, the purpose of the borehole extensometers was to measure the deformation of a pillar as mining takes place in the vicinity. Of specific interest were the nature and order of magnitude of the movement, the locations in the pillar where the movement occurred, and the distance over which mining affected the pillar. The locations of the extensometer sites in pillars 242, 251, 163 and 228 are shown on the longitudinal section, Figure 1, and the enlarged individual sections and plans for each site in Figure 2.

The measurements taken in pillar 163 gave a comprehensive picture of pillar deformation. Extensometers were installed from a central crosscut and measured at intervals along the three axes of the pillar. Measurements started at the beginning of mining and ended with the pillar being blasted out. The graph of total deformation of pillar 163 is shown in Figure 3. These three curves represent the movement in each direction of the end measuring points relative to each other. A record of the time over which the stopes were mined and pillars removed is given below the time axis of the graph.

It is possible to relate, qualitatively, pillar deformation to mining activity from this graph. Between hanging wall and footwall, mining of the adjacent stopes 162 and 164, and the 163 pillar slash, produced appreciable deformation (compression), whereas mining stope 166 and pillar blasts 157, 159, 161 and 165 had no significant effect. The individual measurements along this axis showed that the major movement took place at the centre of the pillar and there was little movement at the hanging wall and footwall. This indicates a stress parallel to strike considerably higher than that perpendicular to strike.

The expansion measured in the vertical direction increased slowly while mining stope 164, 165 pillar blast, and 163 pillar slash. The individual measurements showed that the expansion was almost totally confined by 15 ft above and 30 ft below the crosscut, and the movement between roof and floor of the crosscut was also expansion. These observations could result from a compressive stress acting between hanging wall and footwall, higher than the vertical stress. Also the open stopes, above pillar 163, will have partially diverted the gravitational load to the hanging wall and footwall.

Relatively large expansion was measured between the east and west sides of the pillar during the mining of stopes 162 and 164. The first pillar blasts 157, 159 and 161 had little effect, but 165 pillar blast and 163 pillar slash as well as mining stope 166 resulted in considerable expansion. It would seem that expansion on the east and west sides of the pillar during and after the mining of stope 166 was mainly due to the disturbance caused by blasting rather than the transfer of load, since no significant movement was measured betweeu hanging wall and footwall during the mining of stope 166 and the 165 pillar blast.

The profiles of lateral expansion across pillar 163 in the east-west direction are shown in Figure 4. Most of the expansion was confined to the outside of 14 ft of the west side of the pillar during the mining of the adjacent stope 162 (curve 1). The largest deformation gradient, indicating possible cracking, was between 9 and 14 ft from the pillar edge. This pattern of movement was repeated during the initial mining in stope 164 and the 161 pillar blast (curve 2). On the completion of mining stopes 164 and 166 and the 165 pillar blast, the expansion of the 14 ft at the west side of the pillar increased appreciably (curve 3) indicating definite cracking within this zone. Also expansion occurred on the east side of the pillar with the maximum deformation gradient being within 10 ft of the pillar edge. During all this mining activity the central 50 ft of the pillar remained relatively undisturbed. However, there was a general overall expansion when a 15-ft slash was taken off the east side of pillar 163.

Extensometer bolts were installed in the west side of pillar 228 (Figure 2) after stope 229 on the east side was near completion. Beyond pillar 230 the opening span was 400 ft to pillar 236. Above pillar 228 the stopes and pillars had been mining out. The extensometers measured the lateral expansion of the pillar as stope 227 was mined and pillars 230 and 236 blasted. Curves 4, 5 and 6 in Figure 4 show the profile across the west side of the pillar. Curve 4 is after the 230 and 236 pillar blasts and curve 5 after stope 227 had been partially mined. These two curves indicate that the major expansion was taking place within 5 ft of the centre crosscut with little movement in the rest of the pillar. At this time a diagonal crack was observed running the general direction northwest to southeast which intersected the 5-ft extensometer bolt. On completion of mining in stope 227 (curve 6) there was an overall expansion of the west side of the pillar with the edge moving about 3/4 in., indicating intensive cracking of the pillar.

Measurements of lateral pillar expansion were taken in both the east and west directions in pillar 242, as pillar 244 and stope 241 were mined (Figure 2). The pattern of movement was similar to that obtained in pillar 163, although the magnitude of the expansion was much less. Extensometers installed in the east side of pillar 251 recorded very little expansion during the mining of stope 252 (Figure 2).

The measurements of lateral pillar expansion show that the movement is closely related to nearby mining and takes place along pre-existing joint and fault planes. These geological weakness planes are probably the determining factor concerning pillar sloughing and instability. A structural geological study has been undertaken in pillars 167 and 228 representing the east and west sections of the mine (G. Herget, private communication). It was found that in the east section the joint frequency was much greater than in the west. In addition, the two major joint sets in the east were oriented parallel to the pillar sides and perpendicular to the dip of the orebody, whereas in the west the two major sets of joint and fault planes were nearly vertical and extended diagonally across the pillar. Consequently, the pattern of pillar deformation is likely to be different in the east and west sections. In the east, as exemplified by

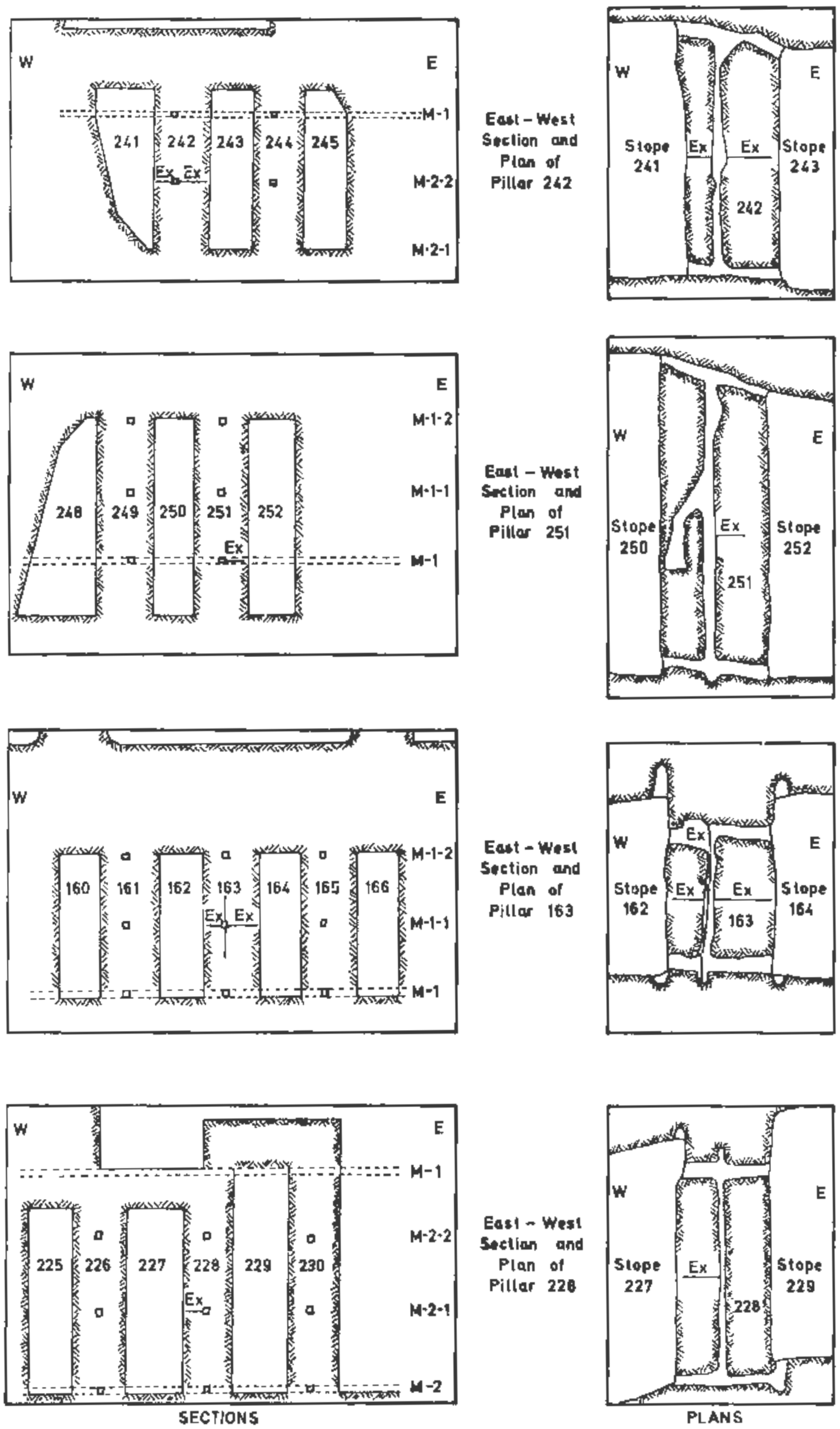

FIGURE 2 — Section and plan of extensometer measuring sites

pillar 163, lateral expansion is concentrated at the sides of the pillar and the rock expands toward the open stopes. In the west, as exemplified by pillar 228, shearing movement takes place along a diagonal fault or joint which intersects the centre of the pillar.

Sonic

Sonic velocities were measured in the 228 pillar near the extensometer site. It was expected that cracks would develop in the pillar as load and confinement were altered by mining. Sonic velocity decreases in fractured rock and the measurements over a period of time could indicate developing pillar instability. Consequently, measurements were repeated at three- to four-month intervals at each location in the pillar.

Two rings of probe holes were drilled 15 ft on either side of the bolt extensometer. Each ring consisted of 6 ft vertical, 25 ft horizontal and two intermediate inclined holes. This configuration provides a number of transmission paths of which 16 were chosen; most of these were parallel to the three axes of the pillar.

During the period of measurement, the 230 and 236 pillars were removed and the 227 stope advanced. The extensometer measurements showed (Figure 4) that a diagonal crack developed which intersected the 5-ft bolt and also the transmission path of the sonic pulse. However, the measurements of sonic velocity varied by less than 10% during this period. Eventually, one set of holes was cut-off by the diagonal crack.

Transmission time is measured to within 5% by the oscilloscope. The field work was done in an active mining area where the background noise level was high and it was difficult to obtain accurate and consistent measurements. Consequently, a difference in sonic velocity of less than 10% is interpreted as not being significant.

The average velocities measured parallel to the pillar axes are given in Table 1. Previous work in the laboratory established that the longitudinal-wave velocity in siderite was of the order of 18,500 – 20,000 ft/sec. The measurements obtained in the present series of tests are slightly higher than those obtained in intact rock (no discontinuity) in the laboratory.

Although the sonic apparatus is designed to measure longitudinal-wave velocity, transit times are quite often measured, which seem to give reasonable values for the shear-wave velocity. These values are also given in Table 1.

Using the average longitudinal- and shear-wave velocities, Poisson's ratio was calculated to be 0.23. The elastic modulus of the rock, which is related to the longitudinal-wave velocity and Poisson's ratio, was calculated to be 17×10^6 psi. The elastic modulus obtained for siderite from compression tests on small samples in the laboratory, ranges between 13 and 21×10^6 psi, which is the same order of magnitude as that obtained from the sonic tests.

In summary, the sonic measurements indicate no general deterioration in the pillar rock. The one isolated crack which developed did not result in any significant change in sonic velocity. The velocities measured along the three pillar axes are consistent and give reasonable values for the elastic constants of siderite.

Microseismic

Four sites were established in pillar 242 to monitor microseismic activity. These consisted of a 5-ft hole drilled into the pillar wall. Three sites were located on the same level, one at the centre of the pillar and the others in two outside corners. A fourth site was located at the base of the pillar some 100 ft below.

Blasting of pillar 244 immediately to the east resulted in a 50% increase in the number of noises. This increased activity continued for about three weeks in the pillar corner facing the

TABLE 1
Results of Sonic Tests

	Along Strike	Normal to Strike	Vertical	Average
Path length, feet	15	30	10	
Longitudinal-wave velocity, ft/sec	20,865	19,974	20,218	20,350
No. of readings	7	16	6	
Shear-wave velocity, ft/sec	11,151	12,352	12,630	12,040
No. of readings	6	4	1	

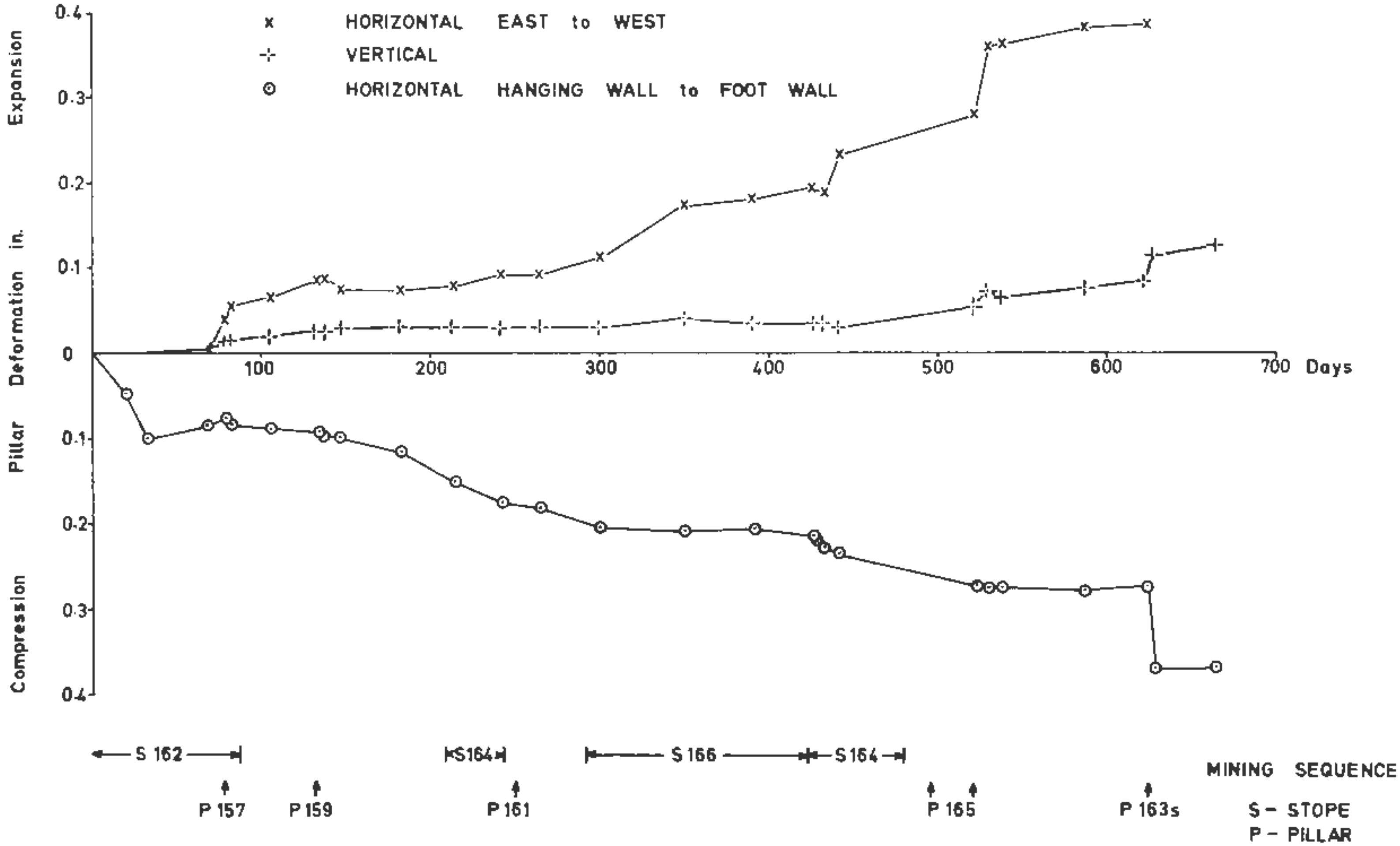

FIGURE 3 – Deformation of pillar 163

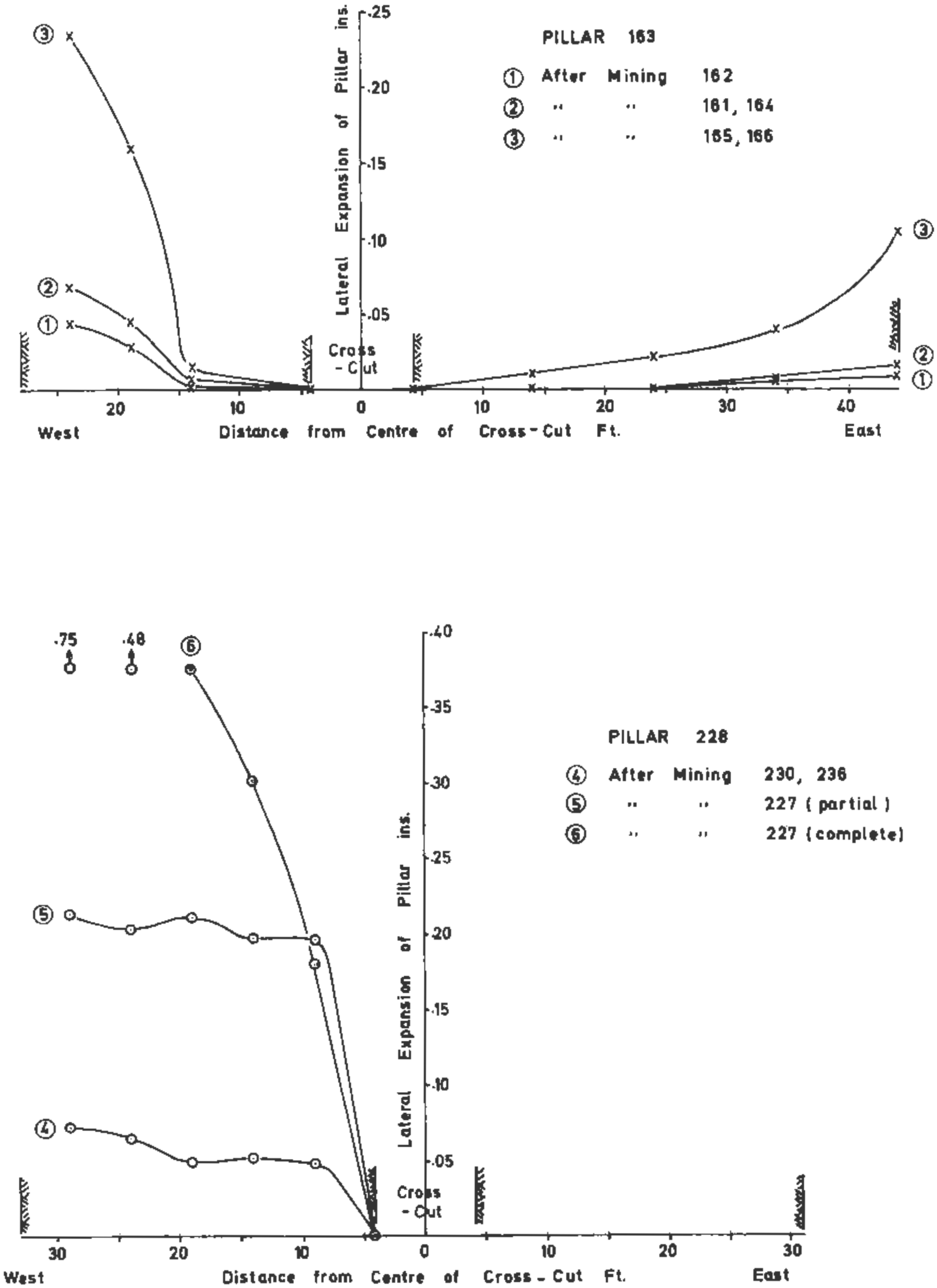

FIGURE 4 – Profiles of lateral expansion, pillars 163 and 228

blast and for one to three weeks at the other sites. Lower noise counts were obtained at the base of the pillar than at mid-height. Subsequently the noise counts declined until the pillar was removed.

Measurements were made in an upper level to monitor stability of an unsupported section of the hanging wall. Between 50 and 100 noises were recorded in different 10-minute intervals. The noise level remained constant and failure in the wall was not observed.

Another series of observations in a crown pillar at the bottom of the mined-out area produced counts of the order of 250 noises/10-minute interval following a 9,000-ton pillar slash. The noise level declined more-or-less linearly in the following two months until the pillar was removed.

The technique was applied here to monitor the stability over large distances, say 100 ft or more. Although the measurements are easily obtained they are difficult to interpret, where the problem is on such a large scale. One of the problems is that the measurement is largely subjective. The operator must choose between the various tones and loudness of the noises without knowing the origin and, hence, significance of any particular noise.

Theoretical Pillar Stresses and Deformations

At present, any theoretical prediction of pillar stresses or deformations can only be made with a two-dimensional analysis. The geometry of the MacLeod mine does not lend itself well to a two-dimensional idealization, which essentially requires that the variations in geometry occur in one plane, with the configuration in the third dimension being essentially constant. In spite of the difficulty, analyses have been made that provide some insight into the reactions, due to adjacent mining, that can be expected in the pillars.

A section, approximately horizontal, has been taken through the first sub-level of a typical pillar as shown in Figure 5. By making a two-dimensional analysis in this plane the implicit assumption is that the geometry is continuous in the third dimension. However, it is only continuous for 100 ft above and below this section, which is of the same order of magnitude as the dimensions of the stopes and pillars. Consequently, load will be diverted above and below the stopes as well as laterally to the pillars. The mining of the crown pillars above the stopes will result in additional transfer of the stresses to the pillars and below the stopes, it being impossible to transfer through the mined-out upper stopes.

The stopes and pillars as shown in Figure 5 were part of a larger model loaded in the directions normal (N – S) and parallel (E – W) to strike. This model was divided up into a series of finite elements, and the effects of mining adjacent stopes aud pillars on a remaining pillar were analyzed using the finite-element technique (Wilson). The sequence of mining in the model was: stope No. 1, stope No. 2, stope No. 3, pillar No. 4, stope No. 5, pillar No. 6, and pillar slash No. 7. Based substantially on tests on the rock substance, it was assumed that the modulus of deformation of the rockmass was uniform and equal to 10×10^6 psi with a Poisson's ratio of 0.2. It was further assumed that the field stress normal to strike, S_o, was 2,500 psi and the field stress parallel to strike, S_t, was 5,000 psi.

The overall deflection of the walls and pillars due to the mining of stopes and pillars No. 1 to No. 6 is superimposed, to an exaggerated scale, on the mine section in Figure 5. The barrelling of the pillar and the bowing-in of the walls are to be expected. However, the absolute movement of the pillar laterally is less likely to be anticipated and must result in a certain amount of working and loosening of the pillar. This lateral movement is even greater during the first stages of mining.

Figure 6(a) shows the movement in the pillar along section B – B relative to the pillar centre at the various stages of excavation. This graph would be comparable to that obtained from a borehole extensometer with the collar at the pillar centre and anchor points at 20, 40 and 60 ft toward the hangingwall or footwall. These curves are similar to that shown in Figure 3, showing that the deformation from hanging wall to footwall in pillar 163 increases with progressive mining of adjacent stopes and pillars. The mining of stopes No. 3 and No. 5 have a very large effect (Figure 6(a)) on the deformation of the pillar, as does the excavation of the adjacent pillar No. 6. The movement per unit length (strain), represented by the spacing between the curves, is greatest at the centre (0 – 20 ft) and decreases toward the walls (40 – 60 ft).

Figure 6(b) shows the profiles of pillar stress in the direction normal to the walls along

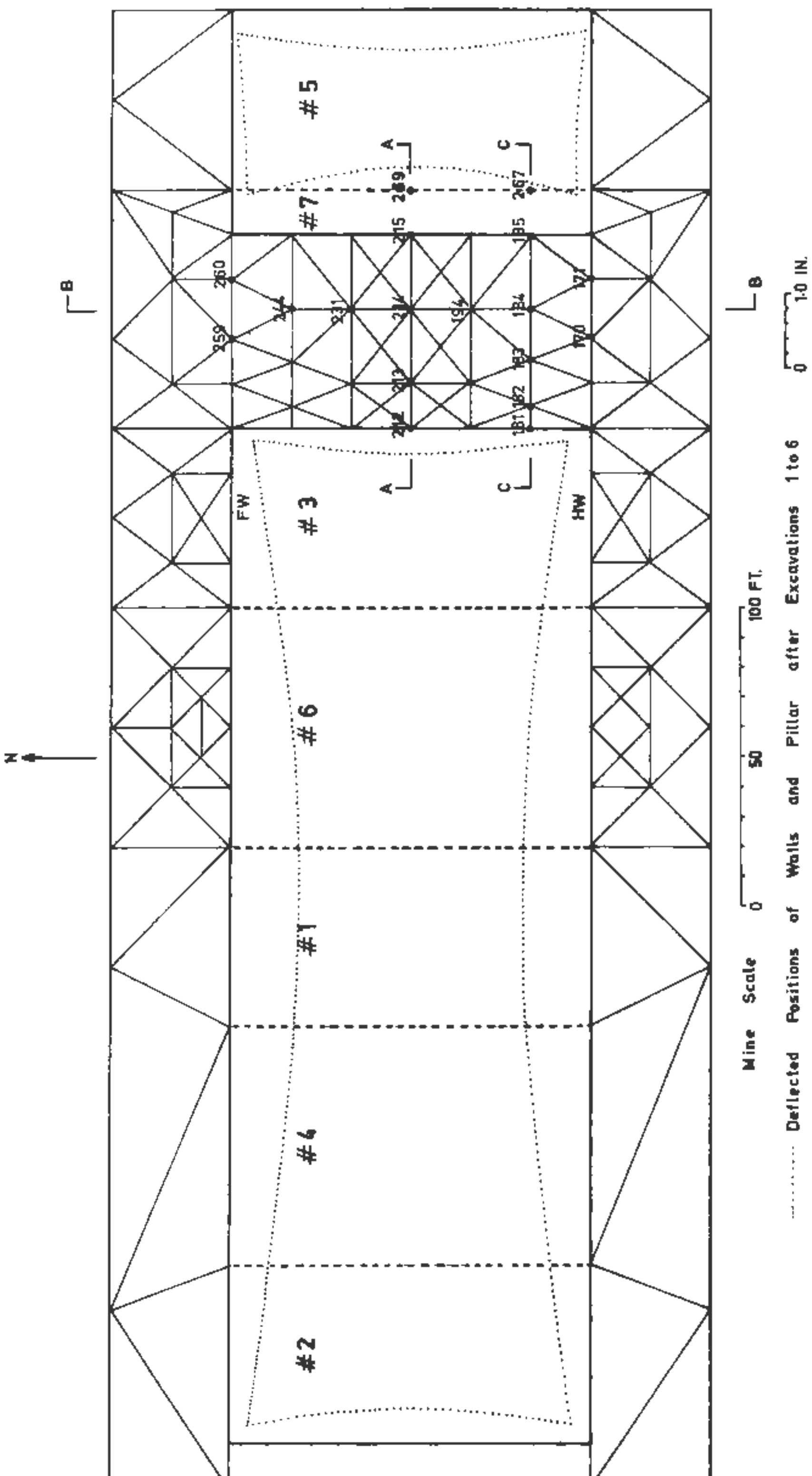

FIGURE 5 — Finite-element Model

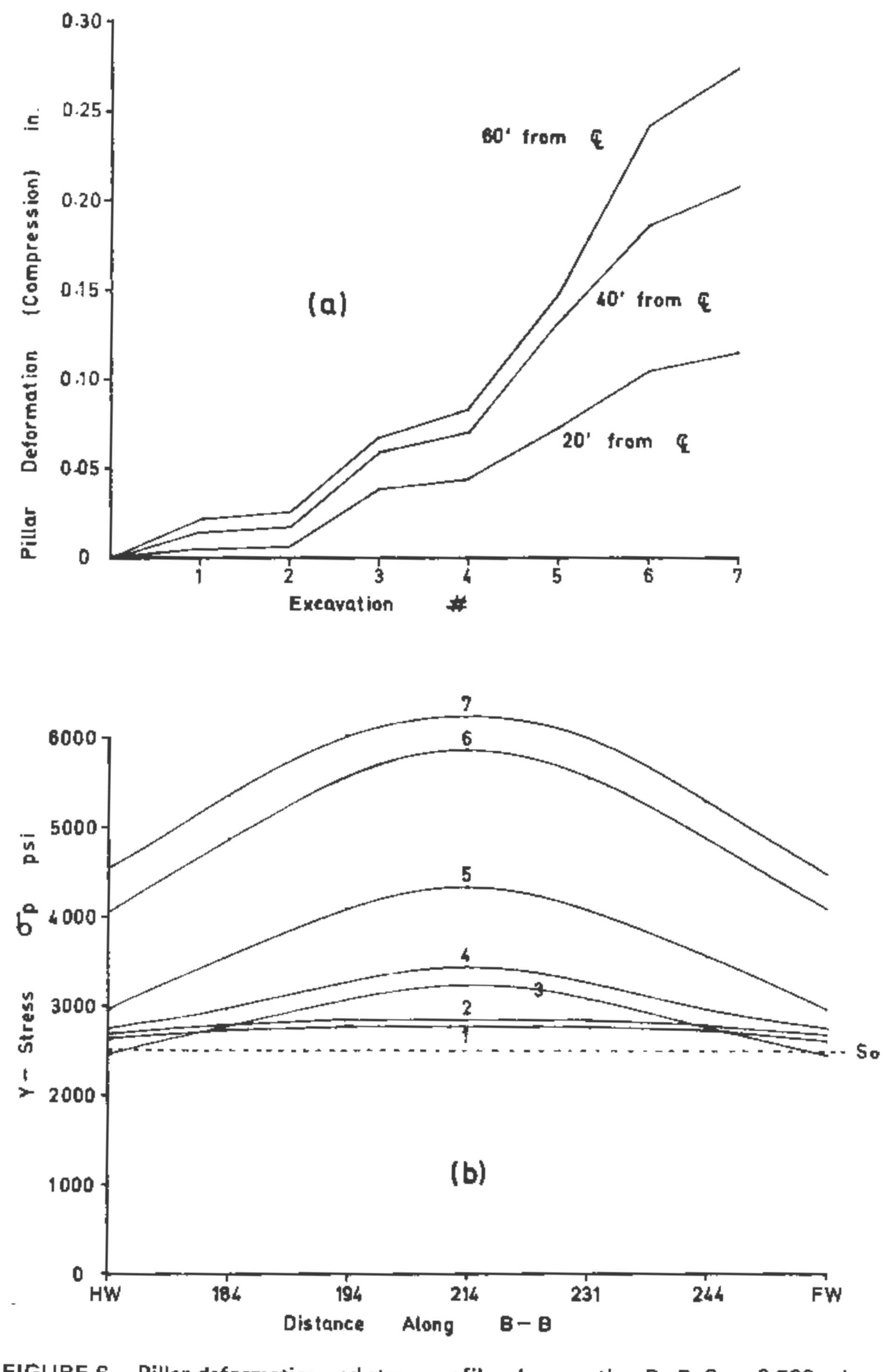

FIGURE 6 – Pillar deformation and stress profiles along section B–B, S_o = 2,500 psi.

the section B – B. The profiles show the increase in stress resulting from successive excavations and the increasing difference in stress between the central portion of the pillar and the zones adjacent to the walls. This stress difference as well as the increase in transverse stress toward the walls accounts for the decrease in pillar deformation near the hangingwall and footwall.

Figure 7(a) shows the displacements across the pillar at section A – A. It can be seen that excavations No. 1 and No. 2 result in a general movement of the pillar to the west. Excavation No. 3 causes an even greater movement to the west as well as a large increase in the expansion between the two sides of the pillar. Excavation No. 4 has little effect. Excavation No. 5 results in a movement back toward the east as well as increased expansion; excavations No. 6 and No. 7 have similar effects.

Figure 7(b) is a re-plot of the lateral pillar expansion along section A – A, comparable to a borehole extensometer with the collar at the pillar centre and anchor points at 25 and 40 ft toward the east and west sides of the pillar. It can be seen that mining stopes No. 3 and No. 5 on either side of the pillar produced most of the expansion.

Figures 7(c) and 7(d) show the profiles of axial pillar stress across the pillar at sections A – A and C – C. The stress pattern is different at the two sections; at A – A the stress is highest at the centre and decreases toward the pillar sides, whereas at C – C it is completely the opposite. It is interesting to see the conspicuous decrease in pillar stress at the west side of the pillar, section A – A, resulting from mining the adjacent stope No. 3. Then with the mining of stope No. 5 on the other side of the pillar these low stresses are increased to give a symmetrical distribution across the pillar. Curiously, the mining of pillar No. 6 results in a relatively large increase in stress on the west side of the pillar contrary to the results of mining stope No. 3. The transverse stress along section A – A was found to be reduced to zero after the excavation of the adjacent stopes No. 3 and No. 5. Along section C – C the restraint coming from the walls was found to be sufficient to preserve a considerable portion of the original stress parallel to strike in the central part of the pillar.

Table 2 shows comparative figures obtained from field measurements of the longitudinal compression and lateral expansion. The measurements are by borehole extensometers (BHE) and the predictions by the finite-element analysis (FE). The predicted figures are obtained from the above analysis using the incremental deformations resulting from the mining of whichever excavations No. 1 to No. 7 are equivalent to the actual block that was excavated. Furthermore, the results from the finite-element analysis are adjusted to correspond to the actual measuring lengths in the pillar.

The measured and predicted results for pillar 163 given in Table 2 are separated into two groups: the total measuring lengths (106 ft N – S, and 68 ft E – W) and over the central portion of the pillar (45 ft N – S and 38 ft E – W) which is relatively unaffected by the constraint of the walls and the zones of cracking at the sides of the pillar.

For the overall movement, the mining of stope 162, pillar 159 and the first stage of stope 164 produced poor agreement for the lateral east-west expansion but good agreement for the longitudinal north-south compression. The mining of blocks 161, 166, second stage of 164, 165 and 163 pillar slash caused the differences between measured and predicted movements to converge in the east-west direction and diverge in the north-south direction.

The measurements in the east-west direction started a month after those in the north-south direction during the mining of stope 162. Consequently, part of the east-west expansion was not measured. If the comparison is made for the mining of block 159 onward then the measured expansion is always greater than the predicted expansion, i.e. after mining pillar 165 the measured movement is 0.30 in. and the predicted movement is 0.22 in. This means that the measured movements might include non-elastic deformation, possibly due to the opening of cracks and joints as deduced from the profiles of laterial expansion shown in Figure 4.

The movements measured in the central portion of the pillar show poor agreement in the east-west direction. After mining of stope 162 no significant east-west expansion was measured until the second stage of mining in stope 164, and there was a large expansion with the 163 pillar slash which probably caused cracking throughout the pillar. The predicted movements show a general increase in expansion for

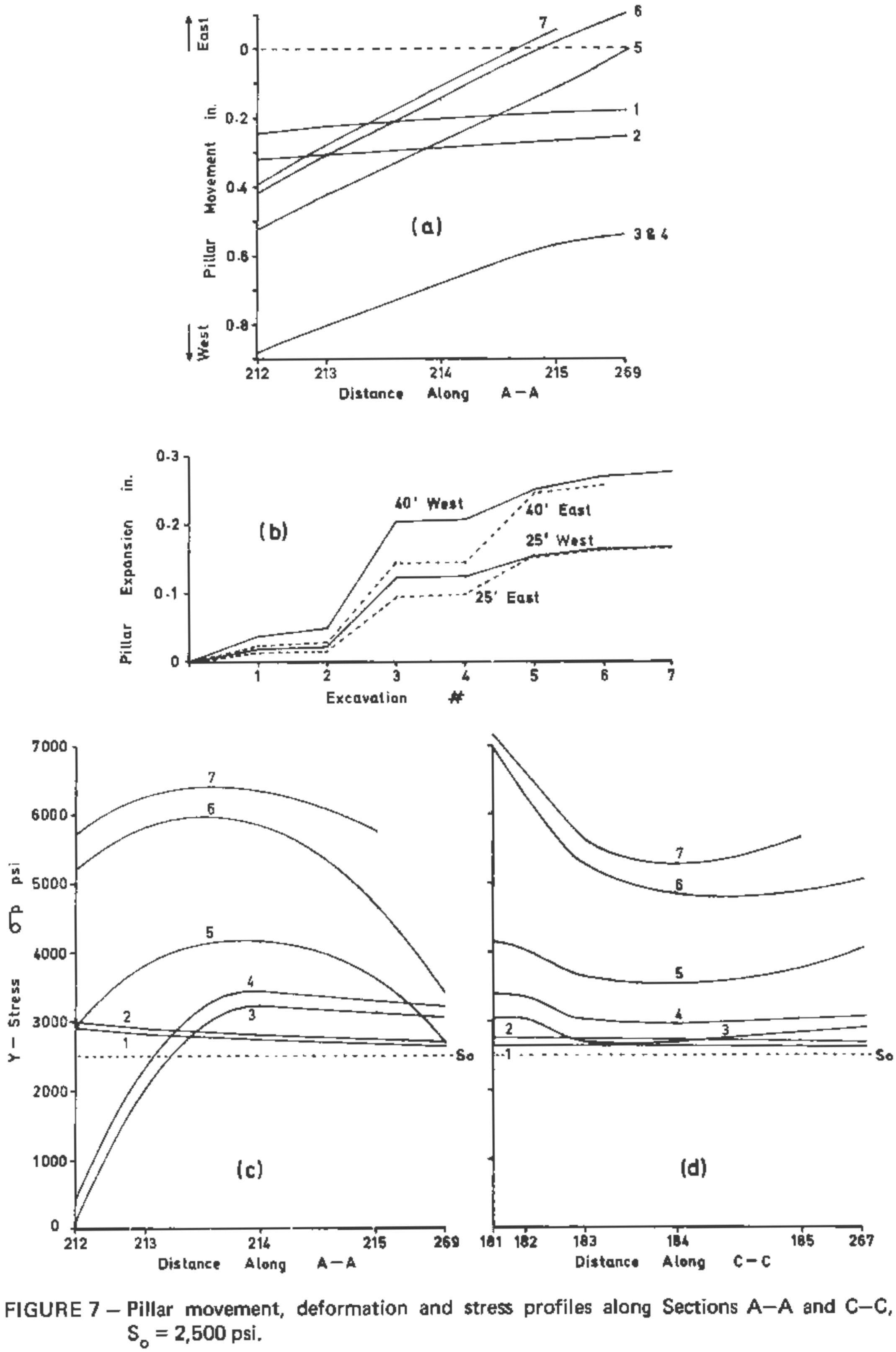

FIGURE 7 – Pillar movement, deformation and stress profiles along Sections A–A and C–C, S_o = 2,500 psi.

TABLE 2
Longitudinal Compression and Lateral Expansion of Pillars Due to Adjacent Mining of Blocks at the MacLeod Mine, Measurements vs Predictions

Pillar Site	Block Excavated	Disp'ts E – W BHE** in.	Disp'ts E – W FE*** in.	Disp'ts N – S BHE** in.	Disp'ts N – S FE*** in.	Measuring Lengths
163	162	0.06	0.21	0.09	0.08	N – S 106 ft
	159	0.08	0.21	0.10	0.11	E – W 68 ft
	164*	0.10	0.28	0.17	0.17	
	161	0.10	0.30	0.18	0.33	
	166	0.20	0.34	0.22	0.37	
	164*	0.28	0.41	0.27	0.43	
	165	0.36	0.43	0.27	0.59	
	163			0.37	0.65	
163	162	0.03	0.14	0.11	0.04	N – S 45 ft
	159	0.02	0.14	0.12	0.06	E – W 38 ft
	164*	0.02	0.17	0.16	0.09	Central
	161	0.02	0.19	0.17	0.16	portion of
	166	0.02	0.22	0.19	0.18	pillar
	164*	0.05	0.25	0.22	0.21	
	165	0.06	0.27	0.23	0.28	
	163	0.18	0.27	0.29	0.30	
242	241, 244	0.10	0.09			E – W 48 ft
251	252	0.01	0.04			E – W 20 ft East side

* Stope 164 mined in two stages, assumed predicted displacement equally divided between stages.
** Measured by borehole extensometer.
*** Predicted by finite-element analysis.

all stages of mining with the 163 pillar slash being a notable exception.

Although there is overall agreement between measured and predicted movements over the 45 ft in the north-south direction the individual increase for each block in some cases do not correspond. The measured movements show that adjacent stopes 162 and 164 and the 163 pillar slash produced the major movement, whereas the predicted movements show that the mining of pillars 161 and 165 should also have produced significant movements. The possible causes which could produce these discrepancies are discussed at the end of this section.

The deformation measured in pillar 242 resulting from the mining of blocks 241 and 244 is in close agreement with the predicted movement. The comparison for pillar 251 is not as good although the order of magnitude is the same. Movements measured in pillar 228 (Figure 4) are not included in Table 1 since most movement was concentrated at a weakness plane and is not predicted by this finite-element analysis.

The comparison between measured pillar stresses and those determined by the model are shown in Table 3. For the assumed field stress (S_o = 2,500 psi, S_t = 5,000 psi), it can be seen that the measured stresses are roughly half the predicted stresses. The fact that there is three-dimensional transfer of stresses around the actual pillars undoubtedly is a major reason for these differences.

In spite of this probable explanation, further analyses were made varying the field stress. These cases might be considered as producing two-dimensional conditions equivalent to the actual three-dimensional transfer; in other words, only a fraction of the field stress is being transferred into the pillar, the other part being diverted above and below the stopes. It can be seen that if field stresses of S_o = 1,600 psi and S_t = 4,000 psi are used, the agreement with the measured stresses is very good. In an alternate

TABLE 3
Stresses in Pillars at the MacLeod Mine,
Measured vs Predicted

Pillar Site	Model Excavations to Approximate Actual Conditions	Pillar Stresses		Remarks
		Measured psi	Predicted psi	
242	1, 3, 5, 6, 7	2600	6000	Pillar breadth 66 ft compared to 80 ft for model. Length of stopes 200 ft which is less than about 600 ft required to fulfill the conditions for a two-dimensional analysis.
251	1, 3, 5, 6, 7	3000	6000	Pillar breadth 60 ft
163	1, 3, 5, 6, 7	3700*	6000	Calculated from Figure 3 at 520 days.
		3000	3300	$S_o = 1{,}600$ psi, $S_t = 4{,}000$ psi.
		1400*	580	$S_o = 600$ psi, $S_t = 7{,}000$ psi. Note that model is not a good representation of actual conditions as there should be an additional block excavated adjacent to No. 5 representing pillar 165.

* $\delta = (\Delta\sigma_p - \mu(\Delta\sigma_t + \Delta\sigma_z))H/E$; $\Delta\sigma_t = -S_t$; $\Delta\sigma_z = 0$; H = 106 feet.

case of S_o = 600 psi and S_t = 7,000 psi the agreement is not good. The seeming paradox of the measured pillar stresses, recorded in Table 3, varying with the field stresses is explained by the fact that deformation is actually measured from which pillar stresses are calculated using assumed values of the field stresses.

In summary, the finite-element analysis on the two-dimensional model predicts movements and stresses greater than those measured in situ. Also it predicts that mining of blocks beyond the immediate stopes on either side of the pillar have a much greater effect on the longitudinal north-south stresses and deformations than is observed in practice. Probably the main reason for these discrepancies is that part of the field stress is being diffracted above and below the stopes instead of all on the pillars as in the model. This diffraction in the third dimension would result in a reduction in the pillar stresses and deformations. In addition, blocks more than one stope distance away from the pillar are nearer to the solid ground above and below the stopes, and the stress field is more likely to be transferred over this shorter distance rather than over the longer distance to the pillar. This would explain why mining beyond the immediately adjacent stopes produces very little deformation in the north-south direction. Other factors which could explain the discrepancies are that the assumed field stresses of S_o = 2,500 psi and S_t = 5,000 psi are too large and should not only be reduced but also the S_o/S_t ratio increased to explain the small measured movements near the hanging wall and footwall. Also, a larger deformation modulus than the value of 10×10^6 psi, while not significantly altering the stresses, would reduce the predicted deformations.

In conclusion, it would seem that the three-dimensional aspects of the actual situation makes it difficult to predict accurately using a two-dimensional model. However, by using this model the mechanics of stress transfer and the behaviour of the structure can be more readily understood. At the same time, it is conceivable that the actual field stresses could be modified by a reduction factor based on some kind of simple three-dimensional analysis the purpose of which would be to determine the equivalent conditions for a central section to be analyzed in two dimensions.

Case History of Pillar Cracking

Noticeable cracking has occurred in several of the pillars mined since underground operations commenced in 1949. At depths from 800 to 1,500 ft, pillar cracking has caused sloughing of the pillar walls and in some cases offset blast holes. Pillar cracking is considered the first sign of instability, and while the whole pillar is not in a state of failure the tensile and shear strengths on certain planes of weakness have been overcome.

Two areas in the west section of the mine (Figure 1), one almost directly above the other, are examined.

Figure 8 shows the locations of observed cracks on the H2, M1–3 and M1–2 levels in Area 1. This area was about 500 feet along strike with the pillars 225 to 300 ft long down-dip. Mining proceeded over a period of 22 months with pillar cracking, and sloughing developing in the final 11 months. The cracks were of three main types: those parallel and near to the sides of the pillar, which are occasionally 1/2 in. wide; those striking in a northwesterly direction; and those striking in a northeasterly direction.

After the mining of 127 stope, partial mining of 125 and 123 stopes and removal of the 130 pillar, cracking was observed in pillar 128. Extensive sloughing took place from the sides of the 124 and 126 pillars, which were probably caused by cracks parallel to the sides of the pillars. Sloughing was also reported from the back of the 125 stope and was thought to be associated with a 15-ft intrusive cutting across the stope.

Figure 9 shows the locations of the observed cracks on the M1, M2–2 and M2–1 levels in Area 2. This area was about 1,000 ft along strike with the pillars 390 ft long down-dip. A thrust zone separated Areas 1 and 2. The direction of the cracks is similar to that observed in Area 1.

Stopes 231, 233, 235, 237 and the block 223 to 225 were mined over a period of 54 months before any pillar blasts. No cracks were observed during this time. Pillar 232 was blasted first, followed by a main portion of pillar 234. Following these blasts a buttress left on the hanging wall at pillar 234 cracked and sloughed off at the M2–1 sub-level. Pillar 236 was the next pillar blasted which produced a 500-ft-long opening to the east of pillar 230.

The hanging wall section of stope 229 was then mined, which produced extensive cracking and sloughing of pillar 230. Cracks up to 1 1/2 in. wide developed in the centre crosscuts on the first and second sub-levels and numerous cracks were observed in the hanging wall and footwall drifts.

The 230 pillar blast produced prominent cracks in the 228 crown pillar on the M1 level. During the mining of stope 227, additional cracks were observed in pillars 226 and 228, with the extensometer monitoring the movement of the cracks in pillar 228 as shown in Figure 4. These two pillars were the last to be blasted above the M2 level in the west section of the mine.

The 41 cracks observed in Areas 1 and 2 can be categorized into three main groups as shown in Table 4. The cracks parallel to the sides of the pillars, set No. 1, mainly occur within 15 ft of the pillar side. These cracks are probably extension fractures and are directly related to the lateral expansion of the pillar, and in some cases result in pillar sloughing. The diagonal cracks, sets No. 2 and 3, probably result from shear movement, which occurs when the frictional resistance is overcome along the joint and fault planes. These crack sets are mainly concentrated in the central portion of the pillar and rarely penetrate into the hanging-wall or footwall.

The progressive pillar deterioration can be visualized as the result of two processes: relief of stresses at the pillar sides permits extension fractures in the rock, not necessarily along any structural weakness planes; shear stresses produce sliding between blocks of rocks, the magnitude, location and initiation of movement is dependent on the structural weakness planes. Considering the susceptibility of the diagonal fault and joint planes to shear movement, it can be deduced that:

1. those planes which intersect both sides of the pillar have the least resistance;
2. those which intersect one side and either the hanging wall or footwall require crushing of the rock or intersecting planes of weakness for movement to occur; and
3. those planes which intersect both the hanging wall and footwall have the greatest resistance. It follows that wide pillars are more stable than narrow pillars since only planes, almost at right angles to the direction of stress, can intersect both sides of the pillar.

The relative magnitude of the stresses acting parallel and normal to the fault planes will determine whether movement occurs. Using the finite-element method of analysis the stresses parallel and normal to the north 30° west and north 30° east fault and joint systems, were calculated. Field stresses of 1,600 psi (S_o) perpendicular to the hanging wall and footwall and 4,000 psi (S_t) parallel to strike were used. An opening of 340 ft was taken on one side of an 80-ft-wide pillar and a 60-ft opening on the

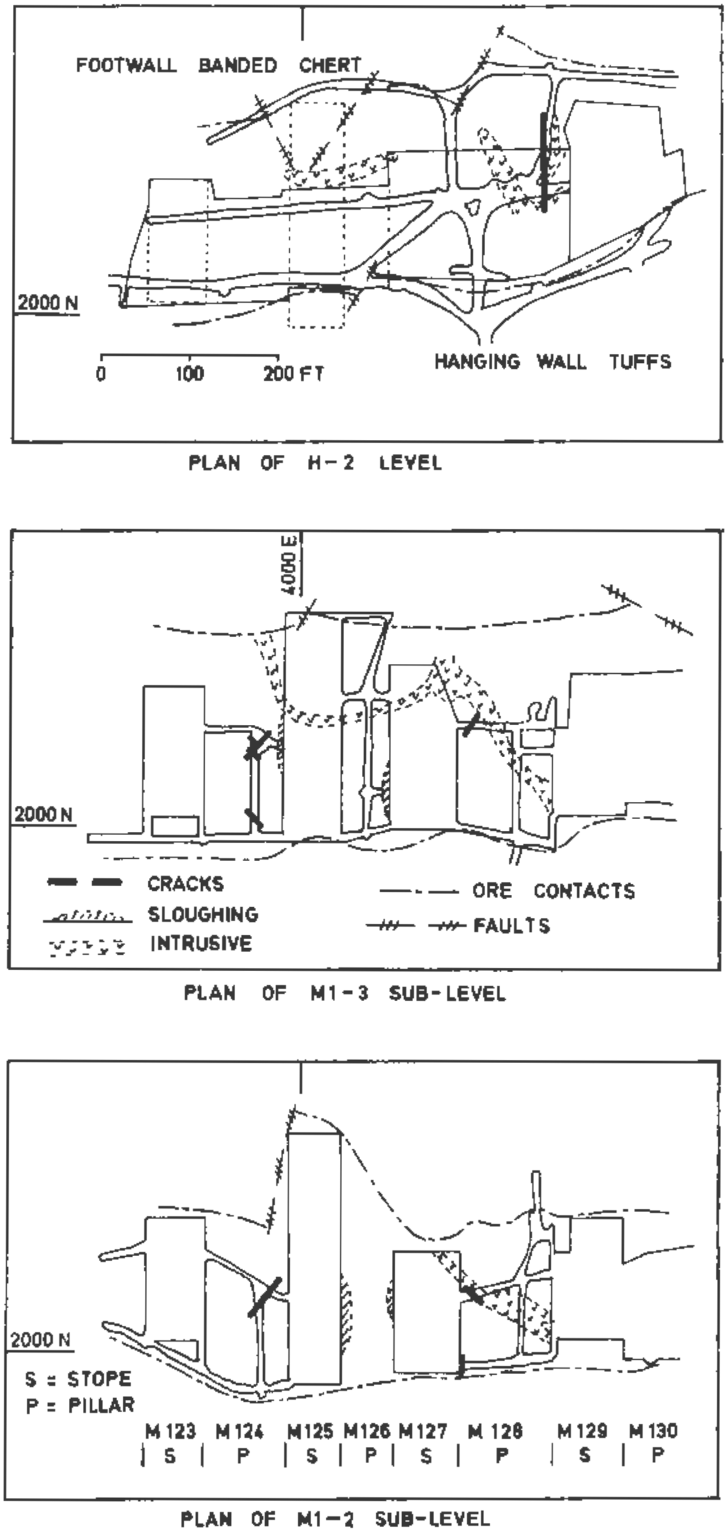

FIGURE 8 – Location of pillar cracks in area 1

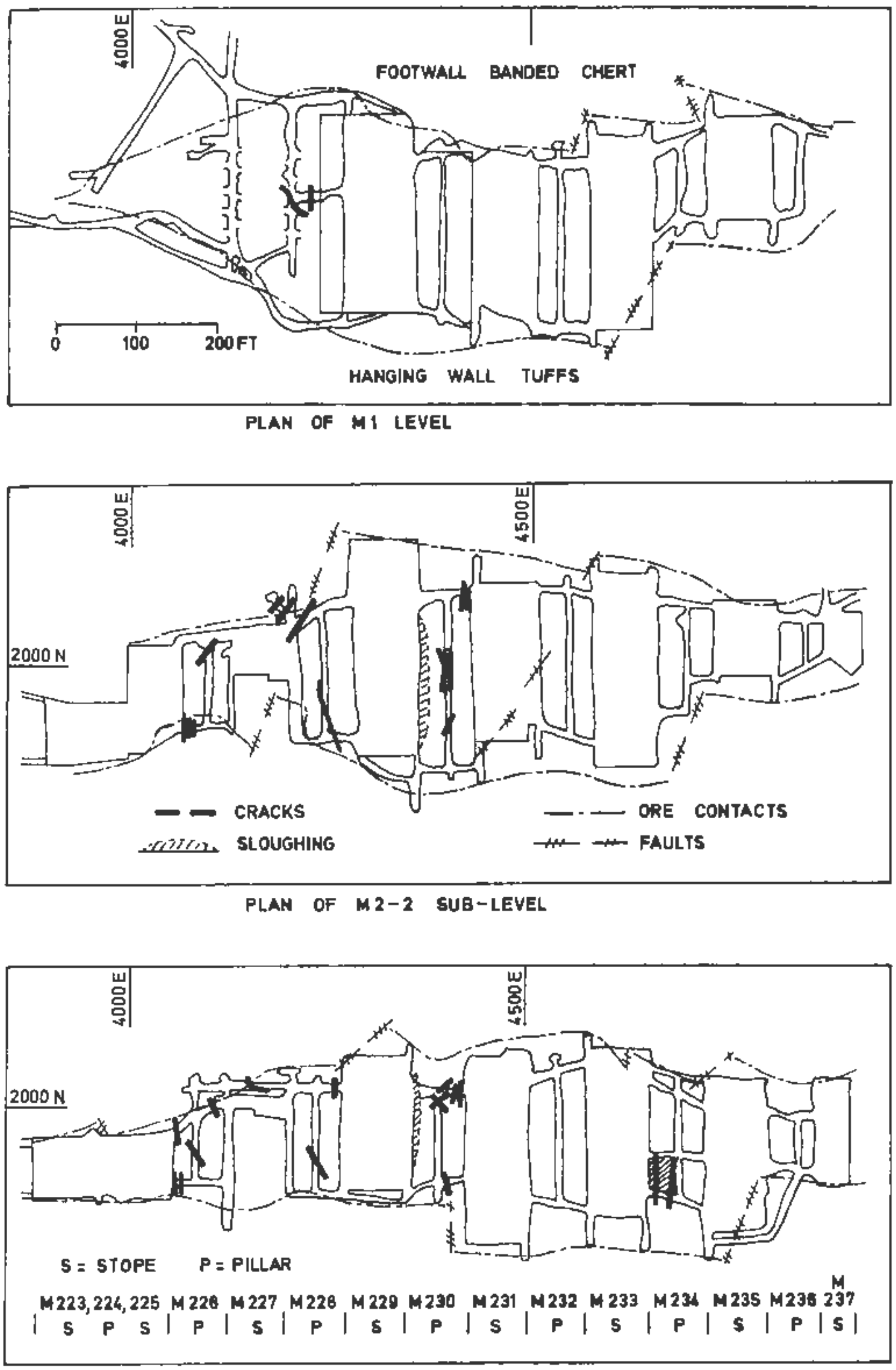

FIGURE 9 – Location of pillar cracks in area 2

TABLE 4
Details of Crack Survey

Set No.	Direction of Cracks	No. of Cracks	Remarks
1	north $\pm 10^\circ$	20	Parallel to pillar sides, not associated with any prominent joint or fault system;
2	north 30° west $\pm 15^\circ$	12	Associated with a steeply dipping fault system;
3	north 30° east $\pm 10^\circ$	9	Associated with a vertical joint system.

other side. The stresses at different locations along the pillar centre line between hanging wall and footwall are given in Table 5.

A high, parallel to normal, stress ratio (τ/σ) indicates the greatest likelihood of shear movement along the planes. The calculated results confirm that the central area of a pillar is more susceptible to shear movement than that near the hanging wall or footwall.

The propagation of pillar cracks has been observed in several pillars and monitored by extensometers in two pillars. The measurements indicate that even during the first stages of mining around a pillar, movement occurs on the fault and joint planes and only during the last stages of mining are the cracks readily visible. The worst cases of pillar cracking occur where an opening at least 300 ft long exists on one side of a pillar and the stope on the other side of the pillar is being mined, e.g. pillar 230 as stope 229 was mined and pillar 228 as stope 227 was mined.

These observations on pillar cracking are only relevant to the west section of the mine. A preliminary structural-geological study in the east section indicates that the fault and joint sets are parallel to the pillar sides. In this case, lateral expansion and the associated cracks should be more prominent than the shear movement along the diagonal faults and joints experienced in the west section.

Conclusions

The research program provided:

1. information on the usefulness of various types of instrumentation;
2. an understanding of the pillar stresses and deformations associated with this method of mining;
3. data for the development of an analytical approach for predicting stresses and deformations; and
4. an understanding of the factors involved in pillar stability.

Extensometers were found to give the most useful information on:

1. the stability of the pillars
2. the location and movement at planes of weakness
3. the extent of load transfer to a pillar, and
4. an estimate of the increase in pillar stress due to mining. Stress measurements, with the equipment used, can give order of magnitude values and define the directions of the principal stresses. Sonic measurements can be used to estimate the elastic modulus and Poisson's ratio of the rock mass. At this mine, this method was not suitable for determining zones of fracture since cracking was already visible before any significant change in sonic velocity occurred. Microseismic measurements indicate working of the rock, but it is difficult to define the origin and significance of the noises. It is considered

TABLE 5
Calculated Stresses Acting on Joint and Fault Planes

Location	Both North 30° West and North 30° East Planes		
	Parallel Stress (τ)	Normal Stress (σ)	τ/σ
Hanging wall or Footwall	600 psi	3,000 psi	0.2
2/3 Distance from Centre	900 psi	1,800 psi	0.5
1/3 Distance from Centre	1,450 psi	1,200 psi	1.2
Centre	1,700 psi	950 psi	1.8

that extensometer measurements provide the same information and are more easily interpreted.

Extensometer measurements in pillar 163 indirectly confirm the field stress measurements as to the direction of the principal stresses, parallel to strike being the major, perpendicular the intermediate, and vertical the minor. Measurements in pillar 163 also indicated that load is transferred to the pillar while the immediately adjacent stopes are being mined. In this location, mining greater than one stope distance from the pillar means that solid ground is nearer above and below the stopes and the load will naturally be transferred over the shorter span. However, this will not always be the case on the second and third levels and it is expected that pillars will be affected by mining over a greater distance as the spans increase.

The finite element analytical model gave values of pillar deformation and stress of the same order of magnitude at those measured. However, there were a number of discrepancies due to trying to represent a three-dimensional stress and geometrical condition as a two-dimensional problem. The possibility exists of modifying the actual field stresses to give equivalent conditions in two dimensions. This type of analysis may be useful in determining the shear and normal stresses acting on the planes of weakness and in conjunction with in situ measurements provide an estimate of pillar strength.

The measurements taken at this mine together with the geological study and survey of pillar cracking indicate that the fault and joint planes of weakness, rather than the strength of the rock substance are the main factors determining pillar stability. The development of these cracks is most noticeable where there is a large opening on one side and mining is advancing in the adjacent stope. In addition the number of cracks observed in the pillars on the second level (Area 2, Figure 9) is greater than those observed on the first level (Area 1, Figure 8). Consequently, the frequency of cracking seems to increase with depth and may be indicative of increasing pillar stress with depth.

Acknowledgments

The authors would like to acknowledge the contribution made by each of the following: the management of the Algoma Ore Division for their participation in the research program; the geological staff at the MacLeod mine who took many of the measurements; Dr. G. Herget who worked on the structural geology aspects; F. Grant, Y. Yu, W. Zawadski, A.V. St. Louis and H. Montone of the Elliot Lake Laboratory; and S. Cook, J. Sullivan and W. Rowe of the Rock Mechanics Laboratory, Ottawa, who participated in the project.

Reference

Wilson, E.L. *Finite-Element Analysis of the Two-Dimensional Structures,* 1963. U. of Calif, Structures and Materials Res. Dept. of Civil Eng. No. 63-2.

D.G.F. Hedley

Education — B. Sc., mining engineering, Royal School of Mines, 1963; Ph D, rock mechanics, University of Newcastle-upon-Tyne, 1965.

Employment Summary — 1965-67, National Research Council of Canada post-doctorate research fellowship. At present, research scientist, Mines Branch Elliot Lake Laboratory, Department of Energy, Mines and Resources, Elliot Lake, Ont.

G. Zahary

Education — B. Sc., mining engineering, University of Alberta, 1955; M Eng, rock mechanics, McGill University, 1963.

Employment Summary — 1958-61 and 1964-66, mining engineer at Steep Rock Iron Mines and International Minerals and Chemical Corp. (Canada). At present, research scientist, Mines Branch Elliot Lake Laboratory, Department of Energy, Mines and Resources, Elliot Lake, Ont;

H.W. Soderlund

Education — B.Sc., University of Saskatchewan, 1950.

Employment Summary — 1950-51, engineer at Magnet Consolidated Gold Mine and Lake Shore Gold Mine; 1951-68, geologist, planning engineer and mine superintendent at the Ore Division of the Algoma Steel Corporation, Limited; at present, chief engineer, Ore Division at Algoma.

D.F. Coates

Education — B. Eng, McGill University, 1948, M. Eng., McGill University, 1954; MA, Oxford University, 1954; Ph D, McGill University, 1965.

Employment Summary — 1951-59, lecturer and supervisor of graduate research at McGill and Carleton universities; 1959-63, consulting engineer; 1963 to the present, head, Mining Research Centre, Mines Branch, Department of Energy, Mines and Resources, Ottawa, Ont.

Ultrasonic Compressional and Shear-wave Velocities of Confined Rock Samples

by M.S. King
Department of Geological Sciences,
University of Saskatchewan,
Saskatoon, Sask.

Abstract

The three basic laboratory techniques for determining compressional and shear-wave velocities on rock samples are reviewed. The conclusion is drawn that the pulse first-arrival method is best suited for rock samples subjected to triaxial loading conditions.

Two systems are described for determining compressional and shear-wave velocities precisely by the ultrasonic pulse first-arrival method on rock samples subjected to hydrostatic pressures to 10,000 psi, and to triaxial loading conditions at confining pressures to 6,000 psi. Emphasized are the advantages of the second system in being able to determine the velocities and static stress-strain relationships concurrently on the same rock sample.

Results of tests on three sandstones subjected to hydrostatic confining pressure are reported. While one sandstone is isotropic in behaviour, the other two are transversely isotropic, with their axis of symmetry perpendicular to the bedding plane. The degree of anisotropy is reduced as the confining pressure is increased.

Static and dynamic elastic moduli have been calculated for the isotropic sandstone from stress-strain data and velocities measured concurrently on the same sample as a function of changes in triaxial loading conditions. While the dynamic moduli are greater in magnitude than the static moduli, the ratio of the two is reduced by an increase in confining pressure. It is concluded that the presence of cracks is responsible for the behaviour of the three sandstones tested: randomly-oriented in all three, but with a higher concentration in the bedding plane of the two anisotropic rocks.

Practical applications of the laboratory results to problems in mining and geological engineering are given. Mention is also made of controlled-pulse acoustic equipment under development for determining in situ compressional and shear-wave velocities, and for locating geologic discontinuities underground.

Introduction

The variation of compressional and shear-wave velocities and attenuation in rocks as a function of changes in triaxial loading conditions is of considerable interest in the fields of mining, geological engineering, geophysics and petroleum engineering. Major factors influencing the velocities and attenuation of acoustic waves in rocks are the degree of anisotropy and fissuring of the solid matrix comprising the rock, the type of fluid saturating the pore spaces, and the effects of the existing stress field and pore-fluid pressure in the rock. In mining, for example, the mechanical state of rock surrounding an opening may often be gauged from the velocities and attenuation of acoustic waves. The distances of geological discontinuities from a mine opening can be determined from the reflection of pulses of acoustic waves.

In geological engineering, the influence of rock matrix anisotropy, pore water saturation and pressure on the strength and elastic moduli of the rock is of prime importance in the selection of suitable foundations for large structures. The dynamic elastic moduli of rocks obtained from velocity measurements are necessary for understanding the mechanisms of drilling and blasting. The interpretation of seismic records demands a knowledge of the velocities of acoustic waves as a function of confining pressure. In the petroleum industry, the effects of changes in rock compressibility, porosity and fluid saturation on the velocities and attenuation of acoustic waves is required for the interpretation of acoustic velocity logs. In order to have the widest possible practical application, the velocities measured in the laboratory must be on rock samples under conditions closely resembling those in the field.

There are, basically, three laboratory techniques suitable for determining the velocities of compressional and shear waves on rock samples subjected to triaxial loading conditions and pore-fluid pressures.

The first of these is the resonance method, in which the rock specimen is caused to vibrate at its resonant frequency in one of several normal modes. For isotropic, homogeneous materials the relationships between resonant frequency and velocity are fairly simple. For materials exhibiting anisotropic behaviour, however, the relationships can be extremely complex. Gardner et al. (1964) describe a method of this type for determining the effects of confining pressure and different fluid saturants on the acoustic-wave velocities and attenuation in rock samples. A limitation of the technique is that corrections must be made for the effects of the frictional forces of the fluid exerting confining pressure on the resonant frequency of the sample. These corrections can assume major proportions at large confining pressures.

The second is the rotating-plate technique, in which a thin parallel-sided sample of rock is rotated in the path of a continuous beam or succession of pulses of ultrasonic energy. At the critical angle of incidence of the beam, for which compressional and shear waves are refracted parallel to the sides of the sample, there will theoretically be no transmission of energy. King and Fatt (1962) have described the continuous-beam method, operating at 1 MHz, for determining shear-wave velocities as a function of hydrostatic confining pressure to 2,400 psi. Wyllie et al. (1962) and Gregory (1963) have reported a gated-pulse rotating-plate method for obtaining compressional and shear-wave velocities at hydrostatic pressures to 10,000 psi. This technique, however, has not been developed further, because of certain problems associated with locating the exact angles for critical refraction of compressional and shear waves.

The third is the pulse first-arrival technique, in which the time is measured for a pulse of compressional or shear waves to traverse a known thickness of the rock. This method has been successfully used on well-compacted rocks by a number of workers, using either X-cut quartz or axially-polarized ceramic transducers for compressional-wave velocities, and AC-cut quartz transducers for shear-wave measurements. A review of this work is contained in an article by Simmons (1965). Difficulties in determining shear-wave velocities on saturated porous rocks were, however, reported by Gregory (1963), because of the high degree of attenuation of shear waves. Jamieson and Hoskins (1963) proposed the use of an axially-polarized ceramic transducer, with its high electromechanical conversion properties, to produce pulses of polarized shear waves from compressional waves at a free surface. Using a development of this method for producing and detecting shear waves, the present author (King, 1964; 1966) has successfully determined the velocities of compressional and shear waves on several dry and liquid-saturated sandstones as a function of hydrostatic confining pressures in the range 500 psi to 10,000 psi. During this research it was observed that several of the sandstones tested exhibited an appreciable degree of anisotropy, especially at low confining pressures. Gregory (1967) has also reported a successful technique for determining shear-wave velocities, which is based on the conversion of compressional waves to polarized shear waves by refraction at a liquid-solid interface.

The stress-strain relationships for materials exhibiting various degrees of anisotropy have been discussed by Hearmon (1961), who also develops expressions for the velocities of compressional and shear waves in these materials. Since the rocks for which results are reported here fall in the categories of isotropic and transversely-isotropic materials, the stress-strain relationships and expressions for velocities in materials of these types are included in the appendix. Walsh and Brace (1966) have reviewed theoretical studies of the elasticity of rock considered as a material containing pores and cracks. The presence of sharp narrow cavities, such as cracks or joints, at low confining pressures is found to influence strongly the mechanical properties of the rock; a considerable reduction in magnitude of the elastic moduli of the rock is associated with them. As the cavities are closed by higher pressures, the elastic properties of the rock approach those of the uncracked porous material. Simmons and Brace (1965) found that for hydrostatic confining pressures in excess of 30,000 psi the static and dynamic elastic moduli for several rocks were closely in agreement with each other, suggesting that any cracks present at lower confining pressures had been closed. Walsh (1966) has used the theory as a basis for a proposed mechanism for the source of seismic-wave attenuation in rocks. This attenuation mechanism predicts results which agree with published values for experiments on granite and limestone.

Biot (1962a) has presented a unified treatment of the mechanics of deformation and acoustic-wave propagation in saturated porous media, which predicts the existence of two coupled compressional waves and one shear wave for an isotropic material. The compressional wave with the lower velocity may usually be neglected, because it is shown to attenuate very much more rapidly than the one with the higher velocity. Two general conclusions may be drawn from Biot's analysis when it is applied to isotropic, saturated rocks. First, the shear-wave velocity in the saturated rock will always be rather less than in the dry rock. Second, the compressional-wave velocity in the saturated rock will generally be higher than in the dry rock, except for rocks having a high value of bulk modulus. Biot (1962a, b) notes, however, that under certain conditions it is possible for the liquid saturant to behave in a non-Newtonian manner, thus invalidating his theory. He shows (Biot, 1962b), for example, that relaxation behaviour can occur at frequencies of the order of 1 MHz in cracks 1 micron thick saturated with water. Geertsma (1961) and King (1966) have noted anomalous behaviour of shear-wave velocities which might be attributed to effects of this kind.

The influence of liquid saturation and confining pressure on compressional and shear-wave velocities in sedimentary rocks has been discussed and determined experimentally by King (1966) and Gregory (1967). It has been found that an increase in hydrostatic confining pressure with constant pore pressure increases both the compressional and shear-wave velocities. Changes in pore pressure were found to indicate a dependence of both velocities on the difference, $(P_e - P_f)$, between the hydrostatic confining pressure, P_e, and the pore pressure, P_f. Gardner et al. (1965) have given a theoretical analysis which shows this dependence on $(P_e - P_f)$ to be true only if the difference in pressure follows a previously established hysteresis cycle. King observed that for all rock types he tested there was an appreciable hysteresis effect, with higher velocities being recorded at a given confining pressure when the pressure was being reduced than when it was being increased. Both King and Gregory noted that once a rock sample had been subjected to the maximum hydrostatic pressure, acoustic-velocity measurements were reproducible during further tests.

The effect of complete liquid-saturation of the rock has been found experimentally by King (1966) and Gregory (1967) generally to increase the velocity of compressional waves, with the effect most marked at low confining pressures. These workers observed a decrease in shear-wave velocities on saturated rock samples at high confining pressures. However, King (1966) reported anomalous behaviour for some sandstones at low confining pressures, when the shear-wave velocity for the saturated rock was found to have a slightly higher value than that for the dry rock at the same confining pressure. Gregory (1967) did not observe this behaviour on the only sandstone he tested for which King had noted the increase in shear-wave velocity upon saturation.

Measurements of compressional and shear-wave velocities of rocks *in situ* have been reported by Nichols (1962) and Onodera (1963), Larocque (1964) and Cannaday and Leo (1966). Onodera mentions the use of a low-frequency electrically-driven vibrator to generate both types of waves, whereas Nichols used small charges of high explosive. Both techniques produced records from which it was a simple matter to obtain the compressional and shear-wave velocities. Onodera (1963) proposed a simple relationship between the elastic moduli of the rock as determined from velocities measured *in situ* and those determined by ultrasonic means on small samples in the laboratory, which gives a measure of the soundness of the rock mass. His theory is in general agreement with that of Walsh and Brace (1966). The two types of apparatus developed by Larocque (1964) and Cannaday and Leo (1966) were developed for use underground in delineating fracture zones and for obtaining the dynamic elastic properties of rocks surrounding mine openings. Larocque made use of hammer blows on a rod embedded in a drill hole behind the rock face as a source of acoustic waves. A piezoelectric transducer embedded in a second drill hole parallel to the first was used to detect the arrival of the acoustic pulses. Cannaday and Leo employed piezoelectric transducers as both a source and a detector of acoustic pulses. With their equipment Cannaday and Leo were able to make velocity measurements over distances of up to 1,400 ft during tests in a New Mexico potash mine.

A description of the acoustic-logging device used in the petroleum industry and methods for interpreting the results from the device in terms of porosity and liquid saturation of the formation being tested have been given by Tixier et al. (1959). Basically, the acoustic-logging tool produces a record of the time required for a pulse of compressional waves of about 20 KHz frequency to traverse a definite length of the formation adjacent to the borehole. A more recent development of this device has been described by Pickett (1963). This device produces a series of seismic records at discrete intervals down the borehole. The velocities and amplitudes of compressional and shear waves can easily be measured from these seismograms.

Duvall and Blake (1968) have shown that the locations of foci and the intensity of rock bursts occurring in mines can be determined from microseismic energy recorded on tape by accelerometers at several locations in the mine. These workers at the USBM, Denver, have found that there is a constant relationship between the reciprocals of compressional and shear-wave velocities, which appears to be independent of the mechanical state of the rock mass. They have been able, therefore, to locate the foci of rock bursts rather precisely. The relationship between the velocities is consistent with the theory proposed by Walsh and Brace (1966) for a porous material containing narrow cavities, if the latter are considered in this case as comprising joints and cracks in the rock mass. Research in South Africa on the location and intensity of rock bursts underground has been reported by Cook (1964). In a later paper Cook et al. (1966) describe the applications of their earlier research to the design of mine openings.

Apparatus

Tests Under Hydrostatic Confining Pressures

The apparatus used for the tests under hydrostatic confining pressures is identical to that described by the present author (King, 1966). Cylindrical rock samples of 3 1/2 in. diameter and up to 1 3/4 in. long are mounted between a matched pair of transducer holders designed either for compressional or shear-wave measurements. The two types of transducer holder are illustrated in Figure 1. The cylindrical surfaces of rock sample and transducer holders are first enclosed in a copper jacket and then in a neoprene sleeve to seal the sample pore spaces from the surrounding fluid which provides the hydrostatic confining pressure. Figure 2 shows a rock sample ready for assembly.

A block diagram of the apparatus is shown in Figure 4, with a sample assembled for shear-wave measurements. The confining and pore-fluid pressures can be varied independently to 10,000 psi and a pore fluid reservoir permits the use of a choice of saturating fluids for the rock sample. A general view of the apparatus is shown in Figure 3.

Compressional and shear-wave velocities are obtained by measuring the time taken for a pulse of either type of waves to traverse the rock sample. The electronic equipment is shown diagrammatically in Figure 4. An Arenberg pulsed oscillator is used to apply a short sinusoidal voltage pulse to a piezoelectric transducer, mounted in the pressure-sealed holder at one end of the rock sample, at its resonant frequency. The acoustic pulse produced by the transducer is transmitted through the rock sample and is detected by a second transducer mounted in a similar cell at the other end of the rock sample. The electrical signal produced by the second transducer is amplified and displayed on the horizontal axis of one beam of a dual-beam oscilloscope. Both the pulsed oscillator and the oscilloscope sweep are triggered by a time-mark generator, which can also be used to provide accurate time marks on the second beam of the oscilloscope.

The time taken for an acoustic pulse to traverse the rock sample and transducer holders is obtained by using the calibrated delayed trigger on the oscilloscope to position the start of a small brightened portion of the trace at some definite point on the received signal. In Figure 9, which shows typical oscilloscope traces obtained with this apparatus, an arrow indicates the reference point chosen on the first positive peak of the received signal. The time taken for the pulse to traverse the rock sample alone is then obtained by subtracting the time taken for the pulse to traverse the transducer holders in face-to-face contact, using the same reference peak for both measurements. In this way, measurements of velocities can be made with an accuracy of ± 1%.

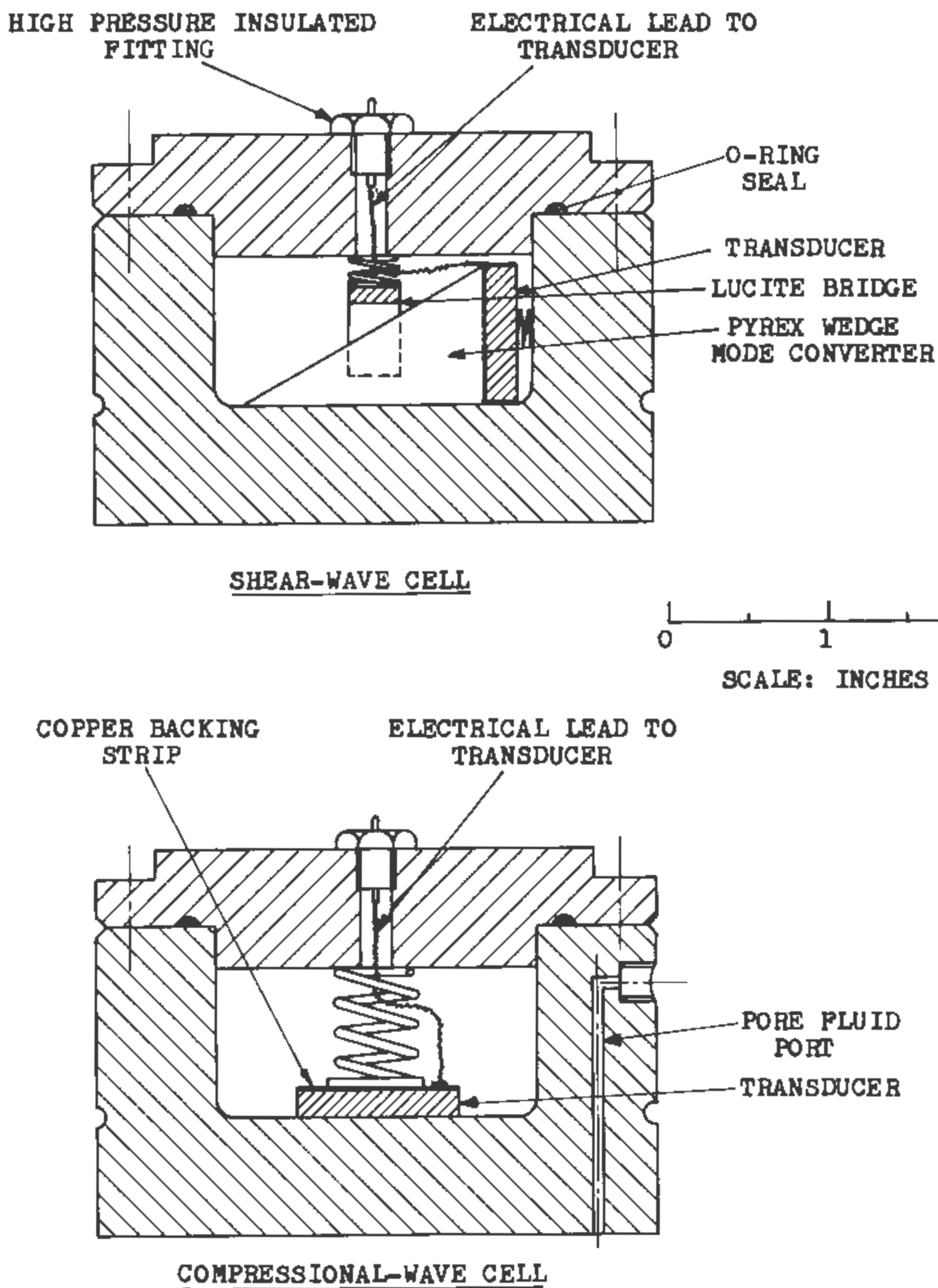

FIGURE 1 — Transducer holders for hydrostatic tests

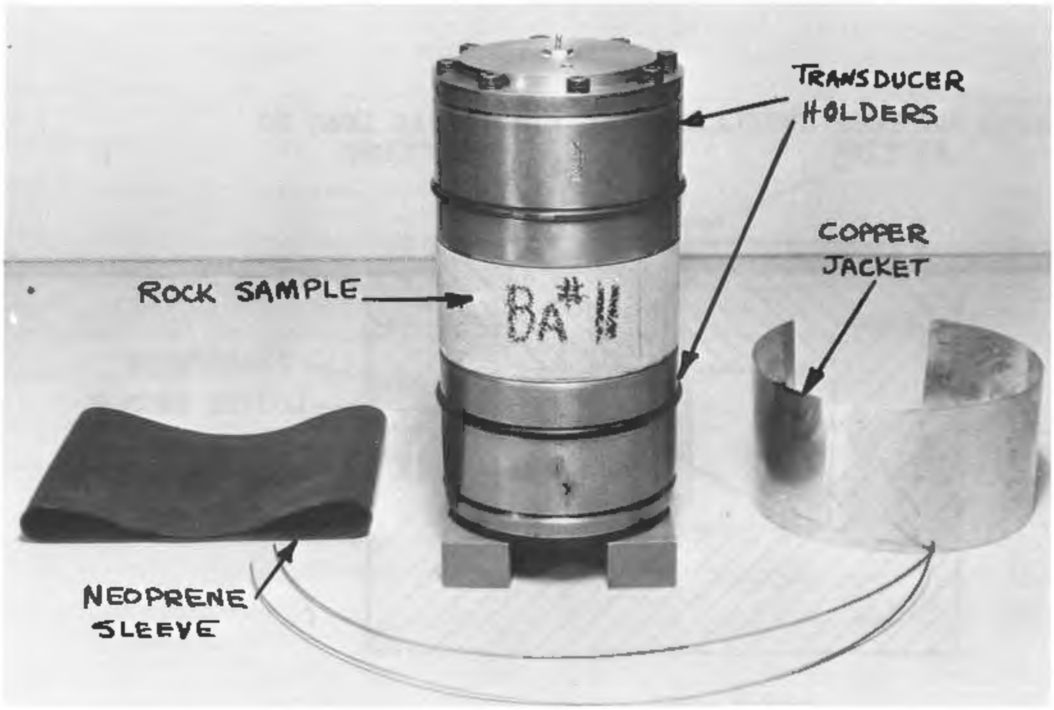

FIGURE 2 — Rock sample ready for assembly — hydrostatic tests

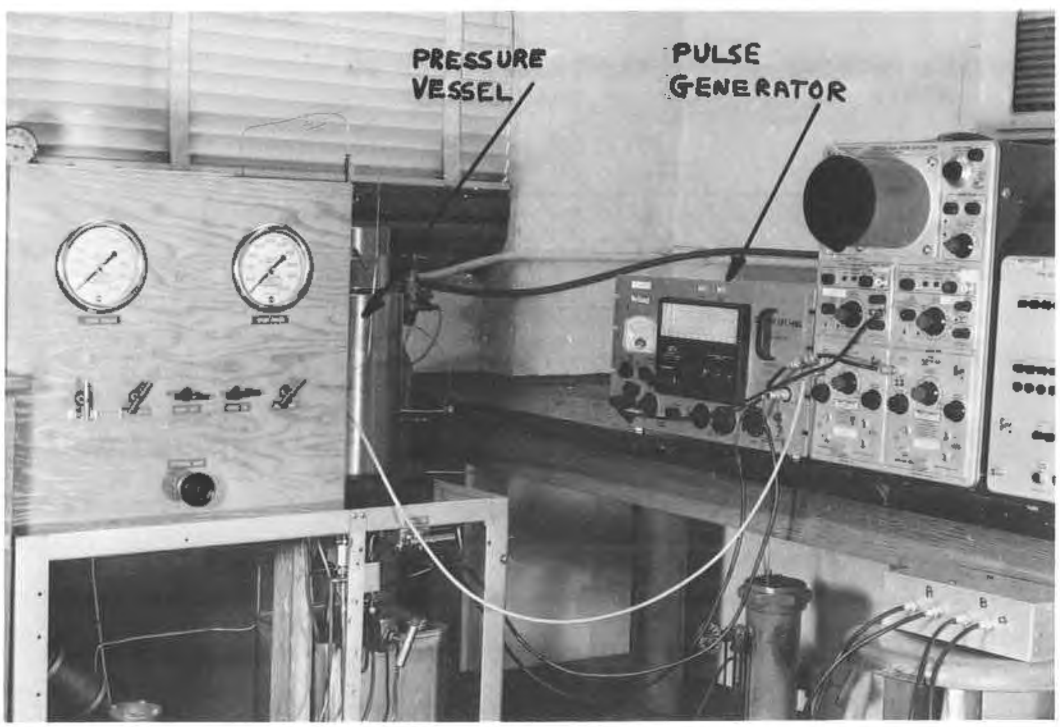

FIGURE 3 — General view of apparatus — hydrostatic tests

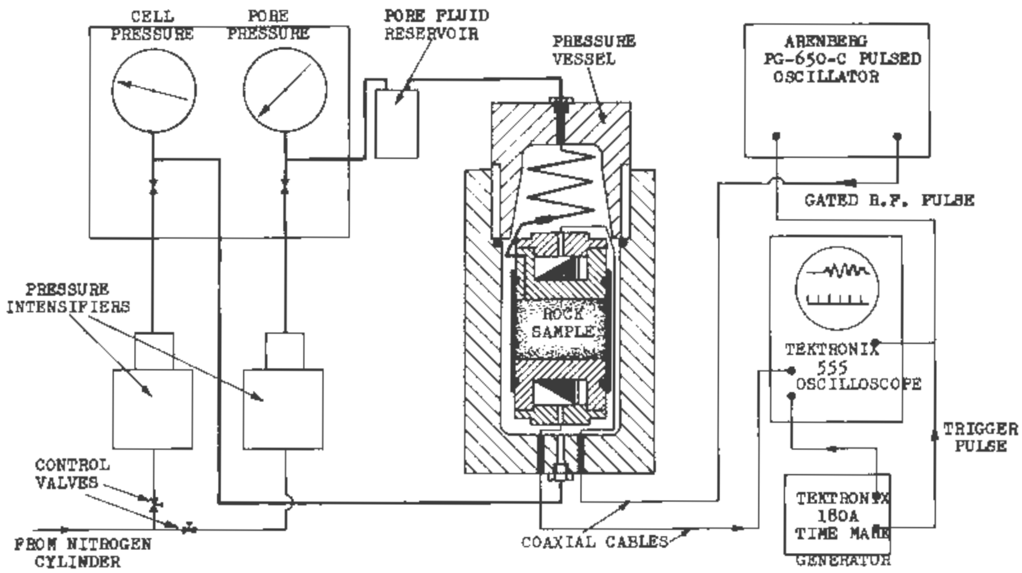

FIGURE 4 — Block diagram of apparatus for hydrostatic tests

Compressional waves are produced by pulsing an axially-polarized ceramic disc of 500 KHz resonant frequency mounted in a pressure-sealed cell as shown in Figure 1. The pulse of mechanical energy generated is in the form of a beam of compressional waves passing through the base of the transducer holder, the rock sample and finally the base of the second transducer holder. A second axially-polarized disc mounted in the second transducer holder detects the pulse after it has traversed the rock sample. A resonant frequency of 500 KHz was chosen so that the wavelengths of compressional and shear waves in the rocks to be tested would be an order of magnitude larger than the largest grain size expected in these rocks.

The method used for generating shear waves was developed from that proposed by Jamieson and Hoskins (1963). An axially-polarized ceramic disc of 500 KHz resonant frequency is attached to one face of a right-angled pyrex-glass prism mounted in a steel pressure-sealed cell as shown in Figure 1. The compressional waves generated by pulsing the transducer are totally converted by critical reflection at the pyrex-glass free surface to polarized shear waves. The latter are propagated in a direction perpendicular to the base of the prism, and pass through the steel cell into the rock sample. On traversing the rock sample, the beam of shear waves passes into a similar transducer holder mounted on the other end of the sample. The polarized shear waves are then converted by critical reflection at the pyrex-glass free surface to compressional waves which, in turn, are detected by a second axially-polarized disc. Based on the theory for this phenomenon, presented by Jeffreys (1962, p. 28), the critical angle for complete mode conversion from compressional to shear waves was determined experimentally for the pyrex glass used.

The manner in which the transducers are mounted in the compressional and shear-wave transducer holders causes the system to be narrow-band in operation, with the transducers tending to ring at their resonant frequency. This behaviour justified the use of the first positive peak as a reference in determining the acoustic velocities.

Tests Under Triaxial Loading Conditions

It was realised during tests on the apparatus described above that improvements in several features could be made. The first was that there would be a considerable advantage in being able to measure the compressional and shear-wave velocities concurrently on a single rock sample. The second improvement was to incorporate facilities for measuring the axial and lateral strains on the rock sample as it was subjected to triaxial loading conditions. Thus the static and dynamic elastic moduli determined on the same sample could be compared, and the theory of Walsh and Brace (1966) tested. The third was to design the transducers for broader-band operation. In this way harmonic analyses of the received pulses would yield information on attenuation of acoustic waves in rocks, and the results could be used to check the seismic-wave attenuation theory proposed by Walsh (1966).

With these points in mind, the apparatus shown in Figure 5 was designed. Mechanical problems associated with the use of pyrex-glass prism mode converters in transducer holders designed for concurrent compressional and shear-wave velocity measurements and broad-band operation, precluded their use in this application. Instead, cross-polarized ceramic shear plates are used to generate pulses of polarized shear waves, and axially-polarized ceramic discs to generate compressional waves.

Three shear plates of 500 KHz free resonant frequency, 1 1/2 in. long and 1/2 in. wide, were carefully mounted with Eastman 910 adhesive side-by-side in the recess of the lower transmitting transducer holder, as shown in Figure 5. The composite form of the shear-wave transducer is employed to eliminate cross-coupling of unwanted resonant modes. A steel disc of 1 1/2 in. diameter and an axially-polarized ceramic disc of 1 1/2 in. diameter and 500 KHz resonant frequency are mounted in turn with heavy grease to the back of the shear plate. A perspex disc serves to insulate the axially-polarized disc from a setscrew which is used to compress the transducers and distance pieces. Similar transducers and distance pieces are mounted with the same configuration in the upper receiving transducer holder. The resulting system permits switching from the measurement of compressional to shear-wave velocities without changing the loading conditions on the rock sample. When the shear-wave transducer is pulsed, the front and back faces of the compressional-wave transducer are electrically shorted. When the compressional-wave transducer is pulsed, the back of the shear-wave transducer is grounded. Typical oscilloscope traces of received pulses are shown in Figure 10. It will be seen that this system operates on a broader band than that used for the hydrostatic tests.

The time taken for either pulse to traverse the rock sample is obtained in the same way as described for the hydrostatic tests, except that the reference point is taken at the first break in the wave-form. The reference point is marked with an arrow on each of the oscilloscope traces shown in Figure 10. Since this system is of fairly broad-band operation, the first positive peak cannot be used as a reference point. The electronic equipment used for these tests is shown in Figure 6.

A block diagram of the apparatus is shown in Figure 8. Cylindrical rock samples 4 in. in diameter and 4 in. long are mounted between the transducer holders as shown in Figure 5. The rock sample is cast in place with a thin sheath of room-temperature-vulcanizing (RTV) silicone rubber. Acoustic contact between the transducer holders and rock sample is maintained by the insertion of annealed copper discs of approximately 1 mil thickness. For static stress-strain measurements, strain gauges can be attached to the rock sample and the leads brought out through the RTV rubber jacket to insulated high-pressure fittings located on the lower transducer holder. The axial deformation of the rock sample is also measured by two linear potentiometers and recorded with a digital voltmeter. Axial stress is applied to the rock sample by a 200-ton compression testing machine. The hydraulic system for applying the confining and pore pressures consists of pressure intensifiers operated by high-pressure nitrogen gas; it is similar to that described for the hydrostatic tests. A general view of the apparatus is shown in Figure 7.

Operational Procedure

The procedures used in the preparation of the 3 1/2-in.-diameter samples and for testing the samples under hydrostatic pressures are identical to those described by King (1966). Basically they are similar to the procedures described below for the triaxial tests.

For the triaxial tests 4-in.-diameter cores of rock were cut with a diamond core drill, using water or kerosene as the drilling fluid. The rock samples were then placed in a specially-designed holder and their flat faces ground parallel to each other and perpendicular to the sample axis, to a maximum difference in length of ± 0.0005 in. across any diameter. The rock samples were then placed in a vacuum oven at 110° C for at least 48 hours immediately before use.

If static stress-strain measurements were to be made, strain gauges were mounted in axial and lateral configuration on the centreline of the cylindrical surface of the rock sample, which had previously been coated with a thin

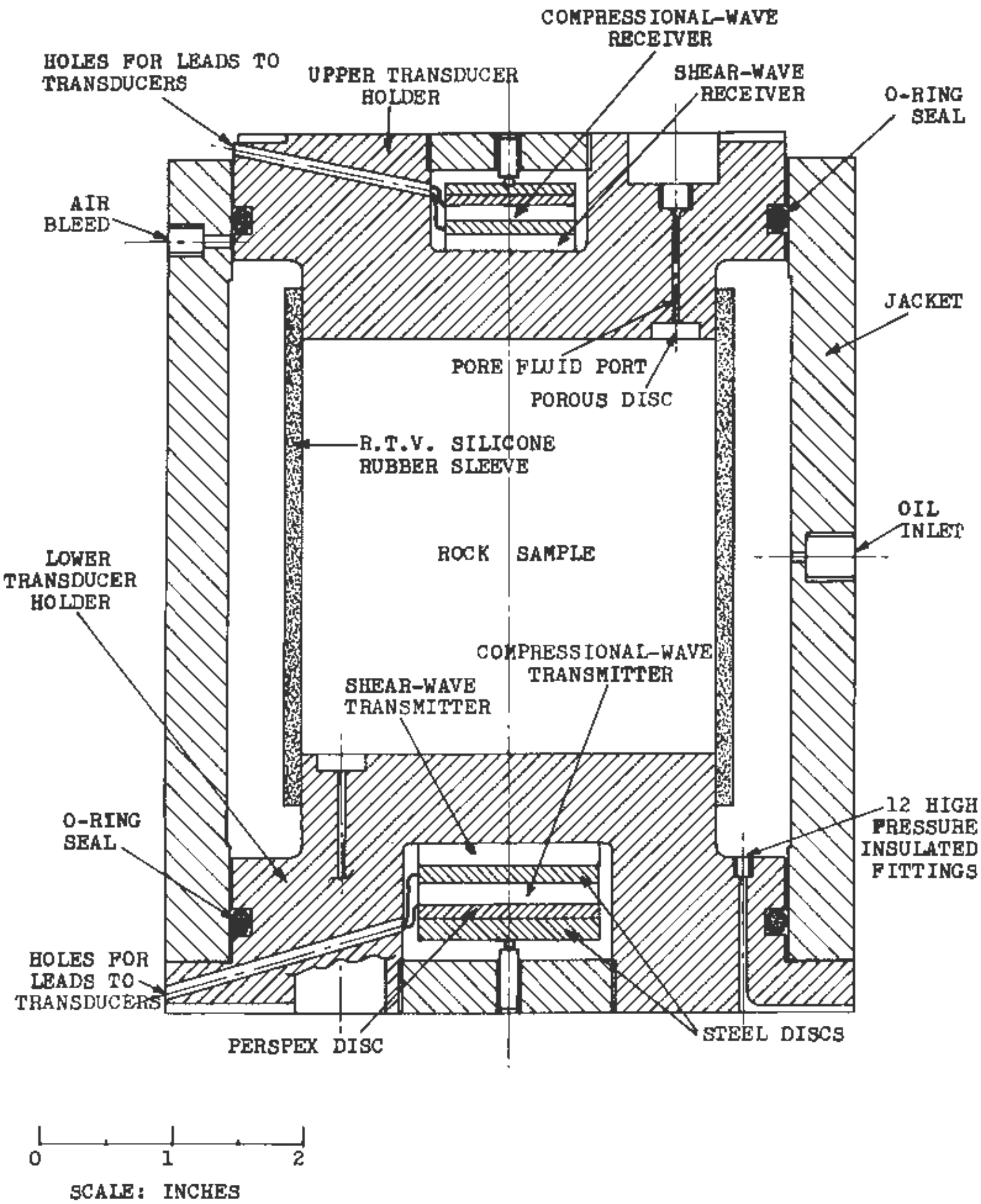

FIGURE 5 – Triaxial loading apparatus

coat of epoxy resin. The sample was then assembled between the transducer holders as shown in Figure 5, with annealed copper discs of 1 1/2 in. diameter and approximately 1 mil thick placed centrally on the top and bottom of the rock sample. After strain gauge leads had been attached, the cylindrical surface was cast in RTV silicone rubber and allowed to set for 24 hours. The assemblage was then transferred to the 200-ton compression testing machine.

As was observed during tests under hydrostatic confining pressures, an appreciable hysteresis effect was apparent during the triaxial tests, with higher velocities being recorded at a given confining pressure and axial load when the latter was being lowered than when it was being raised. During tests, therefore, a previously-established hysteresis cycle was always

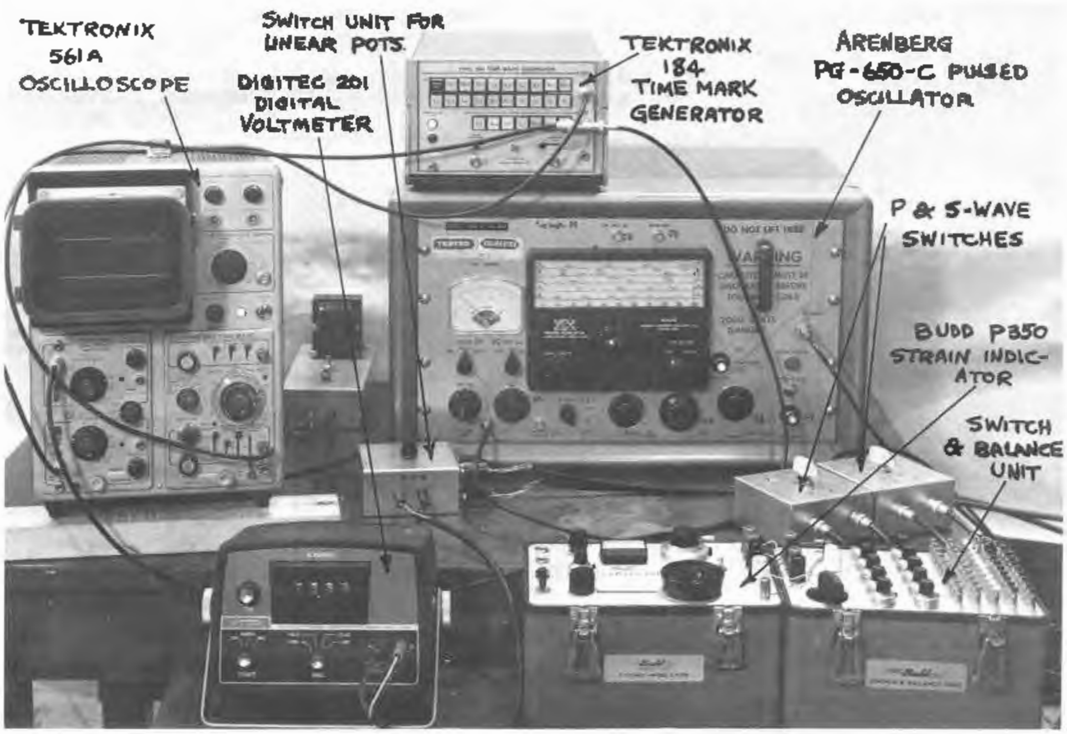

FIGURE 6 — Electronic equipment — triaxial tests

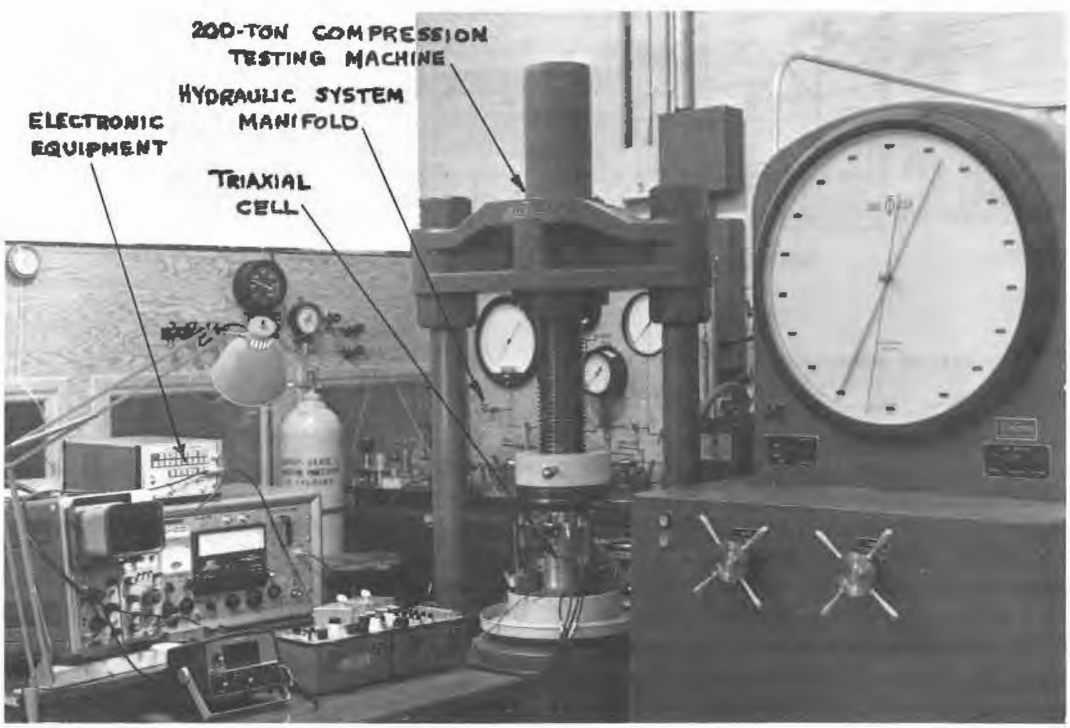

FIGURE 7 — General view of apparatus — triaxial tests

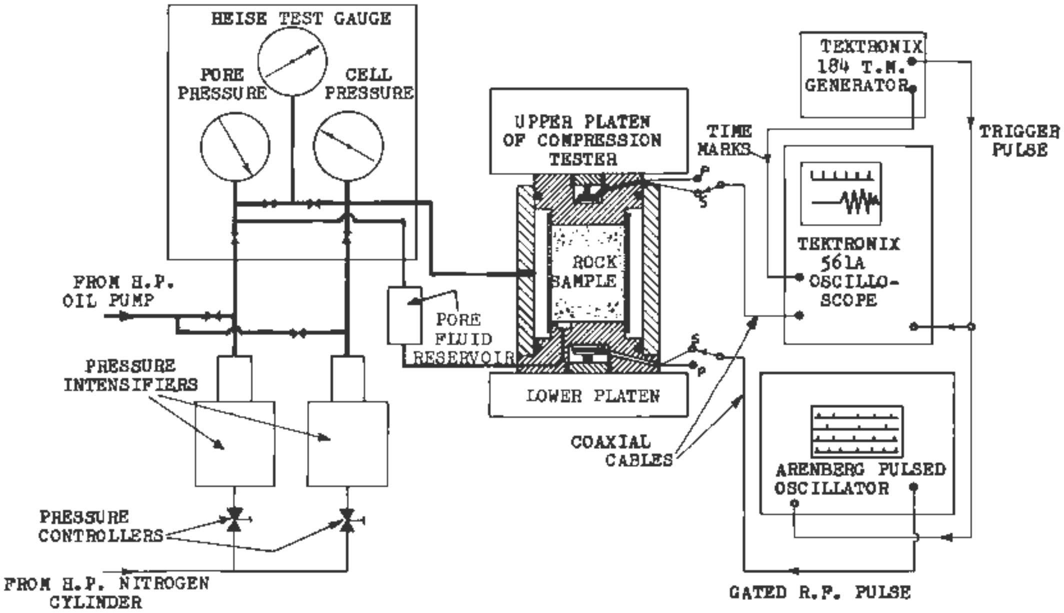

FIGURE 8 — Block diagram of apparatus for triaxial tests

followed, as suggested by Gardner et al. (1965). First, the axial stress and lateral confining pressure were increased together until the rock sample was subjected to a specified hydrostatic pressure. After several minutes had elapsed, strain and velocity measurements were made. Second, a deviator stress was applied by increasing the axial stress in steps, keeping the confining pressure constant. Measurements of strain and velocity were made at each step. The deviator stress was not allowed to exceed a value for which the stress-strain relationships were linear. Third, the deviator stress was removed, leaving the rock sample subjected to the original hydrostatic pressure. This procedure was repeated for each of the hydrostatic stress levels required. Before any measurements were made, however, each rock sample was subjected to a hydrostatic pressure of 6,000 psi to insure reproducibility of the stress-strain and acoustic velocity measurements.

Preliminary experiments were performed with the apparatus, using a standard cylinder of aluminum 4 in. in diameter and 4 in. long. A calibration curve was obtained for the equipment to account for the frictional resistance of the upper O-ring as the top transducer holder moved up and down. These corrections, in terms of axial stress on a 4-in.-diameter sample, ranged from 20 psi axial stress at 500 psi confining pressure to 110 psi axial stress at 8,000 psi confining pressure. The calibration runs were reproducible to within ± 10% of mean values of axial stress. The times of transit of pulses of compressional and shear waves through the aluminum sample were not found to vary more than ± 0.3% during these preliminary tests. The velocities measured were: compressional waves, 20,950 ft/sec; shear waves, 10,270 ft/sec. These values compare well with those reported by King (1966) and Gregory (1967). Measurements of velocities with this system can be made to an accuracy of ± 0.5%.

Discussion of Results

Tests Under Hydrostatic Confining Pressure

Three types of sedimentary rocks were studied in these tests: Boise, Bandera and Berea sandstones, all of which retain fairly uniform properties in bulk. Table 1 indicates some of the physical properties of these sandstones. A more detailed description of these sandstones is given by Mann and Fatt (1960).

For each of these sandstones, three cores were first cut in orthogonal directions perpendicular and parallel to the bedding plane. Before acoustic-velocity measurements were made, each sample was first subjected to a

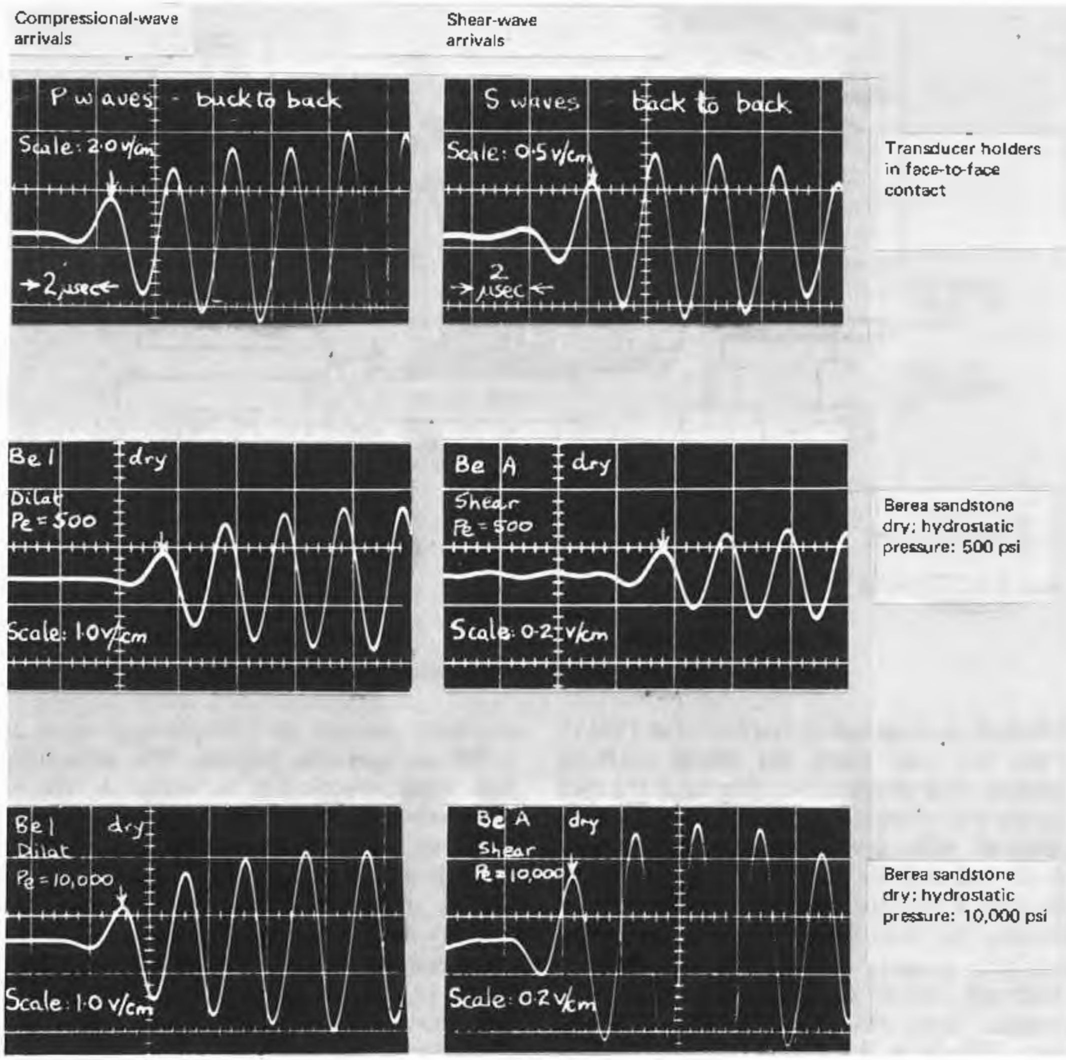

FIGURE 9 — Oscilloscope traces for hydrostatic tests

Table 1

	Boise	Bandera	Berea
Porosity, %	25.0	20.0	20.5
Permeability*, md	1400	3.5	250
Bulk density, gm/cm^3	1.95	2.16	2.14
Mean grain dia., mm	0.25	0.07	0.15
Remarks	Well consolidated, well cemented		

*Measured perpendicular to bedding plane

hydrostatic pressure of 10,000 psi. Measurements of compressional and shear-wave velocities on these cores in the dry state, as a function of hydrostatic pressure to 10,000 psi, showed Boise sandstone to be almost isotropic. The other two sandstones, however, proved to be transversely isotropic, with the axis of symmetry perpendicular to the bedding plane. The compressional and shear-wave velocities have all been corrected for changes in length of the rock sample as the hydrostatic pressure was changed.

Figure 11 shows the compressional and shear-wave velocities measured on three Boise samples as a function of hydrostatic pressures in the range 200 psi to 10,000 psi. The plotted shear-wave velocities are the maximum and minimum ones recorded on the three cores. It will be seen that the measured velocities each

Compressional-wave arrivals

Shear-wave arrivals

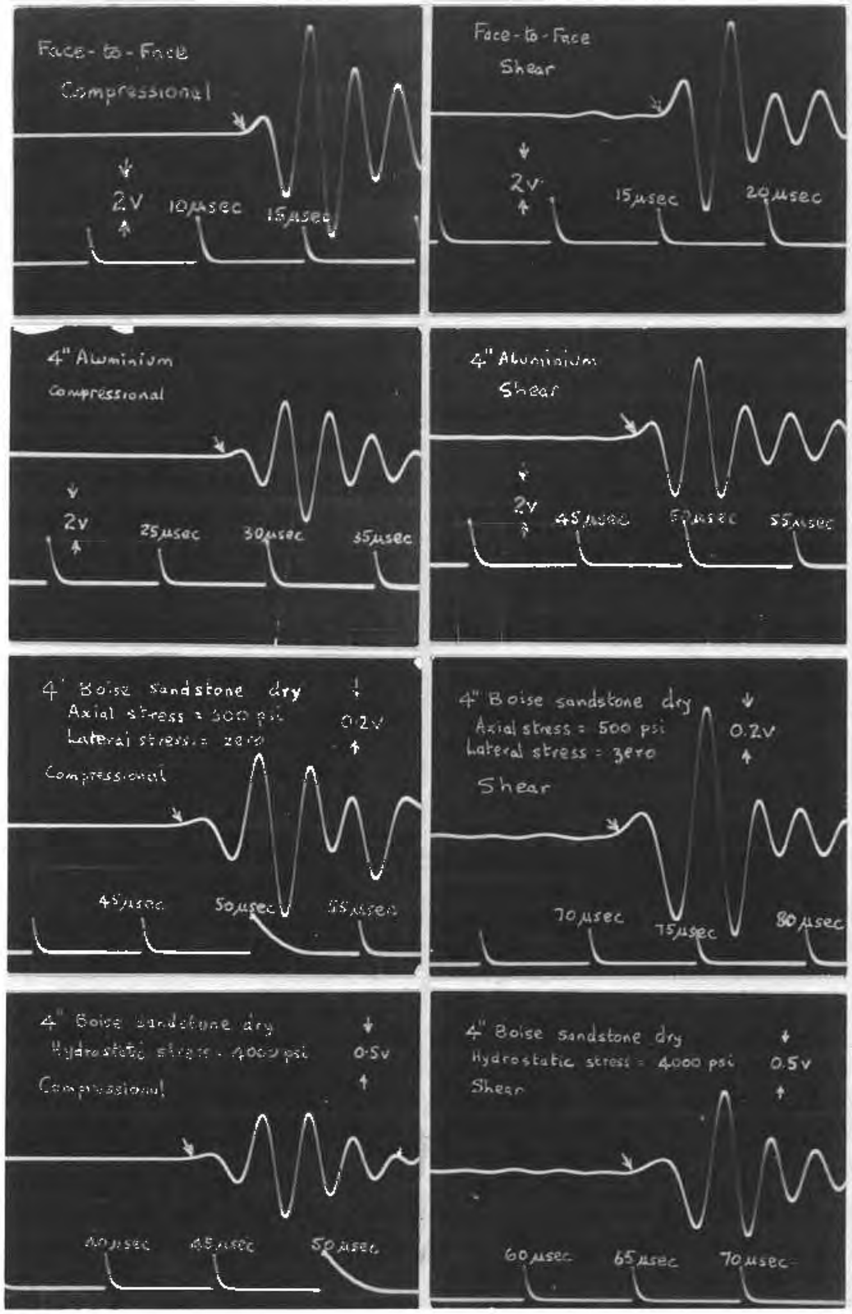

Transducer holders in face-to-face contact

Aluminium test block 4" dia. X 4" long

Boise sandstone dry; axial stress: 500 psi; lateral stress: zero

Boise sandstone dry; axial stress: 4,000 psi; lateral stress: 4,000 psi

FIGURE 10 — Oscilloscope traces for triaxial tests

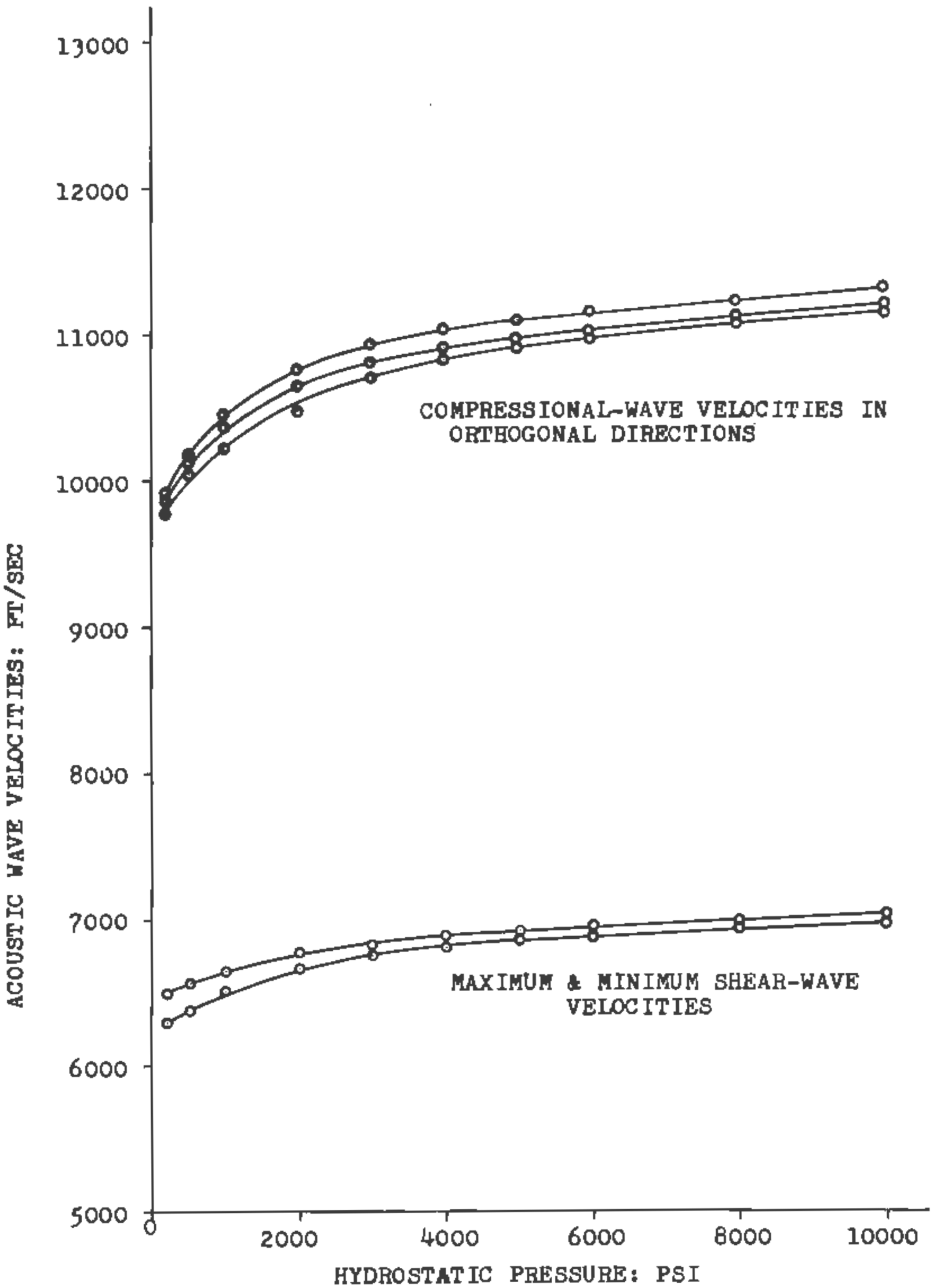

FIGURE 11 — Acoustic wave velocities Boise sandstone hydrostatic tests

lie within ± 1% of the mean. Since this lies within the accuracy of the system, Boise sandstone can be considered isotropic.

The Bandera and Berea sandstones proved to be transversely isotropic, with the axis of symmetry lying perpendicular to the bedding plane. Compressional-wave velocities measured in directions at right angles to each other in the bedding plane were very close in magnitude over the range of hydrostatic pressure 200 psi to 10,000 psi. These velocities were appreciably higher than the compressional-wave velocity

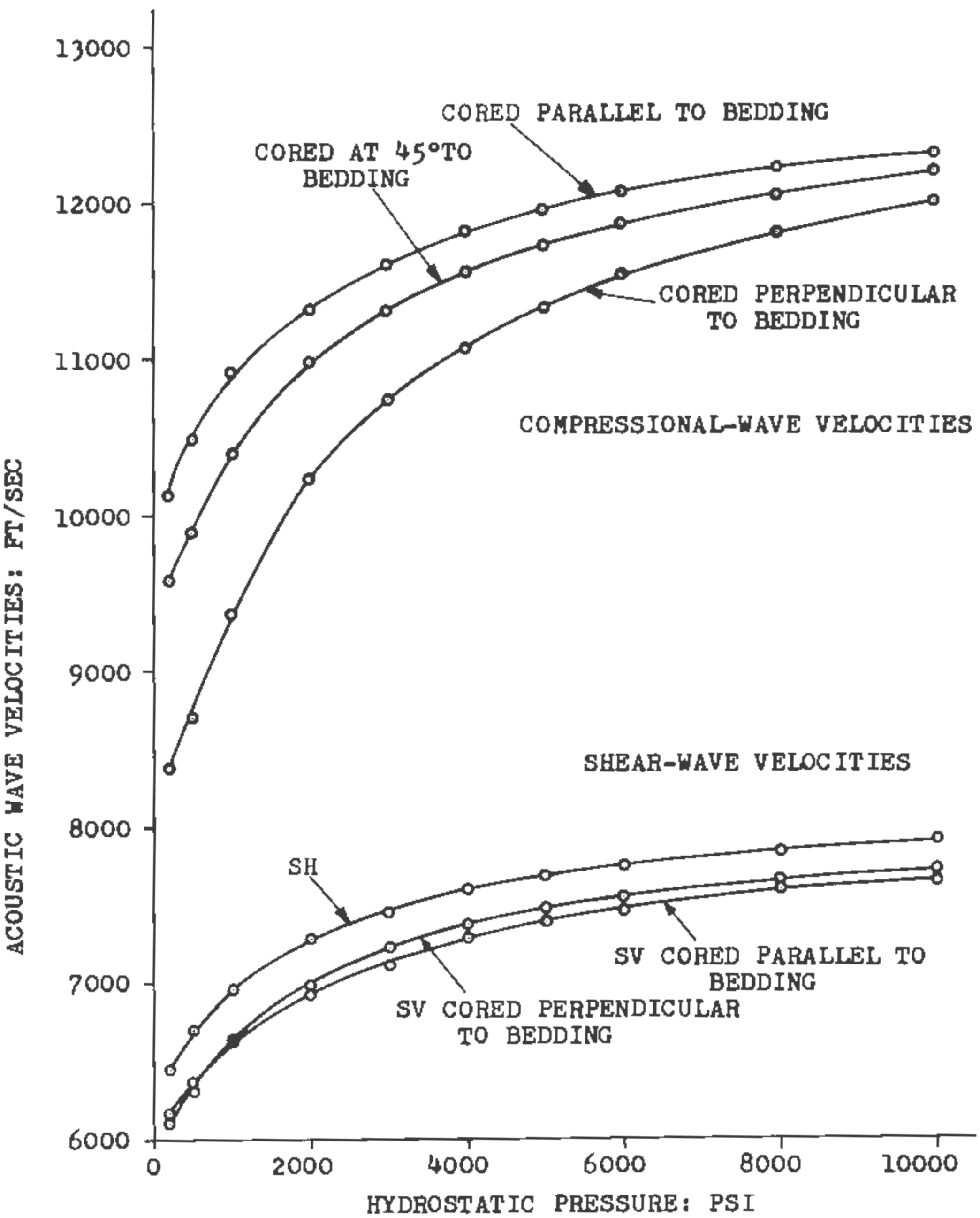

FIGURE 12 – Acoustic wave velocities Bandera sandstone

measured in a direction perpendicular to the bedding plane, especially at the lower confining pressures. Additional samples of these sandstones were cored in a direction at 45° with the bedding plane, and their compressional-wave velocities were measured.

Figure 12 shows the results for Bandera sandstone. It was possible in this case to check the validity of certain of the theoretical equations governing wave propagation in a material exhibiting transverse isotropy. In the Appendix, it is indicated for the condition of transverse isotropy that polarized shear waves can propagate at one velocity, $V_{SV} = \sqrt{\frac{C_{44}}{\rho}}$, in a direction parallel to the axis of symmetry, and at two velocities, $V_{SH} = \sqrt{\frac{C_{11}-C_{12}}{2\rho}}$ and $V_{SV} = \sqrt{\frac{C_{44}}{\rho}}$, in any direction perpendicular to the axis of symmetry. Thus polarized shear waves can propagate at the same velocity, $V_{SV} = \sqrt{\frac{C_{44}}{\rho}}$, in the two directions. These velocities measured on Bandera sandstone are shown in Figure 12. It can be seen that they lie within ± 0.5% of the mean over the range of hydrostatic pressures 200 psi to 10,000 psi, thus further substantiating the fact that Bandera sandstone is transversely isotropic. Figure 13 shows the compressional- and shear-wave velocities as a function of hydrostatic pressure in the range 200 psi to 10,000 psi for Berea sandstone. The behaviour of this sandstone is similar to that of Bandera sandstone, differing only in that the compressional-wave velocities for Berea approach each other in magnitude at high pressures.

Using the mean values of the velocities measured on Boise sandstone samples, the elastic constants were calculated from equations 3, 4 and 5, given in the Appendix for isotropic materials. The Young's modulus, E, and Poisson's ratio, ν, for Boise sandstone as a function of hydrostatic pressure in the range 200 psi to 10,000 psi are plotted in Figure 14. Both Young's modulus and Poisson's ratio increase only slightly, from values of 2.4 to 3.0 $\times 10^6$ psi and 0.14 to 0.18 respectively, with this increase in hydrostatic pressure.

Five velocities measured on both the Bandera and Berea sandstones were used to evaluate the five elastic constants, C_{ij}, from equations 13 given in the Appendix for transversely isotropic materials. From these constants the values of Young's moduli in a direction parallel to the bedding plane, E_H, and parallel to the axis of symmetry, E_V, and Poisson's ratios ν_1, ν_2, ν_3, have been calculated. The Young's moduli and Poisson's ratios are plotted in Figure 15 for Bandera sandstone and in Figure 16 for Berea sandstone as a function of hydrostatic pressure in the range 200 psi to 10,000 psi. Also plotted in these figures is the anisotropy ratio, E_H/E_V. It will be seen that the anisotropy ratio decreases appreciably for both sandstones as the hydrostatic pressure is increased. The decrease in anisotropy ratio, coupled with the tendency for the Poisson's ratios to converge at higher pressures, indicates that the degree of anisotropy of Bandera and Berea sandstones decreases quite appreciably as the hydrostatic pressure is increased to 10,000 psi. The increases in E_H and E_V are more pronounced for Bandera and Berea than for Boise sandstone as the pressure is increased. The average values to which the Poisson's ratios converge at high pressures for Berea and Bandera sandstones are close to the value of Poisson's ratio, 0.18, calculated at high pressures for Boise sandstone.

For both Bandera and Berea sandstones there is a sharp initial decrease in E_H/E_V as the hydrostatic pressure is increased to 2,000 psi. This suggests that a major part of the anisotropic behaviour of these sandstones is due to the presence at low pressures of small lenticular cracks or microcracks parallel to the bedding plane. As these fissures or microcracks are closed with increasing pressure, the loss in stiffness associated with them is considerably reduced and the rock tends to be more isotropic in nature. Berea sandstone is seen to approach a state of isotropy fairly quickly as the hydrostatic pressure is increased. Bandera sandstone, however, approaches this state very much more slowly. The different behaviour of the two sandstones can be explained by the presence of clay partings in the bedding plane of Bandera sandstone, which are not present in Berea sandstone. There is only a gradual increase in stiffness associated with compression of the clay partings, compared with the sharp increase associated with the closure of fissures or microcracks. The fact that the anisotropy ratio for Bandera remains greater than unity at high pressures tends to confirm the validity of this explanation.

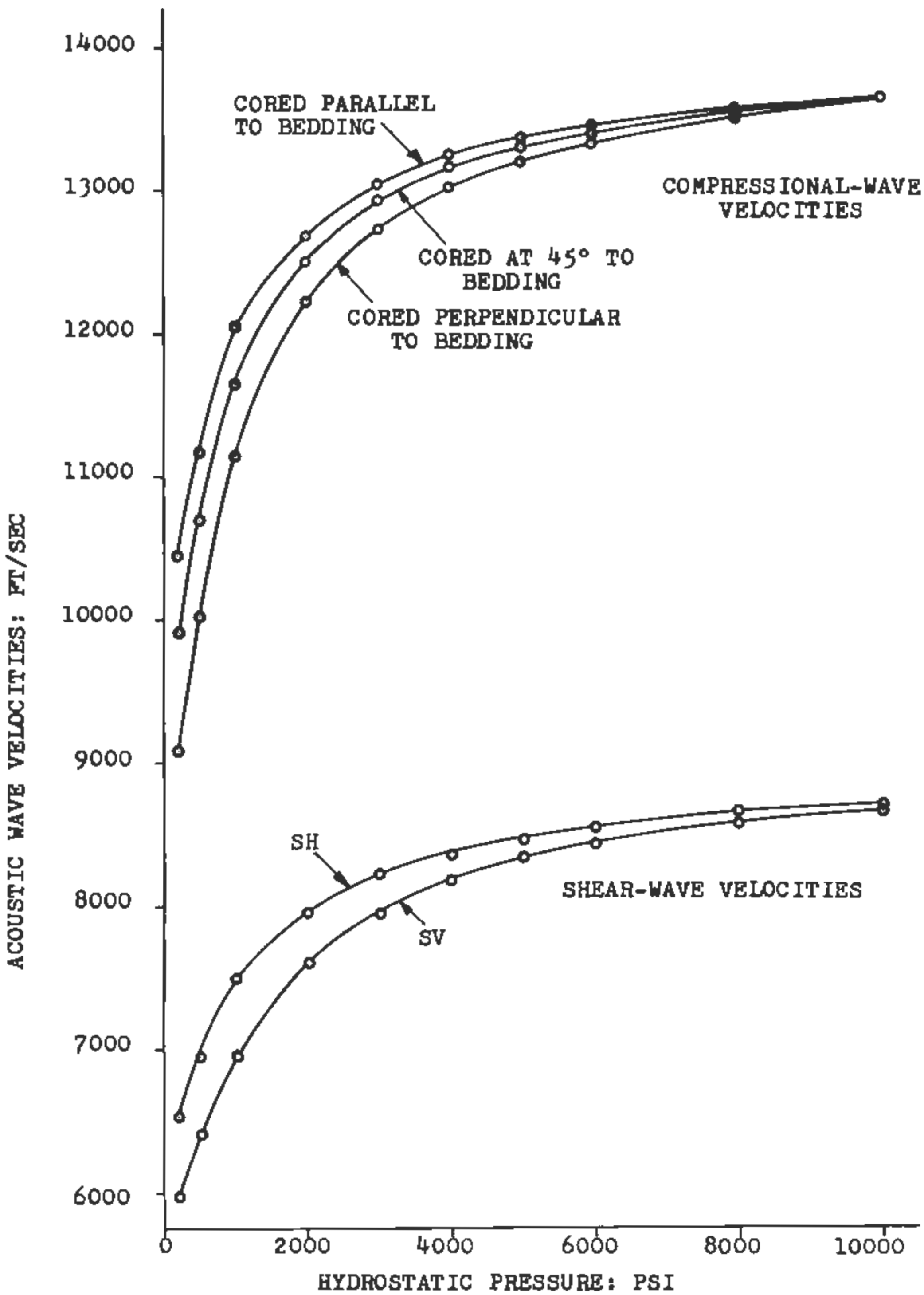

FIGURE 13 — Acoustic wave velocities Berea sandstone

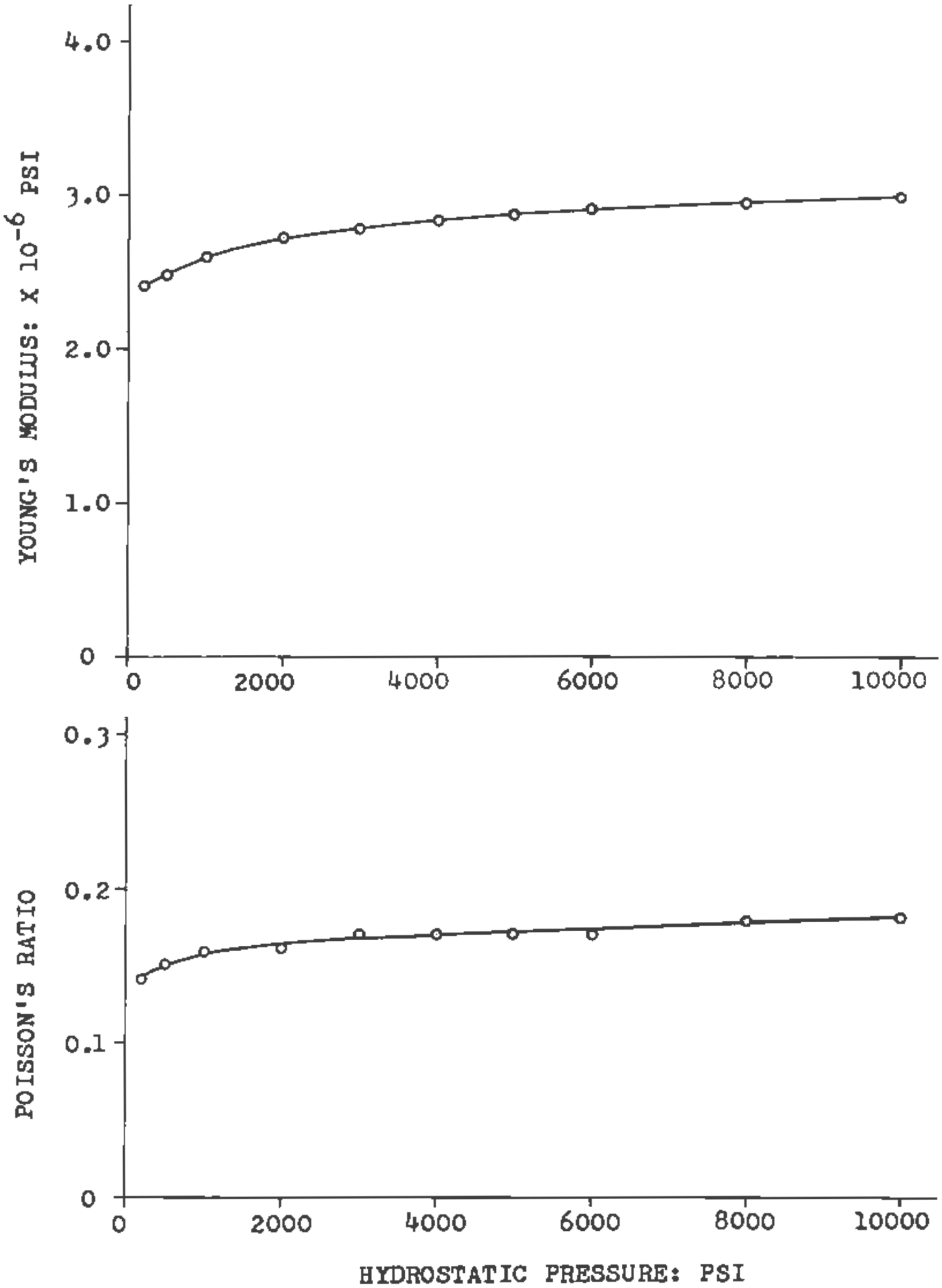

FIGURE 14 — Dynamic elastic moduli — Boise sandstone hydrostatic tests

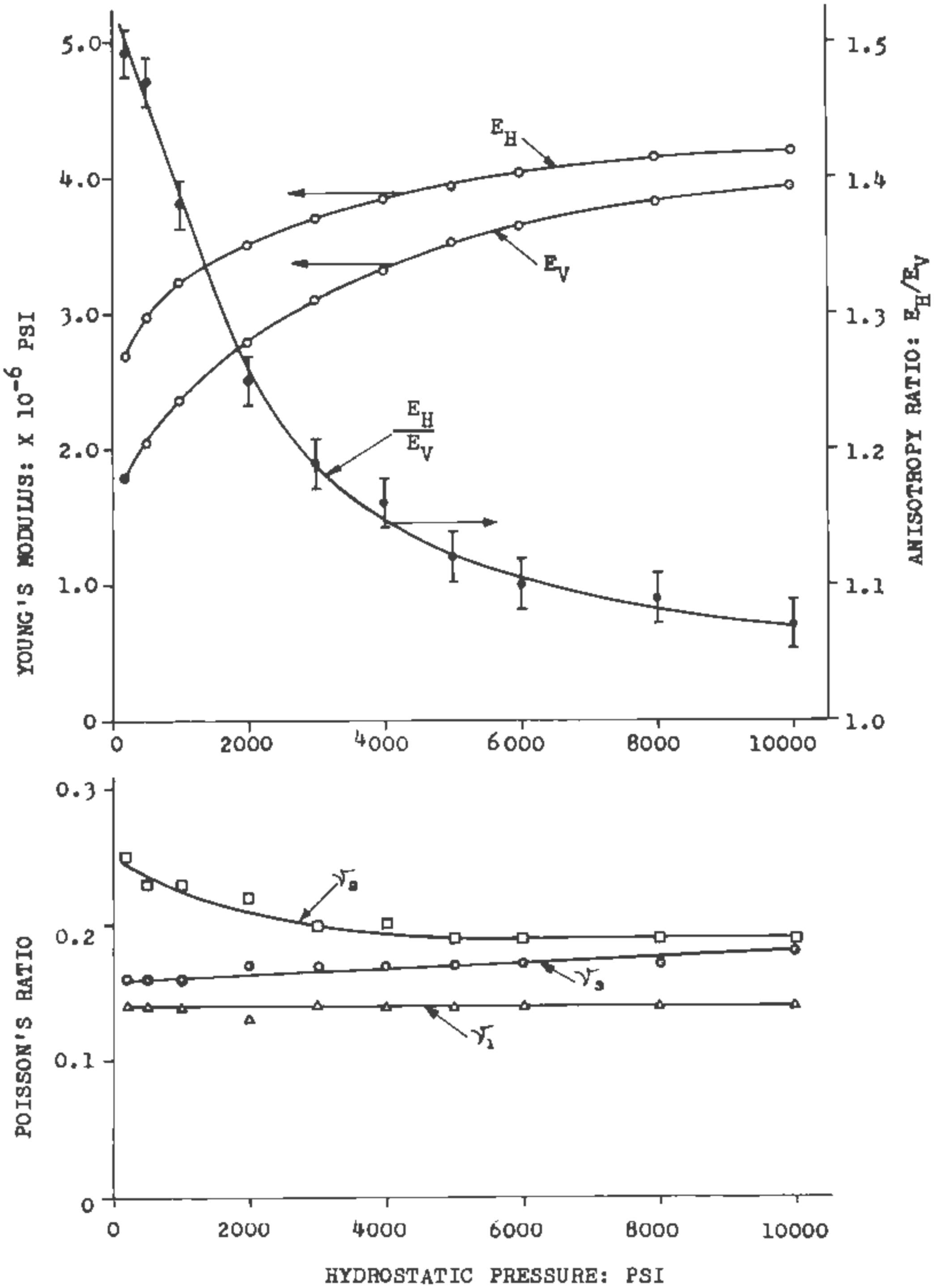

FIGURE 15 – Dynamic elastic moduli – Bandera sandstone hydrostatic tests

Tests Under Triaxial Loading Conditions

Since it had already proved to be almost isotropic in behaviour, Boise sandstone was studied in these tests. The samples were cored from a block quarried more recently than the one from which samples were cut for the previous tests under hydrostatic stress conditions. The bulk density and porosity for these samples were 1.90 gm/cm^3 and 27.0%, respectively. After the samples had been dried in a vacuum oven, five epoxy-backed foil strain gauges were cemented around the circum-

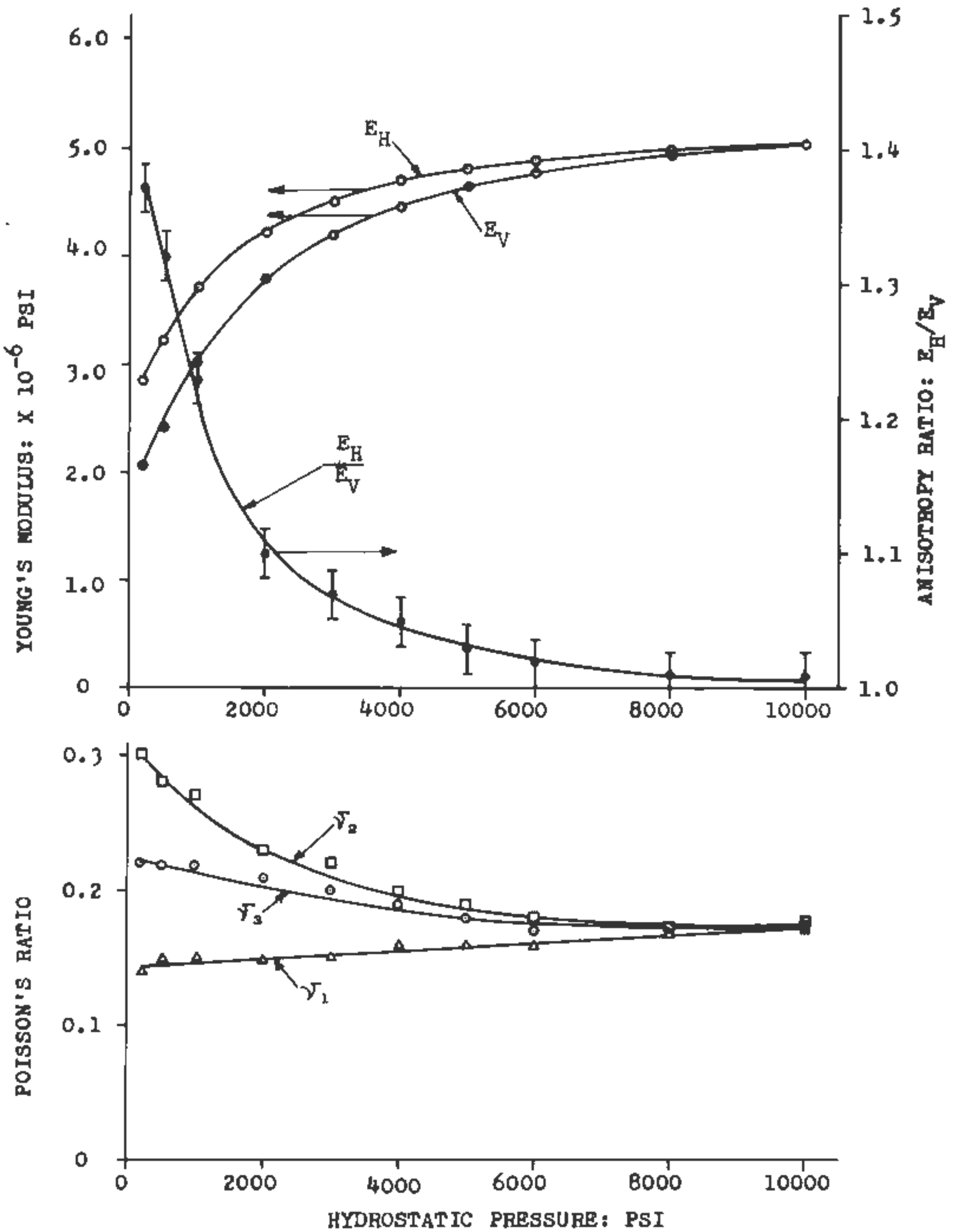

FIGURE 16 – Dynamic elastic moduli – Berea sandstone hydrostatic tests

ference of the samples halfway down: two of 1-in. gauge length spaced at 180° to measure lateral strain, and three of 1/2-in. gauge length spaced at 120° to measure axial strain. The static stress-strain data and acoustic velocities were obtained on samples which had first been subjected to a hydrostatic pressure of 6,000 psi.

The stress-strain relations for Boise sandstone at different lateral confining pressures are shown in Figure 17. The axial and lateral strains plotted are mean values from strain gauges oriented in each direction, recorded as the deviator stress was increased. The strains recorded for each of the axial and lateral gauges did not differ by more than 12% from the mean value in each case throughout the tests. The deviator stress (the difference between the axial stress on the sample and the lateral confining pressure) was not allowed to reach a value sufficiently high to affect the previously established hysteresis cycle. Both the axial and lateral strains show a near-linear relationship to the deviator stress over the range of stresses recorded.

The static Young's modulus, E_S, and Poisson's ratio, ν_S, calculated from the stress-strain data tangent at the origin are plotted in Figure 19 as a function of hydrostatic pressure on the sample. There is an increase in E_S from 1.5 to 2.2×10^6 psi as the hydrostatic pressure is increased from 200 to 5,000 psi, with the rate of increase becoming less at high pressures. Poisson's ratio increases sharply at first from a value of 0.13, and then approaches a constant value of 0.16 for pressures in excess of 1,000 psi.

Figure 18 shows the compressional and shear-wave velocities on Boise sandstone as a function of hydrostatic pressure. The velocities were measured concurrently with the stress-strain data, and they have been corrected for changes in length of the sample as the hydrostatic pressure was changed. The velocities are rather lower over the whole range of pressures than those reported in the previous section, by up to 5% at low pressures and 2% at high pressures. Since the sandstone block from which these samples were cored was cut from a different part of the quarry, these comparatively small differences in velocity tend to confirm the uniformity in mechanical properties of Boise sandstone in bulk.

The dynamic values of Young's modulus, E_D, and Poisson's ratio, ν_D, have been calculated from the acoustic velocities: they are plotted in Figure 19 as a function of hydrostatic pressure. There is an increase in E_D from 2.0 to 2.8×10^6 psi in the range of pressures 100 to 6,000 psi, with E_D always greater in magnitude than the static value, E_S. The ratio E_D/E_S has also been plotted in Figure 19: there is a reduction in this ratio from 1.5 to 1.25 as the hydrostatic pressure is increased from 200 to 5,000 psi. The dynamic value of Poisson's ratio increases sharply from a value of 0.15 to a near-constant value of 0.18 for pressures in excess of 1,000 psi. This behaviour is similar to that noted for ν_S, but the values of ν_D are rather higher than those calculated for ν_S.

The dynamic values of Poisson's ratio agree well with those reported in the previous section. Since the acoustic velocities and bulk density are lower in this case, however, there is a reduction in dynamic Young's modulus, by 10% at low pressures and 7% at high pressures, over the values reported in the previous section for tests under hydrostatic pressure.

Walsh and Brace (1966) have shown theoretically that for materials containing pores and narrow cracks there will be an increase in Poisson's ratio and in Young's modulus as the cracks are progressively closed when the confining pressure is increased. The theory also predicts that as the narrow cracks are closed, the static value of Young's modulus will approach the dynamic value. Simmons and Brace (1965) have found the static and dynamic moduli for rocks subjected to confining pressures in excess of 30,000 psi to agree very well with each other, whereas at low confining pressures the dynamic moduli were considerably higher than the static. The results of the tests reported here indicate that Boise sandstone behaves in a manner similar to that predicted by the theory, but it appears, however, that the maximum confining pressure of 6,000 psi was insufficient to close all the cracks present in the sandstone.

Conclusions and Recommendations

A successful technique has been developed for determining ultrasonic compressional and shear-wave velocities on rock samples subjected to hydrostatic confining pressures to 10,000 psi. The technique has been further developed so that compressional and shear-wave velocities

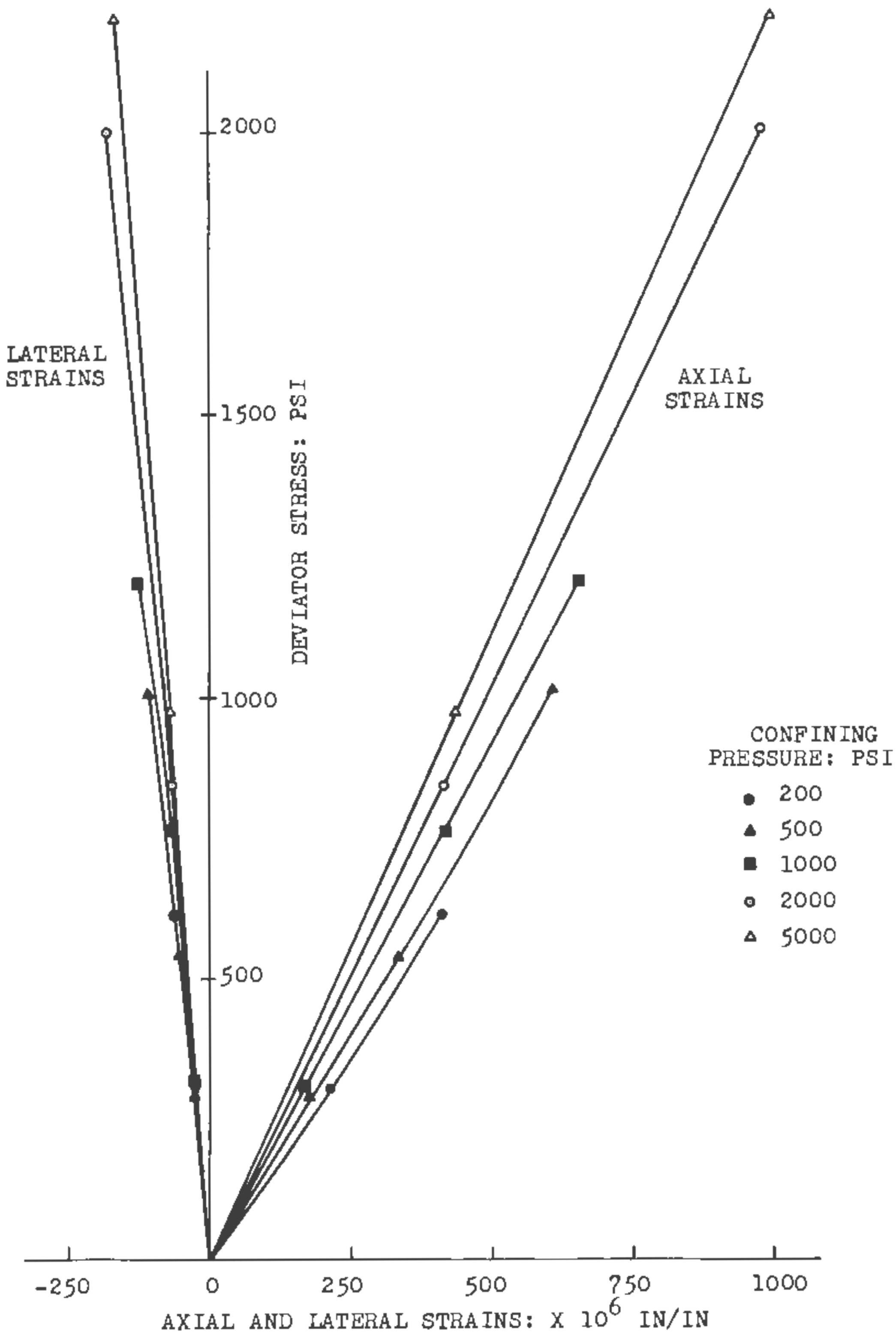

FIGURE 17 – Stress-strain relations Boise sandstone triaxial tests

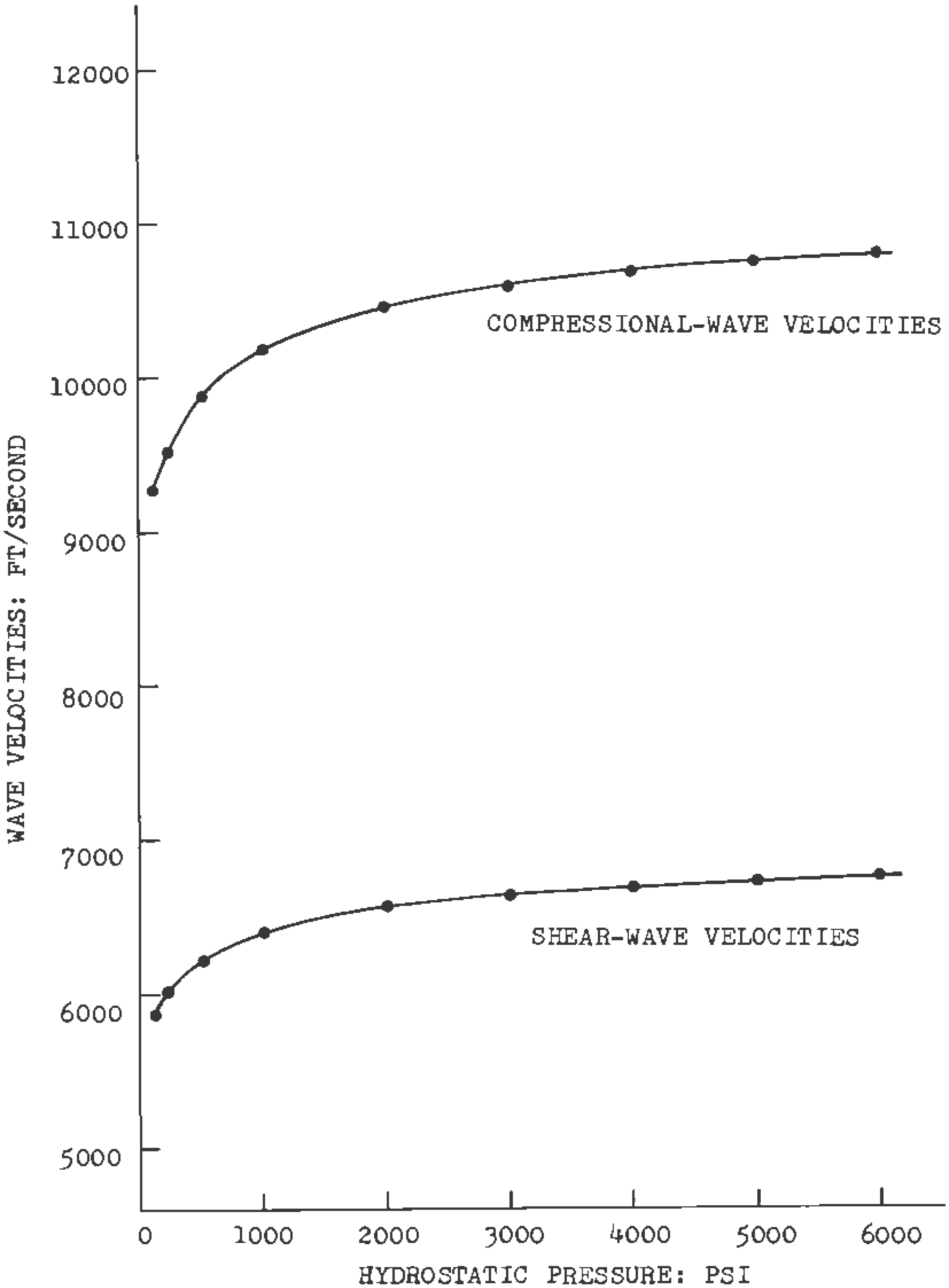

FIGURE 18 — Wave velocities — Boise sandstone triaxial tests

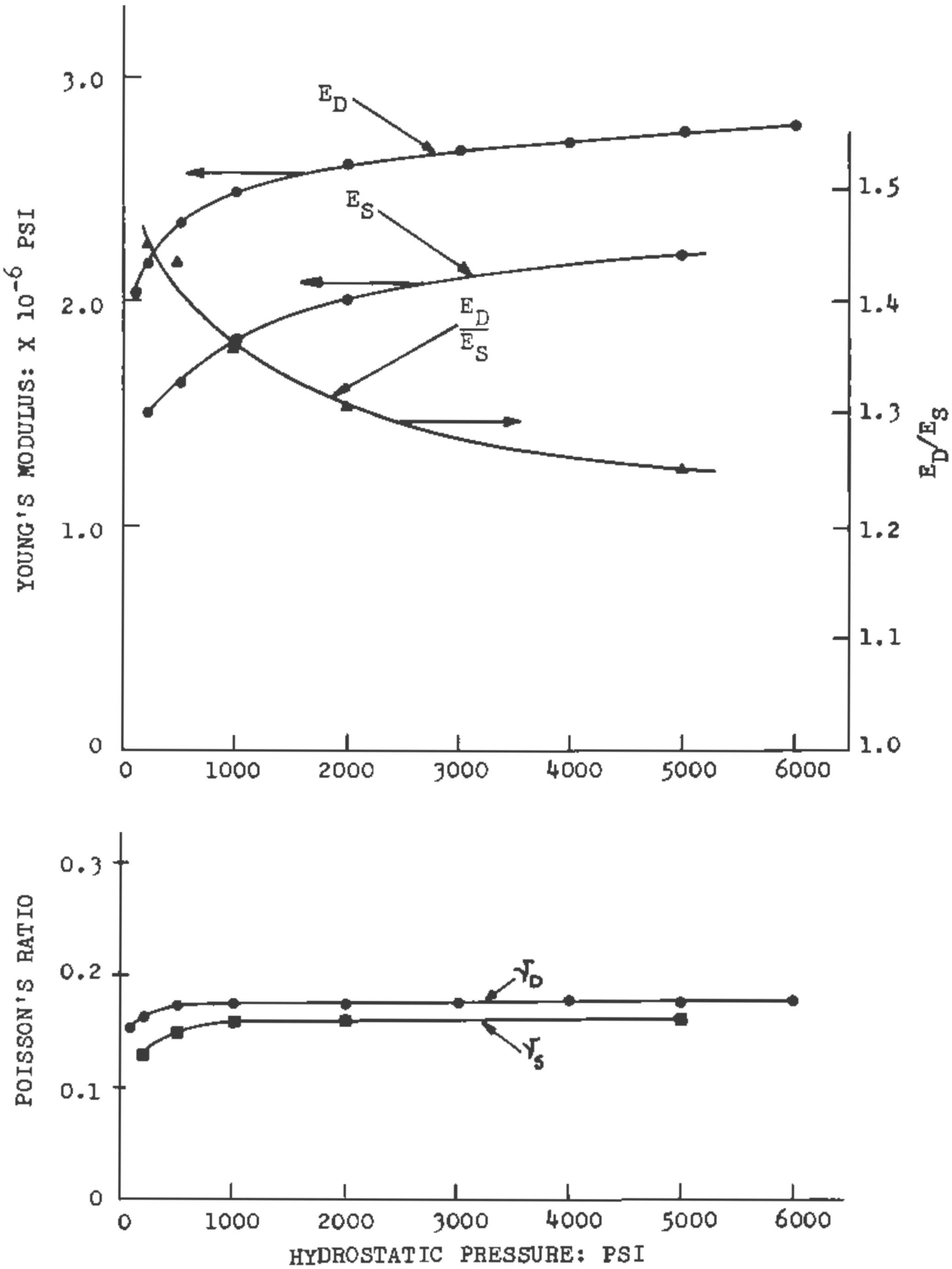

FIGURE 19 — Static and dynamic elastic moduli Boise sandstone — triaxial tests

can be determined concurrently on the same rock sample as a function of changes in triaxial loading conditions. With this apparatus it is also possible to measure the axial and lateral static stress-strain relationships on the sample at the same time as the velocities.

Measurements of compressional and shear-wave velocities in different directions on samples of three sandstones subjected to hydrostatic confining pressures indicate that, while one of them is almost isotropic in behaviour, the other two sandstones are transversely isotropic, with their axis of symmetry lying perpendicular to the bedding plane. The degree of anisotropy was found to decrease appreciably as the hydrostatic confining pressure was increased. It is concluded that the degree of anisotropy is dependent on the presence of

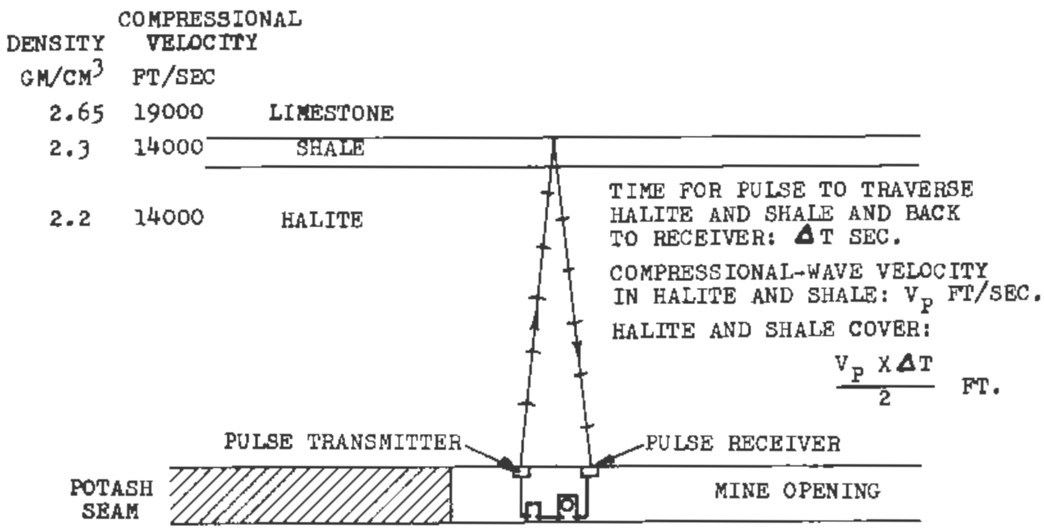

DETERMINATION OF HALITE COVER IN POTASH MINE

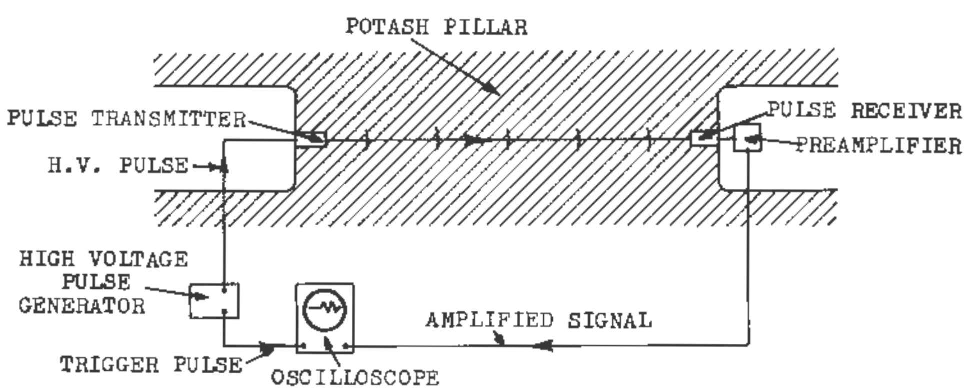

DETERMINATION OF STATE OF STRESS IN POTASH MINE PILLARS

FIGURE 20 — Underground applications of acoustic technique

lenticular cracks or clay partings in the bedding planes of the two anisotropic sandstones.

The dynamic elastic moduli for the isotropic sandstone, calculated from compressional and shear-wave velocities, were higher than the static moduli, determined from strain gauges on the same rock sample at the same time as the velocities were measured. It is concluded that these differences in value can be explained by the presence of randomly-oriented lenticular cracks in the rock, which close progressively as the confining pressure is raised.

Results from measurements of ultrasonic velocities and static stress-strain relationships made concurrently on intact and jointed rock samples in the laboratory could be used to extend the theory of Walsh and Brace (1966) to cover the behaviour of jointed and fractured rock masses. The strong dependence of the static and dynamic moduli on the presence of fissures and joints in the rock could lead to determination of the state of stress around mine openings and to assessment of the suitability of foundations for large structures. Harmonic analyses of the compressional and shear-wave pulses in the proposed tests could be used to test the seismic-wave attenuation theory proposed by Walsh (1966), with similar applications in mining and in the location of the foci of rock bursts.

In potash mining, where the evaporite strata possess good acoustic-wave transmission properties, there appears to be considerable scope for the use of acoustic techniques for locating geologic discontinuities underground, and for determining the state of stress in mine pillars. Controlled-pulse acoustic-wave equipment based partly on that reported by Cannaday and Leo (1966) is presently under development in this laboratory, and it is intended initially to use it for locating precisely the salt and shale cover in a potash mine and for determining the state of stress in mine pillars. For these applications, which are sketched in Figure 20, it will be necessary to determine the compressional and shear-wave velocities and attenuation for potash and halite as a function of triaxial loading conditions in the laboratory. This testing program is now in hand.

Acknowledgments

Continued support for this research by the Defence Research Board under Grant No. 9511-72 is gratefully acknowledged. The earlier research reported here was performed while the author was with the Department of Mineral Technology, University of California, Berkeley.

References

Biot, M.A., 1962a. Mechanics of deformation and acoustic propagation in porous media. *J. Appl. Phys.*, v. 33, p. 1482-1498.

Biot, M.A., 1962b. Generalized theory of acoustic propagation in porous dissipative media. *J. Acoust. Soc. Am.*, v. 34, p. 1254-1264.

Cannaday, F.X., and Leo, G.M., 1966. *Development of Controlled Impulse Technique for In Situ Testing of Rock.* USBM Tech. Rept. No. AFWL-TR-65-156.

Cook, N.G.W., 1964. The application of seismic techniques to problems in rock mechanics. *J. Intern. Rock Mech. Min. Sci.*, v. 1, p. 169-179.

Cook, N.G.W., Hoek, E., Pretorius, J.O.G., Ortlepp, W.D., and Salamon, M.D.G., 1966. Rock mechanics applied to the study of rock bursts. *J. S. African Inst. Min. Met.*, v. 66, p. 435-528.

Duvall, W.I., and Blake, W., 1968. *Trans. AIME*, v. 241, in print.

Gardner, G.H.F., Wyllie, M.R.J., and Droschak, D.M., 1964. Effects of pressure and fluid saturation on the attenuation of elastic waves in sands. *J. Petrol. Tech.*, p. 189-198.

Gardner, G.H.F., Wyllie, M.R.J., and Droschak, 1965. Hysteresis in velocity-pressure characteristics of rocks. *Geophysics*, v. 30, p. 111-116.

Geertsma, J., 1961. Velocity log interpretation: the effect of rock bulk compressibility. *Trans. AIME*, v. 222, p. 235-246.

Gregory, A.R., 1963. Shear-wave velocity measurement of sedimentary rocks under compression. *Rock Mechanics.* New York, Pergamon Press. C. Fairhurst, ed.

Gregory, A.R., 1967. Mode conversion technique employed in shear wave velocity studies of rock samples under axial and uniform compression. *Trans. AIME*, v. 240, p. 136-148 (II).

Hearmon, R.F.S., 1961. *An Introduction to Applied Anisotropy.* Oxford, Clarendon Press.

Jamieson, J.C., and Hoskins, H., 1963. The measurement of shear-wave velocities in solids using axially-polarized ceramic transducers. *Geophysics*, v. 28, p. 87-90.

Jeffreys, H., 1962. *The Earth.* Cambridge, The University Press. 4th ed.

King, M.S., 1964. *Wave Velocities and Dynamic Elastic Moduli of Sedimentary Rocks.* Ph.D. thesis, Univ. of California, Berkeley.

King, M.S., and Fatt, I., 1962. Ultrasonic shear-wave velocities in rocks subjected to simulated overburden pressure. *Geophysics,* v. 27, p. 590-598.

King, M.S., 1966. Wave velocities in rocks as a function of changes in overburden pressure and pore-fluid saturants. *Geophysics,* v. 31, p. 50-73.

Larocque, G.E., 1964. A sonic unit for the determination of *in situ* dynamic properties and for the outlining of fracture zones. *Proc. 6th Symp. Rock Mech.*, Rolla, Univ. of Missouri. E.M. Spokes and C.R. Christiansen, ed.

Mann, R.L., and Fatt, I., 1960. Effect of pore fluids on the elastic properties of sandstone. *Geophysics,* v. 25, p. 433-444.

Nichols, H.R., 1962. *In situ* determination of the dynamic elastic constants of rocks. *Intern. Symp. Mining Res.:* New York, Pergamon Press. G.B. Clark, ed.

Onodera, T.F., 1963. Dynamic investigation of foundation rocks *in situ. Rock Mechanics,* New York, Pergamon Press. C. Fairhurst, ed.

Pickett, G.R., 1963. Acoustic character logs and their applications in formation evaluation. *J. Petrol. Technol.*, p. 659-667.

Simmons, G., 1965. Ultrasonics in geology. *Proc. IEE,* v. 53, p. 1337-1345.

Simmons, G., and Brace, W.F., 1965. Comparison of static and dynamic measurements of compressibility of rocks. *J. Geophys. Res.*, v. 70, p. 5649-5656.

Tixier, M.P., Alger, R.P., and Doh, C.A., 1959. Sonic logging. *Trans. AIME,* v. 216, p. 106-114.

Walsh, J.B., 1966. Seismic wave attenuation in rock due to friction. *J. Geophys. Res.*, v. 71, p. 2591-2599.

Walsh, J.B., and Brace, W.F., 1966. Elasticity of rock: a review of some recent theoretical studies. *Rock Mech. Eng. Geol.*, v. 4, p. 283-297.

Wyllie, M.R.J., Gardner, G.H.F., and Gregory, A.R., 1962. Studies of elastic wave attenuation in porous media. *Geophysics,* v. 27, p. 569-589.

APPENDIX

The general stress-strain relations for an elastic material are

$$\Sigma_i = C_{ij}E_j \quad i,j = 1, 2, 3, 4, 5, 6 \qquad \text{Eq. 1}$$

in which Σ_i = stress
E_j = strain
C_{ij} = elastic constants

Isotropic material [See Hearmon (1961), p. 23 and 71]

$$\begin{aligned} C_{11} &= C_{22} = C_{33} = \lambda + 2\mu \\ C_{12} &= C_{13} = C_{23} = \lambda \\ C_{44} &= C_{55} = C_{66} = \mu \end{aligned} \qquad \text{Eq. 2}$$

where λ and μ are the two independent Lamé constants describing an isotropic elastic material

$$\text{Young's modulus, } E = \frac{\mu(3\lambda + 2\mu)}{\lambda + \mu} \qquad \text{Eq. 3}$$

$$\text{Poisson's ratio, } \nu = \frac{\lambda}{2(\lambda + \mu)} \qquad \text{Eq. 4}$$

In terms of compressional-wave velocity, V_p, shear-wave velocity, V_S, and density, p:

$$\begin{aligned} \lambda &= p\,(V_p^2 - 2V_S^2) \\ \mu &= p\,V_S^2 \end{aligned} \qquad \text{Eq. 5}$$

Transversely Isotropic Material – Axis of symmetry in 3-direction [See Hearmon (1961), p. 23 and 72, and King (1964), p. 114-116]

$$\begin{array}{ll} C_{11} = C_{22} & C_{13} = C_{23} \\ C_{33} & C_{44} = C_{55} \\ C_{12} & C_{66} = \dfrac{C_{11} - C_{12}}{2} \end{array} \qquad \text{Eq. 6}$$

where C_{11}, C_{33}, C_{12}, C_{13} and C_{44} are the five independent constants describing a transversely isotropic elastic material.

Young's modulus, E_V, measured in a direction parallel to the axis of symmetry, is given by:

$$E_V = \frac{\begin{vmatrix} C_{11} & C_{12} & C_{13} \\ C_{12} & C_{11} & C_{13} \\ C_{13} & C_{13} & C_{33} \end{vmatrix}}{(C_{11}{}^2 - C_{12}{}^2)} \qquad \text{Eq. 7}$$

Young's modulus, E_H, measured in any direction perpendicular to the axis of symmetry, is given by:

$$E_H = \frac{\begin{vmatrix} C_{11} & C_{12} & C_{13} \\ C_{12} & C_{11} & C_{13} \\ C_{13} & C_{13} & C_{33} \end{vmatrix}}{(C_{11}C_{33} - C_{13}{}^2)} \qquad \text{Eq. 8}$$

Poisson's ratio, ν_1, which is a measure of the effect of the strain in a direction perpendicular to the axis of symmetry on the strain at right angles to it in the same plane, is given by:

$$\nu_1 = \frac{C_{12}C_{33} - C_{13}{}^2}{C_{11}C_{33} - C_{13}{}^2} \qquad \text{Eq. 9}$$

Poisson's ratio, ν_2, which is a measure of the effect of the strain in a direction perpendicular to the axis of symmetry on the strain parallel to the axis of symmetry, is given by:

$$\nu_2 = \frac{C_{13}(C_{11} - C_{12})}{C_{11}C_{33} - C_{13}{}^2} \qquad \text{Eq. 10}$$

Poisson's ratio, ν_3, which is a measure of the effect of the strain in a direction parallel to ν_3 are the axis of symmetry on the strain at right angles to it, is given by:

$$\nu_3 = \frac{C_{13}}{C_{11} + C_{12}} \qquad \text{Eq. 11}$$

A measure of the degree of anisotropy may be expressed by the ratio, E_H/E_V, known as the anisotropy ratio, where:

$$\frac{E_H}{E_V} = \frac{C_{11}{}^2 - C_{12}{}^2}{C_{11}C_{33} - C_{13}{}^2} = \frac{\nu_2}{\nu_3} \qquad \text{Eq. 12}$$

This relationship indicates that only four of the five elastic constants E_H, E_V, ν_1, ν_2 and independent. To describe the material fully a further independent constant must be used.

In terms of compressional and shear-wave velocities and density, the elastic constants, C_{ij}, are:

$$C_{11} = p\,V_{PH}^2 \quad C_{44} = p\,V_{SV}^2$$

$$C_{33} = p\,V_{PV}^2 \quad C_{12} = p\,(V_{PH}^2 - 2V_{SH}^2)$$

$$C_{13} = p\left\{\sqrt{\left[\frac{4V_{PQ}^2 - V_{PH}^2 - V_{PV}^2 - 2V_{SV}^2}{2}\right]^2 - \left[\frac{V_{PH}^2 - V_{PV}^2}{2}\right]^2} - V_{SV}^2\right\} \qquad \text{Eq. 13}$$

Where V_{PH} = velocity of compressional waves in any direction perpendicular to the plane of symmetry,

V_{PV} = velocity of compressional waves in a direction parallel to the plane of symmetry,

V_{PQ} = velocity of quasi-compressional waves in a direction at 45° to the axis of symmetry,

V_{SH} = velocity of shear waves in any direction perpendicular to the plane of symmetry with particle motion in the same plane,

V_{SV} = velocity of shear-waves in a direction parallel to the axis of symmetry, or velocity of shear waves in a direction perpendicular to the axis of symmetry with particle motion parallel to the axis of symmetry,

p = density of material

From equations 13 it can be seen that

$$V_{SV} = \sqrt{\frac{C_{44}}{p}} \qquad V_{SH} = \sqrt{\frac{C_{11} - C_{12}}{2p}} \qquad \text{Eq. 14}$$

DISCUSSION

John W. Brown, University of Missouri, Rolla, Missouri

Ultrasonic devices have considerable potential for field applications. They have valuable and uncommon capabilities: remote sensing of rock properties and structure, and continuous monitoring of the behavior of a large volume of rock. The microseismic method and conventional seismic methods also share these capabilities to some extent.

Ultrasonic waves from electromechanical transducers may do more than locate single fractures and bedding planes. They may even one day yield three-dimensional pictures of the interior of rock formations. That is, such devices may reveal the complete system of joints, faults, bedding planes, and other discontinuities around excavations.

Though such a development may seem remote, advances have already been made. Optical three-dimensional photographs are now a reality*, and three-dimensional pictures of the interior of industrial materials, using sound waves, are undergoing development**. The latter method in effect employs radiated sound instead of radiated light as for photography.

Admittedly, there are problems to be solved before joints and bedding planes can be reliably located, to say nothing of locating whole systems of discontinuities in rock. Two obstacles to the ultrasonic method are the rapid attenuation of sonic and ultrasonic waves, and the complex variations of density and fracture intensity throughout rock *in situ*.

Field applications of ultrasonics, then, are promising but not well developed. That is true also of the microseismic method of monitoring rock noise. Such methods for remote sensing make up an area of rock mechanics in which further research would clearly be a good investment.

*DeVelis, John B. and Reynolds, George O., *Theory and Applications of Holography*. Addison-Wesley, 1967.

**International Business Machines. Simulating visual reality, *Computing Report*, v. 4, n. 4, July 1968, p. 4-7.

M.S. King

The author agrees with John W. Brown's remarks concerning the potential of different acoustical devices in field applications. With regard to acoustical holography some of the problems facing its use for locating discontinuities underground have been outlined by Metherell* in a recent review. A considerable amount of research will be required before this technique has any practical rock mechanics applications.

P.B. Attewell, University of Durham, Durham, Great Britain

I have had an opportunity of reading a preprint of Prof. King's interesting paper. As part of our own work in rock dynamics at Durham University, we have used the critical-angle tank technique and would concur with Prof. King's remarks at the beginning of his paper concerning the difficulty of locating exact angles for critical refraction of compressional and shear waves.

One of the problems arises, of course, from the very dependence of the velocity determinations on the sines of the critical angles of reflection. Since the critical angles for dilatational waves are much less than those for shear waves, and one is therefore working on the steeper portion of the sine curve, the accuracy of the end result for dilatational velocity must be lower than the corresponding result for shear velocity. Problems of critical-angle location are magnified by specimen internal and external reflections and this uncertainty is reflected in the high Poisson's ratios that are obtained using the standard elastic equations. It is also, of course, absolutely essential that all four quadrants of rotation be examined in order to smooth any anomalies associated with non-parallel faces.

Provided, however, that the tank mechanics are correctly analyzed it can yield valuable results. For example, supplemented by a water displacement technique and *direct compression* ultrasonic tests, a number of experiments have been carried out on a Welsh slate (0.62% porosity) of Cambrian age. The experiments

*Metherell, A.F. Holography with sound, *Science Journal*, v. 4, n. 11, p. 57-62, Nov. 1968.

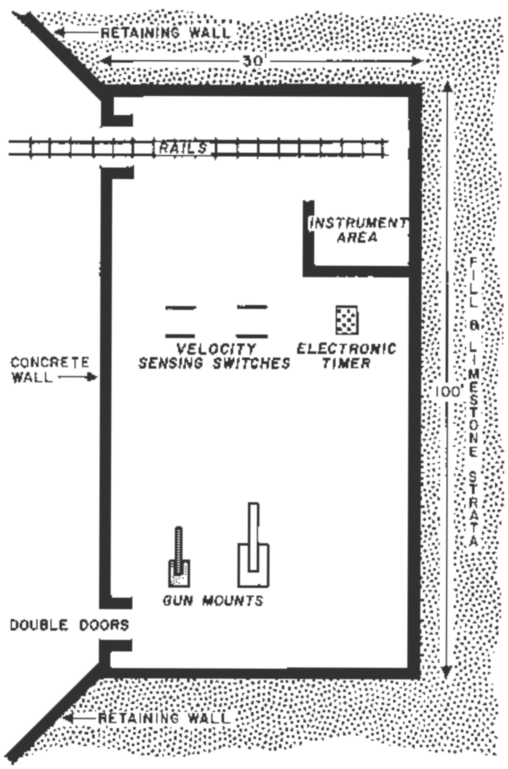

FIGURE 1 — Layout of high-velocity rock impact laboratory.

mount, permit high accuracy when sabot-launched projectiles are used. For the tests with spheres, rather than manufacture special sabots, the spheres were backed by a wad of compressed paper tissue and some accuracy was sacrificed. The gun is fired remotely using a solenoid which may be seen at the left rear of the mount. The .303 cal. gun is also fired from this mount. The 20 mm gun and mount are similar in construction except that the shock absorber is a spring arrangement mounted around the front portion of the barrel. This gun is also fired remotely by solenoid.

The velocity-sensing switch arrangement consists of two sheets of aluminum foil separated by a layer of thin plastic. The shorting of the aluminum sheets by the projectile completes a circuit containing a 6-volt dry cell and triggers an electronic timer. Similarly, the timer is stopped by the projectile passing through a switch 3 feet down range. The timer records in units of 10^{-7} sec. which permits high-accuracy velocity determinations.

Nine different rock types have been tested including varieties of sandstone, limestone, granite and specularite-magnetite.

Discussion of Results

Figures 4 to 13 give the penetration vs impact-velocity data for spherical projectiles. A linear relationship exists between penetration and velocity and for most rocks there is an intercept value of velocity, approximately 500 ft/sec., below which no penetration occurs.

Table 1 gives the values of the penetration-velocity slopes (S_{p-v}) obtained from the plots. By varying projectile density and maintaining a constant diameter, as given in Table 1, the effect of projectile weight was isolated. In Figure 14 S_{p-v} is plotted vs the projectile weight on log-log paper for projectiles of equal diameter. The average value of the slope of these lines is 0.815 and all values are within 4% of this. This gives the relationship:

$$S_{p-v} \propto W^{.815} \propto r^{2.45} \qquad \text{Eq. 1}$$

where:

W is the projectile weight

r is the projectile radius.

Another series of tests was conducted using constant projectile density while varying the radius. S_{p-v} is plotted vs projectile radius ou log-log paper for constant projectile density in Figure 15. The average value of the slopes in this case is 1.21, all values being within 7% of this. This gives the relationship:

$$S_{p-v} \propto r^{1.21} \qquad \text{Eq. 2}$$

Inherent in this relationship is the fact that both the weight of the projectile and the radius have been increased. Since the effect of the weight increase is known from the previous relationship, the effect of the radius increase can be deduced as follows:

$$S_{p-v} \propto r^{1.21} \propto r^{2.45}\, r^{x}$$

where x is the exponent proportionality between S_{p-v} and the contact radius

$$x = 1.21 - 2.45 = -1.24$$

$$\therefore S_{p-v} \propto \frac{W^{.815}}{r^{1.24}}$$

FIGURE 2A – Granite block being loaded on saw cart.

FIGURE 2B – Wire saw in operation cutting granite block.

Within the range of experimental error this can be simplified to:

$$S_{p-v} \propto \frac{W^{4/5}}{r^{5/4}}$$

From the data it is also evident that the penetration is directly proportional to the impact velocity and some rock property. This gives the final relationship:

$$S_{p-v} = \frac{P}{V_o - V_f} = K\frac{W^{4/5}}{r^{5/4}} \quad \text{Eq. 3}$$

where: S_{p-v} = penetration-velocity slope (in/ft/sec.)

P = projectile penetration (in.)

V_o = initial projectile velocity (ft/sec.)

V_f = final penetrating velocity (ft/sec.)

W = weight of projectile (grains).

r = radius of contact area (in.) (radius of sphere).

K = rock penetration constant.

For a sphere, equation 3 can be reduced as follows:

$$S_{p-v} = K\frac{(4/3\,\pi\, r^3\, \rho)^{4/5}}{r^{5/4}}$$

where ρ = projectile density – grains/in^3.

Let $K\,(4/3\,\pi)^{4/5} = K'$

Then: $$S_{p-v} = \frac{K' \, r^{2.45} \rho^{.815}}{r^{1.24}}$$

$$S_{p-v} = K' \, r^{6/5} \rho^{4/5}$$

$$S_{p-v} = K' \, r \rho (r/\rho)^{1/5}$$

$$P = K' (V_o - V_f) \, r \rho (r/\rho)^{1/5} \quad \text{Eq. 4}$$

or: $$P = K'' (M/A) (V_0 - V_f) (r/\rho)^{1/5} \quad \text{Eq. 5}$$

the projectile scaling factor $W^{4/5} r^{5/4}$ obtained from equation 3. The slope of this line represents the average value of the rock penetration constant K. Values of K and the projectile scaling factors used are included in Table 1 for all the tests. Figure 16 also includes the value of K obtained from a series of tests with hemispherical-nosed rod-shaped projectiles, as given in Figure 13. Since the value obtained is identical with that for a sphere of the same weight and radius, it appears that projectile length plays no part for rods with length to diameter ratios up to 3. Equation 3 is apparently valid for any shape in this range provided r is known. This is a preliminary conclusion and further tests are being conducted to establish its validity.

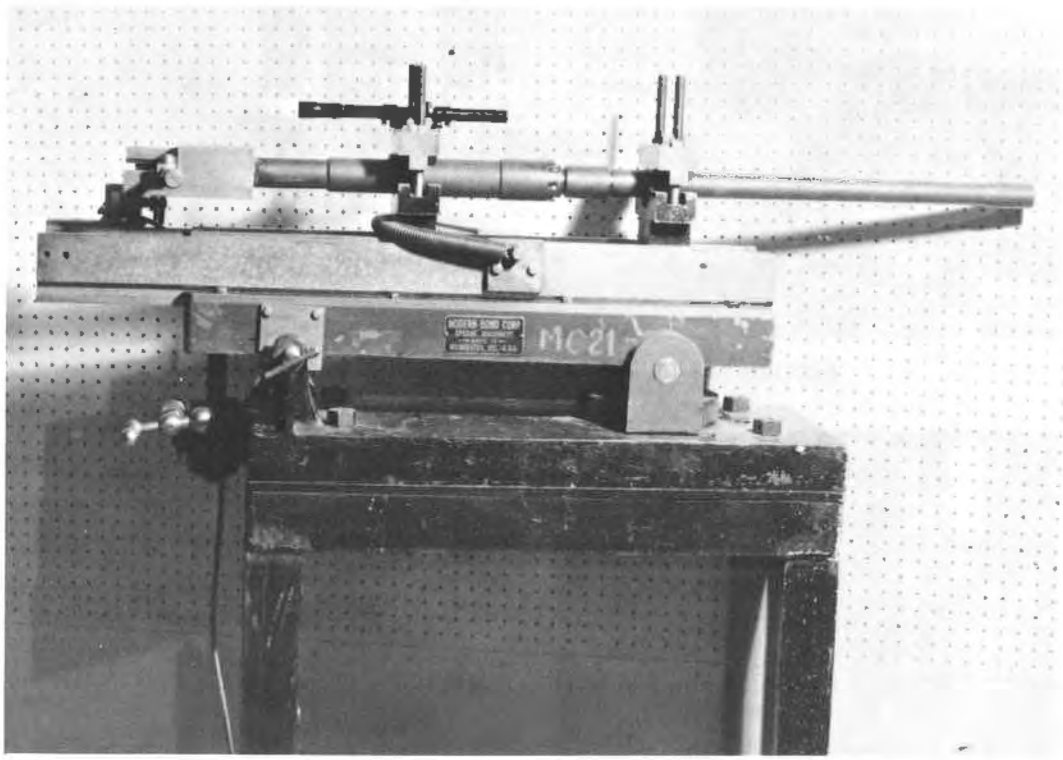

FIGURE 3A — .50-cal. gun — side.

On the basis of similar tests conducted by other workers in this area (1) (2), it was concluded that the penetration of spherical projectiles in rock was proportional to the impact momentum. Their final equation was identical to equation 5 except that the term $(r/\rho)^{1/5}$ was omitted. The addition of this term changes the result significantly and is necessary to accurately predict the effect of changes in projectile density or radius.

In Figure 16, S_{p-v} for five spherical projectile types in Disraeli light granite is plotted vs

Results of a series of tests using .50 cal. armour-piercing projectiles is presented in Figure 17. These projectiles being streamlined (pointed) allow the effect of shape to be studied. The weight of these projectiles is 542 grains and their diameter at the largest section is 0.45 in. The value of S_{p-v} obtained can be com-

Abstract

By measuring closure over a period of six years in different stoping areas in a vertical tabular orebody, several parameters which influence closure have been defined. A number of these parameters have been evaluated, permitting the prediction of closure in most stoping situations. Closure values can be used to predict potential bad-ground conditions, enabling corrective measures to be planned before ground-control problems actually arise.

Closure Studies Improve Ground Control at Falconbridge Mine

K.R. Notley,
Research Engineer, Mine Research Department,
Falconbridge Nickel Mines, Limited,
Falconbridge, Ont.

Introduction

A closure study program was initiated at Falconbridge Mine in 1962 to obtain a better understanding of ground movement and fracture-zone extent under different geometric conditions which are common in the mine.

The orebody, which has been described in detail elsewhere (1), is essentially a near vertical sulphide zone which varies in width from a few inches to over a hundred feet. It extends about a mile east-west on strike and is more than a mile in depth. The footwall rock to the north is norite and the hanging wall is greenstone. In some areas the greenstone has been extensively silicified to a strong quartzite locally known as "jasperoid".

The level interval is 175 ft with the main 8 x 9 ft drifts driven in ore. The principal mining method is longitudinal flat-back cut-and-fill stoping using hydraulic fill and rockbolts for support. Individual stopes are 200 to 350 ft long and are sequenced in three-level blocks to provide adequate production and minimize the number of stope crown or level pillars occurring under mined-out stopes.

Measurements

Closure measurements were first made at Falconbridge Mine between September 1962 and May 1964, on the 3850 level above 4002 27-31 stope. Results of this study indicated that closure measurements, when studied in relation to the mining rate of the ore block under observation, could be useful in yielding data on dynamic behaviour of ground (2). It was decided to instrument further areas for closure studies. These areas were selected on the basis of their geometrical relationship with mined-out stopes.

Case 1, 2975 Level, Above 3102 40-42 Stope (Figure 1) – This stope had solid ground above and at both ends. Closure-measuring plugs were established, in October 1963, at depths of 2 ft and 7 1/2 ft, in each wall at five points on the level above the stope when the back of the stope was some 60 ft below track. Mining in this stope was completed by September 1965, and the last measurements were made in January 1966.

Case 2, 2975 Level, Above 3102 73-79 Stope (Figure 2) – This stope had solid ground above and below, and mined-out areas at each end. Nine closure stations were established on the level above 3102 73-79 stope, two above the mined-out area to the west, and one farther west still, in the undisturbed area.

The instrumentation was installed in December 1963, when the stope back was 95 ft below the 2975 level. Mining in the western half of the stope was suspended at the end of March 1965 at 30 ft below track, and by March 1966, the eastern half had been completely mined out.

Each closure station consisted of two rockbolts anchored at a depth of 7 1/2 ft in colinear horizontal holes about 4 ft above track on opposite sides of the drift. The bolts were supported at the hole collars to permit axial

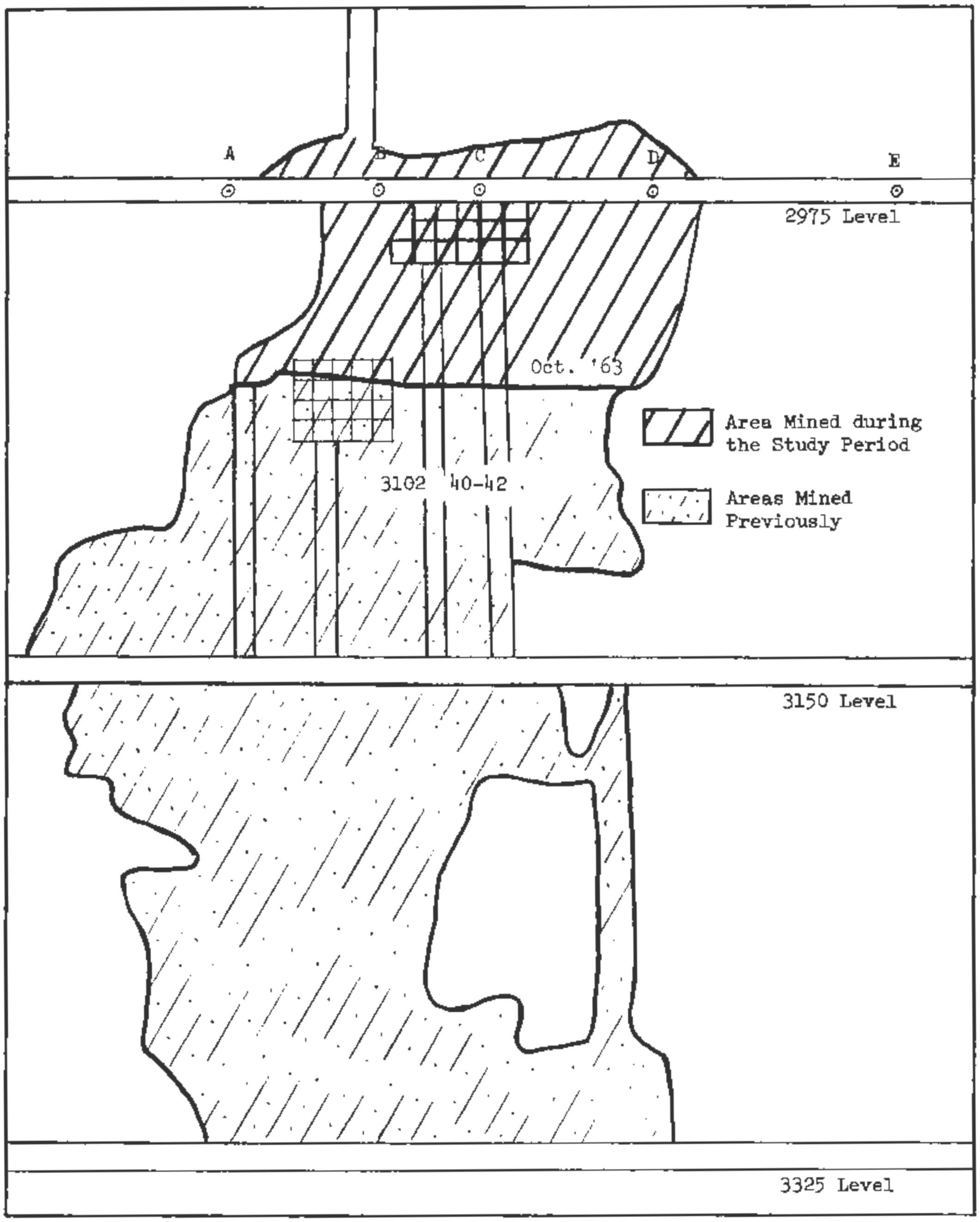

FIGURE 1—Location of closure stations above 3102 40-42 stope.

movement. Closure was measured by means of a turnbuckle micrometer connected by wires to spads welded to the protruding ends of the bolts. Within 6 in. of each hole collar, a surface reference plug was cemented into a hole 6 in. deep. By measuring from each spad on one side of the drift to both spads on the other side (4 measurements) we were able to determine closure at the wall surface, closure between points $7\frac{1}{2}$ ft deep in each wall, and expansion or contraction of each wall to a depth of 7 1/2 ft (Figure 3).

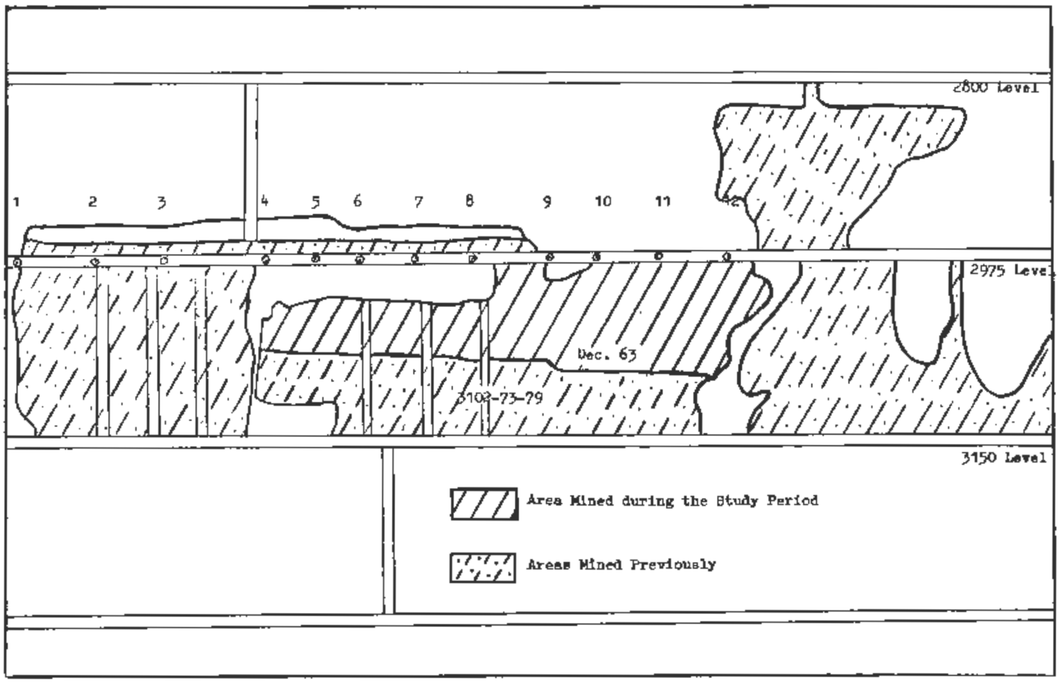

FIGURE 2—Location of closure stations above 3102 73-79 stope.

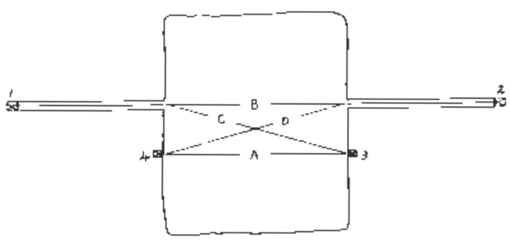

FIGURE 3 – Closure and wall movement measurements.

In Figure 3; 1, 2, 3, 4 are the anchor points of the four closure plugs, and A, B, C and D represent the 4 measurements made at each station. If a, b, c and d are the total changes in A, B, C and D respectively since the initial measurement, the movements are calculated as follows:

Closure between 3 and 4 = a
Closure between 1 and 2 = b
North wall movement between 1 and 4 = $\frac{1}{2}$ (a-c + d-b)
South wall movement between 2 and 3 = $\frac{1}{2}$ (a-d + c-b)

In practice, 3 and 4 are placed as close as possible to the collars of the deeper holes to minimizes errors due to angularity of C and D. The method of calculating wall movement also minimize errors provided the directions of A and B are parallel.

Case 3, 3675 and 3850 Levels, Above and Below 3802 28-31 Stope (Figure 4) – This stope was an island pillar completely surrounded by mined-out areas. The level above the stope was instrumented for closure and extensometer measurements in January 1966. At that time a Potts' extensometer was obtained which permitted direct measurement of relative wall movement at different depths in a single bore-hole.

Six stations were established above 3802 28-31 stope with anchors at depths of 10 and 20 ft in each wall. Closure between the walls was measured from spads attached to the collars of the extensometer holes on opposite sides of the drift.

In May 1966, a similar pattern of instrumentation was installed on the 3850 level below the stope.

Parameters Affecting Closure

In general, closure measurements are made at the end of each month and a graph of closure plotted against time is kept up to date for each station. Longitudinal sections showing the area

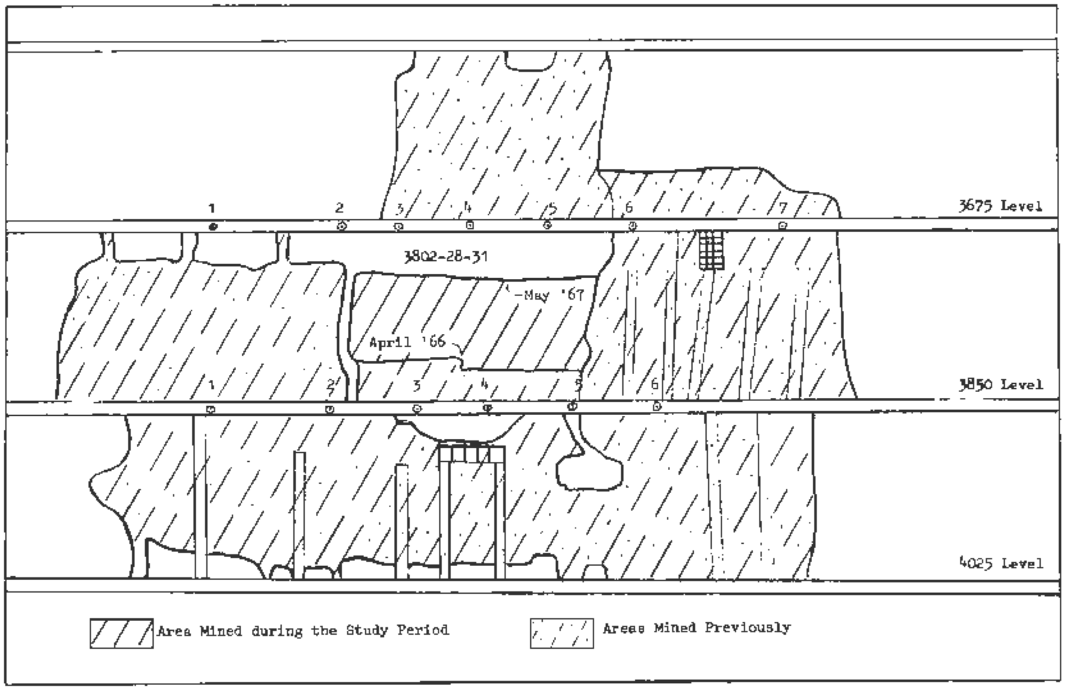

FIGURE 4—Location of closure stations above and below 3802 28-31 stope.

of ground broken in each stope and the area filled between consecutive measuring periods are prepared each month.

It became evident early in the program of study that the closure rate at a particular station above a stope increased when the mining face passed beneath it, and decreased as mining activity moved farther away. As was expected, it was also observed that the closure was greatest above the centre of the stope, and that the closure rate was fairly low and uniform a short distance beyond the stope limits.

For the type of geometry common in the Falconbridge mine it is assumed that the degree of closure is governed by the following parameters.

a. The area of ground broken in the plane of the orebody and its distance from the closure point.

b. The width and height of the opening in which closure is measured, and the height above track and the depth in the walls at which the measuring points are anchored.

c. The physical properties of the wall rocks and the ore, and the inherent stress field.

d. The area and relative position of mined-out stopes in the vicinity and the support factor afforded by the backfill medium.

Analysis of the Effects of the Parameters

1. The Effect of Mining

In the case of closure between the walls of a drift above an active stope, it is apparent from closure measurements, and also reasonable to expect, that the larger the area of ground mined, the greater the amount of closure that will take place. Similarly, the closer the mining activity approaches the measuring station, the greater will be the effect on closure. With these points in mind an inverse square relationship was postulated, which assumes that the effect produced at a closure-measuring station in a drift above a stope is proportional to the area of the excavation in the plane of the orebody, and inversely proportional to the square of the effective distance of the excavation from the closure station. This closure effect due to mining is termed the "excavation factor" and is derived as follows (Figure 5).

In Figure 5, O represents the position of the closure station, and ABCD is the area of ground excavated in a given period. The excavation extends from x_1 to x_2 in length, and is of constant height h at an average distance of y below the closure station along the dip of the orebody.

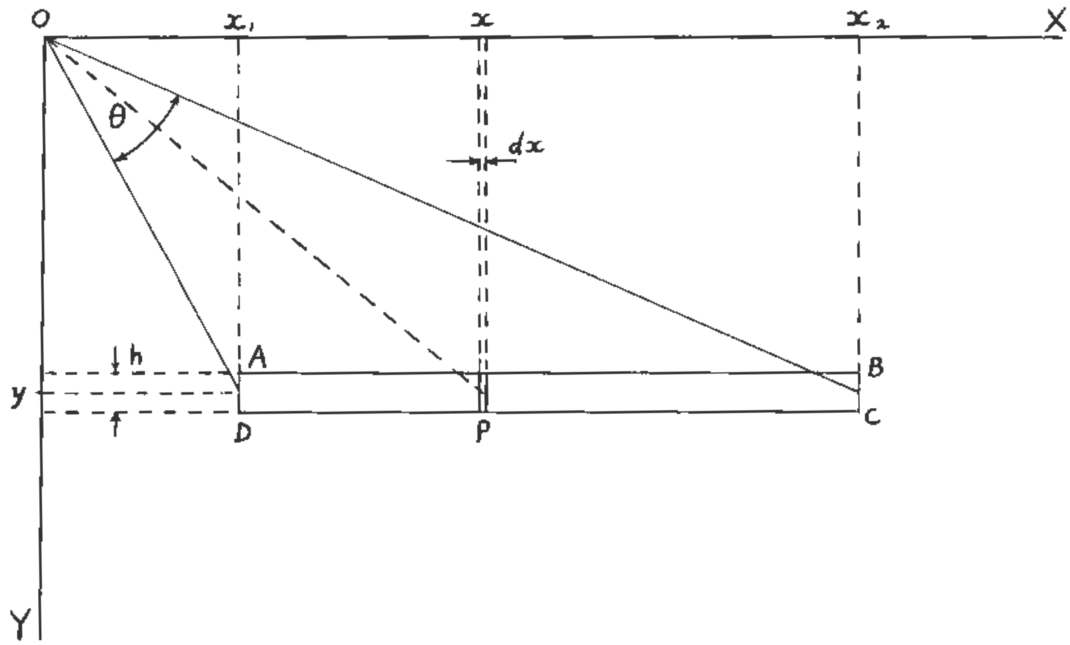

FIGURE 5—Derivation of the excavation factor.

Consider a small element P of the excavation, of height h and length dx, at a horizontal distance x from O.

According to the postulate, the effect of the element P at O is given by

$$\frac{h \cdot dx}{x^2 + y^2}$$

Therefore, the effect of the area ABCD at O is:

$$Fx = \int_{x_1}^{x_2} \frac{h \cdot dx}{x^2 + y^2}$$

$$= \frac{h}{y} \left[\tan^{-1} \frac{x}{y} \right]_{x_1}^{x_2}$$

$$= \frac{h}{y} \left[\tan^{-1} \frac{x_2}{y} - \tan^{-1} \frac{x_1}{y} \right]$$

$$\therefore Fx = \frac{h\theta}{y} \qquad \text{Eq. 1}$$

where θ is the angle subtended at the closure station by the extremities of the excavation. This treatment is sufficiently accurate where the height of the excavation is small in relation to its length and depth below the level. Excavation factors can be calculated for each cut mined, and added together to give the overall effect of mining the whole stope. To calculate the effect of a whole stope in a single operation, however, requires a more rigorous analysis.

Consider the excavation factor at a point above one end of the stoping block (Figure 6).

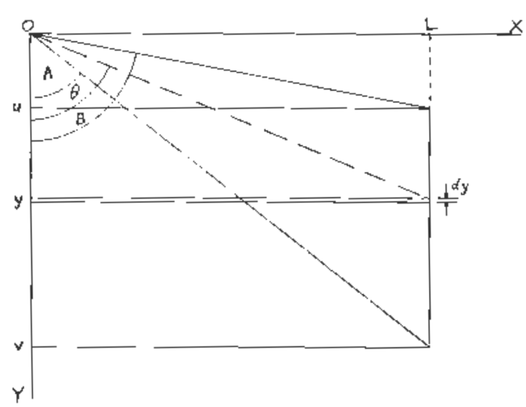

FIGURE 6—Excavation factor for a whole stoping block.

The second component is the buckling component (Cb). This is the closure effect caused by bending of the walls into the opening. Analysis here is more difficult, as in our experience at Falconbridge, fracturing of the walls occurs at an early stage. The beginning of wall failure and the extent of failure depend on the physical properties of the wall rocks and the height of the opening in which closure is measured.

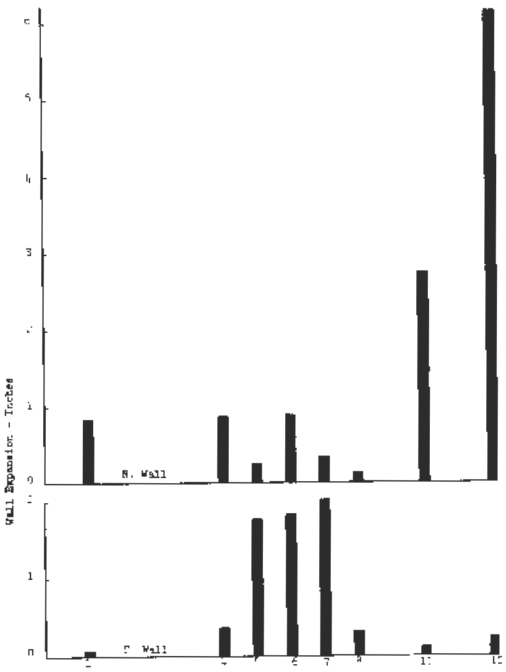

FIGURE 9—Relative wall expansion above 3102 73-79 stope.

Wall movement measurements above 3102 73-79 stope illustrate the effects of these parameters (Figure 9). At stations 29-1, -10 and -12, the north wall expanded much more than the south wall. At stations -5, -6 and -7 however, the south wall movement exceeded that of the north wall. Stations -5, -6 and -7 are in the area where backs had been taken down above the level, making the effective vertical span of the wall some 30 ft. Stations -1, -10 and -12 however, were in raw drift areas where the height of the walls was only 9 ft.

Physical properties of the wall rocks are shown in Table 1.

Table I Physical Properties of Wall Rocks Above 3102 73-79 Stope

	North Wall	South Wall
Rock type	Norite	siliceous greenstone
Young's modulus	10.5×10^6	13.5×10^6 psi
Uniaxial compressive strength	25×10^3 psi	44×10^3 psi
Strain energy content at failure	28 in.lb./cu.in.	78 in.lb./cu.in.
Failure	nonviolent	semi-violent to violent

At stations -1, -10 and -12, the wall pressure applied sufficient bending moment to the 9-ft span of norite to cause failure with consequent high expansion in the wall, since the measurements included the effects of crack opening. The greenstone in the south wall was strong enough to withstand the same bending moment, however, and did not fail. Thus, there was very little expansion measured in the south wall.

At stations -5, -6, and -7, a similar pressure was applied over a 30-ft span and the bending moment was sufficiently high to cause failure of the greenstone as well as the norite. However, the greenstone, having the capacity to store more strain energy, dissipated more energy at failure, and this caused the larger expansions in the south wall as measured in this area.

The buckling component of closure thus depends on the moduli of elasticity of the wall rocks, the moduli of rigidity, the strength of the wall rocks, the height of the opening, the height above track of the closure station, the depth of the closure plugs in the walls and the three-dimensional stress field. Add to this the effect of reinforcement such as rockbolts, tensioned or untensioned grouted bolts, and the mechanism becomes very complex. However, it has been observed at most of the closure stations studied, that the closure is directly proportional to the excavation factor or to some power of the excavation factor. When the excavation factor for a particular station is plotted against the measured closure on logarithmic graph paper, all the points fall generally on a straight line. This is found to be true for the different cases of stope geometry studied, the only difference being in the slope of the lines and their positions relative to the axes of

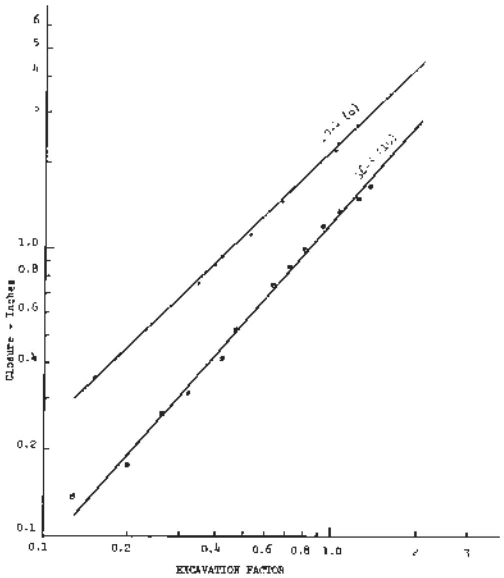

FIGURE 10—Logarithmic plot of closure against excavation factor for stations 29-4 (0) and 36-5 (10).

the graph (Figure 10). Thus, the closure at any one station can be expressed as:

$$\text{closure (inches)} = a\,Fx^{b} \qquad \text{Eq. 5}$$

where Fx is the excavation factor at any stage of mining, and 'a' and 'b' are constants depending on the stope geometry, the position of the closure station and the physical properties of the ore, the wall rocks and the fill in neighbouring mined-out areas.

The IBM 1130 computer was used to calculate least squares estimates of 'a' and 'b' and a correlation coefficient for each set of measurements above 2902 73-79 stope, and above 3602 28-31 stope. Averages for stations in similar geometrical conditions were treated in the same way.

The averages taken were as follows:

Stations 29-1, -2, -3 and -4 – Here the closure was measured beyond the limit of 3102 73-79 stope and above an adjacent mined-out stope (Figure 2).

Stations 29-4, -5, -6, -7 and -8 – These stations were above 3102 73-79 stope, and in the area of drift where two cuts had been mined from the stope above, giving an effective drift height of 30 ft. Mining in this part of 3102 73-79 stope was stopped at 30 ft below track.

Stations 29-10, -11 and -12 – These stations were in a raw drift area above the part of 3102 73-79 stope which was mined right through to the level.

Stations 36-2, -3, -4 and -5 – These stations were located above 3802 28-31 stope with mined-out areas above and at each end (Figure 4).

The values of 'a' and 'b' and the correlation coefficient 'c' for each station or average are shown in Table 2.

Table 2 Relationship Between Closure and Excavation Factor
Closure = a (excavation factor)^{b}.
c = correlation coefficient

STATION	a	b	c
29- 1 (0)	39.3	1.87	0.976
" - 2 (0)	2.42	0.85	0.973
" - 3 (0)	3.37	1.22	0.988
" - 4 (0)	2.30	0.97	0.996
" - 5 (0)	3.21	0.92	0.985
" - 6 (0)	2.11	0.98	0.994
" - 7 (0)	2.59	0.92	0.994
" - 8 (0)	2.24	0.67	0.986
" -10 (0)	1.56	1.16	0.985
" -11 (0)	2.11	1.07	0.995
" -12 (0)	3.58	1.79	0.990
" - 1 (7½)	0.77	0.71	0.958
" - 4 (7½)	1.35	0.86	0.992
" - 5 (7½)	1.31	0.66	0.985
" - 6 (7½)	0.94	0.63	0.992
" - 7 (7½)	1.78	0.79	0.996
" - 8 (7½)	2.17	0.64	0.993
" -10 (7½)	0.54	0.97	0.987
" -11 (7½)	0.52	0.94	0.993
" -12 (7½)	0.67	0.96	0.993
" - 1,-2,-3,-4 (0)*	2.67	0.99	0.990
" - 4,-5,-6,-7,-8 (0)*	2.41	0.87	0.992
" -10,-11,-12 (0)*	2.25	1.20	0.993
" - 4,-5,-6,-7,-8 (7½)*	0.54	0.72	0.995
" -10,-11,-12 (7½)*	0.58	0.98	0.992
36-3 (0)	2.09	1.54	0.997
" -5 (0)-A**	1.82	0.97	0.994
" -5 (0)-B**	2.61	1.50	1.000
" -2 (10)	0.96	1.71	0.977
" -3)10)	0.95	1.66	0.994
" -4 (10)	0.99	1.36	0.995
" -5 (10)	1.21	1.11	0.996
" -3,-5 (0)*	1.66	1.31	0.995
" -2,-3,-4,-5 (10)*	1.09	1.26	0.996

Figures in parentheses are the depths of the closure plugs in the walls (in feet).
*Averages of the stations indicated.
**The data for Station 36-5 (0) was divided into two parts, as the original plot showed two definite straight line portions.

Our ultimate objective is to set up an empirical relationship obtained by numerical analysis which will permit calculation of closure from the excavation factor modified according to the conditions in a given area.

This paper has only dealt with closure on the level above an active stope. As mentioned previously we are also measuring closure on the level below. To correlate mining activity with closure here, we have postulated that closure here is also proportional to the area mined and inversely proportional to the effective distance of the excavation from the closure station. Preliminary investigations show good correlation, but we do not yet have sufficient data for a thorough analysis.

3. The Effect of Neighbouring Mined-out Stopes

Mined-out and filled stopes at the ends of the block have the effect of increasing the effective stope length. This may be regarded as an increase in θ in the excavation factor. Since the increase in θ would be proportionately larger toward the end of the stope next to the filled area, we have the effect of closure being a larger multiple of the excavation factor toward that end.

Where the ground above the level has been mined out, the walls of the drift will already be in a fractured state, and the effect on closure will be that of an increased drift height.

Again, actual calculation of these effects is complicated by the interaction of a number of unknown factors, and our approach has been to evaluate the collective influence of these factors according to their effect on the relationship between measured closure and excavation factor.

So far, we have studied a stope in an unmined area, a stope flanked by mined-out areas, and a stope completely surrounded by mined-out areas. A closure study is currently being conducted in a stope with solid ground at each end and mined-out areas above and below. In addition to closure and extensometer measurements on the levels above and below this stope, we are also making measurements in the manways which are carried up through the fill as mining progresses.

To study the support characteristics of the fill material, half of this stope is being filled with cement-consolidated tailings fill, and the other half with straight tailings fill. Data from this study are not included in this paper, as mining has not yet progressed very far.

Applications in Ground Control

1. Consider mining a block of ore in virgin ground such as 3102 40-42 stope, referred to earlier. As mining progresses up-dip, additional stress is transferred to the unmined portion of the block and also onto the solid rock beyond the stope boundaries. There is thus a strain energy increase in the rock; it is greatest close to the stope back and decreases with distance from the mining activity. Eventually the crown pillar between the stope back and the drift above will start to fail. At this stage more of the stress increase due to mining and part of the strain energy in the pillar will be transferred to the surrounding rock which is still capable of further elastic deformation. Thus the pillar will fail gradually and ground control difficulties will be minimal.

During the stage of pillar failure however, the walls and back of the drift above are subjected to the greatest stress changes due to the drift opening acting as a stress concentrator. Excessive drift maintenance is required due to spalling of the walls and back. In the past, it was often necessary to rebolt the entire drift above a stope, and if this was done too soon, further spalling around the collars of the bolt-holes sometimes necessitated a second re-bolting operation.

The answer to this problem lay in the use of grouted bolts which retain their reinforcing characteristics even if surface spalling does occur (3).

Precalculated closure values can be used to design the length and spacing of the bolts and the time when they should be installed.

2. Where an active stope is coming up under a filled stope, the stress concentration builds up more rapidly on the pillar as this has a much higher modulus of elasticity than the fill, and hence receives a greater share of the induced stress increase. As well as this, the pillar will already be carrying extra stress induced at the time the stope above was mined.

In this situation the pillar will reach the failure stage more quickly, and, having reached that stage, will fail more rapidly. Failure will also be more extensive in this case, as even in its initially fractured condition, the pillar will still have a greater effective modulus of deformation than the fill, and will continue to transmit stress.

Generally, the walls fail along with the ore in the pillar, and it is necessary to convert to square setting when excessive fracturing starts. In some parts of the mine mentioned previously however, the south wall greenstone is highly silicified and is very strong. When mining pillars in these areas, the south wall does not fail readily and very high stresses are built up, often resulting in rockbursts. These rockbursts usually occur at depth in the wall and do not often result in damage to the openings. In the later stages of pillar mining however, the concussion from these bursts can result in falls of ground in the stopes, and the sound of the bursts has a demoralizing effect on the crews.

In one such case, 3802 28-31 stope, we were able to use closure data to predict bursting conditions if failure of the south wall did not occur by the time the stope had advanced to within 60 ft of the level above.

The stope progressed beyond that stage without failure of the south wall, and several rockbursts did in fact occur. It was decided to induce failure of the wall by means of a destressing blast, and this operation was successfully carried out (4).

3. Another application previously reported in the literature (4) is in the modification of timbered gangway design. Since the drifts are driven in the ore zone, a timbered gangway must be installed for each stope as it is started. This gangway has to withstand the closure caused by mining the stope above the level, and also movement caused by future mining below the level if the block below has not been mined previously. It has been recognized that the gangway timber cannot be made strong enough to prevent closure, so the caps are designed with yielding features which serve to maintain the structural integrity of the sets while permitting closure of the walls. Pre-calculation of closure and relative wall movement can be used to determine how much yielding capacity should be allowed on each side of the drift.

Summary

Horizontal closure measurements have led to a better understanding of rock behaviour, including extent of fracture zones, under the influence of mining. The effect of mining activity on closure in the drift above a stope can be pre-calculated from the stope dimensions by means of the excavation factor theory which assumes that closure is proportional to the area mined and inversely proportional to the square of the distance between the excavation and the reference points. The excavation factor (Fx) can be modified according to the expression: closure = a Fx^b where 'a' and 'b' are constants depending on the physical properties of the rocks and the relative size and location of neighbouring mined-out areas.

Actual and estimated closure data can be used to help determine drift support requirements, the amount of yielding capacity to be incorporated into the design of gangway sets, and possibly the rigidity of fill support required in order to minimize stope crown pillar failure.

Acknowledgment

Thanks is expressed to the management of Falconbridge Nickel Mines, Limited, for permission to publish this paper, and to the staff of the Falconbridge Mine Research Department for their assistance in the compilation and analysis of the data.

References

1. The Falconbridge story, *Can. Mining J.*, Vol. 80, June 1959.
2. Moruzi, G.A. and Pasieka, A.R., 1964. Evaluation of a blasting technique for destressing ground subject ro rockbursting. *Proc. 6th Symp. Rock Mech.*, U. of Missouri, Rolla, Mo., Oct. 1964.
3. Ground control and fragmentation at Falconbridge nickel mines, Sudbury operations, *Can. Mining J.*, Vol. 89, March.
4. Slade, A.G., 1968. Some practical applications of rock mechanics in the underground operations of F.N.M. Ltd. – Sudbury operations. *Bull. Can. Inst. Mining Met.*, Vol. 61, No. 678, Oct.

K.R. Notley

Education – ACSM, Camborne School of Metalliferous Mining, 1961.

Employment Summary – Falconbridge Nickel Mines Limited as graduate engineer and mine research engineer.

List of Registrants

Abel, J.J.,
Ryerson Polytechnical Institute,
50 Gould St.,
Toronto 2, Ont.

Adams, J.I.,
Ontario Hydro,
620 University Ave.,
Toronto 2, Ont.

Anderson, I.H.,
Department of Agriculture,
Government of Alberta,
Edmonton, Alta.

Andrew, T.J.G.,
MacLaren, James F.,
321 Bloor St. E.,
Toronto 5, Ont.

Arbour, R.,
Demers, Lemieux & Roy,
Place du Canada,
Montreal 3, Que.

Archambault, G.,
École Polytechnique,
Mining Engineering Department,
C.P. 501, Snowdon,
Montreal 29, Que.

Attewell, P.B.,
University of Durham,
Durham, England.

Babar, N.Y.,
53 Elm Ave.,
Toronto 5, Ont.

Barla, G.,
Henry Krumb School of Mines,
Columbia University,
New York, N.Y., 10027,
U.S.A.

Barron, K.,
Department of Energy, Mines &
Resources,
Mining Research Centre,
555 Booth St.,
Ottawa 1, Ont.

Bauer, G.E.,
University of Ottawa,
Department of Civil Engineering,
Ottawa 2, Ont.

Beck, A.E.,
Department of Geophysics,
University of Western Ontario,
London, Ont.

Belshaw, D.J.,
Peto Associates Limited,
1287 Caledonia Rd.,
Toronto 19, Ont.

Benson, R.,
H.G. Acres Company Limited,
1259 Dorchester Rd.,
Niagara Falls, Ont.

Bettiol, E.I.,
Ecstall Mining Limited,
Box 2002,
Timmins, Ont.

Bielenstein, H.,
Department of Energy, Mines &
Resources,
Elliot Lake Laboratory,
Box 100,
Elliot Lake, Ont.

Bird, S.J.G.,
University of Toronto,
Room 330,
Galbraith Building,
Toronto 5, Ont.

Bladon, L.W.,
Bell Asbestos Mines,
Box 727,
Thetford Mines, Que.

Boghdadi, C.,
Department of Mechanical
Engineering,
University of Toronto,
Toronto 5, Ont.

Blair, P.,
Department of Mining Engineering
and Applied Geophysics,
McGill University,
Montreal, Que.

Botteron, G.,
Demers, Lemieux & Roy,
Place du Canada,
Montreal 3, Que.

Brawner, C.O.,
Golder, Brawner & Associates
Limited,
224 W 8th Ave.,
Vancouver 10, B.C.

Bray, R.C.E.,
Noranda Mines Limited,
Geco Division,
Box 37,
Manitouwadge, Ont.

Bray, W.T.,
Canadian Refractories Limited,
Kilmar, Que.

Broadbent, C.D.,
Kennecott Copper Corporation,
1515 Mineral Square,
Salt Lake City, Utah,
USA

Bromley, P.H.,
Lockwood, Kessler & Bartlett,
Incorporated,
One Aerial Way,
Syosset, Long Island, N.Y., 11791,
USA

Brook, N.
Department of Applied Mineral
Sciences,
The University,
Leeds 2, Yorkshire,
England.

Brooker, E.W.,
Ripley, Klohn Leonoff &
Brooker Limited,
6035-103 St.,
Edmonton, Alta.

Brown, J.W.,
University of Missouri,
Rock Mechanics and Explosives
Research Center,
Rolla, Mo., 65401,
USA

Bullock, W.D.,
Iron Ore Company,
Box 1004,
Schefferville, Que.

Cain, P.M.,
Heath Steele Mines Limited,
Newcastle, N.B.

Calder, P.N.,
Department of Mining Engineering,
Queen's University,
Kingston, Ont.

Cary, A.S.,
Shannon & Wilson,
1105-38th St.,
Seattle, Wash, 98103,
USA

Chan, H.T.,
University of Toronto,
Department of Civil Engineering,
Galbraith Building,
Toronto 5, Ont.

Chan, S.S.M.,
University of Idaho,
Department of Mining Engineering
& Metallurgy,
College of Mines,
Moscow, Idaho, 83843,
USA

Chatterjee, A.K.,
Johns-Manville Mining &
Trading Limited,
Box 2003,
Timmins, Ont.

Chen, J.J.,
H.G. Acres Company Limited,
1259 Dorchester Rd.,
Niagara Falls, Ont.

Cheng, K.L.,
1001 Main St. W.,
Apt. 417,
Hamilton, Ont.

Chrzanowski, A.,
University of New Brunswick,
Department of Surveying,
Fredericton, N.B.

Chyrowski, B.,
Duval Corporation of Canada
Limited,
Box 1320,
Saskatoon, Sask.

Chugh, Y.P.,
Department of Mining,
Pennsylvania State University,
Room No. 2, M. I. Building,
University Park, Pa., 16802,
USA

Chung, S.H.,
Applied Research Group,
Explosives Division,
Canadian Industries Limited,
McMasterville, Que.

Coates, D.F.,
Department of Energy, Mines &
Resources,
Mining Research Centre,
555 Booth St.,
Ottawa 1, Ont.

Cochrane, T.S.,
Department of Energy, Mines &
Resources,
Elliot Lake Laboratory,
Box 100,
Elliot Lake, Ont.

Code, J.,
H.G. Acres Company Limited,
1259 Dorchester Rd.,
Niagara Falls, Ont.

Comeau, W.,
Hydro-Québec,
15th Floor,
Stock Exchange Building,
Victoria Square,
Montreal 3, Que.

Conlon, R.J.,
H.G. Acres & Company Limited,
1259 Dorchester Rd.,
Niagara Falls, Ont.

Corlett, A.V.,
Mining Engineer Consultant,
428 Earl St.,
Kingston, Ont.

Cox, H.H.,
1506-44 King St. W.,
Toronto 1, Ont.

Crawford, C.B.,
National Research Council,
Division of Building Research,
Ottawa, Ont.

Crepeau, P.M.,
Hydro-Québec,
15th Floor,
Stock Exchange Building,
Victoria Square,
Montreal, Que.

Coulombe, B.,
Department of Mining Engineering,
Queen's University,
Kingston, Ont.

Cross, P.S.,
Mogul Mines,
25 Adelaide St. W.,
Toronto, Ont.

Currie, J.B.,
Department of Geology,
University of Toronto,
Toronto 5, Ont.

Davis, H.F.,
Ontario Department of Mines,
Whitney Block,
Parliament Buildings,
Toronto, Ont.

Day, R.A.,
Ontario Hydro,
620 University Ave.,
Toronto 2, Ont.

DeLorimier, A.,
Williams Form Hardware &
Rock Bolt (Canada) Limited,
10351-72nd Ave.,
Edmonton, Alta.

DeLory, F.A.,
Department of Civil Engineering,
University of Toronto,
Toronto 5, Ont.

DeWit, C.,
Warnock Hersey International Ltd.,
250 Madison Ave.,
Toronto 7, Ont.

Dhar, B.,
Mining Department,
McGill University,
Montreal, Que.

Dickhout, M.H.,
International Nickel Company
of Canada Limited,
Copper Cliff, Ont.

Dodds-Hebron, R.,
Bell Asbestos Mines,
Thetford Mines, Que.

Drury, J.J.,
Jones & Laughlin Mining Company,
Box 547,
Kirkland Lake, Ont.

Dubnie, A.,
Department of Energy, Mines &
Resources,
Mining Research Centre,
555 Booth St.,
Ottawa, Ont.

Dudek, F.A.,
Churchill Falls (Labrador)
Corporation Limited,
One Westmount Square,
Montreal 216, Que.

Easterbrook, P.L.,
1236 Mona Road,
Port Credit, Ont.

Eikhoff, W.,
Williams Form Engineering
Corporation,
1501 Madison Ave. SE,
Grand Rapids, Mich.,
USA

Eiler, Z.,
Ontario Hydro,
620 University Ave.,
Toronto 2, Ont.

Everell, M.D.,
École Polytechnique,
C.P. 501, Snowdon,
Montreal 29, Que.

Fairbairn, J.B.,
International Minerals &
Chemical (Canada) Corporation,
Esterhazy Operations,
Esterhazy, Sask.

Favreau, R.F.,
Canadian Industries Limited,
Beloeil, Que.

Fell, F.A.,
Dickenson Mines Limited,
416-25 Adelaide St. W.,
Toronto 1, Ont.

Folinsbee, J.C.,
Sherritt Gordon Mines Limited,
Lynn Lake, Man.

Ford, G.,
Williams Form Engineering
Corporation,
1501 Madison Ave. SE,
Grand Rapids, Mich.,
USA

Ford, R.E.,
Gaspé Copper Mines Limited,
Box 774,
Murdochville, Que.

Forrester, G.N.,
Steel Company of Canada,
525 Dominion St.,
Montreal, Que.

Frame, C.H.,
Denison Mines Limited,
Box 2600,
Elliot Lake, Ont.

Freeman, C.F.,
Peto Associates Limited,
1287 Caledonia Rd.,
Toronto 19, Ont.

Friesen, M.,
International Nickel Company of
Canada Limited,
Box 416,
Levack, Ont.

Gagnon, H.,
Bell Asbestos Mines,
Thetford Mines, Que.

Geller, L.,
Department of Energy, Mines &
Resources,
Mining Research Centre,
555 Booth Street,
Ottawa, Ont.

Gilchrist, G.,
Ripley Klohn Leonoff &
Brooker Limited,
6035-103 St.,
Edmonton, Alta.

Godfrey, G.E.,
Department of Mechanical
Engineering,
University of Toronto,
Toronto 5, Ont.

Golder, H.Q.,
Golder Associates Limited,
3151 Wharton Way,
Cooksville, Ont.

Gorman, G.A.,
Ontario Hydro,
Operations Division,
620 University Ave.,
Toronto 2, Ont.

Grant, H.G.,
Canadian Refractories Limited,
Kilmar, Que.

Graves, A.C.,
Shawinigan Engineering Company,
620 Dorchester St. W.,
Montreal, Que.

Gray, W.M.,
Department of Energy, Mines &
Resources,
Mining Research Centre,
555 Booth St.,
Ottawa 1, Ont.

Greenshields, J.,
Williams Form Hardware &
Rock Bolt (Canada) Limited,
146 Mount Olive Dr.,
Rexdale, Ont.
Gung, G.,
Ontario Hydro,
620 University Ave.,
Toronto 2, Ont.

Gyenge, M.,
Department of Energy, Mines &
Resources,
Mining Research Centre,
555 Booth St.,
Ottawa 1, Ont.

Haflidson, R.S.,
348 Fraser St.,
North Bay, Ont.

Haimson, B.,
Haliburton,
Duncan, Okla.
USA

Hardy, H.R.,
Department of Mining Engineering,
Pennsylvania State University,
University Park, Pa., 16801,
USA

Hastie, L.,
2932 Yonge St.,
Apartment 305,
Toronto, Ont.

Hedley, D.G.F.,
Department of Energy, Mines &
Resources,
Elliot Lake Laboratory,
Box 100,
Elliot Lake, Ont.

Heins, R.W.,
University of Wisconsin,
1509 University Ave.,
Madison, Wis., 53706,
USA

Herget, G.,
Department of Energy, Mines &
Resources,
Elliot Lake Laboratory,
Box 100,
Elliot Lake, Ont.

Hewer, W.A.M.,
Department of Chemical Engineering,
University of Toronto,
Toronto 5, Ont.

Hodgson, S.B.,
Falconbridge Nickel Mines
Limited,
Nickel Division, Sudbury
Operations,
Falconbridge, Ont.

Hogg, A.D.,
Ontario Hydro,
620 University Ave.,
Toronto 2, Ont.

Holubec, I.,
Department of Civil Engineering,
University of Waterloo,
Waterloo, Ont.

Horn, W.R.,
The Mining Association of Canada,
Suite 1403, 372 Bay St.,
Toronto 1, Ont.

Hoyaux, B.,
École Polytechnique,
Department of Mining Engineering,
University of Montreal,
Montreal 25, Que.

Hughes, J.M.,
Ontario Department of Mines,
Parliament Building,
Toronto, Ont.

Imrie, A.S.,
International Power &
Engineering Consultants Limited,
570 Dunsmuir St.,
Vancouver 2, B.C.

Isherwood, B.,
Franki Canada Limited,
105 Nantucket Boulevard,
Scarborough, Ont.

Johannes, P.,
Potash Company of America,
Box 509,
Saskatoon, Sask.

Johnston, C.,
Williams Form Hardware &
Rock Bolt (Canada) Limited,
10351-72nd Ave.,
Edmonton, Alta.

Kawgas, M.,
Sudbury Mining Contractors
Limited,
Box 1045,
Sudbury, Ont.

Keefer, T.C.,
Association of Professional
Engineers of Ontario,
236 Avenue Rd.,
Toronto 5, Ont.

Kenney, T.C.,
Department of Civil Engineering,
University of Toronto,
Toronto 5, Ont.

Kierans, T.W.,
Churchill Falls (Labrador)
Corporation Limited,
One Westmount Square,
Montreal 6, Que.

Kim, R.Y.,
Department of Mining,
Pennsylvania State University,
University Park, Pa., 16802,
USA

King, M.S.,
Department of Geological Sciences,
University of Saskatchewan,
Saskatoon, Sask.

Kostak, B.,
Department of Energy, Mines &
Resources,
Elliot Lake Laboratory,
Box 100,
Elliot Lake, Ont.

Ladanyi, B.,
École Polytechnique,
Department of Mining Engineering,
C.P. 501, Snowdon,
Montreal 29, Que.

Lamb, L.J.,
Bechtel & Company,
5640 Pare St.,
Montreal 9, Que.

LaRochelle, P.,
Department of Civil Engineering,
Laval University,
Quebec 10, Que.

Larocque, G.,
Department of Energy, Mines &
Resources,
Mining Research Centre,
555 Booth St.,
Ottawa 1, Ont.

Lefebvre, M.,
Gaspé Copper Mines Limited,
Box 774,
Murdochville, Que.

Lieszkowszky, I.P.,
Dominion Soil Investigation Limited,
104 Crockford Boulevard,
Scarborough, Ont.

Lo, K.Y.,
Laval University,
Civil Engineering Department,
Ste-Foy, Quebec 10, Que.

Lopes, R.F.,
141 Picton St. E.,
Hamilton, Ont.

Lyall, K.D.,
Department of Energy, Mines &
Resources,
Elliot Lake Laboratory,
Box 100,
Elliot Lake, Ont.

Manuell, H.C.,
Hilton Mines,
Box 190,
Shawville, Que.

Marcil, D.,
Roctest Limited,
435 Norman St.,
Ville St. Pierre,
Montreal, Que.

Marinov, M.G.,
Bulgarian Embassy,
325 Stewart St.,
Ottawa, Out.

Matyas, E.L.,
University of Waterloo,
Waterloo, Ont.

McAnuff, A.L.,
VME Associates Limited,
212 King St. W.,
Room 307,
Toronto 1, Ont.

McAulay, C.,
Ontario Hydro,
620 University Ave.,
Toronto 2, Ont.

McCreath, D.R.,
H.G. Acres Company Limited,
1259 Dorchester Rd.,
Niagara Falls, Ont.

MacDonald, J.E.A.,
ASARCO,
410 Crandall Building,
Salt Lake City, Utah, 84101,
USA

MacDonald, P.R.,
Ryerson Polytechnical Institute,
50 Gould Street,
Toronto 2, Ont.

MacKay, S.A.,
Cyanamid of Canada Limited,
One City View Drive,
Rexdale, Ont.

McLachlan, H.H.,
Hollinger Mines Limited,
Timmins, Ont.

McRostie, G.,
McRostie, Seto, Genest
Associates Limited,
393 Bell St.,
Ottawa 4, Ont.

Milligan, G.C.,
Dalhousie University,
Halifax, N.S.

Milligan, V.,
H.Q. Golder & Associates Limited,
3151 Wharton Way,
Cooksville, Ont.

Mirza, C.,
31-1 Sentinel Rd.,
Downsview, Ont.

Mollison, R.D.,
Texas Gulf Sulphur,
Box 150,
Toronto Dominion Centre,
Toronto 1, Ont.

Morgan, J.R.,
J.D. Paterson & Associates,
1479 Laperriere St.,
Ottawa, Ont.

Morgenstern, N.R.,
Department of Civil Engineering,
University of Alberta,
Edmonton, Alta.

Morrison, R.G.K.,
6195 N.D.G. Ave.,
Montreal 261, Que.

Morton, J.D.,
Department of Civil Engineering,
University of Toronto,
Toronto 5, Ont.

Moruzi, G.A.,
Falconbridge Nickel Mines Limited,
Nickel Division, Sudbury Operations,
Falconbridge, Ont.

Murphy, D.K.,
H.G. Acres & Company Limited,
1259 Dorchester Rd.,
Niagara Falls, Ont.

Naftal, R.,
Cerro Corporation,
300 Park Ave.,
New York, N.Y., 10022,
USA

Nasmith, H.W.,
R.C. Thurber & Associates,
628 Dupplin Road,
Victoria, B.C.

Neave, K.G.,
University of Toronto,
Physics Department,
Toronto 5, Ont.

Neilson, J.M.,
Queen's University,
Department of Geological Sciences,
Kingston, Ont.

Nelson, W.G.,
55 Humber Trail,
Toronto 9, Ont.

Nesbitt, M.C.,
Department of Highways,
4301 Parkside Crescent,
Victoria, B.C.

Nguyen, D.,
Ecole Polytechnique,
Mining Engineering Department,
C.P. 501, Snowdon,
Montreal 29, Que.

Notley, K.R.,
Falconbridge Nickel Mines Limited,
Nickel Division, Sudbury Operations,
Falconbridge, Ont.

Ogilvie, P.I.,
International Nickel Company
of Canada Limited,
Box 44,
Toronto Dominion Centre,
Toronto 1, Ont.

Ola, S.,
Department of Civil Engineering,
University of Toronto,
Toronto 5, Ont.

Oliver, L.K.,
Jones & Laughlin Mining
Company Limited,
Box 547,
Kirkland Lake, Ont.

Oliver, P.H.,
International Nickel Company
of Canada Limited,
286 9th Ave.,
Lively, Ont.,

Ozden, Z.S.,
McMaster University,
Civil Engineering Department,
Hamilton, Ont.

Palmer, J.H.L.,
Department of Civil Engineering,
University of Toronto,
Toronto 5, Ont.

Pandit, B.I.,
Department of Physics,
University of Toronto,
Toronto 5, Ont.

Paquin, J.,
Canadian Formwork Corporation,
2185 Francis Hughes Ave.,
Chomedey Industrial Park,
Laval, Que.

Parfitt, P.O.,
McIntyre-Porcupine Mines Ltd.,
55 Yonge St.,
Toronto 5, Ont.

Pasieka, A.R.,
Falconbridge Nickel Mines Limited,
7 King St., E.,
Toronto 1, Ont.

Patel, J.P.,
Department of Geophysics,
University of Toronto,
Toronto 5, Ont.

Patching, T.H.,
Department of Mining and
Metallurgy,
University of Alberta,
Edmonton, Alta.

Peaker, K.,
William Trow Associates Limited,
90 Milvan Dr.,
Weston, Ont.

Pegler, A.V.,
Department of Mining Engineering,
Queen's University,
Nicol Hall,
Kingston, Ont.

Peltola, A.,
Sudbury Mining Contractors
Limited,
Box 1045,
Sudbury, Ont.

Phukan, A.L.T.,
Civil Engineering Department,
Laval University,
Quebec 10, Que.

Posavec, M.,
40 Lindy Lou Rd.,
Weston, Ont.

Quigley, R.M.,
Faculty of Engineering Science,
University of Western Ontario,
London, Ont.

Rabbidge, A.J.,
Watts Griffis & McOuat Limited,
Suite 911,
159 Bay St.,
Toronto 1, Ont.

Ram, S.,
Department of Electrical
Engineering,
University of Western Ontario,
London, Ont.

Rana, M.H.,
Mining Engineering Department,
Queen's University,
Kingston, Ont.

Reed, J.J.,
Colorado School of Mines,
Mining Department,
Golden, Colo., 80401,
USA

Reik, G.,
Department of Geology,
University of Toronto,
Toronto 5, Ont.

Rice, H.R.,
Civil Engineering Department,
University of Toronto,
Toronto 5, Ont.

Rickaby, A.C.,
Denison Mines Limited,
Box 2600,
Elliot Lake, Ont.

Riddell, W.J.,
Metals, Petroleum & Hydraulic
Resources Consulting Limited,
Suite 1510, 100 Adelaide St., W.,
Toronto 1, Ont.

Ripley, C.F.,
Ripley, Klohn & Leonoff,
665 Stafford St.,
Winnipeg 9, Man.

Robinsky E.,
Department of Civil Engineering,
University of Toronto,
Toronto 5, Ont.

Robinson, R.V.,
Du Pont of Canada Limited,
Box 900,
North Bay, Ont.

Roy, A.,
Mining Department,
École Polytechnique,
4905 Victoria St.,
Montreal, Que.

Royea, M.J.,
Cominco Limited,
Sullivan Mine,
Box 2000,
Kimberley, B.C.

Salvas, R.J.,
Ryerson Polytechnical Institute,
50 Gould St.,
Toronto 2, Ont.

Sanders, J.,
Kennecott Copper,
1515 Mineral Square,
Salt Lake City, Utah,
USA

Sangrey, D.A.,
Department of Civil Engineering,
Queen's University,
Kingston, Ont.

Schwellnus, J.E.G.,
McGill University,
Department of Mining Engineering,
805 Sherbrooke St. W.,
Montreal, Que.

Schwerdtner, W.M.,
Department of Geology,
University of Toronto,
Toronto 5, Ont.

Segsworth, R.S.,
Department of Electrical
Engineering,
University of Toronto,
Toronto 5, Ont.

Seychuk, J.L.,
Golder Associates,
3151 Wharton Way,
Cooksville, Ont.

Singh, V.P.,
Falconbridge Nickel Mines Limited,
Strathcona Mines,
Onaping, Ont.

Singhal, R.K.,
Mining Engineering Department,
The University,
Newcastle-upon-Tyne 1,
England.

Sipe, G.R.,
Queen's University, 347 Albert St.,
Kingston, Ont.

Smith, J.D.,
J.D. Smith and Associates,
106 Holland Cres.,
Kingston, Ont.

Smotrych, S.W.,
Department of Civil Engineering,
McMaster University,
Hamilton, Ont.

Soderlund, H.
Algoma Ore Division,
Algoma Steel Corporation Limited,
Wawa, Ont.

Soles, J.A.,
Department of Energy, Mines &
Resources,
Mines Branch,
40 Lydia St.,
Ottawa, Ont.

Solymar, Z.,
H.G. Acres Company Limited,
1259 Dorchester Rd.,
Niagara Falls, Ont.

Stephens, B.P.R.,
V.M.E. Associates Limited,
212 King St. W.,
Toronto 1, Ont.

Stesky, R.M.,
111 Charleswood Dr.,
Downsview, Ont.

Taylor, B.W.,
Ecstall Mining Limited,
Box 2002,
Timmins, Ont.

Tervo, R.O.
Department of Energy, Mines &
Resources,
Elliot Lake Laboratory,
Box 100,
Elliot Lake, Ont.

Thomas, W.H.,
Cyanamid of Canada,
One City View Dr.,
Rexdale, Ont.

Thompson, C.D.,
William Trow and Associates
Limited,
198 Superior St.,
Hamilton, Ont.

Townsend, D.,
Civil Engineering Department,
Queen's University,
Kingston, Ont.

Turner, A.K.,
Department of Public Works,
Apartment 2E, 2501 Soldiers
Home Rd.,
West Lafayette, Ind., 47906,
USA

Turpin, R.,
Algoma Steel Corporation Limited,
Algoma Ore Division,
Wawa, Ont.

Tuttle, J.K.,
Dames & Moore Limited,
111 Railside Rd.,
Suite 205,
Don Mills, Ont.

Udd, J.E.,
McGill University,
Department of Mining Engineering
& Applied Geophysics,
805 Sherbrooke St. W.,
Montreal, Que.

Utter, S.,
U.S. Bureau of Mines,
Denver Mining Research Center,
Denver, Colo., 80225,
USA

Valent, S.,
Suite 416,
5450 Cote des Neiges,
Montreal 26, Que.

Verity T.W.,
Department of Energy, Mines &
Resources,
Mining Research Centre,
555 Booth St.,
Ottawa 1, Ontario.

Verner, W.J.,
Ohio State University,
College of Engineering,
2070 Neil Ave.,
Columbus, Ohio, 43221,
USA

Voight, B.,
Department of
Geology-Geophysics-Mining,
Pennsylvania State University,
University Park, Pa., 16802,
USA

Walker, B.P.,
Walker Ceponis & Associates,
45 Charles St. E.,
Toronto 5, Ont.

Walton, T.R.,
Steel Company of Canada,
525 Dominion St.,
Montreal, Que.

Williams, R.R.,
Williams Form Engineering
Corporation,
1501 Madison Ave. SE,
Grand Rapids, Mich.,
USA

Wilson, N.E.,
Department of Civil Engineering,
McMaster University,
Hamilton, Ont.

Wilson, R.C.G.,
10 St. Clair Ave. E.,
Suite 5,
Toronto 7, Ont.

Yu, Y.S.,
Department of Energy, Mines &
Resources,
Mining Research Centre,
555 Booth St.,
Ottawa 1, Ont.

Zahary, G.,
Department of Energy, Mines &
Resources,
Elliot Lake Laboratory,
Box 100,
Elliot Lake, Ont.

Zorychta, H.,
Department of Energy, Mines &
Resources,
Mining Research Centre,
Box 111,
Glace Bay, N.S.